PhD thesis

Tests of the isomorph theory by computer simulations of atomic and molecular model liquids

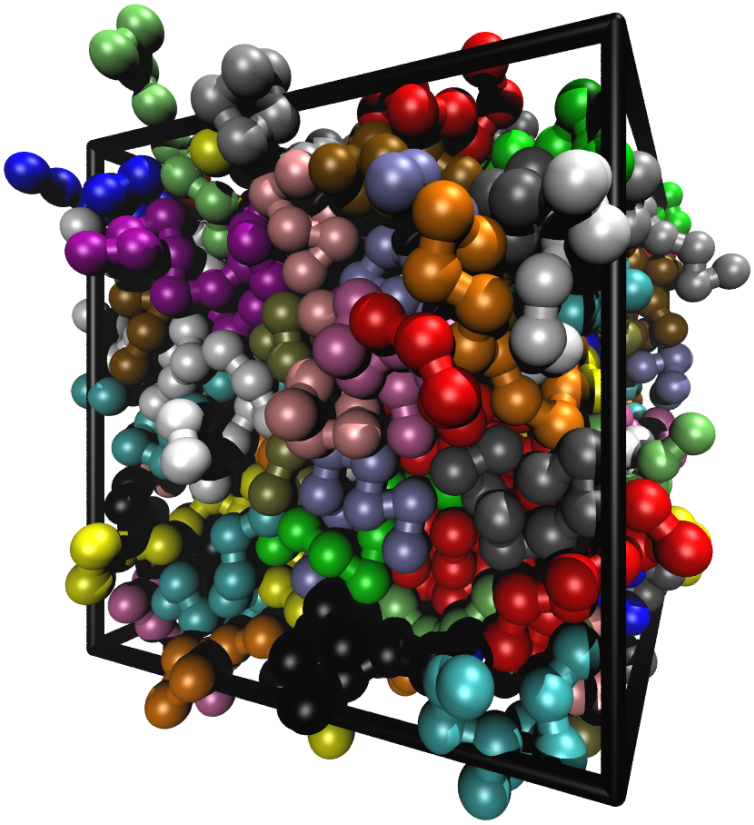

Arno A. Veldhorst, *March 31, 2014*
advisor: Thomas B. Schrøder

Danish National Research Foundation Centre "Glass and Time",
IMFUFA, Department of Science, Systems and Models,
Roskilde University, Denmark

Abstract

Recently, it was discovered that some liquids behave in a particularly simple way in part of their phase diagram (Bailey et al., 2008a,b; Pedersen et al., 2008b). These liquids can be identified in computer simulation by correlations between their potential energy and virial, which is quantified by the correlation coefficient R being higher than 0.9. Their simplicity lies in the fact that they have curves in their phase diagram called isomorphs, along which many properties are invariant to a high degree. This includes for example constant configurational entropy, constant isochoric specific heat, invariant equilibrium dynamics, and invariant equilibrium structure (Gnan et al., 2009; Schrøder et al., 2009). Whereas previous studies have focused mainly on atomic model liquids and small rigid molecules (Ingebrigsten et al., 2012a), this thesis aims to show that the isomorph theory is applicable to a much wider range of systems.

We show that colloidal suspensions and dusty plasmas may also be considered simple by simulating the Yukawa potential. The Yukawa fluid is shown to have correlated energy-virial fluctuations and isomorphs in its phase diagram. We show that it is possible to predict the shape of the isomorph from the form of the potential.

The shape of an isomorph in the density-temperature phase diagram is described by a function $h(\rho)$. Recent results for real liquids show that the logarithmic slope $\gamma = \frac{\mathrm{d}\ln h(\rho)}{\mathrm{d}\ln \rho}$ increases with density (Bøhling et al., 2012). We show with computer simulations of two novel potentials and the Girifalco potential that this may be an effect of the finite molecular volume of many organic glass formers.

Before the development isomorph theory it was already found that for many real liquids, the dynamics can be scaled onto a single curve by a power law of density. A large part of the real liquids that have been shown to obey this scaling are polymers (Roland et al., 2005). For atomic models and small rigid molecules this scaling has been shown to be an approximation of isomorph theory in small density ranges (Gnan et al., 2009; Ingebrigtsen et al., 2012). We simulated flexible chains of Lennard-Jones particles connected by rigid bonds, and show that this liquid has correlations and isomorphs. Interestingly, we find that the structure of a single molecule is not invariant on the isomorph, while the interatomic structure is. Both the dynamics of the Lennard-Jones particles, as well as the dynamics of the entire chain are found to be invariant on the isomorph. Our results indicate that isomorph theory may also hold for liquids consisting of long, flexible chains, like polymers.

Simulations of Lennard-Jones chains where the covalent bonds are simulated as harmonic springs has led to the discovery of so-called pseudo isomorphs. The inclusion of these flexible bond destroys the energy-virial correlations almost completely ($R \approx 0.28$). We show that these chains nevertheless have curves in their phase diagram along which the dynamics and the intermolecular structure is invariant. We show that the energy-virial correlations do persist in the frequency domain at low frequencies.

Abstract in Danish

Inden for de sidste par år er det blevet opdaget, at nogle væsker opfører sig på en særligt simpel måde i dele af deres faserum (Bailey et al., 2008a,b; Pedersen et al., 2008b). Disse væsker kan identificeres i computersimuleringer ved at have en korrelationskoefficient R højere end 0.9. Det simple ved dem vedrører det faktum, at de har kurver i deres faserum, kaldet isomorfer, langs hvilke mange egenskaber udviser en høj grad af invarians. Dette gælder eksempelvis konstant konfigurationel entropi, konstant isochorisk varmekapacitet, invariant ligevægtsdynamik og invariant ligevægtsstruktur (Gnan et al., 2009; Schrøder et al., 2009). Hvor tidligere studier primært har fokuseret på atomistiske modelvæsker og små rigide molekyler (Ingebrigsten et al., 2012a), er formålet med denne afhandling at vise, at isomorfteorien er anvendelig i en langt bredere række af systemer.

Vi viser at kolloidsuspension og støvede plasmaer også kan karakteriseres som simple ved simulering af Yukawapotentialet. Det vises, at Yukawavæsken har korrelerede energi-virial-fluktuationer og isomorfer i sit faserum. Vi viser at det er muligt at forudsige formen af isomorferne fra formen på potentialet.

Formen på en isomorf i densitet-temperatur-faserummet beskrives med en funktion $h(\rho)$. Nylige resultater for virkelige væsker har vist at den logaritmiske hældning $\gamma = \frac{\mathrm{d}\ln h(\rho)}{\mathrm{d}\ln \rho}$ tiltager med densitet (Bøhling et al., 2012). Vi viser ved computersimuleringer af to nye potentialer samt Girifalco potentialet, at dette kan skyldes at mange organiske glasformere har et endeligt molekylært volume.

Før isomorfteorien blev udviklet var det kendt, at for mange virkelige væsker kan dynamikken skaleres til en enkelt kurve ved en potensfunktions af densiteten. En stor del af de virkelige væsker, for hvilke det er blevet vist at de følger denne type skalering, er polymere (Roland et al., 2005). For atomare modeller og små rigide molekyler er det blevet vist, at denne skalering er en approksimation til isomorfteorien i et smalt densitetsinterval (Gnan et al., 2009; Ingebrigtsen et al., 2012). Vi har simuleret fleksible kæder af Lennard-Jones-partikler holdt sammen med rigide bånd, og vi viser, at denne væske har korrelation og isomorfer. Overraskende finder vi, at strukturen af et enkelt molekyle ikke er invariant langs en isomorf, men at den interatomare struktur er. Både Lennard-Jones-partiklernes dynamik og dynamikken af hele kæder vises at være invariant på en isomorf. Vores resultater indikerer, at isomorfteorien muligvis også gælder for væsker bestående af lange, fleksible kæder, så som polymere.

Simuleringer af Lennard-Jones-kæder, hvor de kovalente bindinger simuleres som harmoniske fjedre har ført til opdagelsen af såkaldte pseudoisomorfer. Inklusionen af fleksible bånd ødelægger næsten fuldstændig energi-virial-korrelationen ($R \approx 0.28$). På trods af dette viser vi, at disse kæder har kurver i deres faserum langs hvilke dynamikken og den intermolekylære struktur er invariant. Vi viser, at energy-viriale-korrelationen er bevaret i frekvensdomænet ved lave frekvenser.

Papers

This thesis describes some of the work done during the three years of the Danish PhD program, between April 1st 2011 and March 31st 2014. The work has been supervised by Thomas B, Schrø]der and was done in the Glass and Time group at Roskilde University. The thesis has five companion papers which can be found in appendix C:

I *Isomorphs in the phase diagram of a model liquid without inverse power law repulsion*
A. A. Veldhorst, L. Bøhling, J. C. Dyre, and T. B. Schrøder, Eur. Phys. J. B, **85**, 21, 2012.

II *Do the repulsive and attractive pair forces play separate roles for the physics of liquids?*
L. Bøhling, A. A. Veldhorst, T. S. Ingebrigtsen, N. P. Bailey, J. S. Hansen, S. Toxvaerd, T. B. Schrøder, and J. C. Dyre, J. Phys.: Condens. Matter, **25**, 032101, 2013.

III *Communication: The Rosenfeld-Tarazona expression for liquids' specific heat: A numerical investigation of eighteen systems*
T. S. Ingebrigtsen, A. A. Veldhorst, T. B. Schrøder, and J. C. Dyre, J. Chem. Phys., **139**, 171101, 2013.

IV *Statistical mechanics of Roskilde liquids: Configurational adiabats, specific heat contours, and density dependence of the scaling exponent*
N. P. Bailey, L. Bøhling, A. A. Veldhorst, T. B. Schrøder, and J. C. Dyre, J. Chem. Phys., **139**, 184506, 2013.

V *Isomorphs in flexible Lennard-Jones chains*
A. A. Veldhorst, J. C. Dyre, and T. B. Schrøder (2013), arXiv:1307.5237

Acknowledgements

I would like to start by thanking my advisor Thomas Schrøder and Professor Jeppe Dyre for giving me the opportunity to be a part of the Glass and Time group for three years. Being part of this group has been a true pleasure and a very instructive period of my life. I feel especially indebted to the people of the simulation group, being Nick Bailey, Lasse Bøhling, Lorenzo Costigliola, Jesper Hansen, Heine Larsen, Claire Lemarchand, Andreas Olsen, Ulf Pedersen, Thomas Schrøder, and Søren Toxvaerd, for fruitful collaborations, enlightening discussions, and bugs solved.

I would like to thank Professor Wei Hua Wang from the Chinese Academy of Sciences in Beijing for giving me the opportunity to spend six months in the Ex4 group of the Institute Of Physics. I am also very grateful to all the PhD students there who made me feel right at home. Special thanks to Jiao Wei, Wang Zheng, and Li Yanzhuo, for helping me with a lot of silly problems and for their willingness to explain me whatever about their strange but wonderfull country.

In general I have found my stay at IMFUFA and NSM most comfortable, and I would like to express my gratitude towards whoever joined me in some less scientific adventures. In particular I would like to mention Andreas, Asli, Ben, Elsje, Heine, Jesper, Johanne, Kenneth, Lasse, Lasse, Leila, Lisa, Lorenzo, Mikkel, Sergio, Sif, Thomas, Tina, Trine, and Wence.

Lastly I would like to thank Luna. Without her I probably would not even have started the PhD program, and I would have missed out on these wonderful three years of my life. Having all these good experiences without her would only have compared to living them half, and I am forever grateful for the unconditional support she gives me.

Contents

Chapter 1

Background

This chapter gives some general background information on the research field of glass and viscous liquids, which is the main focus of the Glass and Time group at Roskilde University. After this, a general explanation of the computational method of Molecular Dynamics (MD) is given, as well as some details of the specific implementation used in this thesis.

1.1 Viscous liquids and the glass transition

This section is meant to provide only the most basic background on glasses and viscous liquids. General overviews of this and related subjects can be found in Donth (2001), Debenedetti and Stillinger (2001), Dyre (2006), Kivelson and Tarjus (2008), Cavagna (2009), Ediger and Harrowell (2012), Biroli and Garrahan (2013), and other sources.

1.1.1 The glass transition

In everyday life, the word "glass" is normally used for a solid, transparent material consisting mainly of silicon oxide. The scientific word "glass" however is used to describe a wide range of materials which have as a common denominator that they are: 1. solid and 2. amorphous (i.e., the atoms or molecules are not in an ordered lattice). Glasses can be formed from many different substances, among others organic molecular substances including polymers and biomolecules, and inorganic substances like oxides and metallic alloys.

Glass can be formed in a variety of ways, but the most common way is to start with a liquid and then cool it down. This is illustrated in figure 1.1, where the cooling of the liquid starts at the top right corner. As the temperature is lowered, a typical liquid will at some point encounter the melting temperature T_m at which the solid crystal phase becomes thermodynamically more stable than then the liquid. However, the liquid does not necessarily form a crystal at or below T_m. This depends on the crystal growth and/or nucleation rate. In principle, crystallization can always

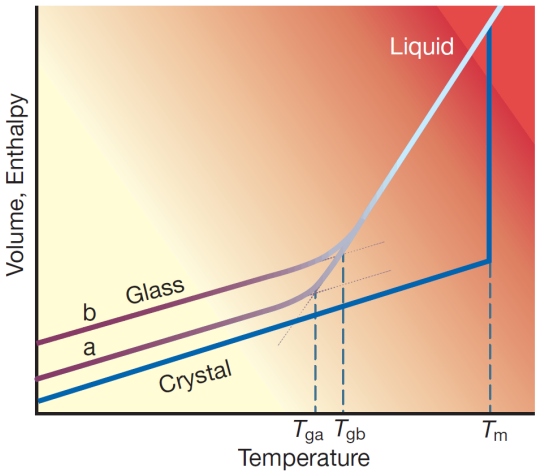

Figure 1.1: Illustration of supercooling a liquid to form a glass. A liquid can prevent crystallization below the melting temperature T_m. At the glass transition temperature T_g the liquid becomes so viscous that relaxation processes cannot keep up with the cooling rate. Here the liquid is not in equilibrium anymore, and is called a glass. The glass transition temperature depends on cooling rate. Taken from Debenedetti and Stillinger (2001).

be avoid by cooling fast enough, although for some liquids this would need cooling rates that cannot (yet) be reached. A liquid below the melting temperature is said to be in the supercooled state.

As the liquid is cooled further, the dynamics of the liquid become slower and slower, as the molecules have less and less kinetic energy. These slow dynamics are usually quantified by some relaxation time τ or viscosity η. At some point, the relaxation in the liquid is so slow that the liquid does not have enough time to "find" the equilibrium. When the liquid is cooled further after falling out of equilibrium it can be considered a glass. This happens at the glass transition temperature T_g, which dependent on the cooling rate. Because the glass transition temperature is not well defined, other definitions exist, such as the temperature where the viscosity or some relaxation time reaches a certain value (see for instance figure 1.2).

The glass transition and the glassy state have been known to physicists for a long time, but the development of a theory that can explain them is still one of the big problems in physics today (Anderson, 1995).

1.1.2 Viscous liquids

It is actually the viscous, supercooled state that has been studied most in research related to the glass transition. Part of the reason for this is that the liquid is in equilibrium, which means that one can use standard thermodynamics to build a theory. Moreover, many properties of the glass such as the high viscosity and the amorphous structure are already developing in the equilibrium liquid state upon approaching the glass transition. The liquid state itself is not well understood either.

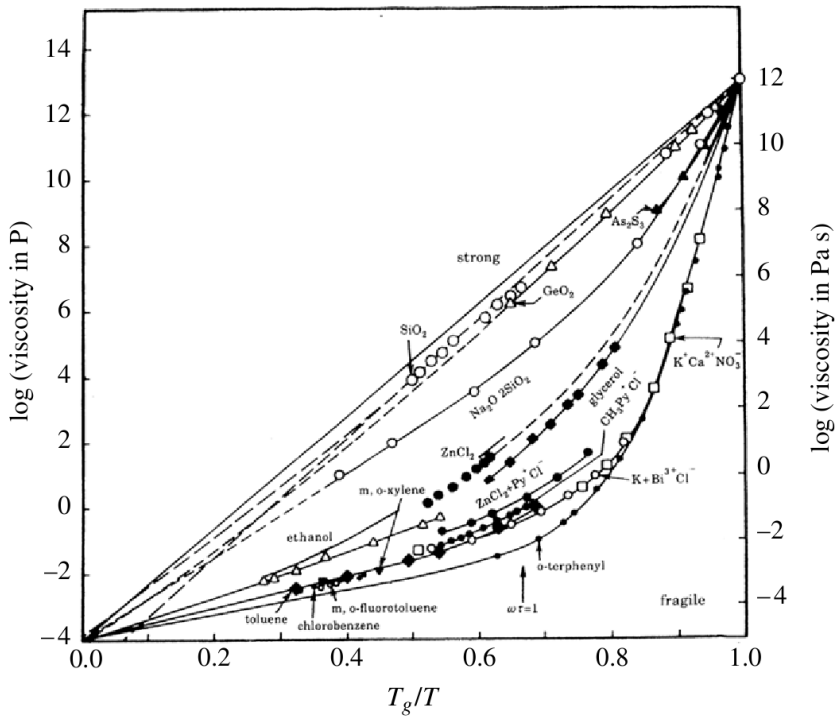

Figure 1.2: The famous Angell plot. Here the viscosity of many different glass forming liquids is plotted versus inverse temperature. The temperature is rescaled by the glass transition temperature, which in this case is defined as the temperature where the viscosity reaches a certain value. The temperature dependence of the viscosity is very different for the different liquids. In this plot, liquids that have an approximate linear dependence $\log(\eta) \propto T_g/T$ are referred to as "strong"liquids, while they are called "fragile" liquids if this is not the case. Taken from Cavagna (2009).

One of the main questions in the study of viscous liquids is what controls the dynamics, such as viscosity and relaxation time. As said before, the dynamics become slower as the liquid is cooled down, and as the glass transition is approached the effect becomes quite extreme. This is visualized in figure 1.2, where the viscosity is shown to increase by a factor of 10^{14} while for some of the liquids temperature only changes a by a factor of two. The huge increase in viscosity in itself is hard to explain, but as can be seen in the figure, the temperature dependence of the viscosity is dependent on the material.

The problem becomes even more complicated when considering that the glass transition including the huge viscosity increase also occurs when pressure (or density) is increased while temperature is kept constant. The problem of what controls the relaxation time is thus a two dimensional problem that may be material specific.

When looking at what happens at the microscopic level, viscous liquid show some typical behavior. This is easily shown in computer simulations by looking at the absolute particle displacement over some period of time. Figure 1.3(a) shows this mean square displacement for different temperatures. At short times, the particles move on average unhindered by their neighbors. After some time the particle

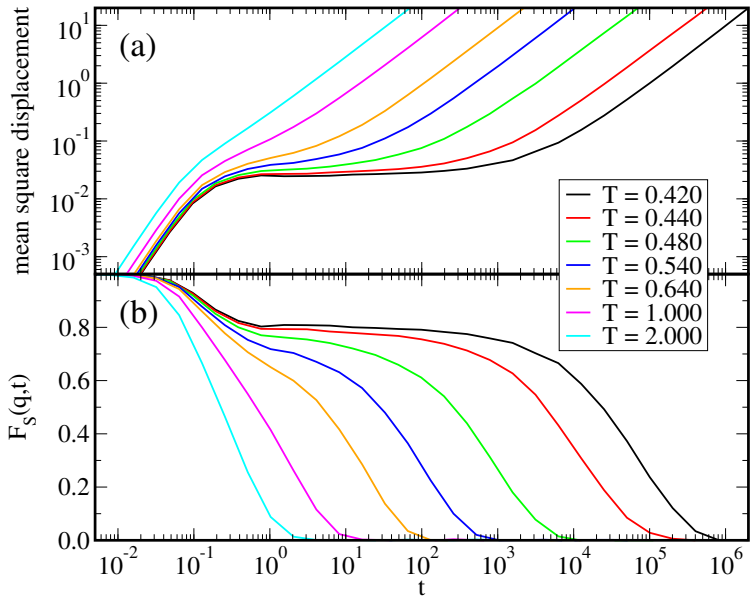

Figure 1.3: The mean square displacement (top) and the Incoherent intermediate scattering function (bottom). For these simulations density is constant $\rho = 1.2$. As temperature is decreased, the dynamics start two show two regimes; a fast ballistic regime at short times and a slower diffusive regime at longer times, with a plateau in the middle. (Data are from simulations of the Kob-Anderson Buckingham liquid. See appendix A for a description of the liquid.)

will the presence of its neighbors; the slope changes. For the lowest temperatures however, the slope becomes zero, indicating that the particle does not move beyond a certain distance that is related to the average interparticle distance in the liquid. This is called the "cage" effect, and at this timescale the liquid behaves as a solid, i.e., it does not flow. Only at longer time scales are particles able to escape from their "cage", and does the liquid flow. Also the intermediate scattering function in figure 1.3(b), which is a common quantity to extract dynamical data from scattering experiments, shows this so called separation of timescales that is typical of viscous liquids.

1.1.3 Power law density scaling

Experimental results by Tölle (2001); Tölle et al. (1998) indicate that the problem of what controls the relaxation time of viscous liquids might be simplified. It was found that the dynamics of *ortho*-terphenyl, measured at different state points (points in the phase diagram with different density ρ and temperature T), can be collapsed onto a single curve by plotting it as a function $h(\rho)/T$. In the case of *ortho*-terphenyl, the function was found to be $h(\rho) = \rho^4$. Later results have shown that the dynamics of many liquids can be collapsed when plotted as a function of $h(\rho)/T$, albeit with a different $h(\rho)$ (Alba-Simionesco et al., 2002; Dreyfus et al., 2003; Paluch et al., 2003b).

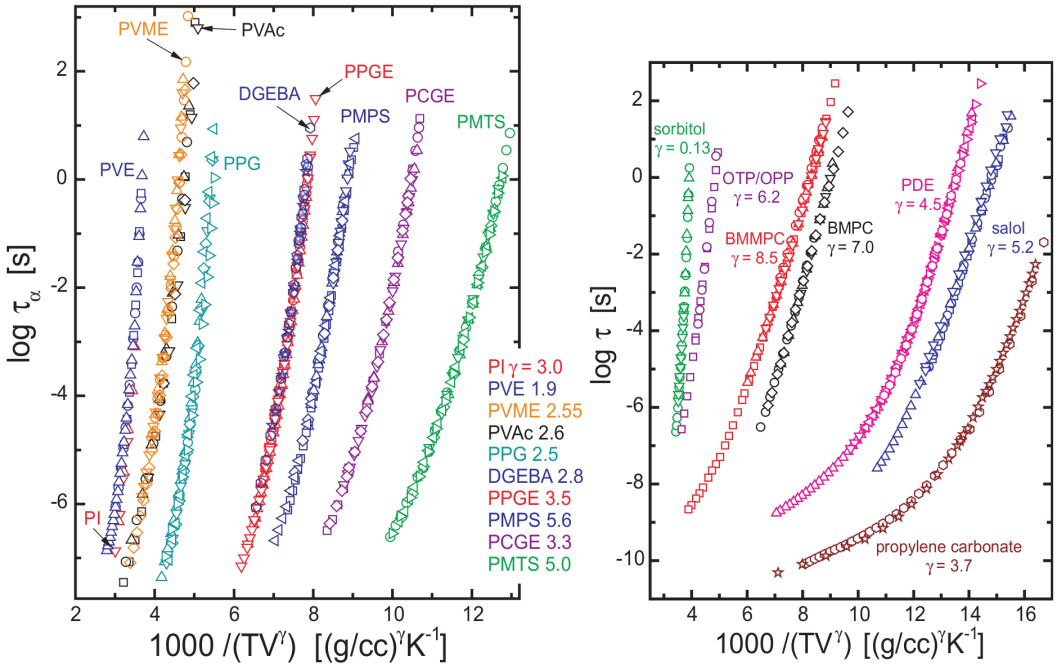

Figure 1.4: Power law density scaling of a selection of polymer melts (left) and small molecular glass forming liquids (right). The dynamical measure that is scaled is the dielectric (α) relaxation time, which collapse when plotted versus ρ^γ/T with γ being dependent on the material. Taken from Roland et al. (2005), where the names of the different substances are explained.

The functional form of $h(\rho)$ and the physical meaning of the functional from were a source of some controversy (Casalini and Roland, 2004; Roland and Casalini, 2004; Tarjus et al., 2004a,b). Nevertheless, it was found that the scaling works well for many liquids if the scaling function is a power law of the density $h(\rho) = \rho^\gamma$ (Roland et al., 2005). This is shown in figure 1.4, where for each liquid the dynamics are only a function of ρ^γ/T, with γ being material dependent. Since $h(\rho)$ is here a power law of the density, we refer to this scaling as *power-law density scaling*.

Figure 1.4 shows data for small molecular glass formers and polymers (which are often also glass forming liquids (Roland, 2010)). However, more recent data have shown that power law density scaling also holds for ionic liquids (Habasaki et al., 2010; López et al., 2011; Paluch et al., 2010; Swiety-Pospiech et al., 2012, 2013) and liquid crystals (Roland et al., 2008; Satoh, 2013; Urban, 2011; Urban and Roland, 2011; Urban and Würflinger, 2005; Urban et al., 2007).

1.2 Molecular dynamics

This is a minimal background on Molecular Dynamics to give the reader a feeling of the method. There exist many good books on the method, with Allen and Tildesley (1987), Frenkel and Smit (2002), and Rapaport (2004) among the classics.

The basic idea of Molecular Dynamics (MD) is to solve Newton's equations of motion numerically, specifically Newton's second law

$$\mathbf{F} = m\mathbf{a}\,, \tag{1.1}$$

which states that the acceleration $\mathbf{a}$ of an object is proportional to the force on that object.

In an MD simulation the objects of interest are usually atoms, groups of atoms, or molecules. Let's call them particles. The force acting on the particles arises from interaction between the particles. In MD the most classic example of such an interaction is the Lennard-Jones potential (Jones, 1924)[1]

$$v_{ij}(r_{ij}) = 4\varepsilon\left[\left(\frac{\sigma}{r_{ij}}\right)^{12} - \left(\frac{\sigma}{r_{ij}}\right)^{6}\right], \tag{1.2}$$

which states how the potential energy depends on the distance r between two particles i and j. For this potential, the particles repel each other at close distance (Pauli exclusion) but attract each other at larger distance (van der Waals attraction). In general, MD is used to solve systems of more than two particles, and in the Lennard-Jones case the total potential energy would then be just the sum of the individual pair interactions $U(\mathbf{R} = \sum_{i<j} v_{ij}$, where $\mathbf{R} = \mathbf{r}_1, \ldots, \mathbf{r}_N$ denotes the positions of all N particles in the system. The force acting on a particle i at position $\mathbf{r}_i$ is then simply the gradient of this potential energy

$$\mathbf{F} = -\nabla_{\mathbf{r}_i} U(\mathbf{R})\,. \tag{1.3}$$

Time is discrete in MD, and a time step Δt is chosen small enough to minimize any errors due to the discretization. Using a central difference, the acceleration at time t can be approximated from the velocities half a timestep before and after t. The same goes for finding the velocities from the positions:

$$\mathbf{a}(t) = \frac{\mathbf{v}\left(t + \frac{1}{2}\Delta t\right) - \mathbf{v}\left(t - \frac{1}{2}\Delta t\right)}{\Delta t}\,, \qquad \mathbf{v}(t) = \frac{\mathbf{r}\left(t + \frac{1}{2}\Delta t\right) - \mathbf{r}\left(t - \frac{1}{2}\Delta t\right)}{\Delta t}\,. \tag{1.4}$$

Putting this in equation 1.1 we get what is known as the Verlet algorithm (Verlet, 1967)

$$\mathbf{r}(t + \Delta t) = 2\mathbf{r}(t) - \mathbf{r}(t - \Delta t) + \frac{(\Delta t)^2}{m}\mathbf{F}(t)\,. \tag{1.5}$$

Thus the position at the next time step can be calculated from the position at the current and previous time steps and the force at the current time step.

Different algorithms exist that are equivalent to the Verlet algorithm, the one used in this thesis being the so called Leap Frog algorithm. The Leap Frog algorithm

[1] One year after the publication Jones married, adding his wife's surname to his own. Hence the name *Lennard-Jones* potential.

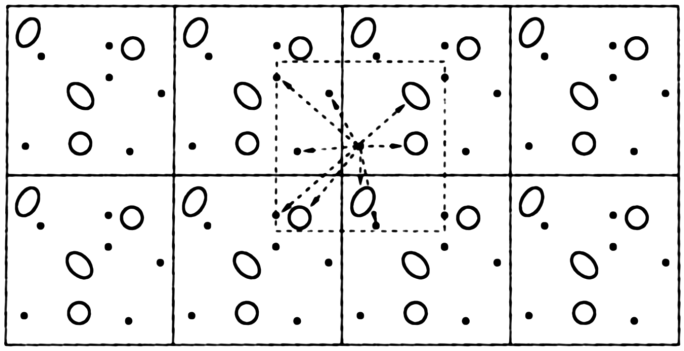

Figure 1.5: Illustration of periodic boundary conditions in two dimensions. The simulation box containing the particles has "virtual copies" of itself as neighbors. If a particle moves out of the box on one side, it is just put back in the box on the other side. Moreover, when the distance to another particles has to be calculated, then the shortest distance to any of the copies is taken (drawn by the dashed box). Taken from Frenkel and Smit (2002).

is also a central difference algortihm, as it uses the rewritten left side of equation 1.4 to calculate the velocities at the intermediate half timestep $t + \frac{1}{2}\Delta t$

$$\mathbf{v}\left(t + \frac{1}{2}\Delta t\right) = \mathbf{v}\left(t - \frac{1}{2}\Delta t\right) + \Delta t \mathbf{a}(t)\,. \tag{1.6}$$

This intermediate velocity is then used to calculate the position at $t + \Delta t$ from the right hand side of equation 1.4

$$\mathbf{r}\,(t + \Delta t) = \mathbf{r}\,(t) + \Delta t \mathbf{v}(t + \frac{1}{2}\Delta t)\,. \tag{1.7}$$

As said before, the Leap Frog algorithm is mathematically equivalent to the Verlet algorithm. It is however more stable on a computer, because is does not take the difference of two large quantities to obtain a small one.

In thesis the simulations were performed in the canonical (NVT) ensemble. To keep temperature constant an extra friction force is added. This has the additional advantage that round off errors do not accumulate during long simulations.

Especially when simulating viscous liquids, one is interested in long time scales, so the computational costs have to be minimized. There are some simple tricks that can be used in MD to reduce the amount of computations:

- Potential cutoff. Most forces come from interactions from particles near each other, so it is not necessary to calculate the force or even the distance between particles that are far away from each other. (As long as you know they far away from each other).

- Less particles. Less particles obviously means less calculations per time step. However, decreasing the system size also means that boundary effects become more important. For this reason one usually uses periodic boundary conditions in MD (see figure1.5).

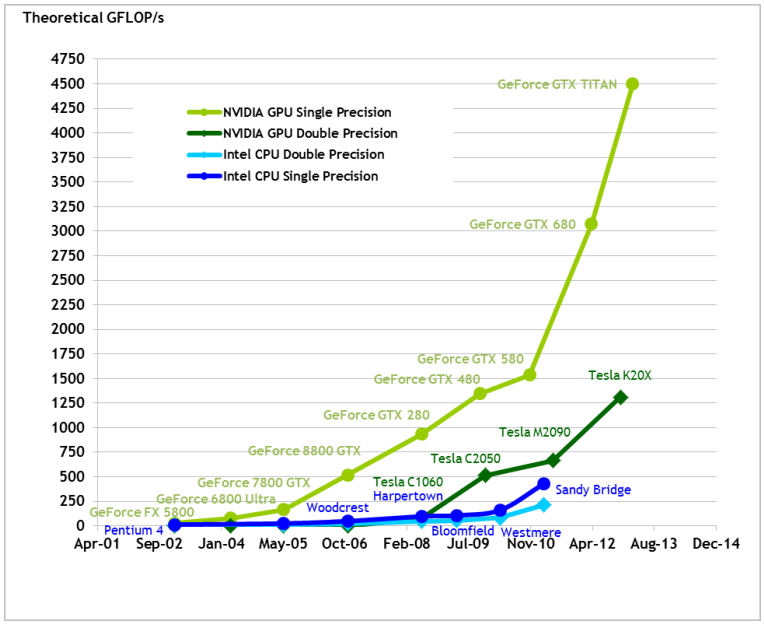

Figure 1.6: Comparison of the development of the number of floating point operations per second (FLOPS) between NVIDIA GPUs and CPUs. Taken from the CUDA programming guide (`http://docs.nvidia.com/cuda/`).

1.2.1 GPU computing: RUMD

In 2007 NVIDIA released the CUDA programming environment, which provides a means to directly program a Graphics Processing Unit (GPU) using C or C++. This made it for the first time relatively easy to harness the power of graphics cards for scientific computing.

GPUs have been around for a long time, but in the last decade or so their speed as measured by the amount of floating point operations per second (FLOPS) has surpassed the speed of the normal Central Processing Unit (CPU) (see figure 1.6). This is partly due to the development of the CPU being slowed down by issues related the energy consumption and heat dissipation. Indeed, any standard CPU nowadays contains multiple cores, which goes in the direction of the GPU which contain many cores[2]. In development of the GPUs, the focus has been purely on increasing the amount of FLOPS due the entertainment industry, where graphics in computer games are demanding ever more floating point operations (Kirk and Hwu, 2010).

Since the architecture of the GPU is focused on bare floating point operations they are perfect for scientific computing. They are not only faster than CPUs when it comes to the amount of floating point operations, but they are also cheaper and use less energy per floating point operation. GPUs are particularly good for MD simulations, since they are optimized to do many identical operations in parallel on different elements of the same data set. In MD this exactly the case for the calculation of the forces on each particle for from the positions of the other particles.

The Glass and Time group has developed its own MD code for GPUs, called

[2]The GTX280, the type of GPU used most for the simulations in this thesis has 240 cores.

Roskilde University Molecular Dynamics (RUMD), which is open source and can be downloaded at https://rumd.org. There are different reasons for writing a new code from scratch. The first reason is that main MD codes are running on CPUs. It is possible to accelerate a CPU code by doing some of the calculations on the GPU, but due to the relatively slow communication between the GPU and the CPU this is not ideal. It is much faster to do the entire simulation on the GPU, keeping communication with the GPU to a minimum. Other MD codes that run completely on the GPU do exist, but these are optimized for large systems $N > 10000$. We on the other hand are interested in simulating small systems very fast to reach long time scales.

Being part of the RUMD development has been a huge pleasure. It has been a blessing to be able to customize the program to my own needs, and knowing the inner workings of the program so well has also proven to be useful in finding new tools in research. A list of functionalities I have implemented in RUMD during the course of my PhD can be found in appendix B.

Chapter 2

Introduction to Roskilde-simple liquids

The aim of this chapter is to give a general overview of the isomorph theory and simple liquids. The theory has been described extensively in a series of publications of the Glass and Time group (Bailey et al., 2008a,b; Gnan et al., 2009; Ingebrigtsen et al., 2012; Schrøder et al., 2009, 2011). Most of the figures used to illustrate the theory in this chapter have been taken from Paper I and contain data from simulations with the Buckingham potential. See appendix A for an introduction to the Buckingham potential and the details of these simulations.

2.1 Liquids with strong energy-pressure correlations

In 2008 it was discovered in Roskilde that some liquids have correlated pressure and energy fluctuations (Bailey et al., 2008a; Pedersen et al., 2008b). More precisely, the correlations appear between potential energy U and the virial W, which are the *excess* or configurational parts of the energy and pressure. These parts only depend on the positions of the particles $\mathbf{r}_i$, in contrast to the kinetic energy and the temperature, which only depend on the momenta of the particles $\mathbf{p}_i$:

$$E = K(\mathbf{p}_1, \ldots, \mathbf{p}_N) + U(\mathbf{r}_1, \ldots, \mathbf{r}_N)\,, \tag{2.1}$$

$$pV = Nk_BT(\mathbf{p}_1, \ldots, \mathbf{p}_N) + W(\mathbf{r}_1, \ldots, \mathbf{r}_N)\,. \tag{2.2}$$

For a system with only pair interaction, the virial (like the potential energy) is calculated as the sum of contributions of each particle pair, from the force acting between that pair:

$$W = -\frac{1}{3}\sum_{i<j} r_{ij} v' r_{ij}\,, \tag{2.3}$$

where i and j denote particles.

In figure 2.1(a) we visualize the correlated fluctuations by plotting the normalized deviations from the average potential energy and virial. The fluctuations clearly

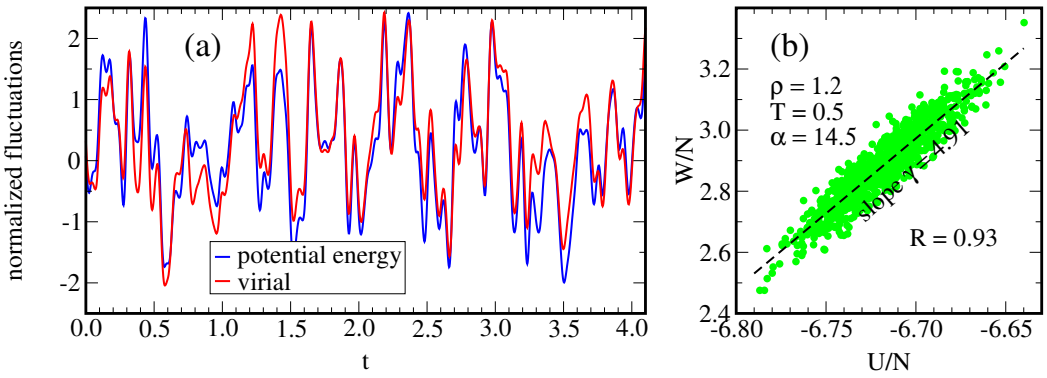

Figure 2.1: (left) The equilibrium fluctuations of the potential energy and the virial versus time for the KABB liquid with $\alpha = 14.5$ at density 1.2 and temperature 0.5. The data have been normalized by subtracting the mean and dividing by the standard deviation. The data show that the potential energy and the virial follow each other, but they are not perfectly correlated. (right) Data from the same simulation, but now visualized as a scatter plot. The correlation coefficient at this state point is 0.93, which is "strongly correlating". The density scaling exponent γ is the slope of the fluctuations in the U,W plane.

follow each other to a good degree. Another way of plotting the fluctuations is as a scatter plot in the U,W plane, as done in figure (b).

The correlations are quantified by the standard correlations coefficient

$$R = \frac{\langle \Delta W \Delta U \rangle}{\sqrt{\langle (\Delta W)^2 \rangle \langle (\Delta U)^2 \rangle}} \,. \tag{2.4}$$

Here Δ denotes the deviation from the average and the angular brackets $\langle\rangle$ denote thermal averaging. The scatter plot in figure 2.1(b) shows that a standard linear regression gives for the slope

$$\gamma = \frac{\langle \Delta W \Delta U \rangle}{\langle (\Delta U)^2 \rangle} \,, \tag{2.5}$$

which turns out to be an important quantity in the isomorph theory. So far people have used the (somewhat arbitrary) threshold of $R \geqslant 0.9$ to define a liquid that is simple in the Roskilde sense.

Many model liquids have been shown to have these correlations (Bailey et al., 2008a), but of course the instantaneous values of the potential energy and the virial are only accessible in computer simulations. Nevertheless, there are indications that some form of energy correlation are also present in real liquids. For a monoatomic system like argon for instance, the configurational part of the energy and pressure fluctuations can be estimated from the isothermal bulk modulus K_T, the isochoric specific heat C_V, and the pressure coefficient β_V as described in Bailey et al. (2008b) and Pedersen et al. (2008b). These estimates for supercritical argon are plotted in figure 2.2, and indicate that argon is indeed a simple liquid. Note also that the correlations depend on state point. For the two model liquids in figure 2.2 the correlation coefficient decreases at low temperature where the systems approaches

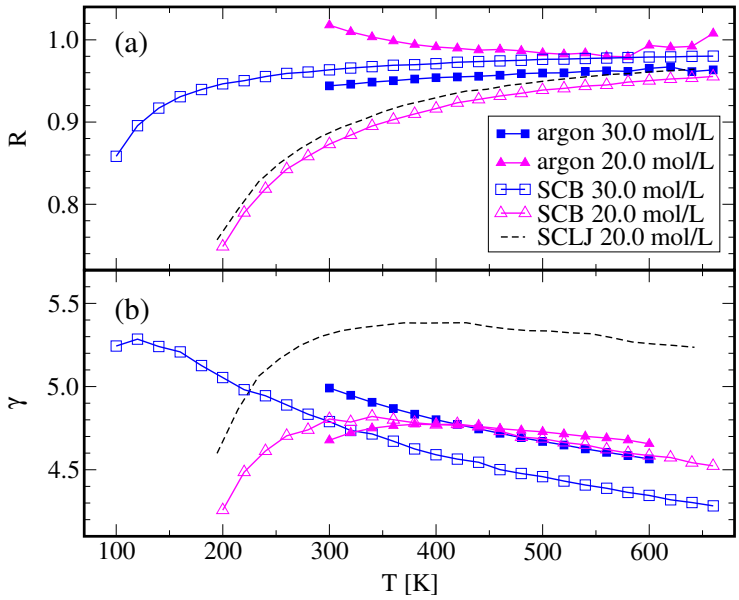

Figure 2.2: The correlation coefficients (a) and γ (b) of the single component Buckingham and Lennard-Jones liquids compared to the estimate for supercritical argon. The estimates for argon were calculated using public data in Pedersen et al. (2008b) and Bailey et al. (2008b), and the potential parameters for argon were taken from Mason and Rice (1954). The data indicate that argon is a simple liquid. Note that the correlation coefficient and γ depend on state point. Taken from Veldhorst et al. (2012).

the coexistence region. With some exceptions, liquids are only simple in part of their phase diagram. Specifically, the simple properties of liquids will disappear upon approaching the critical point.

The correlations of a real liquid have also been estimated by another method for a molecular liquid (Gundermann et al., 2011), which is related to the so-called Prigogine-Defay ratio which is described in section 6.4.

2.2 Isomorphs

2.2.1 Isomorph definition

A microconfiguration in reduced (dimensionless) units $\tilde{\mathbf{R}}$ is obtained by scaling the microconfiguration to density unity:

$$\tilde{\mathbf{R}} = \rho^{1/3}\mathbf{R}\,, \tag{2.6}$$

where R denotes the coordinates of all particles $\mathbf{R} = \{\mathbf{r}_i, \dots \mathbf{r}_N\}$. Two state points ρ_1, T_1 and ρ_2, T_2 are then defined to be isomorphic if microconfigurations $\mathbf{R}_1$ and $\mathbf{R}_2$ at those state points with the same reduced coordinates ($\rho_1^{1/3}\mathbf{R}_1 = \rho_2^{1/3}\mathbf{R}_2$), also have proportional Boltzmann weights (Gnan et al., 2009)

$$\exp\left(-\frac{U(\mathbf{R}_1)}{k_B T_1}\right) = C_{1,2}\exp\left(-\frac{U(\mathbf{R}_2)}{k_B T_2}\right). \tag{2.7}$$

The proportionality should hold for all physically relevant microconfigurations of the two state points with the same constant $C_{1,2}$ which only depends on the state points. An isomorph is then a curve in the phase diagram on which all points are isomorphic to each other.

This definition does not include anything about energy-virial correlations, but it can be shown that only liquids with strong correlation have isomorphs in their phase diagram and vice versa (Gnan et al., 2009).

2.2.2 Predictions from the isomorph theory

Some properties are invariant on an isomorph, but often only in reduced (dimensionless) units, denoted by a tilde. We have already seen (equation 2.6) that dimensionless length can be obtained by scaling with the number density: $\tilde{r} = \rho^{1/3}r$. Likewise other reduced quantities are obtained by scaling with macroscopic properties of the system, for instance for the potential energy U, time t and diffusion coefficient D

$$\tilde{U} = \frac{U}{k_B T}\,, \qquad \tilde{t} = t\rho^{1/3}\sqrt{\frac{k_B T}{m}}\,, \qquad \tilde{D} = D\rho^{1/3}\sqrt{\frac{m}{k_B T}}\,. \tag{2.8}$$

Invariant structure

From equation 2.7 it is obvious that the relative probabilities the microconfigurations have at one state point do not change when scaling them to another state point that is isomorphic. In other words, the normalized probability distribution function of the reduced microconfigurations

$$P(\tilde{\mathbf{R}}) = \frac{\exp(U(\tilde{\mathbf{R}})/k_B T)}{\int \exp(U(\tilde{\mathbf{R}})/k_B T)\,\mathrm{d}\tilde{\mathbf{R}}} \tag{2.9}$$

is invariant on the isomorph. This means that the equilibrium structure is invariant in reduced units, since the configurations are taken from the same probability distribution.

One common structural quantity that is easy to obtain in computer simulations is the radial distribution function $g(r)$, which is the ratio of the local density $\rho(r)$ at a distance r from a particle and the macroscopic density ρ. Since in general particle distribution functions can be rewritten as function of the probability distribution (Hansen and McDonald, 1986), it is invariant on the isomorph in reduced units. The radial distribution function in reduced units $g(\tilde{r})$ has been used extensively in this thesis to test the invariance of the structure.

Invariant thermodynamic properties

Since entropy only depends on the (normalized) probabilities

$$S_{ex} = -k_B \int P(\tilde{\mathbf{R}}) \ln P(\tilde{\mathbf{R}}) \, \mathrm{d}\tilde{\mathbf{R}} \tag{2.10}$$

the excess entropy is an isomorph invariant (Gnan et al., 2009).

Taking the logarithm of equation 2.7 we find

$$\frac{U(\mathbf{R}_1)}{k_B T_1} = \frac{U(\mathbf{R}_2)}{k_B T_2} - \ln(C_{1,2}) \, . \tag{2.11}$$

$U(\mathbf{R}_1)/(k_B T_1)$ is the potential energy in reduced units, so this gives us

$$\tilde{U}(\mathbf{R}_1) = \tilde{U}(\mathbf{R}_2) - \ln(C_{1,2}) \, . \tag{2.12}$$

Since the constant $C_{1,2}$ only depends on the state point, the fluctuations in $\tilde{U}$ as quantified by the variance $\langle(\Delta\tilde{U})^2\rangle$ are the same at two isomorphic state points. Using the fluctuation formula for the excess isochoric specific heat

$$C_{V,ex} = \frac{\langle(\Delta U)^2\rangle}{k_B T^2} = k_B \langle(\Delta\tilde{U})^2\rangle \tag{2.13}$$

is an isomorph invariant (Gnan et al., 2009). This means that for atomic liquids also the total specific heat is constant, since the kinetic contribution is not dependent on state point (there are no rotational contributions).

Invariant dynamics

Equation 2.12 shows that the reduced potential energy of two scaled microconfigurations on an isomorph are the same except for an additive constant. Therefore the reduced force $\tilde{\mathbf{F}} = -\nabla\tilde{U}$ is invariant on the isomorphs, which means that we can write Newton's seconds law in reduced units as $\tilde{m}\ddot{\tilde{\mathbf{r}}} = \tilde{\mathbf{F}}$. This means that the dynamics is invariant as long as it is expressed in reduced time (Gnan et al., 2009). See also Bøhling et al. (2013) for an illustration that identical forces lead to identical dynamics.

This also means that for instance the intermediate scattering function is invariant on the isomorph as long as it is in reduced time and normalized properly (Gnan et al., 2009). The intermediate scattering function is the time correlation function of the spatial Fourier transform of the number density $\rho(q)$ (Allen and Tildesley, 1987), so with the proper normalization

$$F(\tilde{q}, \tilde{t}) = \frac{\langle \rho(\tilde{q}, \tilde{t}) \rho(-\tilde{q}, 0) \rangle}{\langle \rho(\tilde{q}, 0) \rho(-\tilde{q}, 0) \rangle} \tag{2.14}$$

is an isomorph invariant. The mean square reduced displacement $\left\langle [\tilde{\mathbf{r}}(\tilde{t}) - \tilde{\mathbf{r}}(0)]^2 \right\rangle$ is obviously also an invariant.

The fact that both the dynamics and the excess entropy are invariant on the isomorph means that the theory is in agreement with Rosenfeld's excess entropy scaling, according to which the reduced dynamics are a function of excess entropy (Dzugutov, 1996; Rosenfeld, 1999).

2.2.3 Finding isomorphs in a computer simulation

The direct isomorph check

Equation 2.11 can be rewritten to

$$U(\mathbf{R}_2) = \frac{T_2}{T_1} U(\mathbf{R}_1) + k_B T_2 \ln(C_{1,2}) \,, \tag{2.15}$$

which can be used to find isomorphic state points in computer simulations as follows. Doing a standard equilibrium NVT simulation at some density ρ_1 and temperature T_1 it is possible to calculate both potential energies $U(\mathbf{R}_1)$ and $U(\mathbf{R}_2)$ by scaling all configurations to a new density ρ_2 at which you want to find the isomorphic state point

$$\mathbf{R}_2 = \frac{\rho_1^{1/3}}{\rho_2^{1/3}} \mathbf{R}_1 \,, \tag{2.16}$$

keeping the configurations the same in reduced units. According to equation 2.15, the energies calculated should be linear proportional to each other with proportionality constant T_2/T_1. So the temperature T_2 for which the state point at density ρ_2 is isomorphic to state point 1 can be found from the slope in an $U(\mathbf{R}_1)$, $U(\mathbf{R}_2)$ plot.

In practice, it turns out that it is necessary for some liquids to take the density change $|\rho_2 - \rho_1|$ not too big, since the isomorph theory is approximate. Because the reduced structure of the liquid may not be completely invariant, equation 2.6 is not always rigorously obeyed, and $U(\mathbf{R}_1)$ and $U(\mathbf{R}_2)$ are then not perfectly correlating (see for an example figure 5.7 in chapter 5).

The direct isomorph check has been used in chapters 3 and 4 of this thesis.

Curves of constant excess entropy

It is also possible to find an isomorph by using the property that excess entropy is constant on an isomorph

$$\mathrm{d}S_{ex} = \left(\frac{\partial S_{ex}}{\partial V} \right)_T \mathrm{d}V + \left(\frac{\partial S_{ex}}{\partial T} \right)_V \mathrm{d}T = 0 \,. \tag{2.17}$$

That means that on an isomorph we have can rewrite this (using one of Maxwell's relations and with W/V the configurational part of the pressure) to

$$\left(\frac{\partial (W/V)}{\partial T} \right)_V \mathrm{d}V = \left(\frac{\partial (U/T)}{\partial T} \right)_V \mathrm{d}T \tag{2.18}$$

which can be rewritten to (Gnan et al., 2009)

$$\left(\frac{\mathrm{d}\ln T}{\mathrm{d}\ln \rho}\right)_{S_{ex}} = \left(\frac{\partial W}{\partial U}\right)_V = \frac{\langle \Delta W \Delta U\rangle}{\langle (\Delta U)^2\rangle} = \gamma\,. \tag{2.19}$$

So it is possible to find an isomorphic state point by calculating γ form the fluctuations, and then calculating how temperature changes for a small density change or vice versa. For many systems the change in state point has to small, because γ changes on the isomorph (see figure 2.2).

This method of generating state points that are isomorphic has been used in chapter 5.

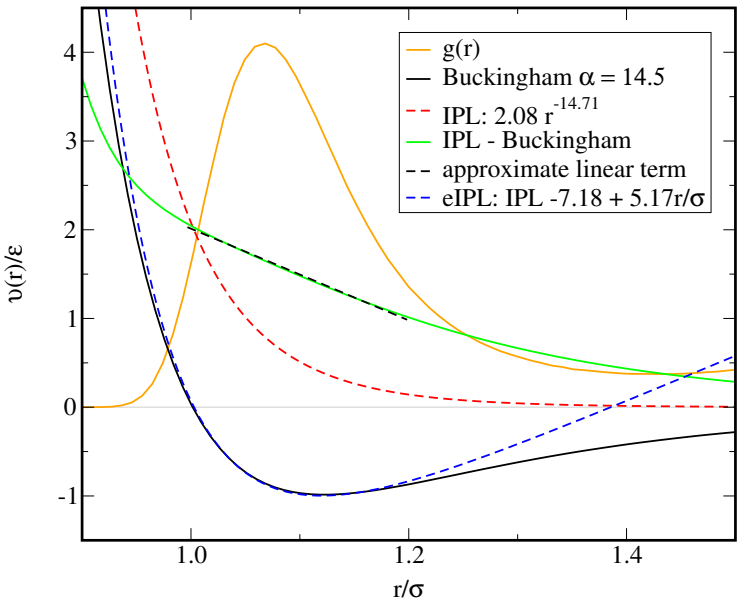

Figure 2.3: The effective IPL approximation (red dashed line) of the Buckingham potential (black line). In Paper I is described how the parameters of the IPL potential were found. The difference between the IPL potential and the Buckingham potential is approximately linear in the first peak of $g(r)$. The eIPL (blue dashed line) is indeed a good approximation of the Buckingham potential. Taken from Paper I.

2.3 Relation to the IPL potentials

In general, the isomorph theory is an approximate theory. However, there is a group of liquids for which the isomorph theory is exact. These are the inverse power law (IPL) systems where the interatomic pair potential is given by $v(r) = r^{-n}$. For an IPL $v(r) = rv'(r)$, which means that from equation 2.3

$$W = -\frac{1}{3}\sum_{i<j} r_{ij}v'(r_{ij}) = \frac{n}{3}\sum_{i<j} v(r_{ij}) = \frac{n}{3}U\,. \tag{2.20}$$

This means that for an IPL potential, the virial and potential energy are perfectly correlated with $\gamma = n/3$.

Moreover, an IPL liquid obeys the isomorph definition (equation 2.7) perfectly for $\rho_1^{n/3}/T_1 = \rho_2^{n/3}/T_2$ with proportionality constant $C_{1,2} = 1$, so the IPL liquid has perfect isomorphs described by curves of constant ρ^γ/T.

Why do non-IPL potentials like the Lennard-Jones and the Buckingham potential also have strong correlations? It has been shown that the fluctuations in U and W mostly depend on contributions from nearest neighbor pairs, and that in this range some attractive potentials are well fitted by an IPL with an extra linear term Bailey et al. (2008b); Veldhorst et al. (2012)

$$v(r) = Ar^{-n} + Br + C \tag{2.21}$$

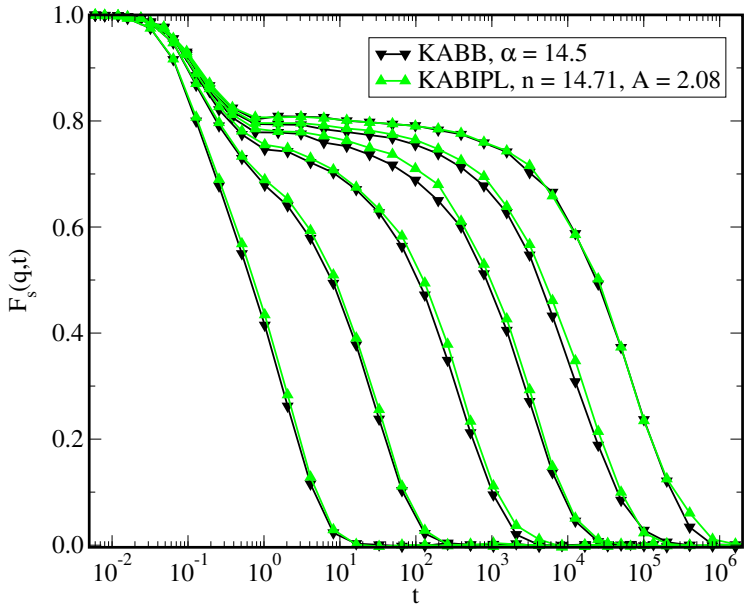

Figure 2.4: The dynamics in the form of the intermediate scattering function for the (binary) Buckingham liquid and the IPL approximation at the standard density $\rho = 1.2$. The temperatures shown are $T = \{0.42, 0.44, 0.46, 0.50, 0.6, 1.0\}$, and the scattering vector is $q = 7.225$. Taken from Paper I.

called the extended IPL (eIPL). In figure 2.3 this is illustrated for the Buckingham potential. The difference between the Buckingham potential and the IPL fit is indeed approximately linear in the first peak of $g(r)$. Since the liquid is dense, all particles are surrounded by a coordination shell of other particles. Because of this, the linear term does not affect the fluctuations in the energy, because making one pair distance longer will have the effect of making another pair distance shorter by approximately the same amount (Bailey et al., 2008b).

It has indeed been shown that the properties of the Lennard-Jones (Pedersen et al., 2010) and the Buckingham (Paper I) potential can be reproduced with an IPL potential. Figure 2.4 shows the dynamics at different temperatures on an isochore for the Buckingham liquid and a IPL approximation. The dynamics are indeed identical over a large range of temperatures. Thus the strong correlations and the isomorphs are not an effect of the potential that can be written as a sum of IPLs, but holds for any potential that may be fitted by an extended IPL to some degree.

The effective IPL also gives a good prediction for specific heat of the Buckingham liquid, as can be seen in figure 2.5. The IPL approximation has has the same temperature dependence of $C_{V,ex}$ as the Buckingham liquid, but there is a slight difference in the absolute value. Moreover, the right side of figure 2.5 shows that C_V at different densities can be scaled using ρ^γ/T to collapse on a single master curve. This confirms that power law density indeed works for small density changes.

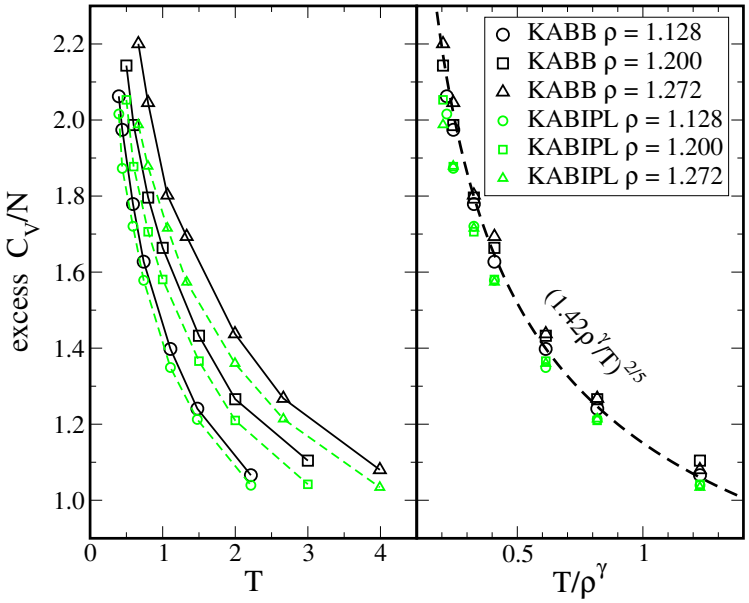

Figure 2.5: The excess isochoric heat capacity per particle $C_{V,ex}/N$ as a function of temperature (a) on three isochores for the binary Buckingham liquid (black data) and the IPL approximation (green data). In (b), the same data are plotted as function of T/ρ^γ. A function of the form $(1.42\rho^\gamma/T)^{2/5}$ as predicted by Rosenfeld and Tarazona (1998) (dashed line, see section 2.5) fits the data well. Taken from Paper I.

2.4 The shape of isomorphs

The excess isochoric heat capacity and the excess entropy are both predicted to be constant on an isomorph. This means that for a simple liquid the specific heat can be written as a function of the excess entropy

$$C_{V,ex} = f(S_{ex})\,. \tag{2.22}$$

Using that $C_{V,ex} = (\partial S_{ex}/\partial \ln T)_V$ and integrating at constant volume, it has been found that the temperature of a simple liquid is a product of a function of excess entropy and a function of density (Ingebrigtsen et al., 2012)

$$T = g(s_{ex})h(\rho)\,, \tag{2.23}$$

where $s_{ex} = S_{ex}/N$ is the excess entropy per particle. Note that from equation 2.19 and 2.23 we find that

$$\gamma(\rho) = \frac{\mathrm{d}\ln h(\rho)}{\mathrm{d}\ln \rho}\,. \tag{2.24}$$

On an isomorph s_{ex} is constant, so an isomorph is defined by

$$\frac{h(\rho)}{T} = \text{constant}. \tag{2.25}$$

This is exactly the scaling function that was proposed in the earlier days of density scaling (Alba-Simionesco et al., 2002, 2004; Tarjus et al., 2004a) as described in section 1.1.3.

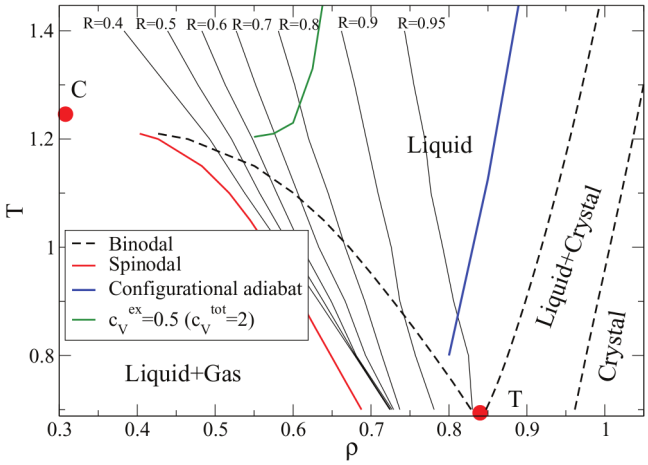

Figure 2.6: The Lennard-Jones phase diagram showing an isomorph (blue line). Also the melting and freezing lines are isomorphs. Taken from Paper IV.

For an IPL potential, the excess entropy is a function of $\rho^{n/3}/T$, so we find $h(\rho) = \rho^{n/3}$. Also for potentials that have a potential energy which can be written as a sum of power laws

$$v(r) = \sum_n v_n r^{-n} \tag{2.26}$$

an analytical expression for $h(\rho)$ has been found. For these potentials, it turns out that $h(\rho)$ is a some of power laws as well, with each term corresponding to a term in the potential (Bøhling et al., 2012; Ingebrigtsen et al., 2012).

$$h(\rho) = \sum_n C_n \rho^{n/3} \,. \tag{2.27}$$

For the Lennard Jones potential this gives $h(\rho) = A\rho^4 - B\rho^2$, where only the ratio between the constant A and B is relevant and can be determined by a single simulation (Bøhling et al., 2012; Ingebrigtsen et al., 2012).

Figure 2.6 shows the shape of three isomorphs for the Lennard-Jones liquid. The liquid isomorph (blue line) is parallel to the melting line, which is also an isomorph (Gnan et al., 2009). This is easily understood be considering the opposite case of an isomorph crossing the melting line. In that case structure would not be invariant on the isomorph. The figure also shows curves of constant correlation coefficient, showing that the liquid loses its simple behavior upon approaching the critical point.

2.5 Rosenfeld-Tarazona

As mentioned before, the isomorph theory is in agreement with Rosenfeld's excess entropy scaling (Dzugutov, 1996; Rosenfeld, 1999). This scaling expresses the relaxation time or another dynamical measure as a function of excess entropy. However, this kind of method cannot predict any state point dependence of thermodynamic quantities.

A prediction of the state point dependence of the potential energy and the specific heat was given by Rosenfeld and Tarazona (1998), using perturbation theory on a hard sphere equation of state they find that

$$U(\rho, T) = \alpha(\rho)T^{3/5} + \beta(\rho)\,, \tag{2.28}$$

$$C_{V,ex}(\rho, T) = \frac{3}{5}\alpha(\rho)T^{-2/5}\,. \tag{2.29}$$

An equation of the second form was fitted to the data in figure 2.5, showing that the Buckingham liquid indeed follows the prediction from Rosenfeld and Tarazona. It has been shown that also the Lennard-Jones and the IPL liquids follow the scaling, which led the the hypothesis that Rosenfeld-Tarazona prediction works well for simple liquids.

This was tested systematically in Paper III for a large group of model liquids including some which have been simulated in thesis. It was found that the Rosenfeld-Tarazona expression indeed describes the behavior of simple liquids better then non-simple liquids.

Chapter 3

Isomorphs in plasmas and colloidal suspensions

3.1 Screened coulomb interactions: The Yukawa potential

The Yukawa potential is named after the physicist Hideki Yukawa, who predicted the existence of the subatomic meson particle (Yukawa, 1935), describing the interaction of two particles in the nucleus by the potential

$$v = -g^2 \frac{e^{-\lambda r}}{r} \,. \tag{3.1}$$

This is the same function as the screened Coulomb potential that is used to describe the electric potential around a charge that is screened by mobile charge carriers in the surrounding medium (see, e.g., Atkins and de Paula (2010))

$$v(r) = \frac{Q^2}{4\pi\epsilon_0} \frac{e^{-k_D r}}{r} \,, \tag{3.2}$$

where Q is the charge, ϵ_0 is the permittivity of the medium and k_D^{-1} is the Debye screening length. The potential was first used by Debye and Hükel (1923) in their theory of electrolyte solutions. For infinite screening length, this potential is simply the Coulomb potential. The screening is caused by the fact that the central charge will attract charge carriers of the opposite charge from the surrounding medium. At longer distances, the potential that is felt will be reduced due to the effect of the accumulated opposite charge carriers.

Although the theory was not able to describe the behavior of anything but the most dilute ionic solutions, the Yukawa potential has still proven itself useful in the description of the potential energy of charge carriers that are much larger than the charge carriers in the surrounding medium. One example is for instance a suspension of charge-stabilized colloids. DLVO theory (Derjaguin and Landau, 1941; Verwey and Overbeek, 1948) says that the interaction energy between two

charged colloids with diameter r_0 is given by

$$\upsilon(r) = \frac{Q^2}{4\pi\epsilon_0(1 + k_D r_0/2)^2} \frac{e^{-k_D(r-r_0)}}{r}\,, \tag{3.3}$$

which has the same functional form as the Yukawa potential. It has been shown that the Yukawa potential of the form in equation 3.2 is actually able to describe the behavior of colloidal suspensions, albeit with a renormalized charge (Alexander et al., 1984). Moreover, if a hard-core repulsion is included in the potential to account for the volume of the colloids, Hynninen and Dijkstra (2003) have shown that the phase diagram of this hard-core Yukawa potential and the point Yukawa potential can be mapped onto each other as long as the temperature relative to the magnitude of the potential is low enough so the hard core is not felt.

It should be noted that depending on the charge of the particles, the Yukawa potential can also be attractive. This is for instance the case in binary suspensions of colloids. In this case, a repulsion needs to be included to prevent the particles from overlapping. This can for instance be done using a hard-core repulsion, but this complicates the simulation when using Molecular Dynamics. González-Melchor et al. (2004, 2012) instead used an steep inverse power law to model the short range repulsion.

Another application of the Yukawa potential is in the field of plasmas. Although ion interactions are not correctly described by the Yukawa potential (Gurnett and Bhattacharjee, 2005), the interaction of charged dust particles screened by the ions of the surrounding plasma can be approximated by a screened Coulomb potential (Fortov et al., 2005; Rowlinson, 1989; Whipple et al., 1985).

Because the Yukawa potential has such wide ranging applications in physics, different parameters have been used to describe the potential and the phase diagram. In the field of dusty plasmas, the phase diagram is often described in terms of the screening parameter κ and the coupling parameter Γ (Vaulina and Khrapak, 2000):

$$\kappa = a k_D\,, \qquad \Gamma = \frac{Q^2}{4\pi\epsilon_0 a T} \tag{3.4}$$

where a is a measure of the interparticle distance, for instance $a = \rho^{-1/3}$, although in earlier studies it was more common to use the Wigner-Seitz radius $a_{WS} = (4\pi\rho/3)^{-1/3}$ (Farouki and Hamaguchi, 1994; Ohta and Hamaguchi, 2000). The screening parameter is thus the ratio between the Debye screening length and the interparticle distance, while the coupling parameter is approximately the ratio between the potential energy and the kinetic energy.

Here, we mostly present our results in terms of density and temperature with σ and ε the usual units of length and energy set to unity:

$$\upsilon(r) = \frac{\varepsilon \exp\left(-\frac{r}{\sigma}\right)}{r/\sigma} = \frac{\exp\left(-r\right)}{r}\,. \tag{3.5}$$

The relation with the other parameters is thus

$$\kappa = \frac{1}{\sigma\rho^{1/3}}\,, \qquad \Gamma = \frac{\varepsilon\sigma\rho^{1/3}}{T}\,. \tag{3.6}$$

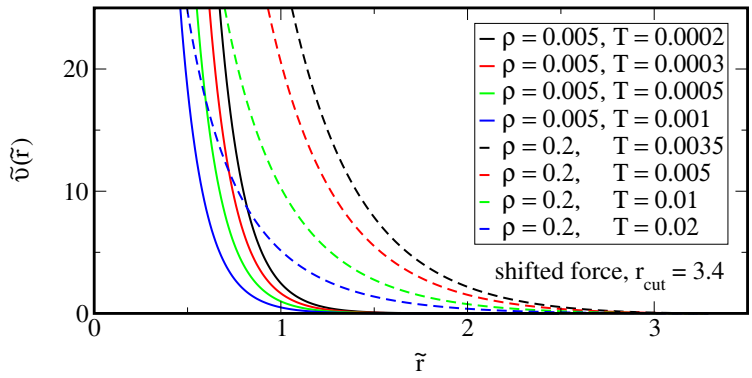

Figure 3.1: The Yukawa potential in reduced units $\tilde{v}(\tilde{r}) = v(\rho^{1/3}r)/T$ for several temperatures at the isochores $\rho = 0.005$ and $\rho = 0.2$. For the high densities, the potential clearly starts to become long-ranged, and the cutoff radius has to be increased to account for this.

The Yukawa potential is of special interest to us, since it has a phase diagram that spans a much larger density and temperature range (Hamaguchi et al., 1997; Meijer and Frenkel, 1991; Robbins et al., 1988) than of the systems that have been shown to obey the isomorph theory so far (Gnan et al., 2009; Ingebrigtsen et al., 2012). Moreover, the "softness" of the potential changes more than any other potential in this range (Khrapak et al., 2012).

Moreover the Yukawa fluid has been shown to obey Rosenfeld's excess entropy scaling (Rosenfeld, 2000; Sanbonmatsu and Murillo, 2001) and Rosenfeld-Tarazona scaling (Rosenfeld, 2001; Rosenfeld and Tarazona, 1998), both of which indicate that the liquid is a simple liquid.

3.2 Simulation procedure

If the screening parameter κ is zero, the potential reduces to the standard Coulomb potential, also called the one-component plasma (OCP). Although we do not simulate the Coulomb potential, the potential already becomes long ranged at densities that would be considered standard for a Lennard-Jones liquid, as shown in figure 3.1. In general, correction algorithms are used when simulating long ranged potentials, e.g., Ewald summation or particle mesh methods. The reason for this is that the error estimate of the energy due to the cutoff

$$U \approx \frac{1}{2} N \rho \int_{r_{cut}}^{\infty} 4\pi r^2 v(r)\, \mathrm{d}r \tag{3.7}$$

diverges for functions that decay slower than r^{-3} (Frenkel and Smit, 2002). Here, we have not used any correction algorithms, using a large cutoff radius and system size, depending on the screening of neighbors to reduce the effect of the long range interaction.

We found the U,W fluctuations to be the most sensitive indicator of a cutoff radius that is too small. This in contrast to for instance the mean square displacement or the radial distribution function. The Yukawa fluid was found to be very

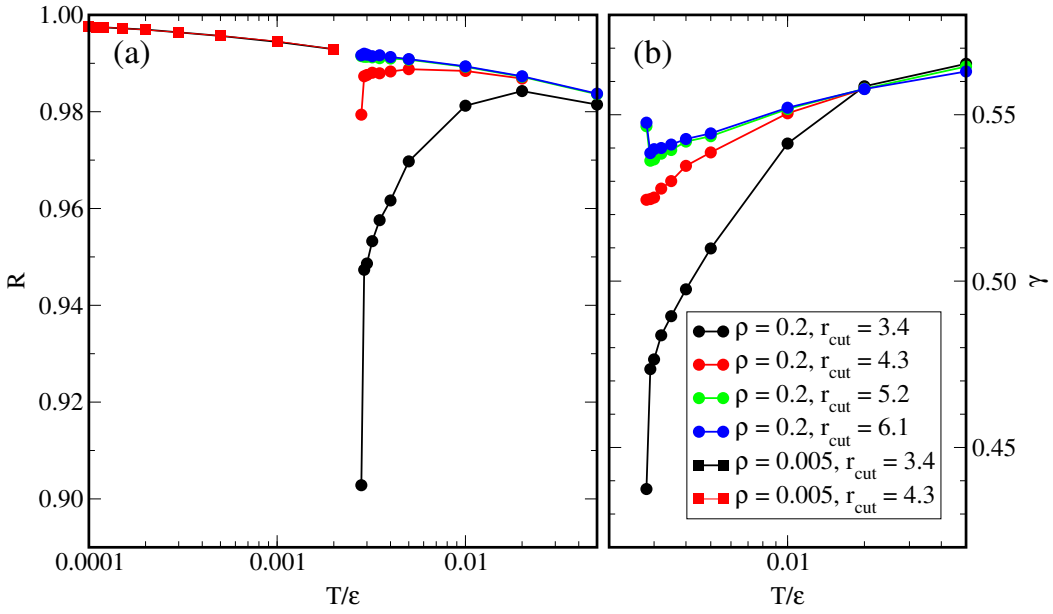

Figure 3.2: The correlation coefficient (a) on two isochores ($\rho = 0.005$ and $\rho = 0.2$) simulated with different cutoff radii r_{cut}. At the low density, the cutoff radius does not affect the correlations, but at the high density, the correlation coefficient only becomes independent of the cutoff radius for $\tilde{r}_{cut} \geqslant 5.2$. As long as the cutoff radius is large enough, the correlation coefficient only seems to depend on temperature. (b) The cutoff radius also affect γ at high density.

strongly correlating at all simulated state points ($R > 0.98$). However, for high density state points, a significant drop in the correlation coefficient was found when simulation with a short cutoff radius. This is visualized in figure 3.2, where we plot the correlation coefficient and γ for a high and a low density isochore. We used a minimum cutoff length $\tilde{r}_{cut} = 3.4$ after the third coordination shell, even for the lowest densities. This is clearly large enough for the isochore $\rho = 0.005$, where increasing the cutoff does not increase the correlation coefficient. For the $\rho = 0.2$ isochore however, both R and γ are dependent on the cutoff ratio up to $\tilde{r}_{cut} = 5.2$.

In our simulations, we have therefore let the reduced cutoff radius $\tilde{r}_{cut}$ depend on density. Likewise, because the steepness of the potential in reduced units increases with lower densities, we have decreased the time step of the simulations at lower densities. The exact details of the simulations are shown in table 3.1. The simulations were performed in the NVT ensemble using a Nosé-Hoover thermostat with the same reduced time constant.

3.3 Predicting the isomorph from the potential

For an inverse power law potential (IPL) with r^{-n}, the density scaling exponent is known: $\gamma = n/3$. For non-IPL potentials it has been shown that it is possible to estimate an approximate IPL exponent n from the potential (instead of calculating γ from the fluctuations). This is done by looking at ratios of consecutive derivatives

	N	$\tilde{r}_{cut}$	$\Delta\tilde{t}$	$\tilde{t}$
$\rho < 0.01$	2048	4.3	0.0010	$3.36 \cdot 10^4$
$0.01 \leqslant \rho < 0.5$	2048	5.2	0.0025	$2.10 \cdot 10^4$
$0.5 \leqslant \rho$	8192	10.0	0.0025	$2.10 \cdot 10^4$

Table 3.1: Simulation details for the Yukawa potential. Depending on the density the number of particles in the system N was changed to allow for a larger reduced cutoff radius $\tilde{r}_{cut}$. The reduced time step $\Delta\tilde{t}$ was somewhat reduced for the lowest densities. The minimum simulation time $\tilde{t}$ in reduced units was the same as the equilibration time.

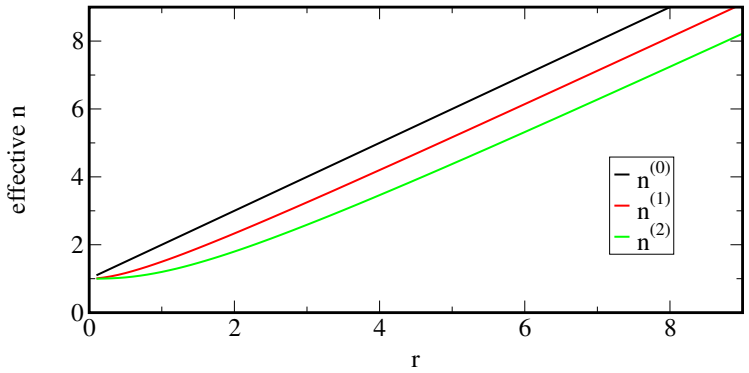

Figure 3.3: Estimates of the effective IPL exponent $n^{(p)}$ for the Yukawa potential using equation 3.8.

of the potential (Bailey et al., 2008b):

$$n^{(p)} \equiv -r\frac{v^{(p+1)}(r)}{v^{(p)}(r)} - p\,, \tag{3.8}$$

where p denotes the pth derivative. For an IPL potential, $n^{(p)}$ is constant and gives the correct exponent for every p. For other potentials, $n^{(p)}(r)$ is dependent on both distance and p. It was found that $p = 2$ gives a good approximation of the IPL exponent at more or less the interparticle distance (Bailey et al., 2008b). Another reason for choosing $p = 2$ is that it gives the correct exponent for an extended IPL (eIPL) that consists of an IPL and a linear term (see figure 2.3).

Figure 3.3 shows the approximations of the effective IPL exponent for $p = \{0, 1, 2\}$. At short distances (which correspond to high densities) we can see that all three predict $n = 1$. This is in agreement with the fact that the potential reduces to the Coulomb potential for infinite screening lengths ($\kappa = 0$). At higher densities, the estimates depend on p. As said, we consider $n^{(2)}$ the most valuable. For the Yukawa potential we find

$$n^{(2)} = -r\frac{v'''(r)}{v''(r)} - 2 = 1 + \frac{r^3}{2 + 2r + r^2}\,. \tag{3.9}$$

From this it is possible to get an estimate of $\gamma = n^{(2)}/3$, if we know at what distance to evaluate this equation. We now that the relevant distance is approximately the

nearest neighbor distance, which scales with $\rho^{-1/3}$ (Bailey et al., 2008b; Ingebrigsten et al., 2012b). Assuming that the relevant reduced nearest neighbor distance Λ is constant on the isomorph, the relevant distance in normal units is $r = \Lambda\rho^{-1/3}$. Substituting this in equation 3.9, we find

$$\gamma(\rho) = \frac{1}{3} + \frac{\Lambda^3}{3\Lambda^2\rho^{1/3} + 6\Lambda\rho^{2/3} + 6\rho} \,. \tag{3.10}$$

For $\rho = 0.2$ and $\Lambda \approx 1$, we find $\gamma \approx 0.53$, which is in agreement with the data in figure 3.2.

Using equation 2.24, we find for the shape of the isomorph

$$h(\rho) = T_0 e^{-\Lambda\rho^{-1/3}} \left[2\rho^{1/3} + 2\Lambda + \Lambda^2\rho^{-1/3}\right] . \tag{3.11}$$

If we express this in the more usual Yukawa parameters, this becomes

$$\Gamma = \frac{1}{c}\frac{e^{\Lambda\kappa}}{2 + 2\Lambda\kappa + \Lambda^2\kappa^2} \,. \tag{3.12}$$

Vaulina and Khrapak (2000) found that a curve of this shape with $\Lambda = 1$ gives a good description of the melting line as found by (Hamaguchi et al., 1997). They derived the equation using Lindemann's melting rule (Gilvarry, 1956), which is in agreement with the isomorph theory (Gnan et al., 2009).

3.4 Testing the predicted isomorph shape

In this section, we test if our $h(\rho)$ indeed gives a good estimate of an isomorph. For this, we of course need to know Λ. Because Vaulina and Khrapak (2000) found equation 3.11 with $\Lambda = 1$ to be a good description of the melting line, and the melting line is predicted to be an isomorph, we of course test if $\Lambda = 1$ is the right value.

We have also tried to calculate the correct value of Λ. For this, we did a simulation at an initial state point ($\rho = 5 \cdot 10^{-3}$ and $T = 1.5 \cdot 10^{-4}$). At this state point γ was found from the fluctuations to be 1.78 using equation 2.5 and therefore $\Lambda = 1.03$ following equation 3.10 (Paper IV).

We check the invariance of the dynamics for both values of Λ in figure 3.4. For $\Lambda = 1$, the dynamics seem to be reasonably invariant on the isomorph. Although the collapse may seem not very good, taking the large density range into considering still makes to collapse quite astonishing. Surprisingly, The dynamics are less invariant for $\Lambda = 1.03$.

In figure 3.5 the radial distribution functions are plotted for both isomorphs. The structure changes a lot on the isomorph, which is to be expected for such a big density change. The steepness of the reduced potential changes a lot (see the plot of γ versus ρ in figure 3.9). Because of this, the steepness of the left slope of the first peak of $g(\tilde{r})$ should also be dependent on density.

The position of the first peak also changes along the isomorph. Since we assumed the relevant reduced interparticle distance Λ to be constant on an isomorph in our derivation of $h(\rho)$, this change in peak position might be the reason for the bad collapse of the dynamics in figure 3.4(b).

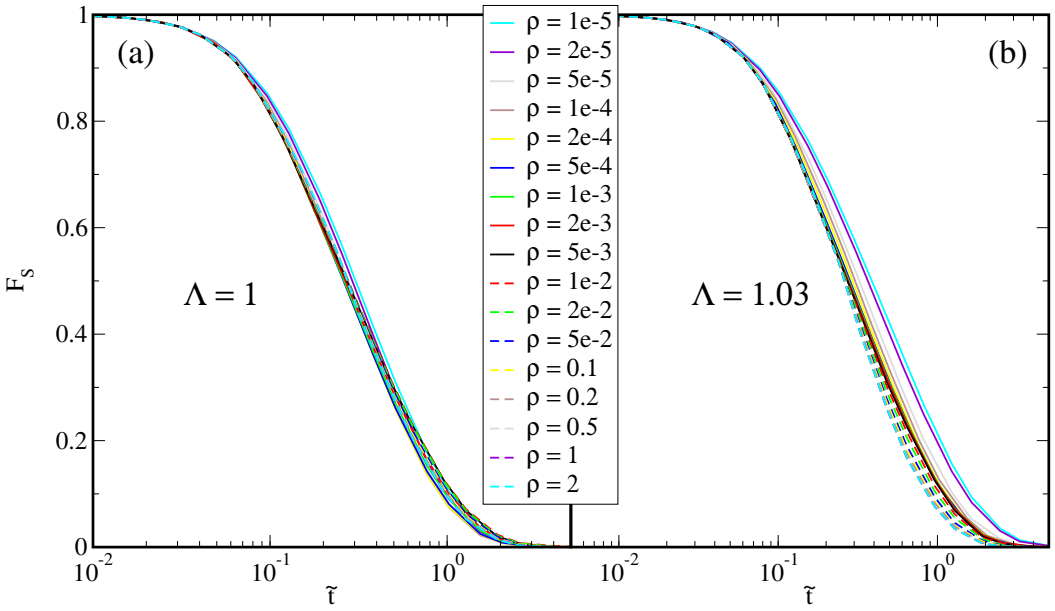

Figure 3.4: The incoherent intermediate scattering function on a curve described by $h(\rho)$ (equation 3.11) for $\Lambda = 1$ (a) and $\Lambda = 1.03$ (b). Both sets of state points contain the point $\rho = 5 \cdot 10^{-3}$, $T = 1.5 \cdot 10^{-4}$. The points lie on the curve $T = T_0 h(\rho)$ with $T_0 = 0.1167$ for $\Lambda = 1$ and $T_0 = 0.01314$ for $\Lambda = 1.03$. We kept the scattering vector constant in reduced units ($\tilde{q} = 7$), close to the first peak of of the structure factor.

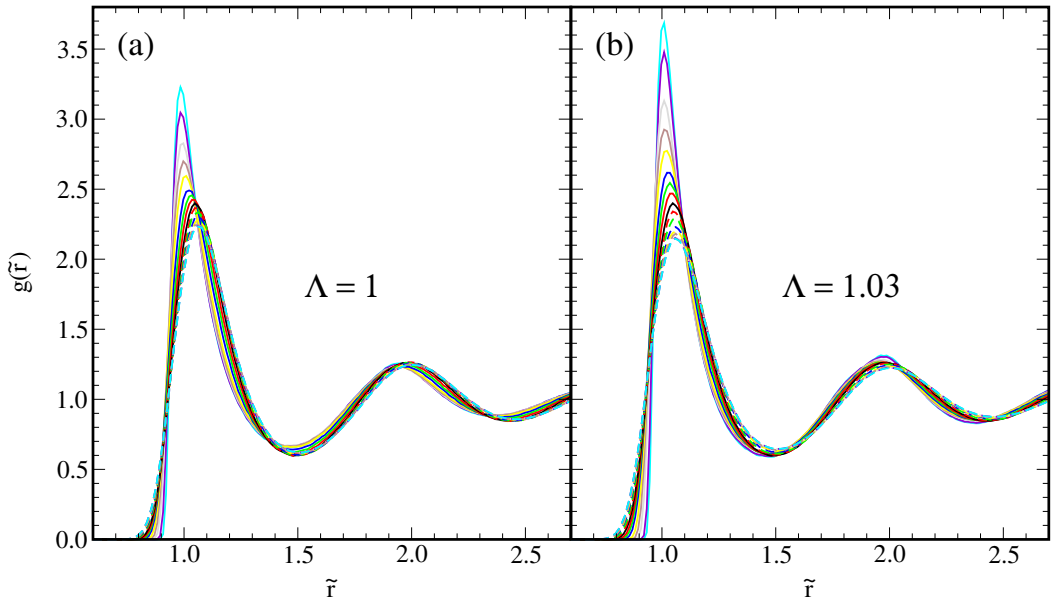

Figure 3.5: The radial distribution functions for state points on $h(\rho)$ (equation 3.11) for two values of Λ. The points lie on the curve $T = T_0 h(\rho)$ with $T_0 = 0.1167$ for $\Lambda = 1$ and $T_0 = 0.01314$ for $\Lambda = 1.03$. See figure 3.4 for the legend.

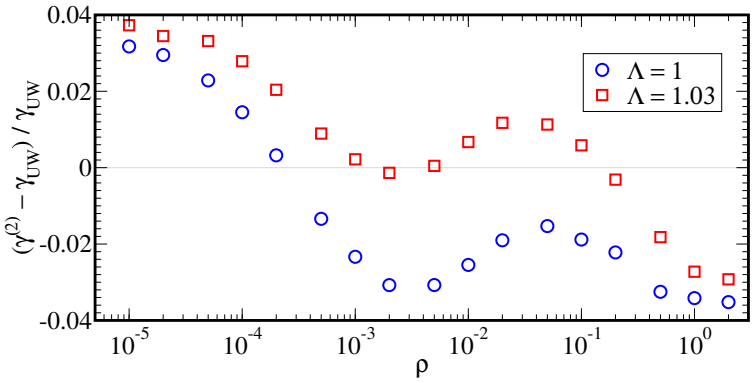

Figure 3.6: The error between the prediction of γ (equation 3.10) and the γ calculated from the fluctuations. Note that the similarity in the errors may be deceiving, since we do not compare two predictions to a single reference γ_{UW}. γ_{UW} is not the same for the two data sets, indicating that γ also depends on temperature.

Bøhling et al. (2014) have also used $n^{(2)}$ to approximate $h(\rho)$ for different potentials consisting of IPLs, including the Lennard-Jones potential. They were able to get good approximations of $h(\rho)$ with a different Λ. Instead of $g(\tilde{r})$, they used the first peak in $\tilde{r}^2 g(\tilde{r})$, which is the most probable distance to find a nearest neighbor. However, also the position of this peak changes a lot in our case; we see a shift of approximately 10% on the isomorph (data not shown). Nevertheless it is surprising that $\Lambda = 1$ gives such a good approximation of $h(\rho)$, since $\Lambda = 1.03$ is closer to the average peak position on the isomorph.

It should be noted that Bøhling et al. (2014) did not find perfect collapse of the calculated and the predicted values of γ. Since we studied a much wider density range, the invariance of the dynamics that we find is not trivial. We plot the relative difference between the prediction (equation 3.10) and the calculated γ (equation 2.5) in figure 3.6. Both predictions are off by no more than four percent, and the prediction with $\Lambda = 1.03$ seems better for most densities. At low densities where the dynamics do not collapse, we find that the error is largest.

3.5 The numerical direct isomorph check

For comparison, we have also constructed an isomorph using more the tested method of the numerical direct isomorph check. We started the isomorph at $\rho = 10^{-3}$ and $T = 3 \cdot 10^{-6}$, changing the density no more than 10% for the next state points. The new temperature was then found from the energies of scaled configurations using equation 2.15. The 10% density change is rather high compared to what is commonly done for other systems see for instance (Gnan et al., 2009). This was done in order to get an isomorph that spans a significant part of the Yukawa phase diagram in a reasonable amount of time. Due to the density dependence of the structure that we found (figure 3.5) simple scaling of the equilibrium configurations at one density may not give the correct energy for the next state point. The variance in the structure in figure 3.5 was however found for density changes much larger

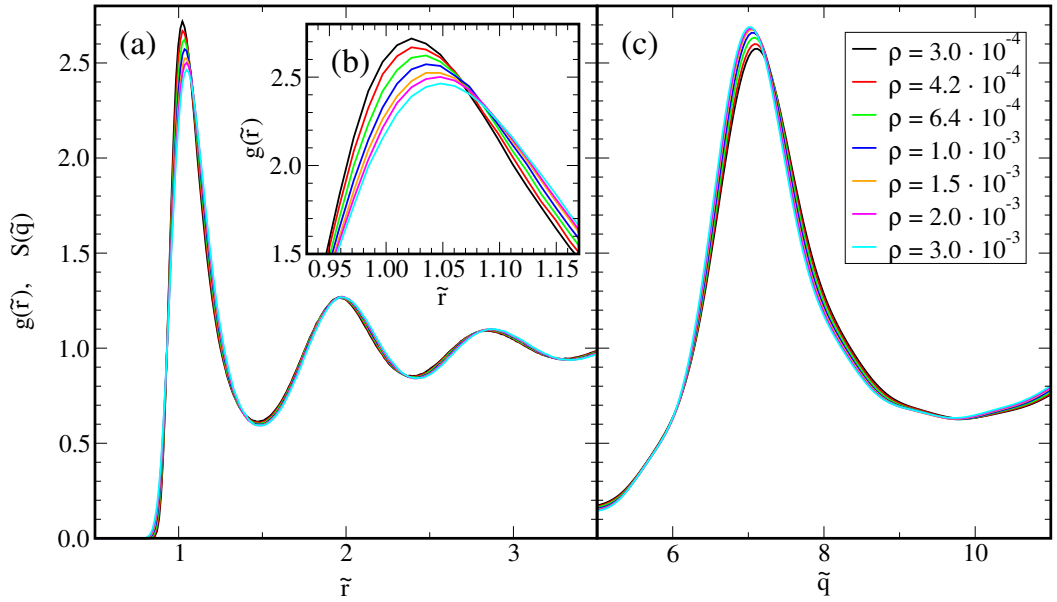

Figure 3.7: The radial distribution function $g(\tilde{r}$ and the static structure factor $S(\tilde{q})$ on the isomorph obtained with the direct isomorph check. Although the change in density is large, the structure does not change significantly in this part of the phase diagram.

than 10%, so the size of the density steps is probably acceptable.

Using the direct isomorph check, we obtained an isomorph spanning a considerable density range ($3.0 \cdot 10^{-4} \leqslant \rho \leqslant 3.6 \cdot 10^{-3}$). The structure for a set of state points on the isomorph is plotted in figure 3.7. Because this density range is much smaller than for the isomorphs from the previous section, we do not see a big change in structure, both for the radial distribution function and the structure factor. This indicates that the 10% steps in density are small enough.

The reduced dynamics also show a perfect collapse for this set of state points (figure 3.8). The collapse is better than for the isomorphs from the previous section, but this is not surprising considering the smaller density range.

3.6 Discussion and conclusion

We have found that the Yukawa fluid is strongly correlating at all investigated densities, with a correlation coefficient above 0.98 (see figure 3.9 and 3.2). This is not surprising for the high density state points, since we know that here the potential becomes the standard Coulomb potential, which should have perfect correlations because it is an IPL. The very high correlations at low densities indicate the the exponential function is also very strongly correlating, because here it is the dominating term in the potential. This in itself is an interesting result, since it has been suggested that exponential potentials provide a simpler basis set of functions than the IPL potentials, and may explain quasiuniversal properties of many different simple liquids (Dyre, 2013). At intermediate densities there is a minimum in the correlation coefficient. This may be due to the change in the liquid structure or a

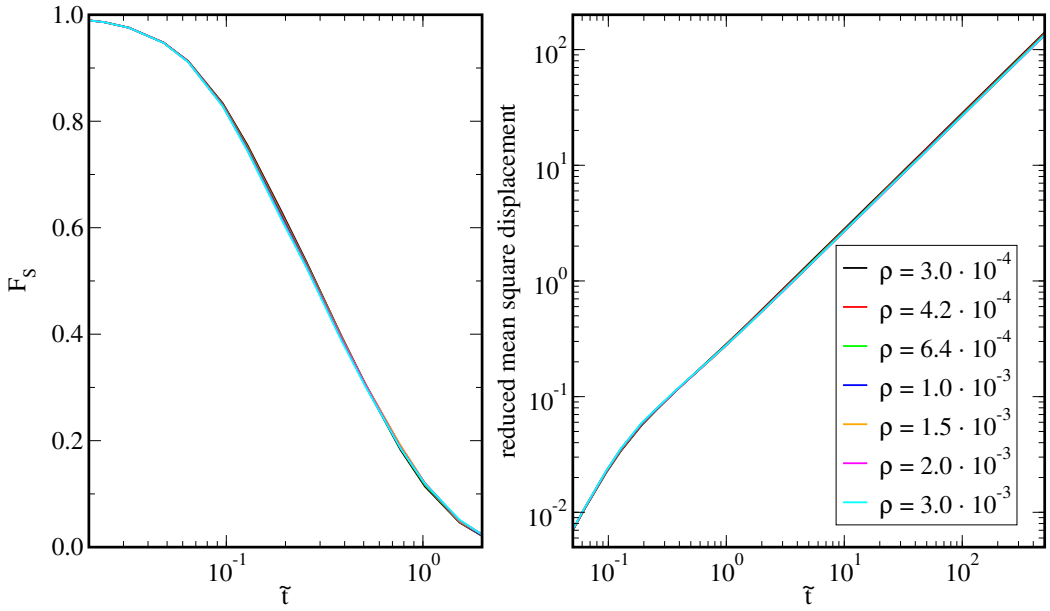

Figure 3.8: The incoherent intermediate scattering function $F_S(q, \tilde{t})$ and the mean square displacement on the isomorph from the direct isomorph check. We kept the scattering vector constant in reduced units $\tilde{q} = 7.042$. The dynamics collapse perfectly for this set of state points.

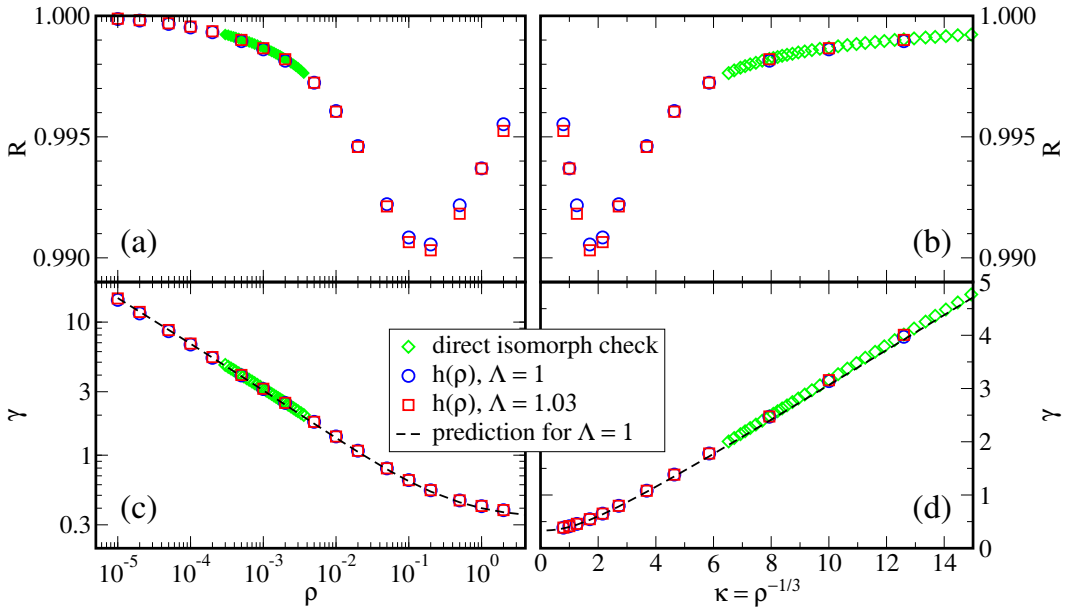

Figure 3.9: The correlation coefficient (top) and γ calculated from the fluctuations (bottom) plotted versus density (left) and screening parameter (right). The yukawa fluid is strongly correlating at all simulated densities. We find that γ changes a lot on the isomorph, from 15.1 at the lowest density to 0.387 at the highest density.

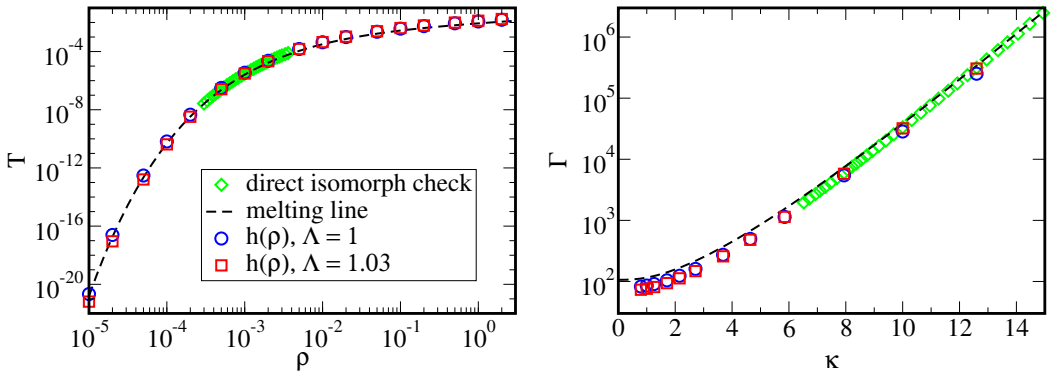

Figure 3.10: Shape of the three isomorphs from the previous sections in the ρ, T (a) and the κ, Γ plane (b). In the κ, Γ plane the difference between the two predicted versions of $h(\rho)$ is visible. The dashed line is the melting line as predicted by Vaulina and Khrapak (2000).

crossover between the the IPL and the exponential potential.

Although the Yukawa potential is purely repulsive, the system has a triple point because it has two stable solid phases. The triple point of the Yukawa system has been found to be at $\rho = 3 \cdot 10^{-3}$ ($\kappa = 6.9$) (Hamaguchi et al., 1997). We find a γ value around 2 here, which is in agreement with data from Agrawal and Kofke (1995) who showed that for IPL potentials with an exponent $n < 6.25$ that BCC is the more stable solid phase. Moreover $\rho = 3 \cdot 10^{-3}$ is also the density range where the largest change in peak position is observed in the radial distribution function (figure 3.5), indicating that this change is caused by a crossover from short to long-ranged interactions.

Our isomorph are plotted in the ρ, T and κ, Γ phase diagram in figure 3.10. In the ρ, T the isomorphs seem to collapse at all but the lowest densities. Due to the different scale in the κ, Γ plane, there is a clear difference between the two predictions of $h(\rho)$. The isomorph from the direct isomorph check seems to collapse on the prediction with $\Lambda = 1.03$. We have compared our isomorphs with the prediction of the melting line from Vaulina and Khrapak (2000) which is given by equation 3.12 with $\Lambda = 1$ and $1/c = 213$. Unsurprisingly, the melting line is parallel to our isomorph prediction with $\Lambda = 1$. However, our isomorph prediction with $\Lambda = 1.03$ actually crosses the melting line at around $\rho = 2 \cdot 10^{-4}$) without any observable crystallization.

We compare the invariance of our three isomorphs in figure 3.11. Data for the direct isomorph check and the prediction with $\Lambda = 1.03$ collapse and are almost constant in that density range, indicating that this is indeed the relevant reduced interparticle distance to evaluate the potential at, at least in this smaller density range. Especially at very low densities the relaxation time changes a lot. For both values Λ, there is a big drop in the relaxation time that starts around $\rho = 10^{-2}$, which is where γ drops below 2 and there are some large changes in peak position. Overall, the prediction with $\Lambda = 1$ gave the most invariant dynamics over the entire density range, but closer inspection of figure 3.11 seems to indicate that this is mostly an effect of cancellation of errors at low and high densities. The distance

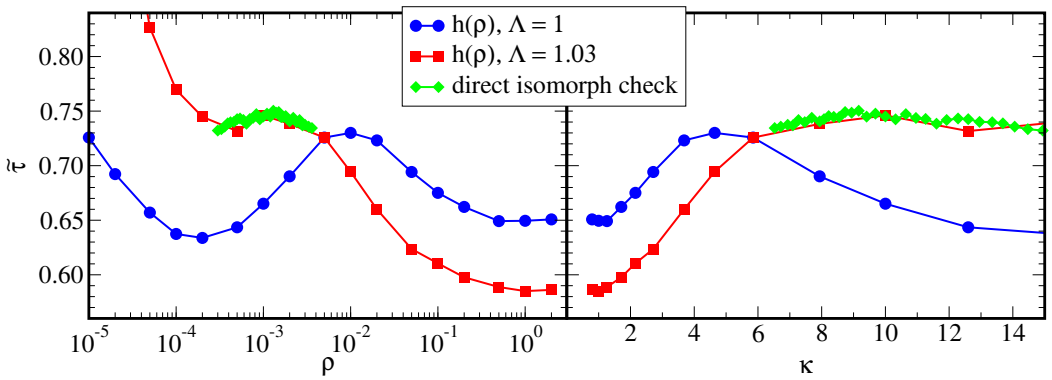

Figure 3.11: The reduced relaxation times on the three isomorphs. The relaxation time is here defined as the time where the intermediate scattering function has decayed to 0.2.

$\Lambda = 1$ does not seem to hold any special significance.

To conclude, we have shown that the Yukawa liquid is a simple liquid in the Roskilde sense, indicating that systems which are generally modelled with a Yukawa potential, like dusty plasmas and colloidal suspensions may show simple behavior in part of their phase diagram. The liquid has very strong correlations, and it is possible to trace out isomorphs with a very big density range. Because the steepness of the potential and γ change a lot over such a large density range, the structure also changes a lot. This has a negative effect on the ability to estimate $h(\rho)$ from the potential. Nevertheless, our prediction of $h(\rho)$ gives a good estimate of the isomorph.

Chapter 4

Simulations of soft particles with a finite, hard-core volume

---

This chapter investigates the applicability of the isomorph theory to different model liquids. The three models studied in this chapter are

- a new repulsive potential with a non-zero divergence (section 4.1 on page 36),
- a new attractive potential with a non-zero divergence (section 4.2 on page 39),
- the Girifalco potential (section 4.3 on page 45).

The similarity between these potentials is that they diverge at non-zero interparticle distance. This is in contrast to other, more common interparticle potentials, like the Lennard-Jones, Buckingham, and the Yukawa potential. The fact that these potentials have a non-zero divergence means that they have a finite volume, while it is more common to model interactions of atoms or even groups of atoms as point particles. These potentials are therefore relevant to explain some experimental observations of real liquids, in which molecules obviously occupy some volume.

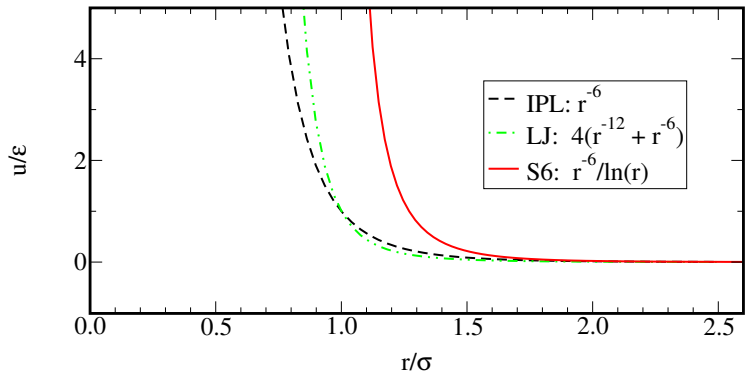

Figure 4.1: The new repulsive potential S6, compared with the IPL6 and repulsive Lennard-Jones. The potential has a hard core of diameter 1.

4.1 New model systems: I. A new repulsive potential

4.1.1 A sum of inverse power laws

The famous Lennard-Jones potential consists of two inverse power-law (IPL) terms, one positive and one negative. This gives the Lennard-Jones potential its attractive well, which makes it useful for simulating systems that have some kind of molecular or atomic attraction. At very high densities, the r^{-12} term in the potential dominates, and the system behaves as an IPL with $\gamma = 4$. When the interparticle distances become larger, the r^{-6} becomes more dominant, but the Lennard Jones potential never behaves as an IPL liquid with $\gamma = 2$ because the system will phase separate at low densities. The attractive term actually makes the potential steeper at intermediate densities, leading to $\gamma > 4$ in most of the Lennard-Jones phase diagram (Bailey et al., 2013).

Recently a new potential has been devised by making both terms in the Lennard-Jones potential positive (Ingebrigtsen et al., 2012; L.Bøhling, 2013). This is a purely repulsive Lennard-Jones potential that shows a smooth transition from r^{-6} behavior to r^{-12} behavior, leading to $2 < \gamma < 4$. This potential was also surprisingly strongly correlating, with $R > 99.9\%$.

This sum of two (repulsive) repulsive IPL potentials gave us an idea for a new potential. Consider for example to sum of all IPLs r^{-n} with $n \geqslant 6$:

$$\int_6^\infty r^{-n}\,\mathrm{d}n = \frac{r^{-6}}{\ln(r)}\,. \tag{4.1}$$

This potential is expected to be a simple liquid in at least part of its phase diagram because it is a sum of power laws. Moreover, the density scaling exponent at low density where the r^{-6} dominates should be $\gamma = 2$, increasing as density is increased. The potential energy diverges at $r = 1$, meaning that the particles have a "hard core" of excluded volume with diameter unity. This means that there is a maximum density, and upon approaching this density the system will behave more and more like a hard sphere system. The hard sphere corresponds to the soft sphere potential with $\gamma \to \infty$.

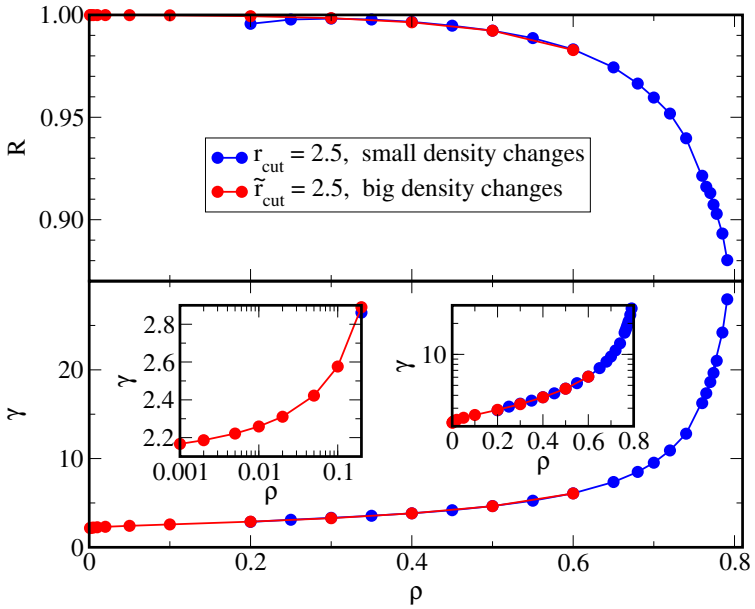

Figure 4.2: The correlation coefficient R (top) and the density scaling exponent γ (bottom) versus density on an the isomorph. The initial state point from which the other isomorphic points were calculated, was $\rho_0 = 0.6$, $T_0 = 1.5$. The blue data set was found by iteratively changing density and calculating the isomorphic temperature at the new state point from the scaled configuration. At low densities (red data) it was possible to change density by a large amount, keeping r_{cut} and Δt constant in reduced units. Thus, all low density state points were found directly from the starting state point. At low density γ approaches 2 as expected, while it increases steeply at high densities.

Since the potential has no name, we shall denote it as "S6". The potential is parameterized as

$$v(r) = \varepsilon \frac{(r/\sigma)^{-6}}{\ln(r/\sigma)}, \tag{4.2}$$

and is plotted in figure 4.1, together with the IPL6 and the repulsive Lennard-Jones potential.

4.1.2 Verification of the isomorph theory

We have simulated one isomorph with this potential, starting at $\rho = 0.6$, $T = 1.5$. We found isomorphic points to this state point using the direct isomorph check (section 2.2.3). We used a cutoff radius of $r_{cut} = 2.5$ for high densities and a reduced $\tilde{r}_{cut} = 2.5$ for the lower densities, shifting the potential to have zero energy at this distance. To take the high temperature at high densities the time step in reduced units can be kept constant. However, due to the increased steepness of the potential at high densities, it was necessary to decrease the reduced time step to $\Delta\tilde{t} = 0.00015$ at the highest density.

The liquid is strongly correlating at most densities, but the correlation coefficient

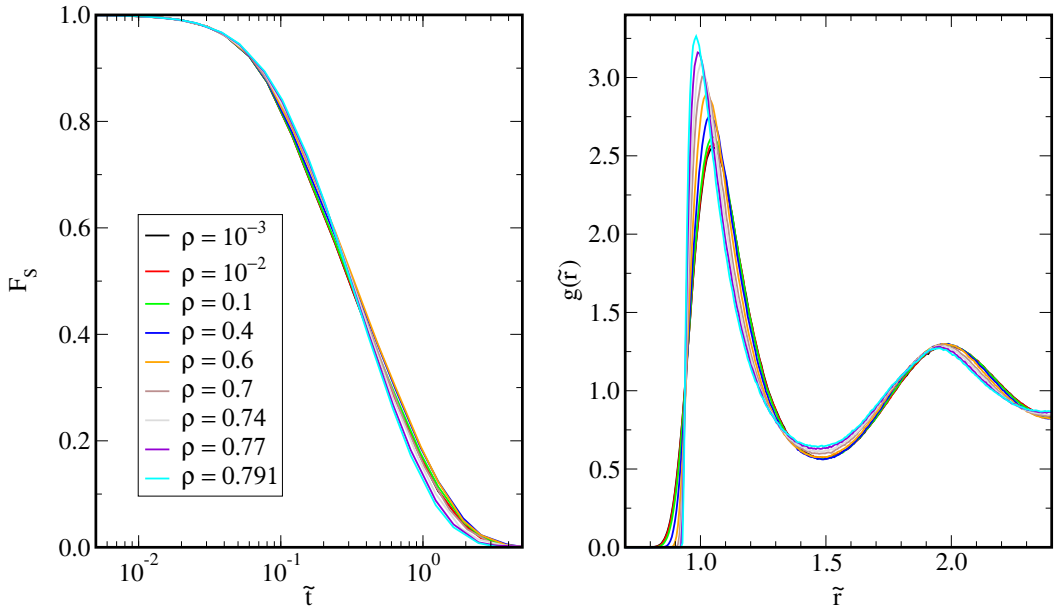

Figure 4.3: (left) The incoherent intermediate scattering function is invariant along the isomorph. The two highest densities plotted here show a slight deviation. (right) The radial distribution function for different isomorphic state points. The structure is quite invariant, although the first peak becomes higher and steeper at the highest densities.

drops below 0.9 for densities above 0.77, as can be seen in figure 4.2. The density scaling exponent is close to the value of the r^{-6} potential at low densities. At high densities γ becomes very dependent on density, with the highest value found being $\gamma = 28$. This corresponds to an effective IPL potential with exponent 84, which as already quite a reasonable approximation of a hard sphere, as shown by Jover et al. (2012) who used a Lennard-Jones potential with exponents 50 and 49 and a WCA cutoff as an approximation for a hard sphere. It is not surprising that the correlation coefficient drops at these high densities. Although a correlation coefficient cannot be calculated for a hard sphere liquid because there is no potential energy, simulations of a square well hard sphere potential yielded a negative correlation coefficient (Bailey et al., 2008a). Also thinking about the density scaling exponent as an indication of an effective IPL potential gives some insight. At high densities, the effective IPL exponent estimated by 3γ becomes very dependent on density, and therefore also on the interparticle distance. Thus the effective potential that the particles feel is no longer approximately a single IPL, at least not over the range of distances comparable to the width of the first peak of $g(r)$.

We test the isomorph invariance of the structure and the dynamics in figure 4.3. The dynamics do indeed show as good an invariance as any simple liquid. The radial distribution function changes mainly at the first peak, which becomes narrower as the potential gets steeper.

4.2 New model systems: II. A new attractive potential

In the last couple of years, many systems have been shown to obey the isomorph theory. Except for the IPL liquids, all systems also have a density dependent γ, indicating that power law density scaling is an approximation that only holds for small density changes. Most model liquids have γ decreasing with density. This includes the Lennard-Jones potential (Bailey et al., 2008a) and the Buckingham potential (chapter 2), but also rigid (Ingebrigsten et al., 2012a) and flexible (chapters 5 and 6) molecular systems. Considering data for supercritical argon, the decrease of γ seems to be in agreement with experimental data as shown in figure 2.2.

Experimental data from empirical density scaling studies show that a constant γ gives satisfactory collapse of the dynamics (Roland, 2010; Roland et al., 2005). There is no a priori reason to believe that γ should indeed be constant (Tarjus et al., 2004a,b), and indeed it would be surprising if this was the case for all experimental data on molecular glass formers, given the fact that the opposite is seen in computer simulations. It is more probable that the density range accessible in experiments and/or the density dependence of γ was to small to compare different functional for forms of $h(\rho)$.

Recently, Bøhling et al. (2012) published the first experimental proof that–at least for two real liquids–the shape of an isochrone ($h(\rho)$) is not well approximated by a power law. For this it was necessary to change density much more than usual in experiments; the maximum density increase was 20% (Paluch et al., 2003a). It was found that γ increased with density, which is the opposite of what is normally seen in computer simulations.

4.2.1 The potential

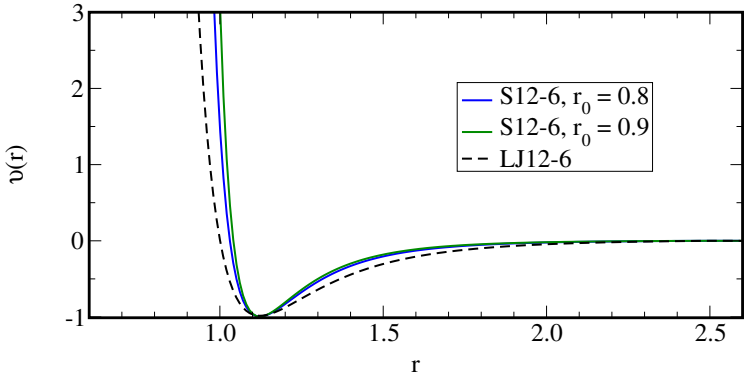

Figure 4.4: The S12-6 pair potential as described in equation 4.4 plotted for two values of r_0. The minimum of the potential was kept at $r_m = 2^{1/6}$ to make it comparable to the Lennard-Jones potential (dashed line).

New potentials like the one in the previous section are interesting in view of this increasing γ with density. In order to simulate a physically more realistic liquid we constructed a physically more relevant interatomic potential by including an attraction at longer interparticle distances. Inspired by the Lennard Jones potential that is sum of two power laws, the new attractive potential is a sum of two potentials

as described in the previous section:

$$A\int_p^\infty r^{-n}\,\mathrm{d}n - B\int_q^\infty r^{-n}\,\mathrm{d}n = A\frac{r^{-p}}{\ln(r)} - B\frac{r^{-q}}{\ln(r)}\,, \qquad p>q\,. \tag{4.3}$$

Like the Lennard-Jones potential, the exponents are chosen to be $p = 12$ and $q = 6$, and the potential will be denoted S12-6. To facilitate comparison with the Lennard-Jones potential, the potential is parameterized as

$$v(r) = \varepsilon\,\frac{A\,(r/r_m)^{-12} - B\,(r/r_m)^{-6}}{\ln\,(r/r_0)}\,, \tag{4.4}$$

where

$$A = \ln\,(r_m/r_0) + 1/6\,, \qquad B = 2\ln\,(r_m/r_0) + 1/6\,, \tag{4.5}$$

and r_0 and r_m are the hard core radius and the position of the potential minimum, respectively.

The potential is plotted in figure 4.4. In order to get densities comparable to the Lennard-Jones liquid, the position of the potential minimum was chosen to be the same ($r_m = 2^{1/6}$). Two values of the hard-core diameter were simulated ($r_0 = 0.8$ and $r_0 = 0.9$). We simulated both the single component liquid, as well as a Kob-Andersen mixture to test the dynamical invariance on the isomorph in the viscous state.

4.2.2 Isomorphs in single component systems

An isomorph was traced out using the direct isomorph check, starting at $\rho = 0.9$ and $T = 1.5$. W simulated with a time step $\Delta t = 0.001$, decreasing it for the state points with the highest values of γ to $\Delta t = 0.0002$. The dynamics and structure are plotted in figure 4.5 and are invariant. There is not much difference between the two values of r_0, except for the range of densities (see also the left side of figure 4.7).

The liquids are very strongly correlating, except for the lower densities where there is a sharp decrease in the correlation coefficient (see figure 4.6). For both particle sizes we see an initial decrease of γ at the lower densities, similar to what is seen for liquids consisting of point particles like the Lennard-Jones liquid (Bailey et al., 2008a).

The change of γ on the isomorph is hardly visible in a $\log(\rho), \log(T)$ plot. For a constant γ the isomorph is a straight line shown as a fit (dashed line). We find $\gamma = 7.92$ for $r_0 = 0.8$ and $\gamma = 10.55$ for $r_0 = 0.9$. These "constant γ" fits are shown as dashed lines in figure 4.6. Especially for the particles with $r_0 = 0.8$ the linear fit approximates the shape of the isomorph well, because the change of γ is small, and changes sign. The experimental observation from power law density scaling that γ is constant for many liquids may therefore also be caused by a "cancellation of effects" in the experimental density range.

4.2.3 Isomorphs in a viscous mixture

We used the same parameters as the Kob-Andersen Lennard-Jones system (Kob and Andersen, 1994), i.e., a 80 : 20 mixture of A and B particles that interact via the potential in equation 4.4 with parameters $\varepsilon_{AA} = 1.0$, $\varepsilon_{AB} = 1.5$, $\varepsilon_{BB} =$

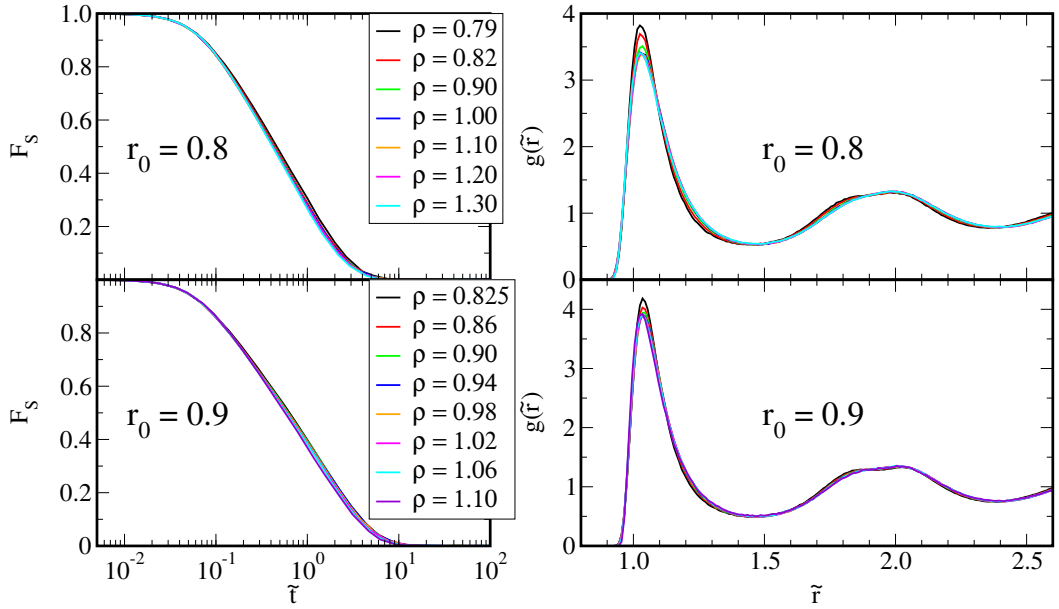

Figure 4.5: The incoherent intermediate scattering function (left) and the radial distribution function (right) in reduced units for the new attractive potential with hard core diameter $r_0 = 0.8$ (top) and $r_0 = 0.9$ (bottom). The results are very similar for both potentials, there are only small differences in reduced relaxation time and peak height. $\tilde{q} = 7.11$ for both isomorphs.

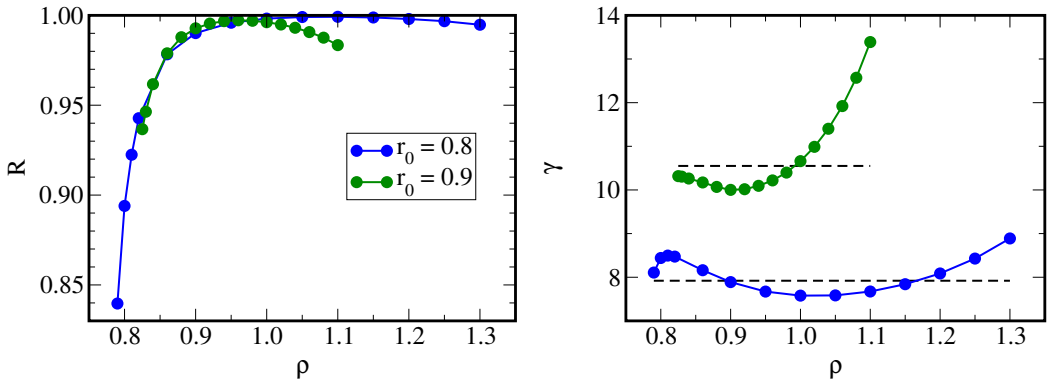

Figure 4.6: The correlation coefficient (left) and γ (right) as a function of density. The lowest density state point with $r_0 = 0.8$ has a negative pressure.

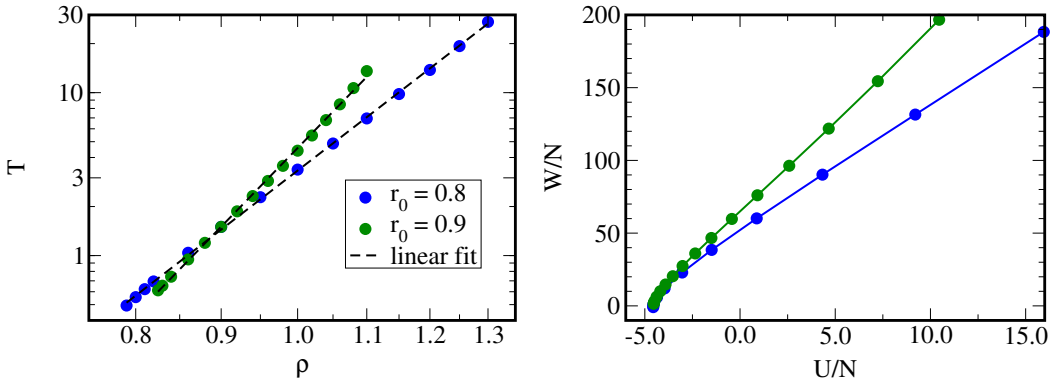

Figure 4.7: The shape of the isomorphs in the $\log(\rho), \log(T)$ plane (left) and the U, W plane (right). In the log-log plot, there is only a small visible deviation from a straight line.

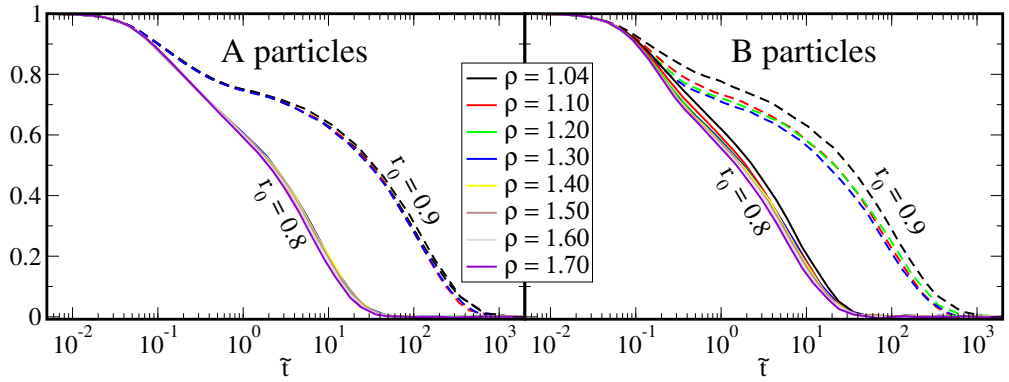

Figure 4.8: The incoherent intermediate scattering functions on isomorphs of the binary Kob-Andersen mixtures. Due to the larger size, the particles with $r_0 = 0.9$ (dashed lines) have slower dynamics. The dynamics of the A particles (left) collapse well, but the dynamics of the B particles (right) cannot be called invariant. The scattering vector was kept constant in reduced units at $\tilde{q} = 6.785$ for the A particles and $\tilde{q} = 5.449$ for the B particles.

0.5, $r_{m,AA} = 2^{1/6}$, $r_{m,AB} = 0.8 \cdot 2^{1/6}$, $r_{m,BB} = 0.88 \cdot 2^{1/6}$, $r_{0,AB} = 0.8 r_{0,AA}$, and $r_{0,BB} = 0.88 r_{0,AA}$. The potentials were cut and shifted at $r_{cut} = 2.5 r_m$. The time step used was $\Delta t = 0.001$ for all but the highest densities, where the time step had to be decreased down to $\Delta t = 0.0005$ for the highest density due to the increased steepness of the potential and the high temperature.

The isomorphs of the Kob-Anderson mixture were started at the standard density for this mixture $\rho = 1.2$ and $T = 1.6$ and state points a consecutive densities were found using the direct isomorph check. The dynamics are plotted in figure 4.8 for both values of r_0. The larger particles (dashed lines) have slower dynamics. There is a good collapse of the dynamics in reduced units for the A particles. The dynamics of the B particles do not collapse on both isomorphs, although it must be noted that the correlation coefficient for the black lines is below 0.9.

The structure on the isomorph is also invariant (figure 4.9), more so for the AA

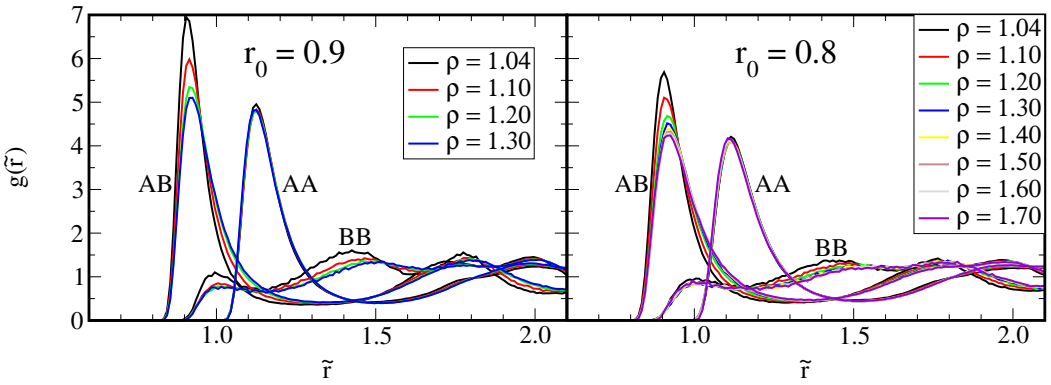

Figure 4.9: The radial distribution functions on isomorphs of the binary Kob-Andersen mixtures. For the AA pairs, the structure is perfectly invariant, but there is some difference in the height of the peak for the AB pairs. Again, the black line has a correlation coefficient below 0.9.

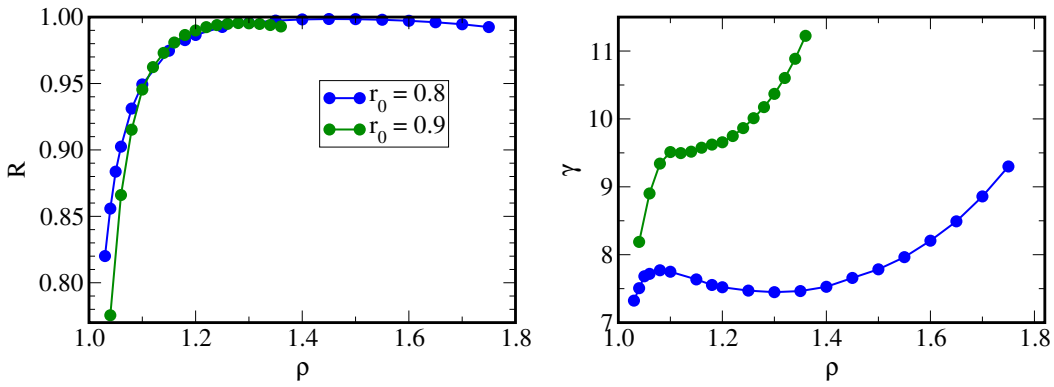

Figure 4.10: The correlation coefficient and γ versus density for the isomorphs of the Kob-Andersen binary mixture. The lowest density state point with $r_0 = 0.9$ has a slightly negative pressure.

particle pairs than for the AB and BB pairs. This seems the be a general feature of Kob-Anderson mixtures, since a similar thing has been observed for the binary Lennard-Jones system (Gnan et al., 2009) and the binary Buckingham system (Paper I).

The behavior of the correlation coefficient and the density scaling exponent is plotted in figure 4.10. The correlation coefficient decreases sharply when the pressure approaches zero, which is also seen in other systems (Bailey et al., 2008a; Veldhorst et al., 2012). The density scaling exponent γ increases significantly at the higher densities for both values of r_0. It seems that at the highest densities, the correlation coefficient starts to go down again due to the strong change in steepness of the potential.

The shape of the isomorphs are plotted in figure 4.11, and shows qualitatively the same behavior as the isomorphs of the single component liquid.

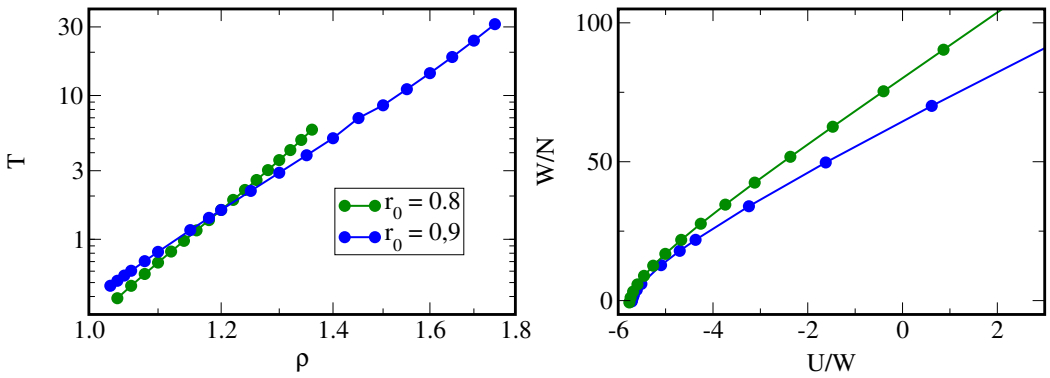

Figure 4.11: Shape of the isomorphs of the Kob-Andersen mixture in the $\log(\rho), \log(T)$ phase diagram (left) and the U, W phase diagram (right)

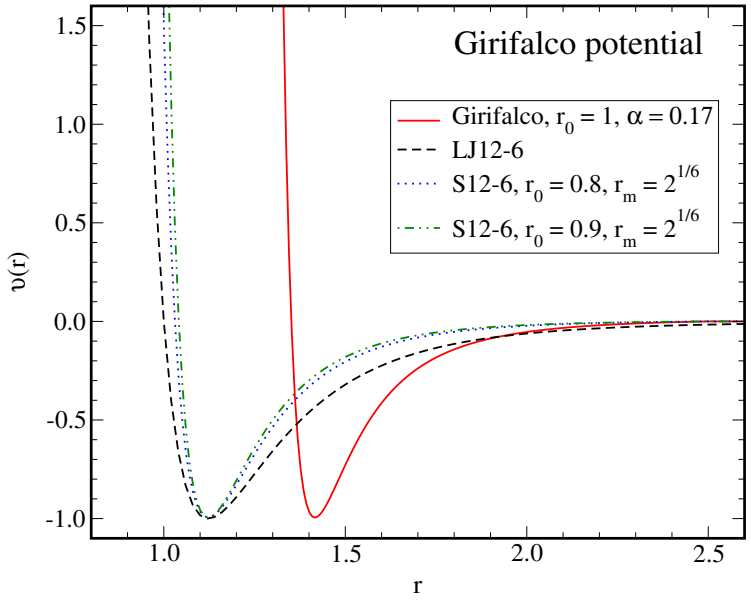

Figure 4.12: The Girifalco potential as plotted with the parameter values used in the simulations, compared with the Lennard-Jones potential and the S12-6 potential from the previous section.

4.3 The Girifalco potential

This section describes a small study to test if the results encountered with the new potential can be reproduces qualitatively with an existing potential, namely the Girifalco potential.

The Girifalco potential was devised by Girifalco (1992) to simulate molecular C_{60}, also known as Buckminsterfullerene or simply Buckyballs. The C_{60} molecule was first discovered by Kroto et al. (1985) and was found to have an almost spherical shape, with the carbon atoms positions on the surface of the sphere. The molecules rotate even in the solid phase (Tycko et al., 1991; Yannoni et al., 1991), indicating that the shape of the molecule is well approximated by a sphere.

Girifalco (1992) derived the potential by assuming that the carbon atoms interact via the standard Lennard-Jones potential. Because of the (fast) rotations of the molecule, the effect of the 60 carbon atoms can just be averaged out rotationally to a spherical surface with a uniform density of carbon atoms. The interaction between two molecules is then found by integrating over the surface of two spheres.

The potential thus obtained has the form

$$v(r) = -\frac{\alpha}{s}\left[\frac{1}{(s-1)^3} + \frac{1}{(s+1)^3} - \frac{2}{s^3}\right] + \frac{\beta}{s}\left[\frac{1}{(s-1)^9} + \frac{1}{(s+1)^9} - \frac{2}{s^9}\right], \quad (4.6)$$

where

$$s = \frac{r}{r_0} \qquad \alpha = \frac{N^2 A}{12 r_0^6} \qquad \beta = \frac{N^2 B}{90 r_0^{12}}. \quad (4.7)$$

Here r_0 is the diameter of the molecule, N is the number of atoms per molecule, and A and B are the prefactors for each term in the Lennard-Jones potential for a carbon

atoms in different sheets of graphite ($\upsilon(r) = -A/x^6 + B/x^{12}$). For C_{60}, the diameter of the molecule $r_0 = 0.71$ nm, $\alpha = 7.494 \times 10^{-21}$ J, and $\beta = 1.3595 \times 10^{-23}$ J (Girifalco, 1992).

A more general from of this potential has been used to describe the interaction between fullerene molecules of different sizes (Kniaź et al., 1995):

$$\begin{aligned}\upsilon(r) = &-\frac{\alpha}{r_a r_b r}\left[\frac{1}{(r-r_a-r_b)^3} - \frac{1}{(r+r_a-r_b)^3} - \frac{1}{(s-r_a+r_b)^3} + \frac{1}{(r+r_a+r_b)^3}\right] \\ &+\frac{\beta}{r_a r_b r}\left[\frac{1}{(r-r_a-r_b)^9} - \frac{1}{(r+r_a-r_b)^9} - \frac{1}{(r-r_a+r_b)^9} + \frac{1}{(r+r_a+r_b)^9}\right],\end{aligned} \tag{4.8}$$

where r_a and r_b are the diameters of the two molecules. The values of α and β are also defined in a different way:

$$\alpha = \frac{1}{48} N_a N_b A\,, \qquad \beta = \frac{1}{360} N_a N_b B\,. \tag{4.9}$$

4.3.1 Simulation procedure

The potential was simulated with parameter values $r_0 = 1$, $\alpha = 0.17$, and $\beta = 1.8141 \times 10^{-3}\alpha$. This gives a potential that diverges at $r = 1$, and has a potential well of unity depth. The ratio between α and β is as found by Girifalco (1992). The implementation of the potential was verified to be correct by comparing to simulation data from Alemany et al. (2000). We used a cutoff radius of $r_{cut} = 2.5$ and time steps between $10^{-5} \leqslant \Delta t \leqslant 5 \cdot 10^{-4}$. To facilitate comparison with literature data on the Girifalco potential we present our results in Kelvin and nanometers.

There has been some controversy about the existence of a liquid phase in the phase diagram of the Girifalco fluid (Ashcroft, 1993; Cheng et al., 1993; Hagen et al., 1993; Hasegawa and Ohno, 1999), but we only present from simulations at supercritical temperatures.

4.3.2 Simulation of isomorphs

We construct an isomorph using the direct isomorph check, starting at density $\rho_0 = 1.118\ \text{nm}^{-3}$ and $T_0 = 3193$ K. The dynamics and the structure are invariant on the isomorph, as shown in figure 4.13

As shown in figure 4.14, the density scaling exponent is very high, as can be expected for such a steep potential. γ shows first a decrease in density to later increase again at higher densities. At the very lowest densities, there is a steep drop in γ and the fluid stops being strongly correlating.

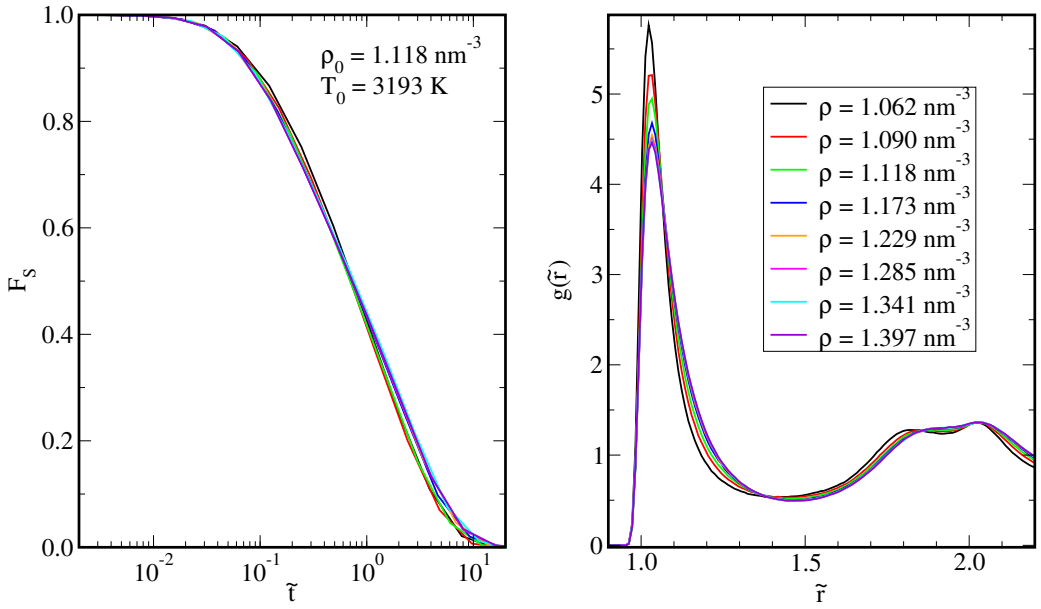

Figure 4.13: The incoherent intermediate scattering function and the radial distribution function on the isomorph started at $\rho_0 = 1.118\ \mathrm{nm}^{-3}$, $T_0 = 3193$ K.

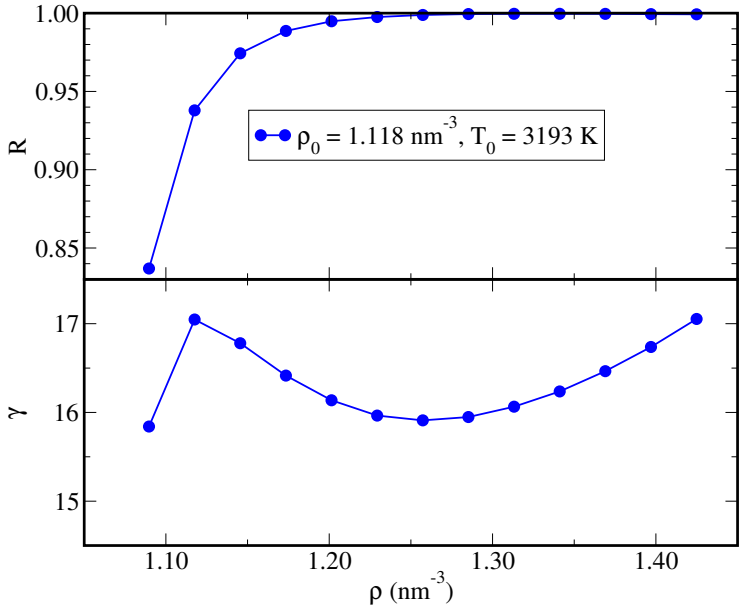

Figure 4.14: The behavior of the correlation coefficient and the density scaling exponent γ versus density.

4.4 Conclusion

The systems studied in this chapter all have potential that diverges at non-zero particle separation, giving the particles a "hard core" of finite volume, in contrast to the point particles of the Lennard-Jones and related potentials. All potentials here have been shown to be strongly correlating and have isomorphs in their phase diagram. Unlike the Lennard-Jones and the Buckingham potential, the hard core potentials studied here have a density scaling exponent that is increasing with density, as is the case for recently published experimental data (Bøhling et al., 2012). The results presented in this chapter point to the presence of inaccessible excluded volume as a possible explanation for the discrepancy between the experimental density scaling data from Bøhling et al. (2012) and most simulation results of atomic and molecular liquids such as presented in chapter 2, 5, 6, and by Ingebrigsten et al. (2012a). Moreover, the results for the Girifalco potential indicate that at high densities and pressures, Buckminsterfullerene is a simple liquid, although it is not clear if this part of the phase diagram is physically relevant.

Chapter 5

Isomorphs in the phase diagram of flexible Lennard-Jones chains.

I. Results for rigid bonds

5.1 Introduction

As mentioned in chapter 2, the isomorph theory has so far been tested for atomic systems and rigid molecular systems. Real liquids for which we expect the theory to hold are–among others–the molecular glass formers that obey power-law density scaling. A large part of the liquids that have been shown to obey power-law density scaling are polymers, which are clearly very different form the simple model systems for which the isomorph theory has been tested. Our aim in this chapter is to bridge this gap somewhat by showing that the isomorph theory also holds for flexible molecules with intramolecular degrees of freedom.

5.1.1 Model and simulation procedure

The Lennard-Jones chain model

The Lennard Jones chain consists of a series of Lennard-Jones particles connected by bonds. The Lennard-Jones chain was first simulated by Grest and Kremer (1986), who used it as a coarse-grained model to study the properties of polymeric liquids. They used their early version of the model to simulate chains consisting of 5 to 400 segments (Kremer and Grest, 1990; Kremer et al., 1988). The particles in chain do not correspond to a single atom, but rather to groups of atoms, like one CH_n unit in an alkane or one or several monomers in a polymer. For this reason we refer to the Lennard-Jones particles in the chain as "segments".

Starting at the end of the 90's, extensive simulations of the model have been done to investigate the behavior of polymer melts around the glass transition (Bennemann et al., 1998, 1999a,b,c,d; Binder et al., 1999). At that time the model had

already undergone some changes compared to the original version. The main difference was that the new simulations used a longer cut-off radius, including also the attractive part of the Lennard-Jones potential (Kopf et al., 1997), whereas the earlier versions cut and shifted the potential at the minimum. A second difference was that Grest and Kremer (1986) did not use standard Molecular Dynamics, but Langevin Dynamics, including a stochastic force similar to what is done when simulating an implicit solvent (Schlick, 2002).

The Lennard-Jones chain has since been used often to model viscous polymer melts close to the glass transition. The recurring chain length in these simulations is ten segments (Aichele et al., 2003; Binder et al., 2003; Puosi and Leporini, 2011, 2012). Even though one segment may correspond to several monomers, a chain of ten segments can hardly be called a polymer in chemical or physical sense. The reason for simulating such short chains is the fact that one is usually interested in the equilibrium properties of the viscous liquid. Increasing the chain length greatly increases the equilibration time, as does increasing the viscosity, so there is always a trade-off to be made (Barrat et al., 2010; Glotzer and Paul, 2002). When it is not the equilibrium liquid, but the non-equilibrium properties that are of interest this issue does not arise (as much), and simulations with longer chains have been performed (Riggleman et al., 2009; Shavit et al., 2013).

The Lennard-Jones model is a good candidate for the isomorph theory, since has been shown to obey power law density scaling (Galliero et al., 2011), and Rosenfeld's excess entropy scaling (Galliero and Boned, 2009; Galliero et al., 2011; Goel et al., 2008; Voyiatzis et al., 2013).

Simulation procedure

In order to investigate the applicability of the isomorph theory to flexible molecules, we have simulated the Lennard Jones chain model. All particles except the bonded particles interact by a cut and shifted Lennard-Jones potential (equation 1.2) with the standard cutoff radius $r_c = 2.5\sigma$. The potential parameters were set to unity $\epsilon = \sigma = 1$. In this chapter the Lennard-Jones particles are connected by "covalent" bonds to form a linear chain. In the next chapter we also present results for chains where the covalent bonds are modelled as harmonic springs.

The bond lengths are also fixed to be unity: $b = \sigma$. The bonds are completely rigid during the simulation, which is achieved using constraint dynamics (Allen and Tildesley, 1987). When simulating constraint dynamics, one calculates the forces on all particles that come from interactions between non-constraint particle pairs. An additional force is than added to keep the relative velocities of bonded particles zero along the direction of the bonds, using Gauss principle of least constraint (Edberg et al., 1986). We use here a recently improved constraint algorithm that has the advantage that it is energy conserving and time symmetric (Toxvaerd et al., 2009). It should be noted that the constraint algorithm adds an extra force that contributes to the pressure of the system via the virial, but it does not give a (direct) contribution to the potential energy.

We have simulated chains of different lengths $L = \{2, 4, 8, 10, 16, 32\}$ segments. While in the introduction and section 5.2 we investigate the effect of chain length, in later sections we only focus on chains with 10 segments. For most systems the

L	N	M
2	2048	1024
4	2048	512
8	2048	256
10	2000	200
16	2048	128
32	2048	64

Table 5.1: System size in number of segments N and number of molecules M for the different chain lengths L.

total number of segments in the simulation N was 2048, except for chains with ten segments. This resulted in a variable number of molecules in the system, as listed in table 5.1.

The simulations were performed in the NVT ensemble with a Nosé-Hoover thermostat in a cubic box with periodic boundary conditions. The time step was set to $\Delta t = 0.0025$.

5.1.2 The structure of linear molecules

In this and the follow section we discuss the structure and dynamics of linear molecules in terms of some standard models. This can be found in standard textbooks like Doi and Edwards (1986), Ferry (1980), and Rubinstein and Colby (2003).

The origin of the Lennard-Jones chain model in Molecular dynamics lies in early (analytical) models of polymers. The Gaussian chain is one of the simplest models for polymer structure, and consists of a series of connected springs. The springs have a reference length b. The "particles" in the Gaussian chain do not interact with each other, i.e., it is an *ideal* chain. Also, the angles between the bonds are random, so the equilibrium configuration of the polymer in this case is essentially a random walk. If the position of the first and last position in the chain are denoted by $\mathbf{r}_1$ and $\mathbf{r}_L$, and the bond vector between positions $\mathbf{r}_i$ and $\mathbf{r}_{i+1}$ is denoted by $\mathbf{b}_m = \mathbf{r}_{m+1} - \mathbf{r}_m$ the end-to-end vector of the chain is defined by

$$\mathbf{R} = \mathbf{r}_L - \mathbf{r}_1 = \sum_{m}^{L-1} \mathbf{b}_m \,. \tag{5.1}$$

Normally, it is the mean square end-to-end distance that is used to characterize the size of a chain, which for a random walk is given by

$$\left\langle R^2 \right\rangle = \left\langle \mathbf{R}^2 \right\rangle = (L-1)b^2 \,, \tag{5.2}$$

for a chain of length L. Another common way to quantify the size of a molecule is the radius of gyration R_g, defined by:

$$R_g^2 = \frac{1}{2L^2} \sum_{i,j}^{L} \left(\mathbf{r}_i - \mathbf{r}_j\right)^2 \,, \tag{5.3}$$

where i and j denote positions in the chain. This is a more general quantity because it is also defined for non-linear molecules, and can be measured in scattering experiments. For the Gaussian chain, it can be shown that $R_g^2 = \langle \mathbf{R}^2 \rangle / 6 = (L-1)b^2/6$.

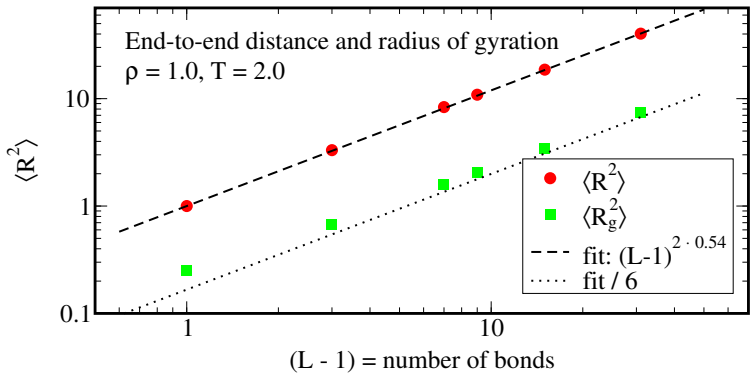

Figure 5.1: The mean square end-to-end distance $\langle R^2 \rangle$ and radius of gyration $\langle R_g^2 \rangle$ as a function of the number of bonds $L-1$. Both are almost proportional L. The Flory exponent ν is found to be 0.54 by fitting the function $(L-1)^{2\nu}$. The dotted line shows the same fit divided by 6.

For a real molecule, the assumption that the directions of consecutive bonds are uncorrelated is of course not correct. However, for two bonds $\mathbf{r}_m$ and $\mathbf{r}_{m+k}$ separated by an amount k, their orientation will be uncorrelated if k is large enough. k is called the Kuhn length, and can be calculated by

$$k = \frac{\langle \mathbf{R}^2 \rangle}{R_{max}}, \tag{5.4}$$

where $R_{max} = (L-1)r_{bond}$ is the maximum end-to-end distance of the chain. For the Gaussian chain $k = r_{bond}$, so the "particles" in the Gaussian chain model correspond to the Kuhn segments of a molecules.

Even considering the particles in a Gaussian chain as Kuhn segments, the model does not describe the size of real molecules, because there are no interactions between the segments. In real molecules, particles do interact when they are far away from each other in the chain. This is called the excluded volume effect and was first taken into by Flory (1949) for polymers in solution. Flory theory predicts that $\langle R^2 \rangle \propto r_{bond}^2 (L-1)^{2\nu}$ with $\nu = 3/5$ for a perfect solvent.

The Lennard-Jones chain is of course not ideal, but the prediction of Flory (1949) for the size of the chain does not hold either, as shown in figure 5.1. By fitting, we obtain a Flory exponent $\nu = 0.54$, which is somewhere in between the theoretical values for the ideal Gaussian chain (0.5) and the Flory model for a perfect solvent (0.6). Figure 5.1 also shows that at low chain lengths, the prediction $R_g^2 = \langle \mathbf{R}^2 \rangle / 6$ is not exact.

5.1.3 Dynamics of linear molecules

The Rouse model

One of the earliest theories that is successful in explaining the dynamics of polymers and linear molecules was published by Rouse (1953). In Rouse theory the molecule is represented as a series of particles connected by harmonic springs. The particles experience friction as they move through their surroundings, quantified by a friction

coefficient ζ. The friction coefficient of the Rouse chain is the sum of the friction coefficients of the particles $L\zeta$, and so the diffusion coefficient of the chain D_R is found from the Einstein relation to be

$$D_R = \frac{k_B T}{L\zeta} \,. \tag{5.5}$$

The Rouse time, the time it takes for the molecule to move approximately it's own length is given by

$$\tau_R \approx \frac{\langle \mathbf{R}^2 \rangle}{D_R} \approx \frac{\zeta b^2 L (L-1)^{2\nu}}{k_B T} \,. \tag{5.6}$$

Similarly, the characteristic time in which one segment moves a distance comparable to its own size (b) is predicted to be

$$\tau_0 \approx \frac{\zeta b^2}{k_B T} \,, \tag{5.7}$$

and therefore

$$\tau_R \approx \tau_0 L (L-1)^{2\nu} \tag{5.8}$$

For long chains, $L-1$ is approximately L, so the relaxation time of a long ideal Rouse chain is proportional to $\tau_0 L^2$.

The dynamics of an ideal Rouse chain is commonly expressed in its normal modes, analogous to the modes of a vibrating string. The modes are often called Rouse modes, and for a chain of L beads the Rouse modes $\mathbf{X}_p$ are given by the discrete cosine transform of the position of the segments by (Meyer et al., 2008; Verdier, 1966)

$$\mathbf{X}_p(t) = \frac{1}{L} \sum_{i=1}^{L} \cos\left(\frac{\left(i - \frac{1}{2}\right) p\pi}{L} \right) \mathbf{r}_i(t) \,, \quad p = 0, 1, \ldots, L-1 \,. \tag{5.9}$$

The zeroth mode corresponds to the position of the center of mass of the chain:

$$\mathbf{X}_p(t) = \frac{1}{L} \sum_{i=1}^{L} \mathbf{r}_i(t) = \mathbf{r}_{cm}(t) \,, \tag{5.10}$$

while the higher modes correspond to (sub)chains of L/p segments. For an ideal Rouse chain, the Rouse modes are independent of each other, but this is not the case for more realistic chains that have interactions between the segments, including the Lennard-Jones chain (Barkema et al., 2011; Meyer et al., 2008).

The relaxations of the Rouse modes can be visualized by plotting autocorrelation functions of the Rouse modes; $\langle \mathbf{X}_p(t) \mathbf{X}_p(0) \rangle$ (Bennemann et al., 1999d). Different Rouse modes characterized by p are plotted for the different chain lengths L in figure 5.2. The figure clearly shows that according to Rouse theory, small sections of a molecule behave in the same way as a molecule with the same size as the section.

Each mode has its own relaxation time corresponding to the relaxation time of a chain with length L/p (see equation 5.8)

$$\tau_p \approx \tau_0 \frac{L}{p} \left(\frac{L}{p} - 1 \right)^{2\nu} \,. \tag{5.11}$$

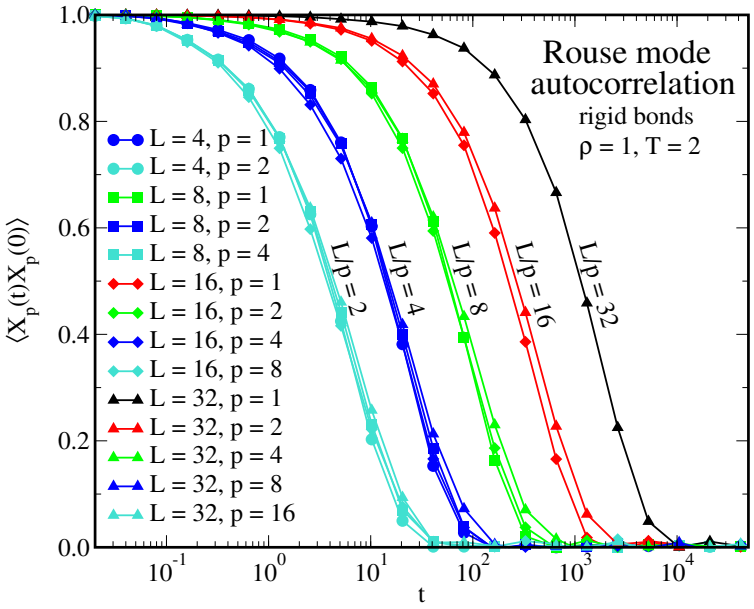

Figure 5.2: Normalized Rouse mode autocorrelation functions for different chain lengths. Symbol shapes correspond with chain length L, while autocorrelation functions with the same value of L/p have the same color. The data show that (sub)chains with the same length have similar relaxation.

For long subchains, we can assume for the size of a segment to be $L/p + 1 \approx L/p$ and we can rewrite equation 5.11 to

$$\left(\frac{L}{p}\right)^{2\nu} \approx \left(\frac{\tau_p}{\tau_0}\right)^{2\nu/(1+2\nu)} . \tag{5.12}$$

During this time τ_p, the segments move a distance of approximately the size of a segment, which for the longer chains is well approximated by $b^2(L/p)^\nu$, so for the mean square displacement we can write

$$\left\langle [\mathbf{r}_i(\tau_p) - \mathbf{r}_i(0)]^2 \right\rangle \approx b^2 \left(\frac{L}{p}\right)^{2\nu} \approx \left(\frac{\tau_p}{\tau_0}\right)^{2\nu/(1+2\nu)} . \tag{5.13}$$

Since the relaxation times of the modes τ_p are time dependent, we can rewrite this to get the time dependence of the mean square displacement

$$\left\langle [\mathbf{r}_i(t) - \mathbf{r}_i(0)]^2 \right\rangle \approx \left(\frac{t}{\tau_0}\right)^{2\nu/(1+2\nu)} \tag{5.14}$$

for the timescale of the Rouse mode relaxations ($\tau_0 < t < \tau_R$). For our Lennard-Jones chains $\nu = 0.54$ so we expect a slope in the mean square displacement of $2\nu/(1+2\nu) = 0.52$, close to the slope of 0.5 for ideal chains.

Figure 5.3 shows the mean square displacements of the segments and the centers of mass for different chain lengths. The data clearly show three regions for the segments in the longest chains. At short times, the segments move ballistically because they are not hindered by their neighbors. At long distances, their movement

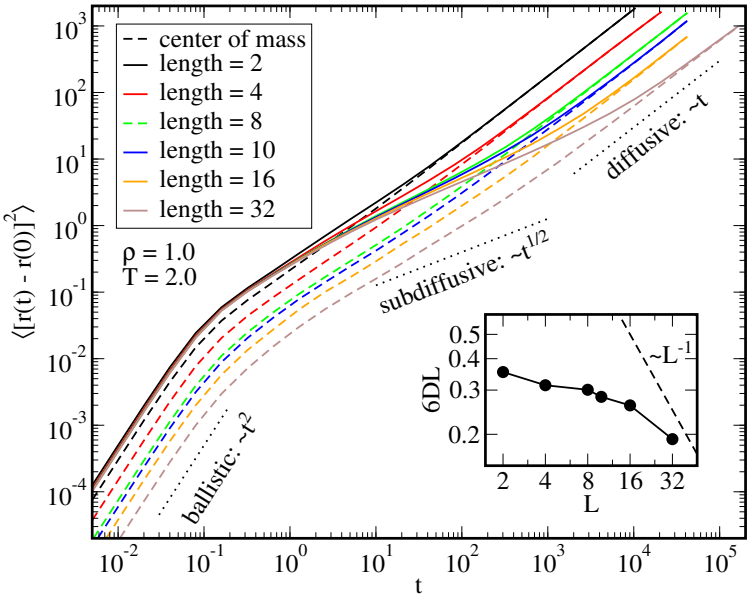

Figure 5.3: The mean square displacement for chains with two to 32 segments at the state point $(\rho, T) = (1.00, 2.00)$. Solid lines are for the segments while the dashed lines are for the centers of mass of the chain. For the longer chains the mean square displacement of the segments shows a ballistic, subdiffusive, and a diffusive regime. In the diffusive regime the mean square displacement of the segments and the center of mass collapse and the slope is related to the diffusion coefficient $\left\langle [\mathbf{r}_i(t) - \mathbf{r}_i(0)]^2 \right\rangle \propto 6Dt$. (inset) The diffusion coefficients were obtained by fitting to the center of mass mean square displacement for $\left\langle [\mathbf{r}_{cm,j}(t) - \mathbf{r}_{cm,j}(0)]^2 \right\rangle > 10$. For the short chains, the diffusion coefficient does not follow the prediction for Rouse dynamics: $D \propto L^{-1}$ which would correspond to a horizontal line in this plot. At longer chain lengths the chain length dependence of the diffusion coefficient becomes larger, closer to the prediction of reptation dynamics, $D \propto L^{-2}$ (dashed line).

is diffusive and the same as the movement of the whole molecule. At intermediate times, there is a regime where the mean square displacement is almost proportional to $L^{-1/2}$ as is predicted from Rouse theory.

The Rouse model was first conceived to describe the dynamics of a polymers in dilute solutions (Rouse, 1953), but the theory is not correct under these circumstances. The reason for this is the hydrodynamic effect, which is a long ranged interaction between the moving polymer and the solvent. The dynamics of dilute polymer solutions are more correctly described by the Zimm model, which takes into account the hydrodynamic interaction (Zimm, 1956).

The Rouse model is however useful in the description of melts of short polymers, because here the hydrodynamic interactions are screened. For instance, the Rouse model predicts the correct chain length dependence of the viscosity for short polymer melts (Colby et al., 1987; Rubinstein and Colby, 2003). For long chains however, the Rouse theory is incorrect due to the effect of entanglement.

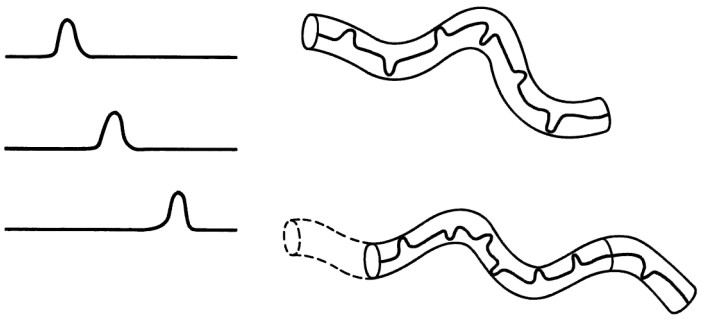

Figure 5.4: (left) Movement of a "defect" in the chain. (right) Movement of the entire chain in and with its tube. Taken from Doi and Edwards (1986).

Entanglement

Long chains have topological interactions because they cannot cross each other. For linear molecules, these interactions do not affect the structure because all configurations are still accessible. There is however a strong effect on the dynamics, especially for long chains in the melt or in concentrated solutions. The effect of entanglements is usually discussed in terms of the tube model.

In the melt, the conformation of a chain is limited by topological constraints due to the neighboring chains. Within these constraints there is however some room for small (local) changes in the conformation. The idea of the tube model is that the space that is occupied by all this different local changes in the conformation has the shape a tube, and movement of the chain is confined to this tube (see figure 5.4). Local conformational changes can be considered "defects" and can move back and forth on the chain, but do not change the shape of the tube. The tube only changes by extension or reduction at the end points due to the moving defects within the tube. Movement of the chain through these "defects" resembles the movement of caterpillars and is called *reptation* (de Gennes, 1971). The importance of the topological constraints has been demonstrated convincingly in computer simulations, where the topological constraints can be easily removed by allowing chains to cross each other (Everaers, 1999).

In the tube model the minimum length L_e (in segments) at which a chain becomes entangled is related to the width of the tube a by assuming an ideal chain:

$$a \approx b\sqrt{L_e} \tag{5.15}$$

The average contour length of the tube $\langle C_t \rangle$ is then the width times the number of sections of length L_e in the chain:

$$\langle C_t \rangle \approx a\frac{L}{L_e} \approx \frac{bL}{\sqrt{L_e}} \tag{5.16}$$

The longest relaxation time τ_{rep} of the reptation model is related to the time it takes the chain to diffuse out of its original tube. The diffusion constant D_t for this movement along the tube is characterized by the standard Rouse friction coefficient

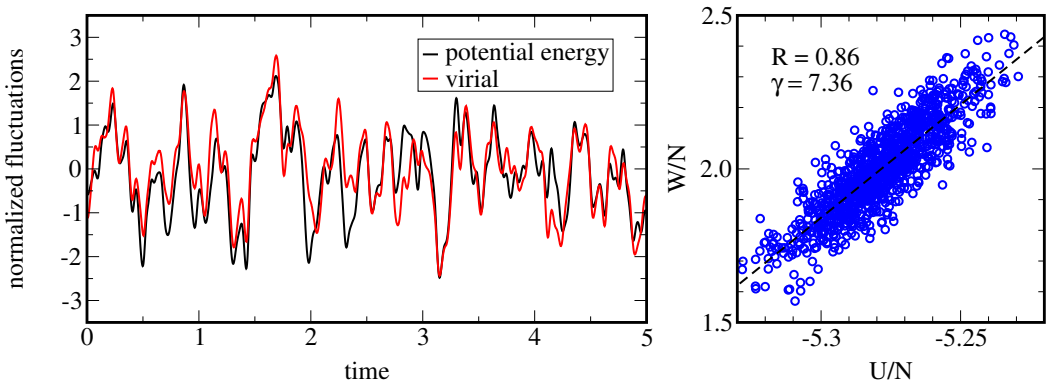

Figure 5.5: (left)Normalized fluctuations in the the potential energy and virial versus time, for a length $L = 10$ chain at density $\rho = 1.00$ and temperature $T = 0.70$. (right) Data for the same state point, now in a scatter plot in the U-W plane. The correlation coefficient and the slope γ are obtained by linear regression and are found to be $R = 0.86$ and $\gamma = 7.36$.

of the chain by $D_t = k_B T/(L\zeta)$ (equation 5.5). Thus, for the reptation time

$$\tau_{rep} \approx \frac{\langle C_t \rangle^2}{D_t} \approx \frac{L\zeta L^3}{k_B T L_e}\,, \tag{5.17}$$

and we can get the diffusion coefficient of the chain from the size of the chain and the relaxation time:

$$D_{rep} \approx \frac{\langle \mathbf{R}^2 \rangle}{\tau_{rep}} \approx \frac{k_B T L_e}{\zeta L^2}\,. \tag{5.18}$$

So the reptation model predicts that the diffusion coefficient is proportional to L^{-2}, in contrast to the L^{-1} for the Rouse model. Experimental data show that the chain length dependence of entangled polymers is even stronger, approximately $L^{-2.3}$ (Lodge, 1999).

The inset of figure 5.3 shows the diffusion coefficient obtained from the mean square displacement versus chain length. For the short chains the product DL should be constant according to Rouse theory, while the reptation model predicts a negative slope of unity ($\log(DL) \propto -\log(L)$). Although the Rouse prediction does not hold for short chains, the slope clearly increases for higher chain lengths and the longest chains can be considered to be in the crossover regime between Rouse and reptation dynamics. This is in agreement with the findings of Kremer and Grest (1990) and Sen et al. (2005) who found an entanglement length $L_e \approx 35$ and $L_e \approx 28$, respectively. This means that the chains of ten segments that have been simulated in the following sections of this chapter may be considered as a coarse grained model of short polymers in the Rouse regime.

5.2 Strong correlations

As usual when investigating isomorphs in a new model, we first look at the fluctuations in the energy and the virial. As shown in figure 5.5 there are correlations in the instantaneous values of the potential energy and the virial for a liquid with

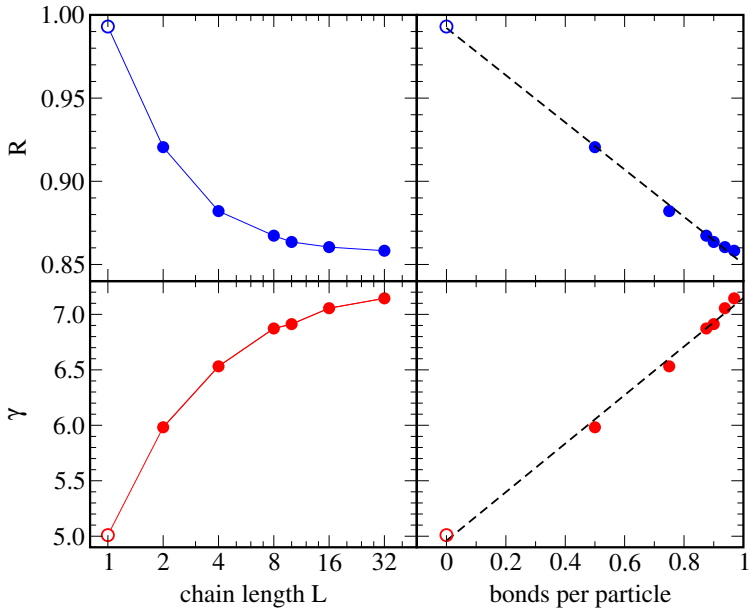

Figure 5.6: The correlation coefficient R (top) and γ (bottom) of chains with different lengths at density $\rho = 1.00$ and temperature $T = 2.00$. Data for the single component Lennard-Jones liquid (open symbols) have been included for comparison ($L = 1$). The data have been plotted in two ways; as function of the number of segments L in the chain (left), and as a function of the number of bonds per particle $(L-1)/L$ (right). The dashed lines are linear fits to the data (including the data points of the single component Lennard-Jones liquid).

chains of length 10. Often the energy and virial follow each other perfectly, while other times there is a clear difference in the fluctuations. At density $\rho = 1.00$ and temperature $T = 0.70$, the correlation coefficient is $R = 0.86$. This is lower then $R = 0.90$ which has previously been the limit for liquids to be called "strongly correlating" (Bailey et al., 2008b), and lower than the standard single component Lennard-Jones liquid (Bailey et al., 2008a).

Also the slope γ of the fluctuations in the U-W plane is markedly different from the value of the single component Lennard-Jones liquid, which has $4 < \gamma < 6.5$ (Bailey et al., 2008a). It is however in the range of γ values for the coarse-grained *ortho*-terphenyl model from Lewis and Wahnström (1993, 1994), which has $6.3 < \gamma < 8.0$ (Ingebrigsten et al., 2012a). This model is similar to the Lennard-Jones chain model in the sense that it also consists of Lennard-Jones particles connected by rigid bonds. It was found that contributions to the virial from the constraints increases the the value of γ (Ingebrigsten et al., 2012a).

Figure 5.6 shows the effect of the chain length on the correlations of the potential energy and the virial. The correlation coefficient decreases with increasing chain length. When plotting the data as a function of the number of bonds per particle $(L-1)/L$ shows an almost linear dependence. The opposite behavior is seen for γ, which is increasing for increasing chain length. Again there is a much more linear dependence on the bonds per particle, although there is clear systematic deviation

from linearity. The data indicate that the correlation coefficient is not expected to decrease much for chains longer than 32 segments. This is may not be true for γ, although care should be taken by concluding anything about long chains when plotting the data as function of the number of bonds per particle since this removes most of the details foor longer chains.

An intuitive explanation for the higher γ values of the longer chains is that the rigid bonds can be viewed as a very steep repulsion between the segments. Nevertheless, higher γ values for the longer chains are somewhat surprising in view of experimental data; power law density scaling in general gives lower γ values for polymers than for small molecular liquids (Roland, 2010). On the other hand, experimental data from power law density scaling of viscosity data are not conclusive for alkanes. Pensado et al. (2008) found that γ decreases for increasing alkane length, while Galliero et al. (2011) found the opposite.

A possible explanation is the fact that we compare different chain lengths at the same density and temperature. Experimental data are generally obtained around ambient temperatures and pressures. In our simulations we find that pressure is lower for the longer chains at the same density and temperature. This means that if we would compare our chains at the same pressure, the density of the longer chains would be higher, which leads to lower γ values (see section 5.3).

It might be that the Lennard-Jones chain model just does not capture the behavior of γ in real molecules correctly. For example, Tsolou et al. (2006) found $\gamma = 2.8$ from power-law density scaling of simulation data of a realistic united atom model of *cis*-1,4-polybutadiene. Chain length is far from the only variable influencing γ. Previously, Ingebrigsten et al. (2012a) found that γ decreases with increasing bond lengths in the assymetric dumbbel model, and Xu and Freed (2013) showed using the generalized entropy theory that polymer rigidity (quantified by the bending energy between consecutive bonds) significantly decreases the power law density scaling exponent γ.

5.3 Isomorphs

In this section we show that the Lennard-Jones chain liquid has isomorphs in its phase diagram. Chains of length $L = 10$ have been used for this, because these shorter chains were still reasonably fast to equilibrate at state points where the segmental dynamics start to show the typical two-step relaxation of viscous liquids. Moreover, chains of length ten have been simulated extensively in previous works (see section 5.1.1).

5.3.1 Isomorph definition

Previously, Ingebrigsten et al. (2012a) tested the isomorph theory for small molecules that were simulated with rigid bonds. Because the bonds do not scale with density, the isomorph theory was changed to include rigid molecules. For a liquid consisting of rigid molecules, configurations at two state points (1) and (2) with density ρ_1 and ρ_1 and temperature T_1 and T_2 are considered scaled versions of each other if the molecules have the same reduced position of the center of mass $\mathbf{r}_{cm}$:

$$\rho_1^{1/3}\mathbf{r}_{cm}^{(1)} = \rho_1^{1/3}\mathbf{r}_{cm}^{(1)}\,, \tag{5.19}$$

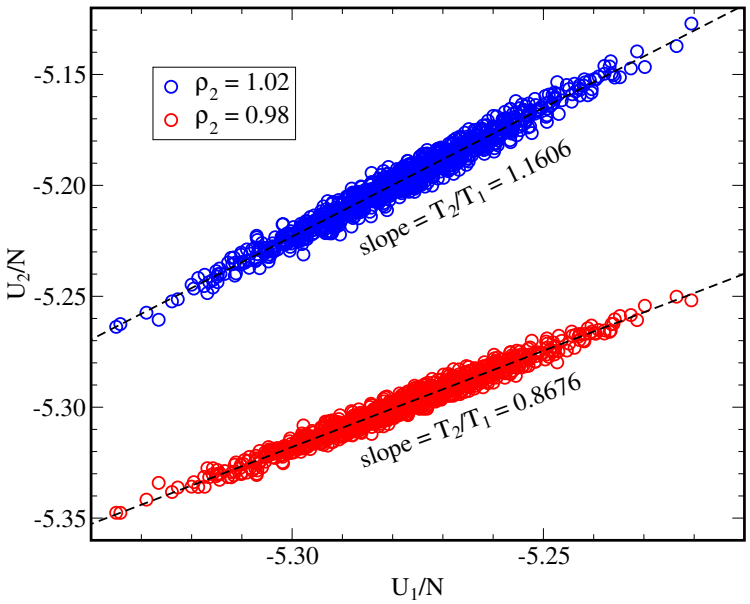

Figure 5.7: The numerical direct isomorph with Lennard-Jones chains. configurations of an equilibrium simulation at $\rho_1 = 1.00$ and $T_1 = 0.70$ were scaled to a new density ρ_2 while keeping intramolecular distances constant. From these scaled configurations we calculated U_2. The slope in the U_2, U_1-plane than gives the ration of temperatures for the isomorphic state points. We find for $\rho_2 = 0.98$ that $T_2 = 0.607$, and for $\rho_2 = 1.02$ that $T_2 = 0.8124$.

while the distances within the molecules and the orientations of the molecules are the same. Denototing the energy of two such scaled configurations U_1 and U_2, the two state points are then isomorphic to each other if each physically relevant pair of scaled configurations has proportional Boltzmann weights

$$e^{-U_1/k_BT_1} = C_{1,2}e^{-U_2/k_BT_2}\,, \tag{5.20}$$

with the same factor $C_{1,2}$ that only depends on the two state points (Ingebrigsten et al., 2012a).

This definion could then be used to perform the numerical direct isomorph check in a similar way as is done for atomic liquids. Taking the logarithm on both sides, one obtains

$$U_2 = \frac{T_2}{T_1}U_1 + k_BT_2\ln(C_{1,2})\,. \tag{5.21}$$

Thus, if one performs a simulation at state point 1 one can calculate U_2 by scaling configurations to the density at state point 2 while keeping all intramolecular distances constant. When U_2 is then plotted versus U_1, the slope simply gives fraction T_2/T_1, from which we can calculate the temperature T_2 of the isomorphic state point.

We have performed the numerical direct isomorph check exactly in this way, but now for flexible molecules. A long equilibrium simulation was performed at density $\rho_1 = 1.00$ and temperature $T_1 = 0.7$. Every 512 timesteps, the configuration was scaled to the new densities $\rho_2 = 0.98$ and $\rho_2 = 1.02$ while keeping intramolecular

distances and angles fixed. The energies U_2 were calculated from these scaled configurations. The result is plotted in figure 5.7. We find temperatures of 0.6073 and 0.8124 for the two new densities. This is very close to the 0.6033 and 0.8099 we find using the slope $\gamma = 7.36$ of the U,W fluctuations (figure 5.5). Nevertheless, we have not used this method to create the isomorphs, because it is not known if the intramolecular structure of flexible molecules is constant on the isomorph. This definition of the isomorphicc state points may therefor not be true. Moreover, our method of scaling only centers of mass to a new density cannot hold for longer chains, since it might create significant overlap of segments in different molecules.

5.3.2 Generating isomorphs

Instead of the numerical direct isomorph check we have here used the "old-fashioned" method of creating a curve of constant excess entropy S_{ex} using equation 2.19, calculating γ from the fluctuations using equation 2.5. Five different isomorphs were made, starting from five different starting state points with temperatures T_0 between 0.50 and 0.80 on the isochore $\rho_0 = 1.00$. The lengths of the simulation runs are listed in table 5.2. Before the start of the simulation, an equilibration run was done with at least the same length. Also the segmental and longest (chain) relaxation times are given in table 5.2. This shows that the simulation time for the most viscous isomorph is approximately $40\tau_R$.

After obtaining γ at the starting state point, density was changed by 0.02 and equation 2.19 was used to find the temperature with the same excess entropy. In this way a set of state points is obtained with the same excess entropy, which should be an isomorph according to the theory. As is the case with other model systems, these small density increments are necessary because γ is density dependent.

Table 5.2 also lists the smallest and largest density for each isomorph. These are the real limits of the isomorph; at densities lower than ρ_{min} we observed phase separation or the formation of cavities in the system due to too negative pressures, while at higher densities than ρ_{max} we observed crystallization. This seems to be in contradiction with the isomorph theory, which predicts that the melting line is an isomorph (Gnan et al., 2009). This prediction holds well for the single component

T_0	t	τ_0	τ_R	ρ_{min}	ρ_{max}
0.50	$1.34 \cdot 10^6$	198	$3.29 \cdot 10^4$	1.00	1.04
0.60	$6.71 \cdot 10^5$	31.6	$7.40 \cdot 10^3$	0.98	1.14
0.65	$6.71 \cdot 10^5$	18.2	$4.65 \cdot 10^3$	0.98	1.16
0.70	$3.36 \cdot 10^5$	12.1	$3.33 \cdot 10^3$	0.96	1.20
0.80	$1.68 \cdot 10^5$	6.66	$1.98 \cdot 10^3$	0.96	1.20

Table 5.2: Starting temperature T_0, simulation time t and relaxation times at the starting state points of the five isomorphs. The simulation time is the minimum time of all state points on the isomorphs. Relaxation times are determined from the segmental intermediate scattering function (τ_0) and the autocorrelation of the end-to-end vector (τ_R). ρ_{min} and ρ_{max} correspond to the lowest and highest density state point on that isomorph. All data are in standard Lennard-Jones units (not in reduced units).

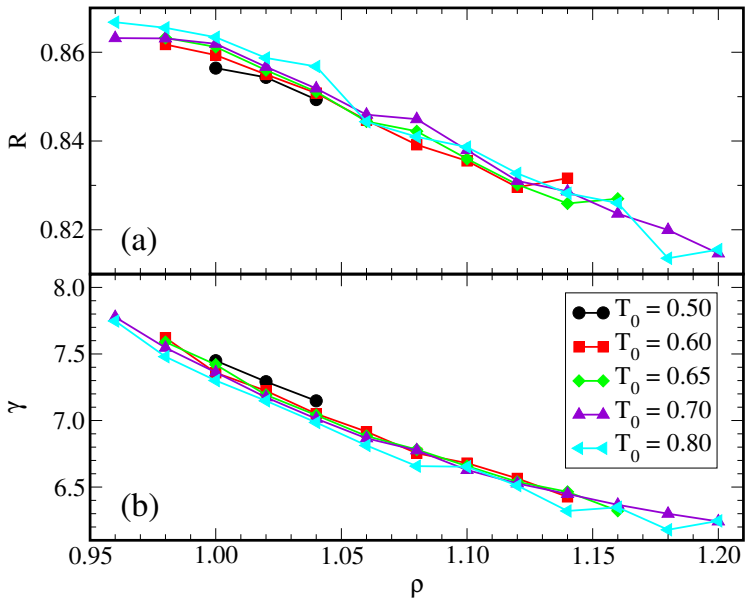

Figure 5.8: The correlation coefficient R and the slope of the fluctuations γ on the isomorphs, calculated using equations 2.4 and 2.5. The different colors correspond to the five isomorphs (see table 5.2). As for other model liquids and in agreement with the theory, γ depends only on density and not on temperature. Taken from Paper V.

Lennard-Jones liquid (Pedersen, 2013), but for the Lennard-Jones chain liquid the isomorphs cross the melting line instead of being parallel to it. We explain this by the presence of the rigid bonds, which do not scale with density, i.e., their length is not constant in reduced units. This means that at high densities, the bond length is comparable to the interparticle distance of the non-bonded particles, which is favorable for crystallization. At lower densities however, there is a discrepancy between the interparticle distances of the bonded and non-bonded particles, supressing crystallization

Figure 5.8(b) shows γ at the state points of the five isomorphs. γ ranges from 7.8 at low densities to 6.1 at high densities. This behavior is similar to the behavior of the single component Lennard-Jones liquids (Bailey et al., 2008a) and the small molecular liquids consisting of Lennard-Jones particles (Ingebrigsten et al., 2012a). The data agree with the theory in the sense that γ is only dependent on temperature, and not on density (Gnan et al., 2009; Schrøder et al., 2011). This is quantified by derivatives of γ on the isochore and isotherm. We find for the temperature dependence $\left.\frac{\partial \ln \gamma}{\partial \ln T}\right|_{\rho=1} \approx 0.05$ and for the density dependence $\left.\frac{\partial \ln \gamma}{\partial \ln \rho}\right|_{T=0.7} \approx 0.89$.

We plot the correlation coefficient R on the isomorphs in figure 5.8(a). The correlations coefficient is decreasing with density as is the case for the single component Lennard-Jones liquid (Bailey et al., 2008a, 2013). The correlation coefficient is however much lower, and even below the (somewhat arbitrary) 0.9 limit for simple liquids. Despite the low correlation coefficient, we show in the following sections that the Lennard-Jones chain can be considered a simple liquid, and that these curves of constant S_{ex} do indeed have many of the traits that isomorphs have.

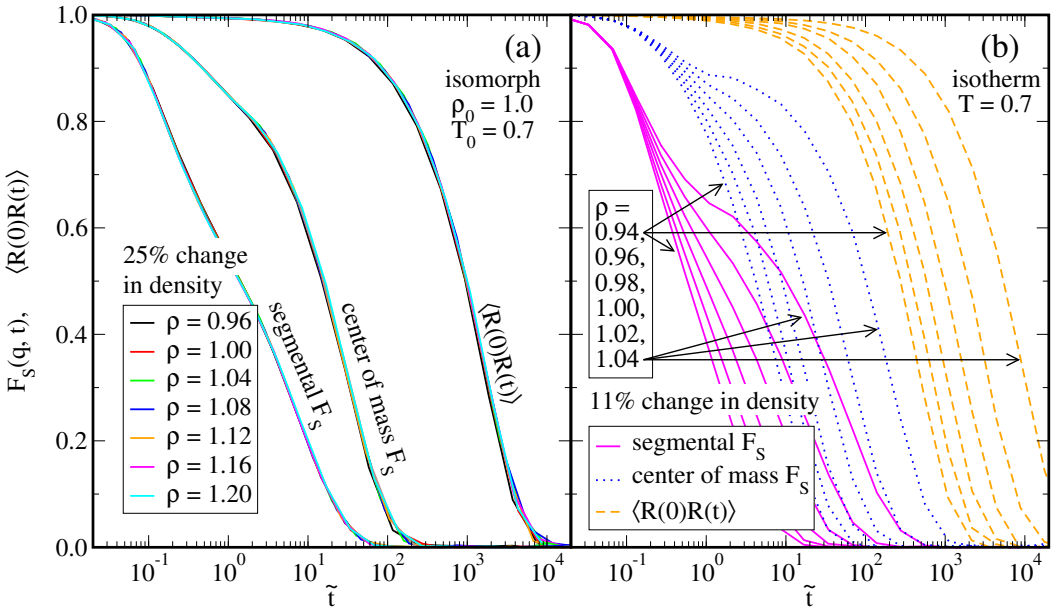

Figure 5.9: The self part of the intermediate scattering functions of the segments and the centers of mass, and the orientational autocorrelation of the end-to-end vector on the isomorph with $T_0 = 0.7$ (a) and on an isotherm for comparison (b). For each of these dynamical measures, the data at the isomorphic state points collapse when plotted in reduced units, in contrast to the isothermal state points in (b). We kept the wave vector constant in reduced units at $\tilde{q} = \rho^{1/3}q = 7.09$, which is close to the position of the main peak in the static structure factor. Adapted from Paper V.

5.3.3 Equilibrium dynamics on the isomorph

The first isomorph prediction we verify is the invariance of the dynamics in reduced units. In figure 5.9(a) we probe the dynamics at three different time and length scales for one of the isomorphs. The segmental and center of mass intermediate scatter function $F_S(\tilde{q}, \tilde{t})$ and the orientational autocorrelation of the end-to-end vector $\langle \mathbf{R}(0)\mathbf{R}(\tilde{t})\rangle$ collapse on a single curve for the isomorphic state points. Especially when we compare the dynamics on the isomorph to the dynamics on the isotherm (figure 5.9(b)) the collapse is striking. On the isotherm, an 11% change in density changes the dynamics by more than a decade, while the dynamics on the isomorph are invariant over a 25% change in density.

Figure 5.10 shows the self part of the segmental intermediate scattering function as well as the end-to-end vector autocorrelation for all five isomorphs. The data show that both the segmental and the chain dynamics are invariant in a significant part of the phase diagram; from high temperature non-viscous state points to viscous state points where the dynamics show the typical two-step relaxation. For the most viscous isomorph with $T_0 = 0.5$, the end-to-end-vector autocorrelations do not fall exactly on top of each other. This is probably caused by a too short simulation or equilibration time (see table 5.2). The liquid may not be completely in equilibrium, or the data may not have been averaged over long enough time scales.

In figure 5.9 and 5.10 we have plotted the self intermediate scattering function

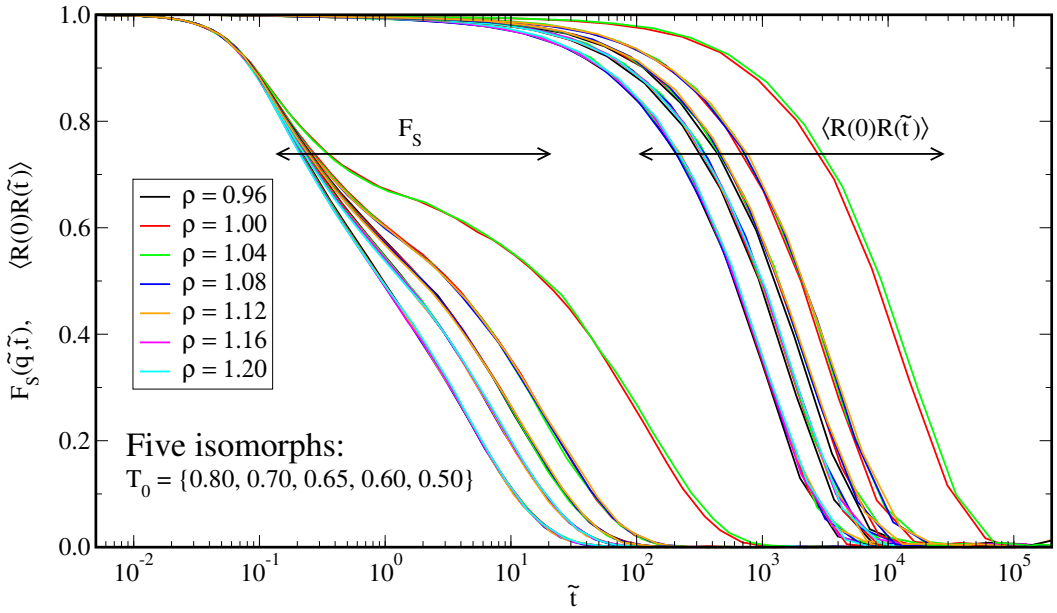

Figure 5.10: The self part of the segmental intermediate scattering function and the autocorrelation function of the end-to-end vector for all five isomorphs, plotted versus reduced time.

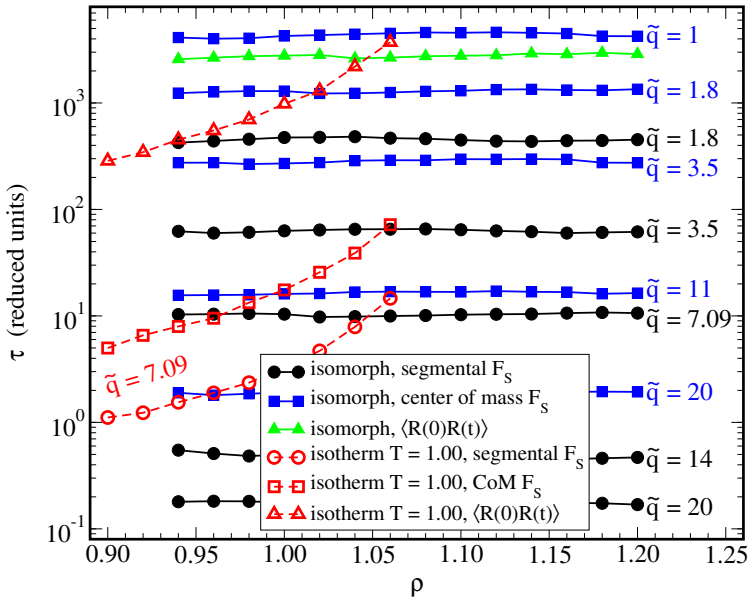

Figure 5.11: Reduced relaxation times obtained from the segmental self intermediate scattering functions for different reduced scattering vectors $\tilde{q}$. On the isomorph, the relaxation times corresponding to different length scales are constant. Red open symbols are for an isotherm and are not constant. Taken from Paper V.

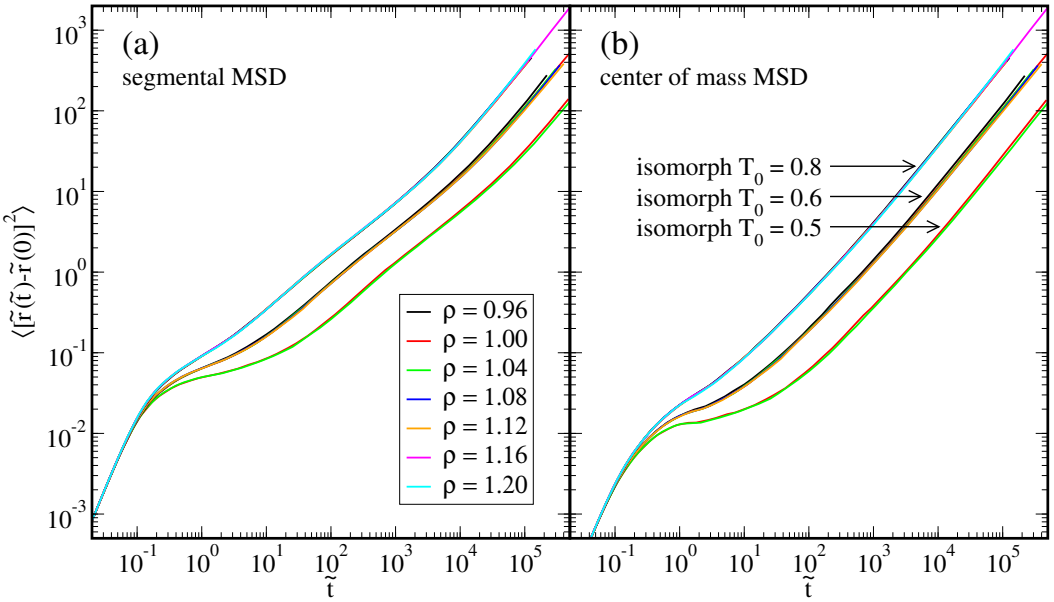

Figure 5.12: The segmental (a) and center of mass (b) mean square displacement for three of the five isomorphs with $T_0 = \{0.5, 0.6, 0.8\}$. Both the mean square displacement and time are in reduced units. For each isomorph, the data of the different state point collapse.

for only one value of the magnitude of the reduced scattering vector $\tilde{q}$. We now compare the dynamics for different wavevectors by plotting the relaxation times obtained from the self intermediate scattering vectors in figure 5.11. The relaxation times are defined as the time at which the scattering function has decayed to 0.2. For all tested wavevectors the reduced relaxation time is constant on this particular isomorph. For comparison, we included the relaxation times obtained from the isothermal scattering functions in figure 5.9.

The invariance of the dynamics is also confirmed by plotting the mean square displacement in reduced units (figure 5.12). The movement of the molecule as a whole, as probed by the center of mass displacement, and the movement of the segments collapse for all five isomorphs (only three isomorphs are shown for clarity). The invariance holds for all three regimes of the segmental mean square displacement, including the subdiffusive regime at intermediate times that is typical for chain molecules. The fact the curves collapse in the diffusive regime at long time means that also the diffusion coefficient in reduced units is invariant as predicted by the theory.

As mentioned in section 5.1.3, the dynamics of chain molecules are often expressed in terms of the Rouse modes (equation 5.10). We plot the normalized autocorrelations of the Rouse modes $\langle \mathbf{X}_p(t)\mathbf{X}_p(0)\rangle$ in figure 5.13. The Rouse modes correspond to the movement of subchains of L/p segments, so the autocorrelation function of the first mode is almost the same as the autocorrelation of the end-to-end vector (Doi and Edwards, 1986), and indeed they have the same relaxation time. Also the Rouse mode autocorrelation functions collapse for isomorphic state points. For the higher modes however, the collapse is not as good. This is

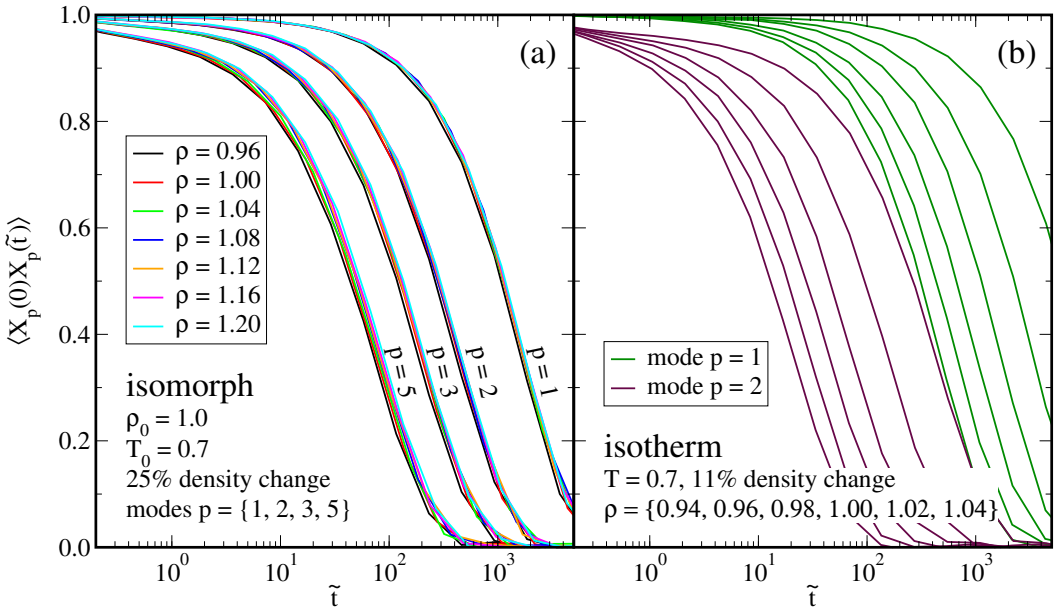

Figure 5.13: Auto-correlation functions of some of the Rouse modes on the isomorph with $T_0 = 0.7$ (a). Only the modes with $p = 1, 2, 3, 5$ are shown. The collapse is good on the isomorph, but gets a little bit worse for the higher modes. (b) On the isotherm none of the Rouse modes collapse. Adapted from Paper V.

probably not relevant for the overall dynamics, since it is not seen in any of the previous figures in this section. Moreover, these higher modes do not contribute much to the dynamics; the amplitude of the Rouse modes is predicted to scale as $\langle \mathbf{X}_p^2 \rangle \propto 1/(L \sin^2(p/L))$ (Bennemann et al., 1999d), which is also seen in our simulations (data not shown).

5.3.4 Structure on the isomorph

We now test the prediction that the liquid structure is invariant on the isomorph. Traditionally this is done for atomic liquids by plotting the radial distribution function $g(\tilde{r})$ in reduced units. We also plotted this for the segments of the chain in figure 5.14(a). Due to the bond lengths, which are constant in real units but not in reduced units, the total segmental distribution function is not invariant on the isomorph. The delta functions around $\tilde{r} \approx 1$ are the most obvious, but also around $\tilde{r} \approx 2$, there is an effect of the next-nearest neighbors in the chain. For this reason we split the radial distribution in an intermolecular and an intramolecular contribution, plotted in figures 5.14(b) and (c), respectively. The intramolecular $g(\tilde{r})$ is clearly less invariant than the intermolecular $g(\tilde{r})$.

We also plotted the radial distribution function of the centers of mass in figure 5.14(d). These are invariant as well on the isomorph, but when compared with isothermal density changes the invarance is not surprising. It seems that the distribution of the centers of mass is not dependent on state point at all when plotted in reduced units.

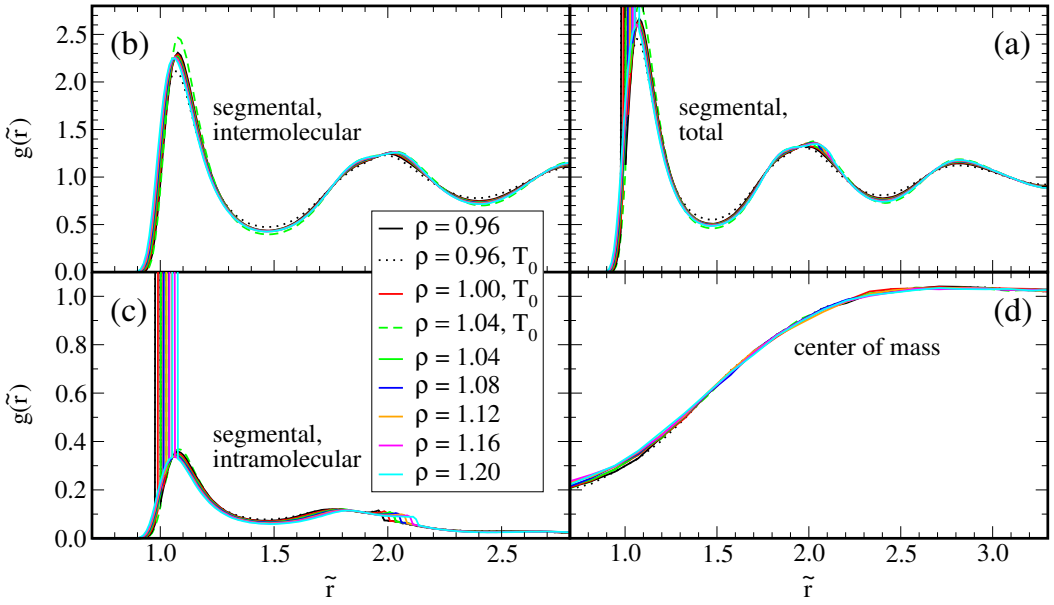

Figure 5.14: Four different radial distribution functions on the isomorph with $T_0 = 0.7$. (a) The total segmental distribution function, which has been split into contributions of the particle pairs in different molecules (b) and the contributions from the pairs in the same molecule (c). (d) The radial distribution function of the center of mass. The isomorphic state points (solid lines) collapse reasonably for the total and intermolecular distributions. Small deviations from collapse of the total radial distribution function are caused by the intramolecular contribution. The center of mass distribution function is invariant on the isomorph, but is not state point dependent at all when plotted in reduced units. Two isothermal state points are included in each plot for comparison (dotted and dashed lines). Data in (b) and (c) taken from Paper V.

In figure 5.15 we plot two more quantities related to the molecular structure, the mean square end-to-end distance $\langle \mathbf{R}^2 \rangle$ and the mean square radius of gyration $\langle R_g^2 \rangle$. These are clearly not invariant on the isomorph. Comparison with isothermal data, these quantities seem to be purely dependent on density. Comparison with isochoric data indeed shows that there is only a small dependence on temperature on the isochore. Moreover, any temperature dependence on the isochore may be caused by the fact that the molecular structure has not completely equilibrated. Bennemann et al. (1999c) also noted that the size of the molecule is not dependent on temperature.

In conclusion, the structure is not completely invariant on the isomorph, especially compared to the atomic liquids. This is not surprising, since the bonds do not scale with density. The effect of the bonds is however completely captured by the intramolecular structure, leaving the intermolecular structure invariant on the isomorph.

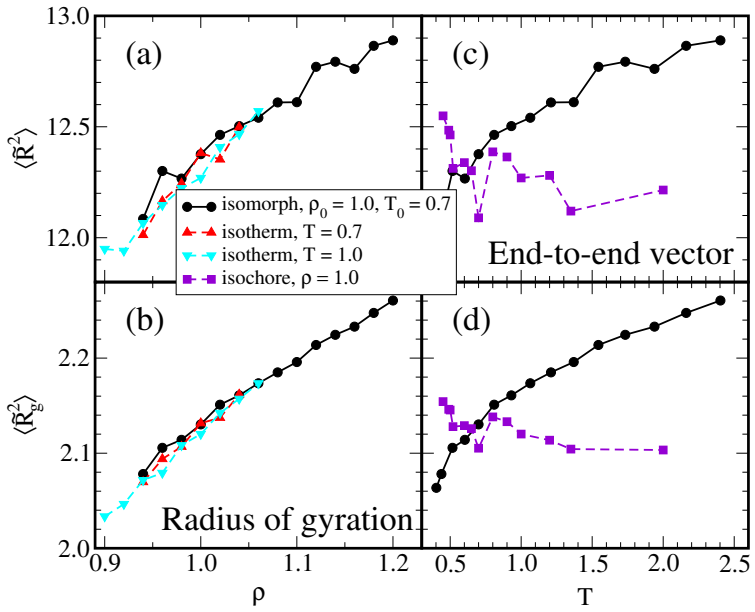

Figure 5.15: The mean square end-to-end distance, and the mean square radius of gyration of the molecules in reduced units. Black circle are data for the isomorph with $T_0 = 0.7$. These quantities are not invariant on the isomorph, their density dependence is the same as on the isotherm, indicating that the quantities only depend on density. The isochoric data indeed do not change very much, although there is a lot of noise in the data. The low temperature data may have the additional problem that they system has not equilibrated long enough. The increase in the molecular size with increasing density may seem counter-intuitive, but is an effect of the reduced units. When plotted in standard units, the molecular size does in fact decrease with density. Taken from Paper V.

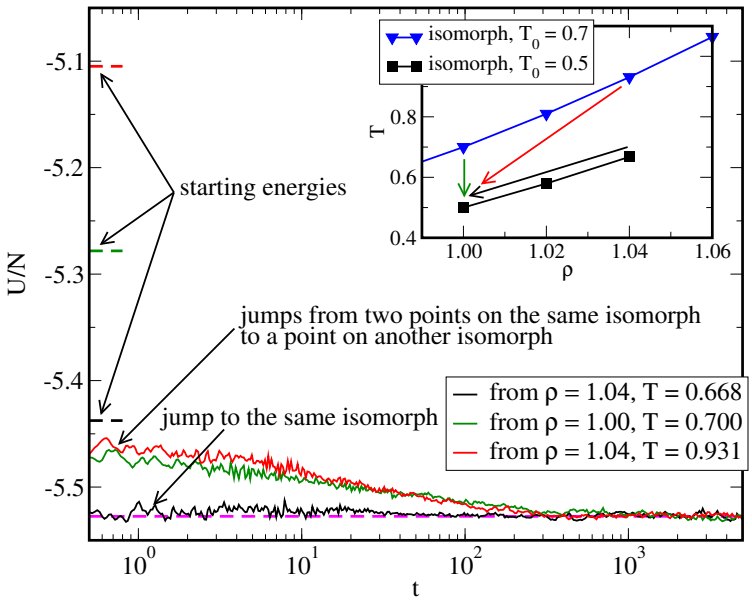

Figure 5.16: The relaxation of the potential energy after three different instantaneous jumps in the phase diagram. All three jumps are towards the state point $\rho = 1.00$, $T = 0.5$. The jump from the same isomorph (black line) does not show any relaxation in the potential energy. The other two jumps are from the isomorph with $T_0 = 0.7$, and show a similar relaxation in potential energy. Each relaxation curve is the average of eight simulations with independent starting configurations. The inset shows the jumps in the ρ,T phase diagram. The dashed lines show the average energies before the jumps. Adapted from Paper V.

5.3.5 Non-equilibrium dynamics on the isomorph

Because isomorphic state points have proportional Boltzmann factors for all configurations, it is possible to scale an equilibrium configuration from one state point to another on the same isomorph while staying in equilibrium (Gnan et al., 2009). We show this by performing different instantaneous jumps between equilibrium configurations. When jumping to another density, we scale only the box with the centers of mass of the molecules. The intramolecular distances are kept constant as in the formal definition of the isomorphs by Ingebrigsten et al. (2012a), and to satisfy the constraints.

We plot the relaxation of the of the potential energy after the isomorphic jump in figure 5.16 (black line). The average potential energy before the change in density is shown by the black dashed line, while the average equilibrium energy of the state point that is jumped to is given by the pink dashed line. Even though the state points have different average energies, there is no relaxation when jumping between them, especially when compared to jumps from state points that are on another isomorph (black and red lines).

Jumping from two isomorphic state points to a third (non-isomorphic) state point will give the same relaxation, because scaling an equilibrium configuration anywhere on an isomorph will give an equilibrium configuration at the new den-

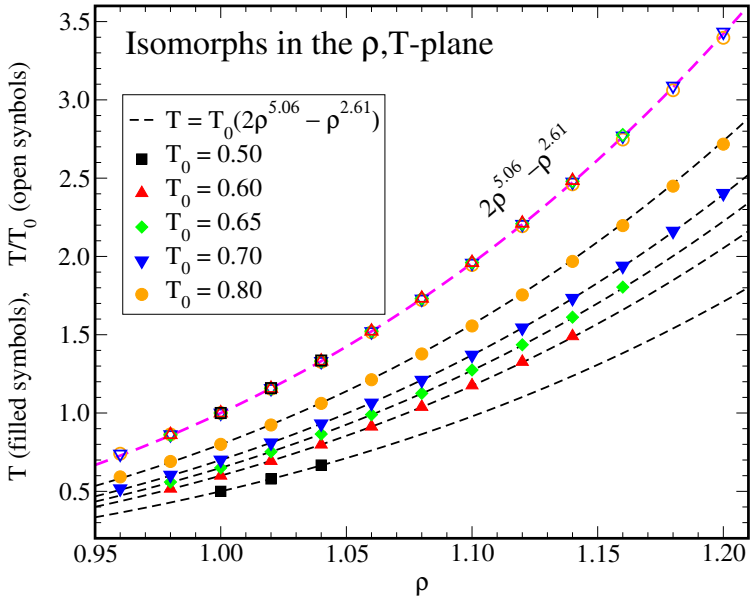

Figure 5.17: All five isomorphs in the ρ,T phase diagram (filled symbols). The isomorph can be scaled by the initial temperature to collapse on a single curve (open symbols), the shape of which is given by $h(\rho)$. Fitting to a sum of power laws gave us $h(\rho) = 2\rho^{5.06} - \rho^{2.61}$ (dashed lines). Taken from Paper V.

sity (Gnan et al., 2010). This is shown by the green and the red curves in figure 5.16, which show the relaxation in the potential energy when jumping from two state points on the isomorph with $T_0 = 0.7$, to a point that is not on the isomorph (at $\rho = 1.00$, $T = 0.5$). The data show that even though the two state points have different equilibrium energies before the jump (dashed red and green lines), they have the same energy immediately after the jump. The relaxation is then the same for both starting state points.

It should be noted that since the intramolecular structure is not invariant on an isomorph, some relaxation of the individual chains will still occur, but this does not seem to have an effect on the potential energy of the system.

5.4 Isomorphic scaling

According to the theory, the shape of the isomorphs in the phase diagram is described by $h(\rho)$ with a multiplicative constant T_0 (see equation 2.25). It is easy to The isomorphs therefore have the same shape, as shown in figure 5.17. It is possible to scale the isomorphs with their starting temperature T_0 to collapse on a single curve (open symbols).

For particles interacting with (sums of) inverse power laws, the functional form of $h(\rho)$ is known. For instance, for the single component Lennard-Jones liquid, $h(\rho) = \alpha\rho^4 + (\alpha - 1)\rho^2$ (Bøhling et al., 2012; Ingebrigtsen et al., 2012). Due to the rigid bonds, we do not have an analytical expression $h(\rho)$, and it is found that the $h(\rho)$ from the single component Lennard-Jones liquid does not describe the shape

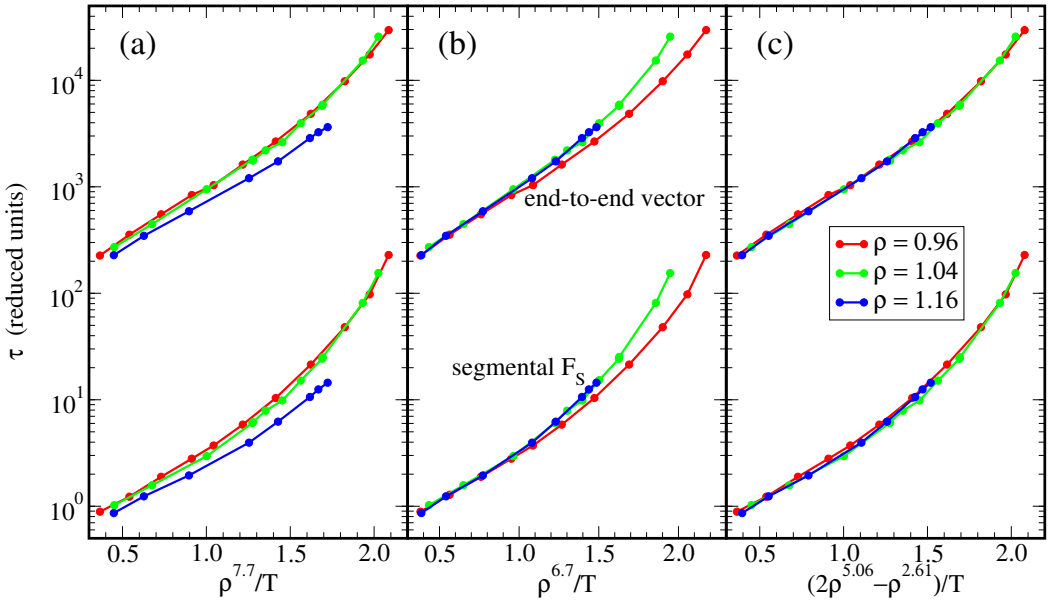

Figure 5.18: Relaxation times from the end-to-end autocorrelation (top) and the segmental intermediate scattering function (bottom). In (a) and (b) attempts are made to collapse the relaxation times of different isochores onto a single master curve by power law density scaling. This is not possible, $\rho^{7.7}$ collapses only the low density isochores, while $\rho^{7.7}$ collapses the high density isochores. When using equation 5.22, the data collapse well over the entire density range. Adapted from Paper V.

of Lennard-Jones chain isomorphs correctly. Instead, we have fitted the shape of the isomorphs with a function of the form $h(\rho) = 2\rho^{\alpha} - \rho^{\beta}$ where α and β are fitting parameters. The choice of the functional form is rather arbitrary; there is no reason why $h(\rho)$ should be a sum of two power laws. Nonetheless, this function with $\alpha = 5.06$ and $\beta = 2.61$ was found to fit the isomorphs well (pink dashed line in figure 5.17. The shape of each isomorph is thus described by the function

$$h(\rho) = T_0 \left(2\rho^{5.06} - \rho^{2.61}\right) , \tag{5.22}$$

shown as black dashed lines in figure 5.17.

Our empirical $h(\rho)$ indicates that power law density scaling may not work for the Lennard-Jones chain system. We test this in figure 5.18(a) and (b) by plotting the segmental and chain relaxation times of three isochores. We plot the relaxation times versus ρ^{γ}/T for two values of γ. The higher γ collapses the relaxation times for the two lowest densities, while the low γ works for the high densities. This is in agreement with the γ values obtained from the fluctuations, where we find higher values for the lower densities (figure 5.8). It is however not possible to scale all three isochores on top of each other with a single power law. Instead, this can be achieved by using our empirical $h(\rho)$ (equation 5.22), which collapses all three isochores perfectly. The scaling works for both the fast segmental dynamics, as well as for the slow chain dynamics, which is also found to be the case for power law density scaling of polymers over a small range of densities (Casalini and Roland,

2005; Roland, 2007; Roland et al., 2004).

5.5 Conclusion

The Lennard-Jones chain liquid with rigid bonds is simple in part of its phase diagram. For all chain lengths simulated we found correlations in the fluctuations of the viral and the potential energy. Although the correlation coefficient is lower than 0.9, the fluctuations can still be used to trace out isomorphs in the phase diagram.

On the isomorph, both the segmental and the chain dynamics are invariant in reduced units. Indeed all dynamics are invariant. Because γ is found to change with density, power law density scaling does not hold in the density range that was simulated. Although no analytical expression for $h(\rho)$ exists for the model, the empirical expression $h(\rho) = 2\rho^{5.06} - \rho^{2.61}$ can be used to collapse the dynamics of the entire density range.

Not all structure in the liquid is constant on the isomorph, due to the fixed bond length that does not scale with density. However, we have shown that this is captured completely in the structure within the chain. Intermolecular structure is constant, while intramolecular structure like the molecular size is not. Also the non-equilibrium dynamics, probed by the relaxation of the potential energy after a jump in the phase diagram is found to obey the isomorph theory.

Chapter 6

Isomorphs in the phase diagram of flexible Lennard-Jones chains.

II. Results for harmonic bonds

6.1 Introduction

Although the Lennard-Jones chain model has been used extensively in the field of (glass-forming) liquids and polymers, different versions of the model have been simulated. Apart from the length of the chain, which is often varied depending on the system under investigation and the technical capabilities, the bond type is another property which often differs between works.

In the field of chemical and biochemical Molecular Modelling, one generally uses empirical force fields to paramerize the different interatomic interactions (Leach, 2001). Both all atom and united atom force fields (Brooks et al., 2009; Cornell et al., 1995), as well as coarse grained force fields (Marrink et al., 2007) approximate the covalent bonds by a harmonic potential, given by

$$v_{ij}(r_{ij}) = -0.5k(r_{ij} - r_0)^2 \,. \tag{6.1}$$

where k is the spring constant and r_0 is the reference bond length where the bond energy is zero. The harmonic bond has the advantage that it is fast to calculate, and it is easily parameterized using the reference bond length. Although it does not take into account the anharmonicity of real covalent bonds, it is usually a reasonable approximation because the deviations from harmonicity are small or not relevant when simulating equilibrium configurations (Leach, 2001).

On the other hand, Grest and Kremer (1986) used a finitely extensible nonlinear elastic (FENE) potential in their original simulations of Lennard-Jones chains. The FENE potential is given by

$$v_{ij}^{FENE}(r_{ij}) = -0.5kr_{max}^2 \ln\left[1 - \left(\frac{r_{ij}}{r_{max}}\right)^2\right] , \tag{6.2}$$

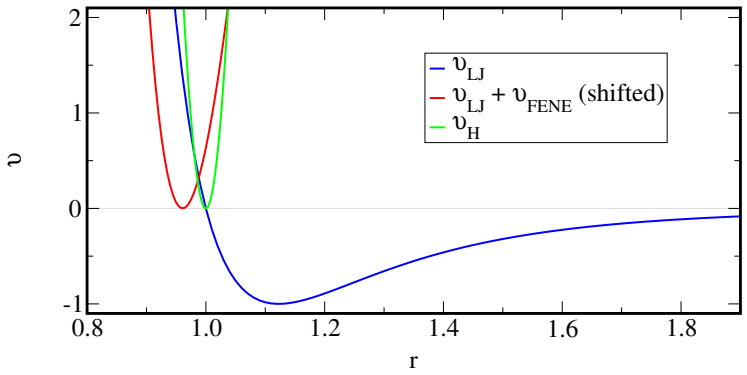

Figure 6.1: Comparison between the FENE potential and the harmonic potential for bonded particles as used in Lennard-Jones chains. The FENE potential is always used in addition to a potential with repulsion, in this case the Lennard-Jones potential. The FENE potential has a spring constant $k = 30\epsilon_{LJ}$ and a maximum bond length $r_{max} = 1.5\sigma_{LJ}$., resulting in a potential minimum around $0.96\sigma_{LJ}$ for low pressures. The harmonic potential has a spring constant of $k = 3000\epsilon_{LJ}$ and a bond length $r_0 = \sigma_{LJ}$.

where k_s is the spring constant and r_{max} is the maximum bond length. The FENE potential was proposed as an empirical bond potential that behaves as an harmonic spring and therefore gives a Gaussian bond length distribution at small bond lengths ($r_{ij}/r_{max} < 0.2$), but becomes stiffer at larger bond lengths (Warner, 1972). This second property has been of importance in the theory of coarse-grained bead-spring polymer models, because it prevents the chain to from being stretched to infinite length (Bird et al., 1987).

The potential is purely attractive, and is therefore often used in addition to another potential to prevent particle overlap. For the Lennard-Jones chain, the repulsion is provided by including the Lennard-Jones interaction for the bonded particles: $\upsilon_{ij} = \upsilon_{ij}^{FENE} + \upsilon_{ij}^{LJ}$. The FENE bonds in the Lennard-Jones chain have a spring constant $k = 30\epsilon_{LJ}$ and maximum bond length $r_{max} = 1.5\sigma_{LJ}$. This results in a potential minimum for a bond length of about 0.96 (see figure 6.1). This choice of potential parameters leads however to non-Gaussian bond length distributions.

More recent simulations of Lennard-Jones chains have also used harmonic bonds, and in that case have a spring constant of $k = 3000\epsilon_{LJ}$ and a reference bond length of $r_0 = \sigma_{LJ}$ (Riggleman et al., 2009, 2010; Shavit et al., 2013). In figure 6.1 this potential is plotted, together with the FENE bond an the Lennard Jones potential. As can be seen the harmonic bond is longer than the FENE bond, and more narrow. Both bonds are shorter than the average interparticle distance in the low pressure liquid. The different bond length will probably have a significant effect on the molecular structure. On the other hand, the Lennard-Jones chain with harmonic bonds is expected to have very similar behavior to the Lennard-Jones chain with rigid bonds, due the the similar bond length and the narrow potential of the potential well. The Harmonic bond was therefore chosen for comparison with the rigid bond results from the previous chapter.

Section 6.1.1 shows the effect of bond type on the dynamics, structure, and fluc-

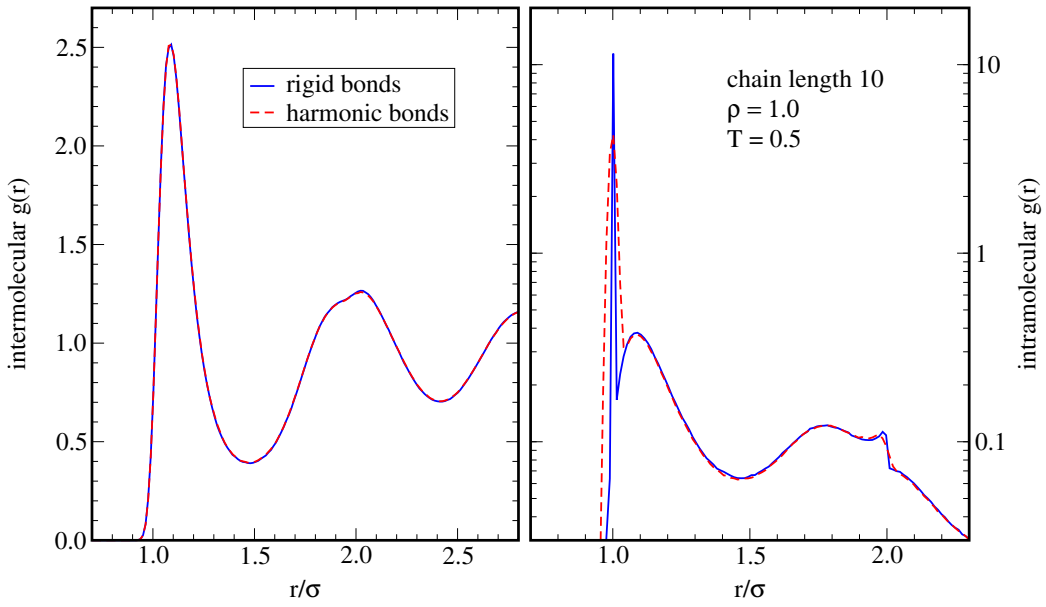

Figure 6.2: The intermolecular (left) and intramolecular (right) radial distribution functions for chains with rigid (blue solid lines) and harmonic (dashed red lines) bonds. The intermolecular structure is identical for both bond types. The intramolecular structure is slightly different, mainly due to the bond length distribution for the harmonic bonds.

tuations of the Lennard-Jones chain liquid. The following sections discuss different methods to obtain isomorphs for the liquid with harmonic bonds.

6.1.1 Rigid bonds versus flexible bonds

Since the rigid and harmonic bonds have the same length, the difference in the overall liquid structure is expected to be minimal. This is indeed the case for the intermolecular radial distribution function $g(r)$ plotted in figure 6.2. When varying only the bond type, the intermolecular $g(r)$ is unchanged. The only structural effect of the harmonic bonds can be seen in the intramolecular $g(r)$, where a widening of the bond peak can be seen.

Figure 6.3 shows the effect of the bond type on the dynamics, in this case the segmental and center of mass incoherent intermediate scattering function $F_S(q,t)$ and the orientational autocorrelation function of the end-to-end vector $\langle \mathbf{R}(0)\mathbf{R}(t)\rangle$. Here the bond type causes bigger differences. For the high temperature ($T = 0.7$) state point, the dynamics are slightly but visibly faster for the harmonic bonds. However, when temperature is decreased towards a more viscous state point ($T = 0.5$), the effect of bond type becomes more pronounced.

So far the effect of bond type on the liquid seems qualitatively very small. There is however a big effect on bond type that becomes immediately apparent when looking for strong correlations. In chapter 5 it was shown that the rigid bonds have correlations between their potential energy U and virial W, albeit not as strongly as many atomic liquids. For the state point $(\rho, T) = (1, 0.7)$ The correlation coefficient

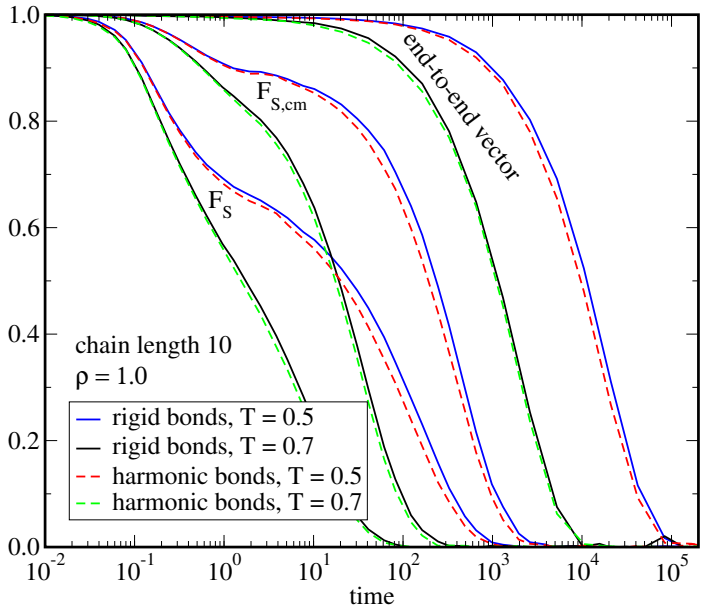

Figure 6.3: The effect of bond type on the liquid dynamics. The segmental and center of mass incoherent intermediate scattering function $F_S(q,t)$ as well as the orientational autocorrelation of the end-to-end vector are plotted for rigid bonds (solid lines) and harmonic bonds (dashed lines). For the lower temperature ($T = 0.5$, red and blue lines) there is bigger difference than for the higher temperature ($T = 0.7$, black and green lines).

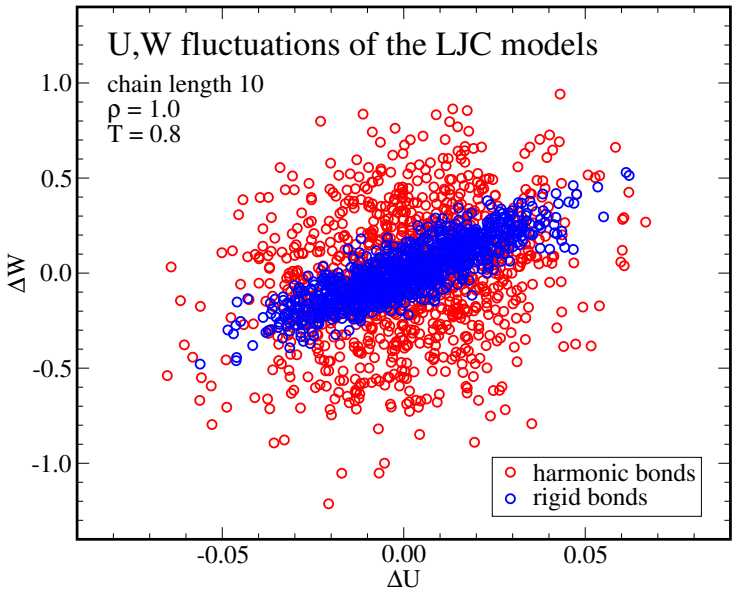

Figure 6.4: Scatter plots of the potential energy U and virial W equilibrium fluctuations for different bond types. The data have been normalized ($\Delta U = U - \langle U \rangle$). Where the rigid bond simulations (blue points) still have U, W correlations, the use of harmonic bonds (red points) removes the correlations completely.

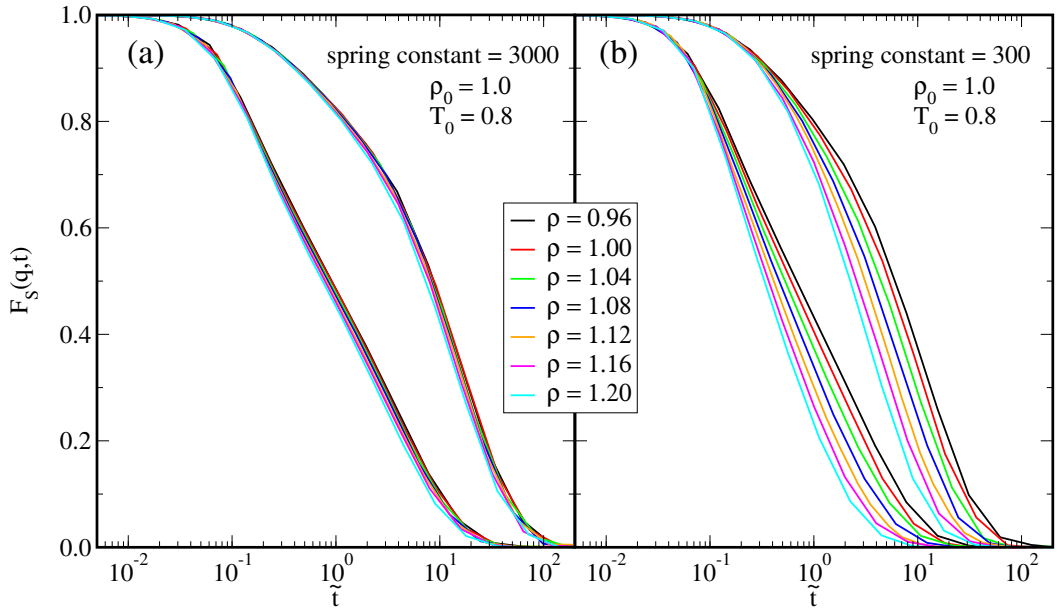

Figure 6.5: State points from the rigid bond chain isomorph with starting state point $\rho_0 = 1.0, T_0 = 0.8$, now simulated with harmonic bonds. (a) With a spring constant of $k = 3000$, the dynamics are slightly less invariant than for the rigid bonds. (b) With more flexible bonds (spring constant $k = 300$) the dynamics become much less invariant.

was $R = 0.86$ and the slope $\gamma = 7.36$. Figure 6.4 shows that these correlations completely disappear when using harmonic bonds. For the same state point we find for the harmonic bonds $R = 0.28$ and $\gamma = 4.36$. This value of γ cannot be used to trace out an isomorph, it leads to dynamics that are far from invariant. The absence of correlations raises the question if any of the molecular liquids that are simulated using flexible bonds have correlations and/or conform to the isomorph theory.

6.2 Simulating rigid bond isomorphs using flexible bonds

Since the differences in the dynamics of the chains with rigid bonds and harmonic bonds is small, an obvious first attempt to obtain an isomorph with the harmonic springs, is to use the same isomorphic state points as the rigid bond isomorph. In order for this to work, the shape of the isomorphs, $h(\rho)$, has to be the same for the rigid bonds and the harmonic bonds. The small difference in the dynamics in figure 6.3 is not necessarily a problem if this difference is constant along the isomorph.

Figure 6.5(a) shows the dynamics of the harmonic bond chain at the state points of the least viscous isomorph from chapter 5 (with $\rho_0 = 1.0, T_0 = 0.8$). For the stiff spring with spring constant $k = 3000$, the collapse of the curves is not perfect, but the dynamics are reasonably similar. For the more flexible harmonic bonds however, the set of state points clearly does not resemble a curve with invariant dynamics. The chains with harmonic spring thus have dynamics that are not only faster than

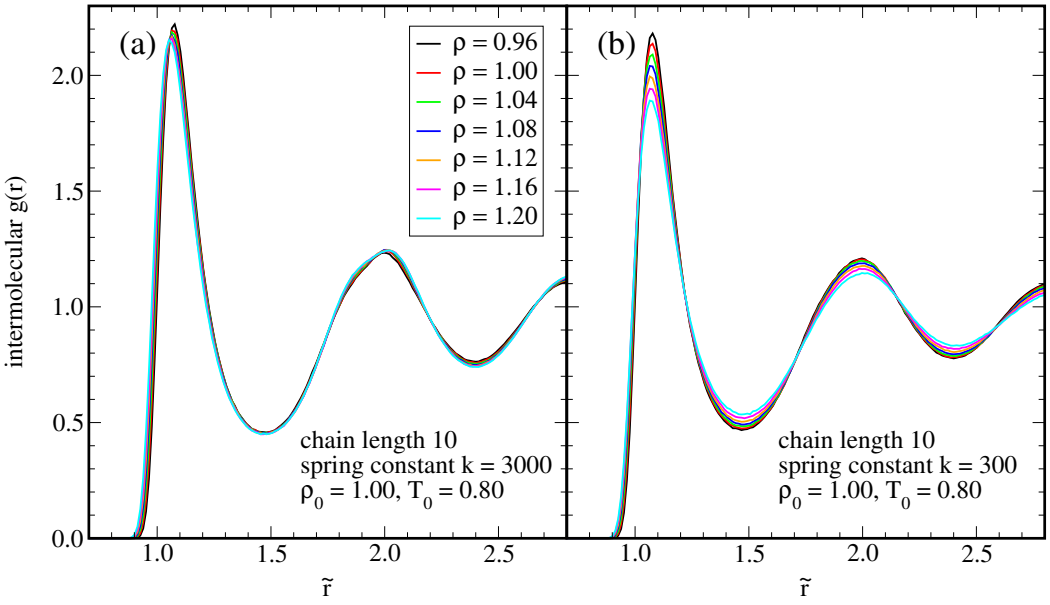

Figure 6.6: The intermolecular structure for chains with harmonic bonds with spring constants $k = 3000$ (a) $k = 300$ (b). The state points simulated are the state points of the isomorph for rigid bond chains which starts at $\rho_0 = 1.0, T_0 = 0.8$. The collapse is not perfect; for the high spring constant the left side of the first peak seems to shift slightly, for the low spring constant the height of the peaks changes significantly.

the dynamics of rigid bond chains (figure 6.3), but also have a different state point dependence. In other words, curves of invariant dynamics are not described by the same $h(\rho)$ for the different bond types.

We now investigate the structure for the same set of state points for both spring constants by calculating plotting the intermolecular radial distribution function (figure 6.6). Here there is no obvious difference between the chains with the harmonic bonds, and the isomorph of the rigid bond chains. So the observation that rigid bonds have the same intermolecular structure as stiff harmonic bonds seems to be correct over a large range of densities. The simulations of the low spring constant obviously different; here the it is especially the peak height that changes.

If we go to more viscous isomorphs, where the dynamics are more temperature dependent, the difference between rigid and harmonic bonds becomes even more pronounced. Figure 6.7 shows the dynamics and the structure of the harmonic bond chain with spring constant $k = 3000$ at the state points from the rigid bond isomorph with $\rho_0 = 1.0, T_0 = 0.7$. The spread of the intermediate scattering functions is larger than in figure 6.5(a) and it is quite safe to assume that this will only be worse when going to more viscous state points.

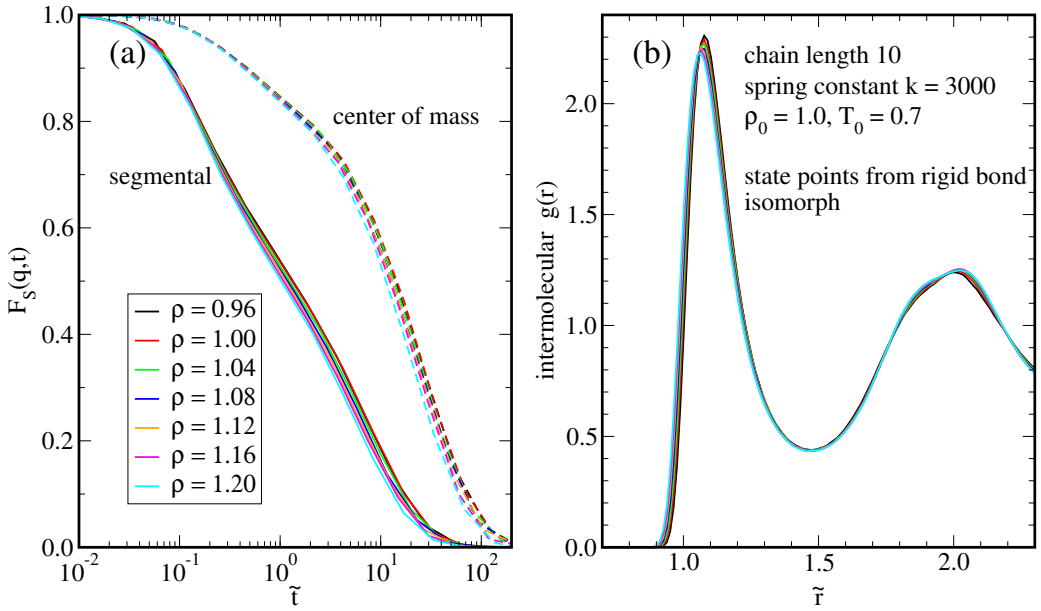

Figure 6.7: State points from the rigid bond chain isomorph that was started at $\rho_0 = 1.00$, $T_0 = 0.7$, simulated with harmonic bonds with spring constant $k = 3000$. (a) Especially for the dynamics, it is clear that the invariance is less at these lower temperatures then at the higher temperature state points of figure 6.5(a). (b) The collapse of the intermolecular radial distribution functions is not very good at these state points.

6.3 Density scaling of Lennard-Jones chains with harmonic bonds

So far we have found that the chains with stiff harmonic bonds have similar behavior to the chains with rigid bonds. Apart from the absence of potential energy-virial correlations, the dynamics are a little bit faster and have a different density dependence. We therefore expect that also Lennard-Jones chains with flexible bonds should have isomorphs in their phase diagram, at least if isomorphs are defined as curves in the phase diagram along which structure and dynamics are invariant. However, due to the lack of correlations between the potential energy and virial fluctuations, it is not possible to use equation 2.5 to obtain the scaling exponent γ from the fluctuations. Moreover, it is not possible to use the numerical direct isomorph check (equation 2.15) by scaling the simulation box to a different density during the simulation, because it is known that the intramolecular structure, and especially the bonds do not scale with density.

Instead, we have attempted to use a more "old fashioned" approach to obtain curves of invariant dynamics. Where in section 5.4 we used our $h(\rho)$ obtained from the isomorphs to scale the dynamics at different isochores on to of each other. We now do the opposite by empirically scaling the dynamics of harmonic bond chains to obtain values of $h(\rho)$.

The relaxation times as determined from the segmental incoherent intermediate scattering function and the orientational autocorrelation function of the end-to-end

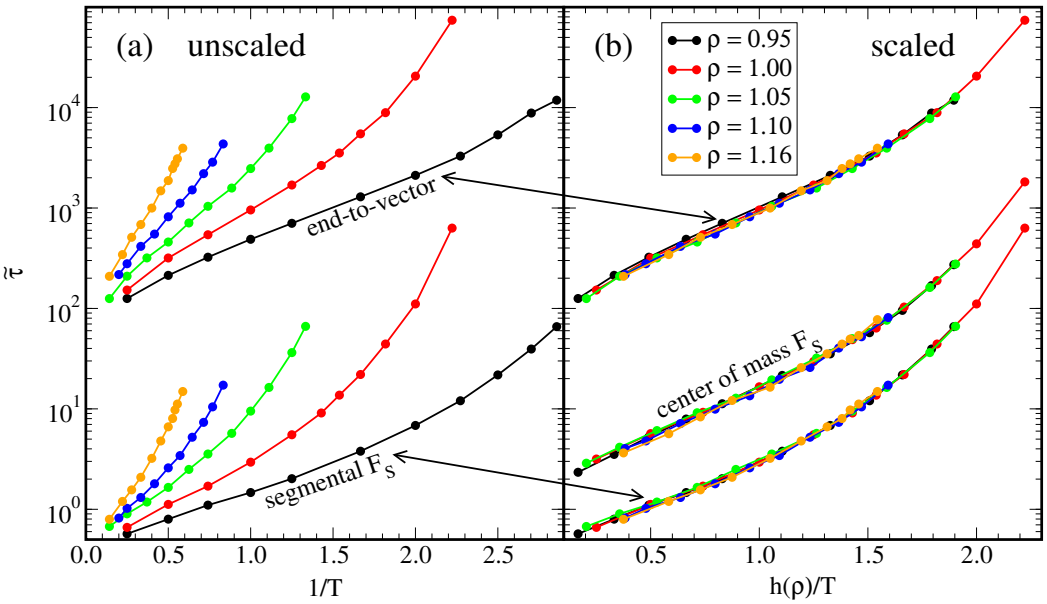

Figure 6.8: Density scaling of the (reduced) relaxation time for the harmonic bond chains. On the left the unscaled data from the segmental incoherent intermediate scattering function and the orientational autocorrelation of the end-to-end vector are shown for different isochores. On the right, the segmental relaxation data have been scaled by hand to obtain some values for $h(\rho)$, and the other measures of relaxation times have been scaled by the same factor.

vector are shown for five different isochores in figure 6.8(a). Again it was not possible to go to the higher relaxation times for all densities due to phase separation (or negative pressure) at low densities and crystallization at high densities. Nevertheless a large range of relaxation times could be reached for some densities. Each isochore was then scaled by hand to collapse onto the $\rho = 1.00$ isochore, using $h(\rho)$ as a scaling parameter. Thus for each isochore, a scalar h was chosen by hand to collapse the relaxation times. The result of the scaling is plotted in figure 6.8(b), showing a good collapse.

The $h(\rho)$ that is thus obtained for the harmonic bond chain is compared with the $h(\rho)$ of the rigid bond chains in figure 6.9. There is a noticeable difference in the shapes of $h(\rho)$ for the two models. The Difference is most obvious at high density, where the harmonic bond $h(\rho)$ is lower than the rigid bond $h(\rho)$. This is in agreement with the data in figure 6.7, that show that the rigid bond $h(\rho)$ results in too fast dynamics for the harmonic spring isomorph at high density, which means that the temperature is too high at those state points. Again, we fit the $h(\rho)$ values of the harmonic springs to a function of the form $2\rho^{\alpha} - \rho^{\beta}$. The resulting function $h(\rho) = 2\rho^{4.32} - \rho^{1.07}$ fits the data well.

From this, we can calculate $\gamma(\rho)$ using $\gamma(\rho) = \mathrm{d}\ln h(\rho)/\mathrm{d}\ln\rho$ using equation 2.24. At low densities the harmonic bond chain has a lower γ than the rigid bonds while at high densities the rigid bonds have a higher γ. There might be a significant error in the data at low density, due to the fitting. In figure 6.9 there is a visible difference between the fit and the data point at $\rho = 0.96$. Moreover, calculating $\gamma(\rho)$ for the rigid bonds also gives a function that disagrees at low density with the γ values from the fluctuations.

Now that we have an expression for $h(\rho)$, we can use it to simulate an isomorph[1]. We create a set of isomorphic state points using $T_0 = 0.7$ at $\rho = 1$ (the same state point was in the rigid bond isomorph simulated in section 6.2) using $T = T_0(2\rho^{4.32} - \rho^{1.07})$. Different measures of the dynamics are plotted in figures 6.11 and 6.12. The dynamics are exactly invariant, except for the higher Rouse modes, which were also not invariant on the isomorphs of the rigid bond chains.

As we have seen in the previous chapter, not all structure is invariant on the isomorph for the Lennard-Jones chains with rigid bonds. The reason for this is that the bonds do not scale with density, and are therefore not constant in reduced units. Since we now have harmonic bonds, their length may depend on density and the intramolecular structure may be invariant on the isomorph. The bond length distributions are plotted in figure 6.11 and are clearly not invariant on the isomorph. Comparison with the bond length distributions along the isochore and isotherm shows that the width of the distribution depends solely on the temperature. The average bond length is slightly state point dependent (in normal Lennard-Jones units), but this is only a small effect and the average bond length does not become constant when expressed in reduced units.

When plotting the mean square end-to-end vector $\langle \mathbf{R}^2 \rangle$ and mean square radius of gyration $\langle R_g^2 \rangle$ the results are qualitatively the same as for the rigid bonds. The molecular size is only dependent on density; it is practically constant on an isochore.

[1] "Isomorph" may not be the best name for this set of state points. Since only the relaxation time has been used as a criterion in the selection of these state points, "isochrone" might be a more appropriate term (Roed et al., 2013; Tölle, 2001).

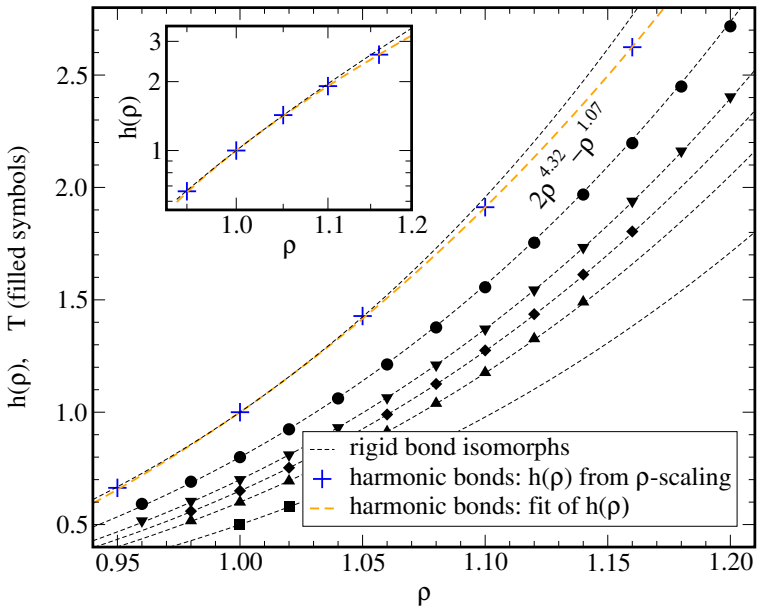

Figure 6.9: The values of the harmonic bond $h(\rho)$ obtained by fitting (blue crosses) compared to the rigid bond $h(\rho)$ (dashed line). All data of the rigid bonds are identical to the data presented in figure 5.17 These values have then been fitted to obtain $h(\rho) = 2\rho^{4.32} - \rho^{1.07}$ (orange dashed line). The inset shows the same but in a log-log plot.

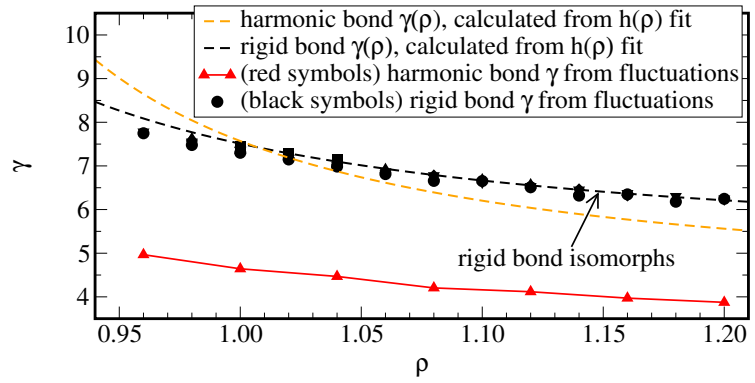

Figure 6.10: $\gamma(\rho)$ for the harmonic bond chains (orange dashed line) calculated from the $h(\rho)$ fit in figure 6.9. This was compared to the rigid bond $\gamma(\rho)$ (black dashed line) calculated from $h(\rho)$ and the rigid bond γ values calculated from the fluctuations.

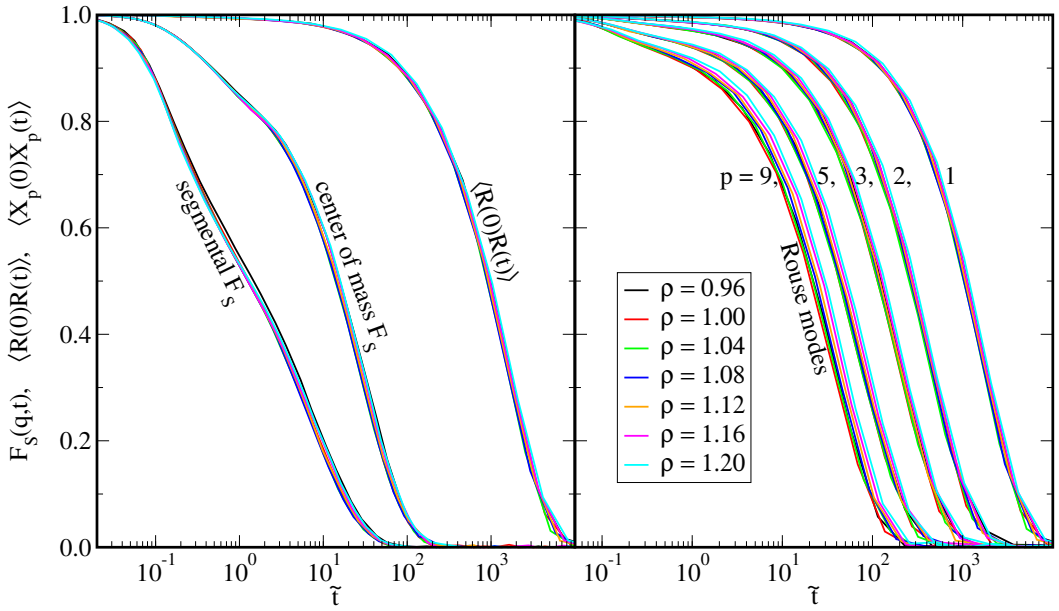

Figure 6.11: The different measures of the dynamics for the isomorphic state points obtained from density scaling. The curves collapse over the entire times span, except for the higher Rouse modes.

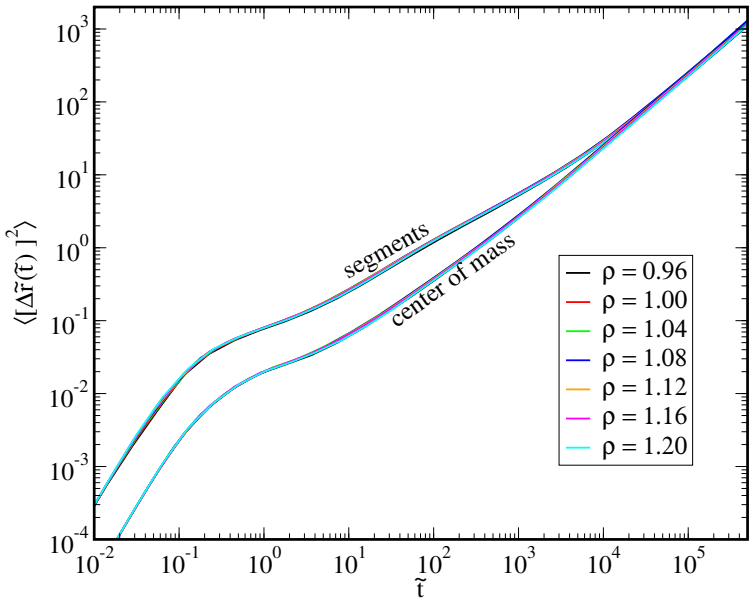

Figure 6.12: Mean square displacement of the segments and centers of mass on the isomorph obtained by density scaling. Both collapse well at all time scales.

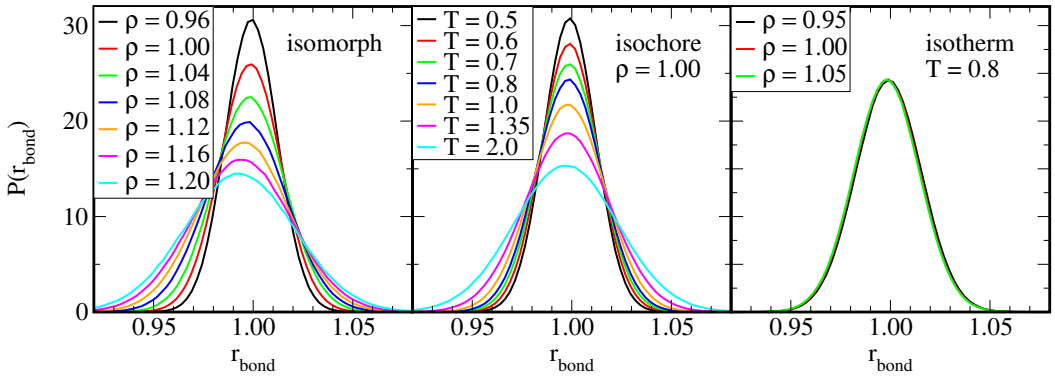

Figure 6.13: Bond length distributions along the isomorph, an isochore, and an isotherm. The width of the bond length distribution changes along the isomorph, as it does on the isochore. The average bond length changes slightly in all three plots.

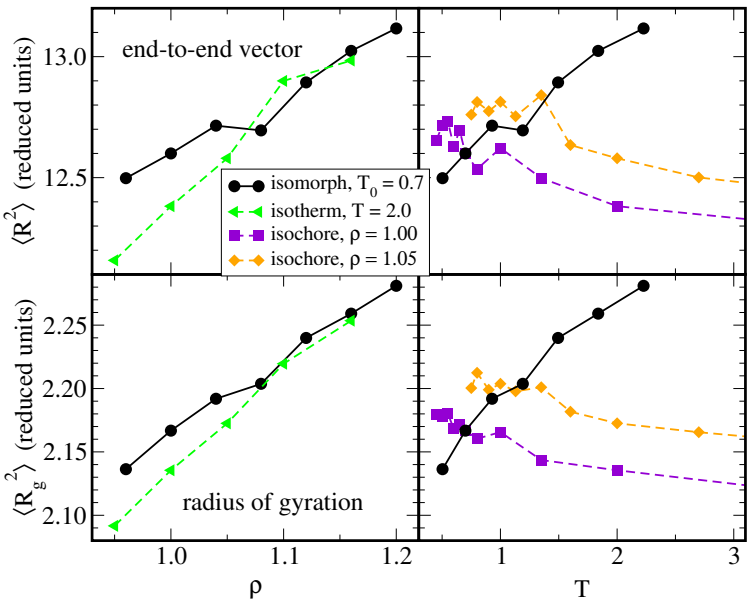

Figure 6.14: The mean square end-to-end vector $\langle \mathbf{R}^2 \rangle$ and mean square radius of gyration $\langle R_g^2 \rangle$ for on the isomorph, compared to the isotherm and isochore. These measures of the molecule size seem only dependent on density.

6.4 The dynamic Prigogine-Defay ratio

Since the dynamics at long time are so similar for the harmonic bonds and the rigid bonds, but the short time dynamics very different, we expect that the harmonic bonds only have affect the U,W correlations at high frequencies. We test this by looking at the frequency dependence of the correlations. This is closely related to earlier work related to the Prigogine-Defay ratio, hence first explain some background on this.

6.4.1 Background

The idea of a single-parameter liquid is not a new idea, and already in the early days of glass science the idea was used in the investigation of the glass transition. It was found that *if* it is possible to describe the a liquid system with only one order parameter, then the Prigogine-Defay ratio given by

$$\Pi = -\frac{\Delta c_p \Delta \kappa_T}{T_g (\Delta \alpha_p)^2} \tag{6.3}$$

is unity (Davies and Jones, 1953a,b; Prigogine and Defay, 1954). Here T_g is the glass transition temperature, c_p is the isobaric specific heat per unit volume, κ_T is the isothermal compressibility, α_p is the isobaric thermal expansion coefficient, and Δ denotes the difference in these quantities when going from the liquid to the glass, extrapolated to T_g. The equality also follows from the Ehrenfest equations for second order phase transitions, although the glass transition was not considered a phase transition (Davies and Jones, 1953a; Gee, 1947).

Moreover, it was argued that the Prigogine-Defay ratio can never be smaller than unity (Davies and Jones, 1953b; Gupta and Moynihan, 1976). This was later confirmed by experimental data; most glass formers do indeed have a Prigogine-Defay ratio larger than one (Berg and Simha, 1976; Gupta and Moynihan, 1976; Oels and Rehage, 1977), meaning that in general, a single order parameter description of glasses did not seem feasible.

This definition of the Prigogine-Defay ratio in equation 6.3 is however not rigorous, firstly because T_g is not well defined, and secondly because material properties of a glass can change slightly over time. Therefore the differences in the material properties of the glass and the liquid at T_g are ill defined as well. Moreover, extrapolation is inherently not rigorous. A more rigorous definition was proposed using linear response measurements of viscous liquids (Moynihan and Gupta, 1978; Roe, 1977):

$$\Pi^{lin} = -\frac{[c_p(\omega \to 0) - c_p(\omega \to \infty)][\kappa_T(\omega \to 0) - \kappa_T(\omega \to \infty)]}{T[\alpha_p(\omega \to 0) - \alpha_p(\omega \to \infty)]^2}\,, \tag{6.4}$$

called the linear Prigogine-Defay ratio. This definition has the advantage that it is defined for a viscous liquids of any temperature T, so it only depends on the well defined equilibrium quantities. On the other hand, the definition has the disadvantage that it is hard to do linear response measurements over such a large frequency range; so far, Π^{lin} has only been determined once experimentally (Gundermann et al., 2011). This experimental challenge led to the definition of a linear dynamic

Prigogine-Defay ratio by Ellegaard et al. (2007), using the imaginary (loss) part of the linear response functions:

$$\Lambda_{pT}(\omega) = -\frac{c_p''(\omega)\kappa_T''(\omega)}{T[\alpha_p''(\omega)]^2}\,, \tag{6.5}$$

Ellegaard et al. (2007) also showed the definitions of the dynamic Prigogine-Defay ratio that naturally occur when using other combinations of control variables than p and T; $\Lambda_{SV}(\omega)$, $\Lambda_{Sp}(\omega)$, and $\Lambda_{VT}(\omega)$. It was moreover shown that if one of these $\Lambda(\omega) = 1$ at one frequency, then $\Lambda(\omega) = 1$ at all frequencies for all control variables.

6.4.2 Calculating the Prigogine-Defay ratio in simulations

Our simulations are done in the NVT ensemble, so the natural dynamic Prigogine-Defay ratio for this ensemble is (Ellegaard et al., 2007)

$$\Lambda_{VT}(\omega) = -\frac{c_V''(\omega)K_T''(\omega)}{T[\beta_V''(\omega)]^2}\,, \tag{6.6}$$

where β_V is the isochoric pressure coefficient, and K_T the isothermal bulk modulus.

Using the fluctuation-dissipation theorem, it is possible to calculate the response functions from equilibrium fluctuations. For instance, the isochoric specific heat can be calculated from the autocorrelation function of the energy using (Nielsen, 1999; Nielsen and Dyre, 1996)

$$c_v(\omega) = \frac{\langle(\Delta E)^2\rangle}{k_BT} - \frac{i\omega}{k_BT}\int_0^\infty \langle\Delta E(0)\Delta E(t)\rangle(\cos(\omega t) + i\sin(\omega t))\,\mathrm{d}t\,. \tag{6.7}$$

Since we are only interested in the imaginary part we write (for the excess part)

$$c_{v,ex}''(\omega) = \frac{\omega}{k_BT}\int_0^\infty \langle\Delta U(0)\Delta U(t)\rangle\cos(\omega t)\,\mathrm{d}t\,. \tag{6.8}$$

The autocorrelation function is a real and even function, so $\int_0^\infty = \frac{1}{2}\int_\infty^\infty$. Denoting the cosine transform as $\hat{\mathcal{F}}_\omega^c(g(t)) = \int_\infty^\infty g(t)\cos(\omega t)dt$ we can write following Pedersen (2009) for the three response functions per particle

$$c_{V,ex}''(\omega) = \frac{\omega}{2Nk_BT^2}\,\hat{\mathcal{F}}_\omega^c\langle\Delta U(0)\Delta U(t)\rangle_{VT}\,, \tag{6.9}$$

$$\beta_{V,ex}''(\omega) = \frac{\omega}{2NVk_BT^2}\,\hat{\mathcal{F}}_\omega^c\langle\Delta U(0)\Delta W(t)\rangle_{VT}\,, \tag{6.10}$$

$$K_{T,ex}''(\omega) = -\frac{\omega}{2NV^2k_BT}\,\hat{\mathcal{F}}_\omega^c\langle\Delta W(0)\Delta W(t)\rangle_{VT}\,. \tag{6.11}$$

This is now the excess quantity per particle.

On a computer, one usually calculates (auto)correlation functions of discrete data using the Wiener-Khinchin theorem, which states that the autocorrelation function of a function $g(t)$ is the inverse transform of its power spectrum $|G(\omega)|^2 = G(\omega)\overline{G(\omega)}$. Likewise, the crosscorrelation of two functions $g(t)$ and $h(t)$ is the inverse transform of $G(\omega)\overline{H(\omega)}$ (Press et al., 2007). Denoting the inverse Fourier transform as $\hat{\mathcal{F}}_\omega^{-1}$ and the Fourier transform of $\Delta U(t)$ as $\Delta U(\omega)$ the Wiener-Khinchin states

that $\langle \Delta U(0)\Delta U(t)\rangle_{VT} = \hat{\mathcal{F}}_\omega^{-1}|\Delta U(\omega)|^2$. Taking the specific heat as example, equation 6.9 can then be rewritten as

$$c''_{V,ex}(\omega) = \frac{\omega}{2Nk_BT^2}\,\hat{\mathcal{F}}_\omega^c\,\hat{\mathcal{F}}_\omega^{-1}|\Delta U(\omega)|^2\,. \tag{6.12}$$

This can be simplified further by noting that the inverse Fourier transform of an real and even function yields a real and even function (Press et al., 2007). In other words, the inverse Fourier transform $\hat{\mathcal{F}}_\omega^{-1}$ (and also the forward Fourier transform $\hat{\mathcal{F}}_\omega$) of an even function reduces to the cosine transform $\hat{\mathcal{F}}_\omega^c$. Therefore

$$c''_{V,ex}(\omega) = \frac{\omega}{2Nk_BT^2}\,\hat{\mathcal{F}}_\omega^c\,\hat{\mathcal{F}}_\omega^{-1}|\Delta U(\omega)|^2 = \frac{\omega}{2Nk_BT^2}|\Delta U(\omega)|^2\,, \tag{6.13}$$

because, as we have just seen, the cosine transform is its own inverse. This can also be done for the compressibility and the pressure coefficient, yielding a total of three response functions

$$c''_{V,ex}(\omega) = \frac{\omega}{2Nk_BT^2}|\Delta U(\omega)|^2\,, \tag{6.14}$$

$$\beta''_{V,ex}(\omega) = \frac{\omega}{2NVk_BT^2}\Delta U(\omega)\overline{\Delta W(\omega)}\,, \tag{6.15}$$

$$K''_{T,ex}(\omega) = -\frac{\omega}{2NV^2k_BT}|\Delta W(\omega)|^2\,. \tag{6.16}$$

Figure 6.15 shows these response function for the Lennard-Jones chain system. The α-relaxation peak can be seen in all three response functions at a frequency of around $\omega \approx 0.15$, which corresponds to a relaxation time of 42. This value is reasonably close to the time at which the (segmental) intermediate scattering function vanishes. At low frequencies all three response functions have a slope of around 1, which is expected for the low frequency side of the α-relaxation. The fact that all three slopes are the same also indicates that the linear dynamic Prigogine-Defay ratio is constant in that frequency range. At high frequencies on the other hand, the response functions show very dissimilar behavior due to the effects of the springs.

To show how similar the shapes of the response functions are, they are scaled to collapse at low frequencies in figure 6.17. Only at high frequencies the shapes of the three response functions differ significantly. The scaling parameters we determined by fitting a linear function $y = x + b$ to the low frequency part of the response functions in the log-log plane. From the fitting parameters we estimate the dynamic Prigogine-Defay ratio to be $10^{b_c+b_K-2b_c}/T = 10^{0.318+2.04-2\,\cdot\,1.13}/0.7 = 1.80$ using equation 6.6.

If we now express the dynamic Prigogine-Defay ratio in terms of the Fourier transforms of fluctuations as

$$\Lambda_{VT}(\omega) = -\frac{c''_{V,ex}(\omega)K''_{T,ex}(\omega)}{T[\beta''_{V,ex}(\omega)]^2} = \frac{|\Delta U(\omega)|^2|\Delta W(\omega)|^2}{[\Delta U(\omega)\overline{\Delta W(\omega)}]^2}\,, \tag{6.17}$$

we see that this definition resembles the inverse square of the definition of the correlation coefficient R (see equation 2.4). We therefore define a frequency dependent correlation coefficient

$$R(\omega) = \frac{1}{\sqrt{\Lambda_{VT}(\omega)}} = \frac{\Delta U(\omega)\overline{\Delta W(\omega)}}{\sqrt{|\Delta U(\omega)|^2|\Delta W(\omega)|^2}}\,. \tag{6.18}$$

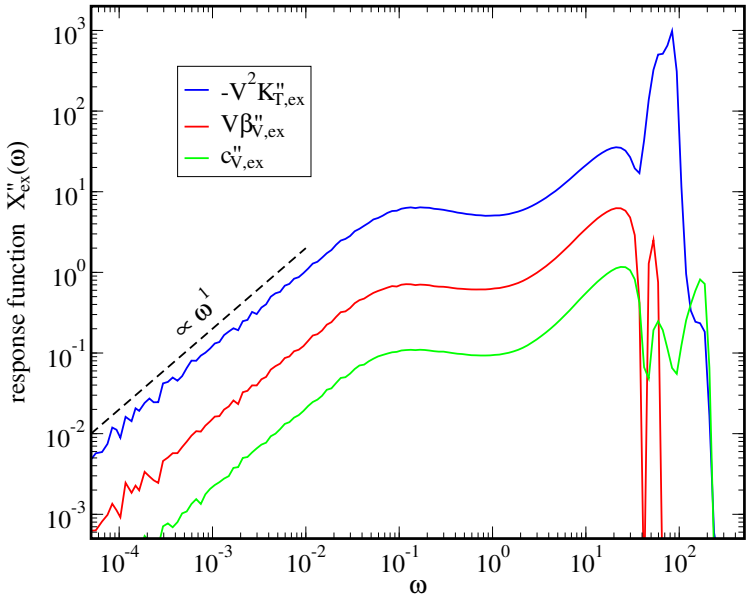

Figure 6.15: The imaginary (loss) parts of the isochoric specific heat $c''_{V,ex}$, the negative isothermal bulk modulus $-K''_{T,ex}$ and the isochoric pressure coefficient $\beta''_{V,ex}$ for the Lennard-Jones chain model at density 1.00 and temperature 0.7, calculated using equations 6.14 - 6.16. The data have been obtained by averaging over 17 independent simulations. The simulations were run for 2^{27} steps, sampling the potential energy and virial every four steps. This high sampling frequency was shown to be high enough to prevent aliasing (Press et al., 2007). Logarithmic data binning with 20 bins per decade has been used to smooth the final data.

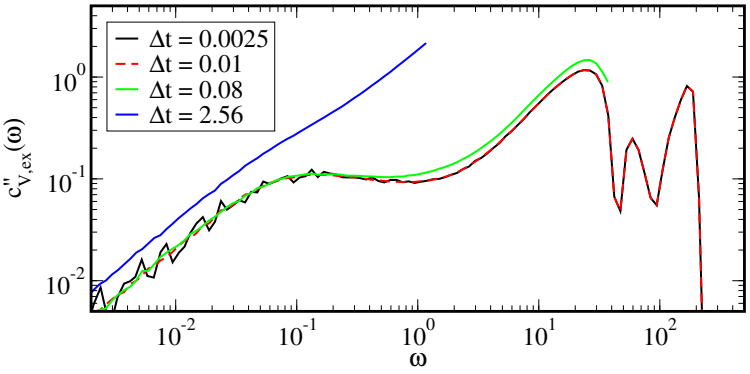

Figure 6.16: The imaginary part of the frequency dependent configurational isochoric specific heat, calculated from data with different sample frequencies. The two lowest sample intervals correspond to saving the energy every timestep and every four timesteps, And the resulting response functions are indistinguishable at high frequencies, indicating an absence of aliasing. For the larger sampling intervals, it is clear that there is spectral density from outside the frequency window is folded into the frequency window (Press et al., 2007).

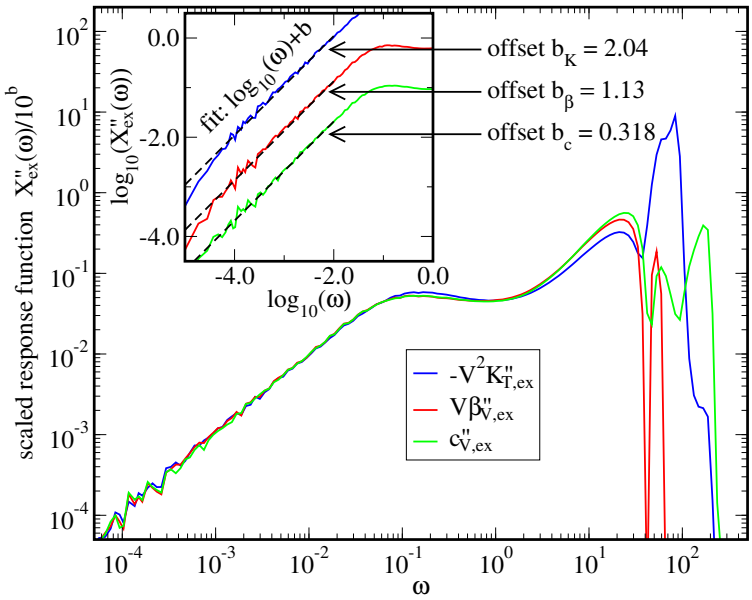

Figure 6.17: The same data as in figure 6.15, but now the data have been scaled to collapse at low frequencies. At low frequencies the collapse is good, although there appear to be small deviations at the top of the α-peak. The inset shows the determination of the scaling parameters. A linear function of $\log_{10}(\omega)$ with slope unity was fitted to the data for $\omega < 0.01$, with the offsets b as fitting parameters. The response functions in the main graph were scaled by 10^{-b}.

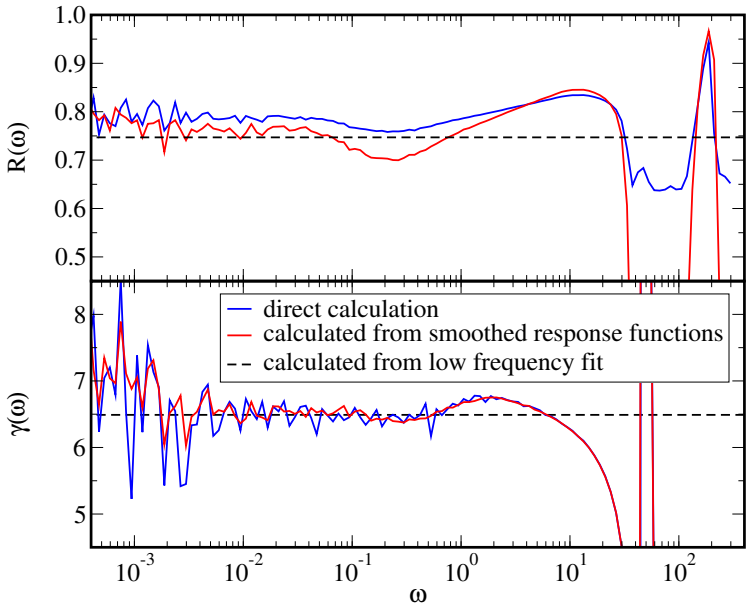

Figure 6.18: The frequency dependent correlation coefficient (top) and slope (bottom). The data have been calculated from the same simulations as figure 6.15, using equations 6.18 and 6.19. Zero padding has been used to prevent end effects in the Fourier transforms (Press et al., 2007), and data binning has been used to smooth the result. At low frequencies, the different calculations agree, and give reasonable values (dashed lines show results from the low frequency fits (see figure 6.17).

Similarly, we define a frequency dependent version of γ:

$$\gamma(\omega) = \frac{\Delta U(\omega)\overline{\Delta W(\omega)}}{|\Delta U(\omega)|^2} = \frac{V\beta''_{V,ex}(\omega)}{c''_{V,ex}(\omega)}\,. \tag{6.19}$$

The link between the Prigogine-Defay ratio is nothing new, Pedersen et al. (2008a) have shown for instance that the strongly correlating Kob-Anderson Lennard-Jones liquid indeed has a Prigogine-Defay ratio close to unity. Moreover, the Prigogine-Defay ratio of molecular and polymeric van der Waals-bonded glass formers is lower (closer to unity) (Gundermann et al., 2011; Takahara et al., 1999; Zoller, 1982) than that of inorganic and hydrogen bonded glass formers (Dingwell et al., 1993; Gupta and Moynihan, 1976; Samwer et al., 1999; Wondraczek and Behrens, 2007)[2].

The low frequency correlation coefficient as shown in figure 6.18 is around 0.8, which is much higher than the standard correlation coefficient $R = 0.28$ as found from the instantaneous values. The low frequency coefficient is comparable to the instantaneous correlation coefficient of the chain with rigid bonds. This indicates that also the LJC model with harmonic springs may have isomorphs in its phase diagram.

At low frequencies we find that $\gamma(\omega < 1) \approx 6.5$ which is lower than the value for the LJC liquid with rigid bonds at the same state point, where we find $\gamma = 7.36$.

[2]For an overview of Prigogine-Defay ratios from the literature, see Pedersen (2009) and Gundermann et al. (2011).

This indicates that the two LJC model have a different state point dependence of the dynamics. In particular, the dynamics of the spring model has a smaller density dependence.

Although it seems that it is possible to determine the scaling exponent γ necessary to trace out an isomorph, this method has some disadvantages. To prevent aliasing, it is necessary to choose the sample interval small enough to include all high frequency contributions to the spectrum. This means that the sample interval should not be bigger than 0.01 LJ units. On the other hand, the total simulation time has to be large enough to get good statistics at low frequencies. This means that the length of the simulation has to be longer than for a normal equilibrium simulation, making the construction of the whole isomorph in an iterative fashion a very time consuming process. For this reason the frequency dependent $\gamma(\omega)$ has not been used to show that this model obeys the isomorph theory. The data do however show that the liquid has "hidden correlations" in the low frequency component of the U and W fluctuations, and how these correlations can be found.

6.5 Conclusion

We have shown that the Lennard-Jones chain liquid with harmonic bonds has curves in its phase diagram that resemble the isomorphs found for the rigid bond chains. However, the harmonic bonds destroy the energy-virial correlations almost completely, and the γ value found from the fluctuations cannot not be used to find a curves of invariant dynamics. This means that the *pseudoisomorphic* curves we have identified are not configurational adiabats.

By going to the frequency domain we have found that the harmonic bonds only destroy the correlations at high frequency. At low frequency we find a correlation coefficient and γ that are close to the values found for the chains with rigid bonds.

Bibliography

Abrahamson, A. A. (1963). "Repulsive interaction potentials between rare-gas atoms. Homonuclear two-center systems". In: *Phys. Rev.* 130.2, pp. 693–707. DOI: 10.1103/PhysRev.130.693 (cit. on p. 106).

Agrawal, R. and D. A. Kofke (Jan. 1995). "Solid-Fluid Coexistence for Inverse-Power Potentials". In: *Phys. Rev. Lett.* 74.1, pp. 122–125. DOI: 10.1103/PhysRevLett.74.122 (cit. on p. 33).

Aichele, M., Y Gebremichael, F. W. Starr, J Baschnagel, and S. C. Glotzer (2003). "Polymer-specific effects of bulk relaxation and stringlike correlated motion in the dynamics of a supercooled polymer melt". In: *J. Chem. Phys.* 119.10, p. 5290. DOI: 10.1063/1.1597473 (cit. on p. 50).

Alba-Simionesco, C., D. Kivelson, and G. Tarjus (2002). "Temperature, density, and pressure dependence of relaxation times in supercooled liquids". In: *J. Chem. Phys.* 116.12, pp. 5033–5038. DOI: 10.1063/1.1452724 (cit. on pp. 4, 20).

Alba-Simionesco, C., A. Cailliaux, A. Alegría, and G. Tarjus (2004). "Scaling out the density dependence of the α-relaxation in glass-forming polymers". In: *Europhys. Lett.* 68.1, pp. 58–64. DOI: 10.1209/epl/i2004-10214-6 (cit. on p. 20).

Alemany, M. M. G., C. Rey, O. Diéguez, and L. J. Gallego (2000). "A computer simulation study of the static structure and dynamic properties of liquid C_{60} using Girifalco's potential". In: *J. Chem. Phys.* 112.24, pp. 10711–10713 (cit. on p. 46).

Alexander, S., P. M. Chaikin, P. Grant, G. J. Morales, P. Pincus, and D. Hone (1984). "Charge renormalization, osmotic pressure, and bulk modulus of colloidal crystals: Theory". In: *J. of Chem. Phys.* 80.11, pp. 5776–5781. DOI: 10.1063/1.446600 (cit. on p. 24).

Allen, M. P. and D. J. Tildesley (1987). *Computer simulations of liquids*. Oxford University Press (cit. on pp. 6, 15, 50).

Anderson, P. W. (Mar. 1995). "Through the glass lightly". In: *Science* 267, pp. 1615–1616. DOI: 10.1126/science.267.5204.1610 (cit. on p. 2).

Ashcroft, N. W. (Sept. 1993). "Elusive diffusive liquids". In: *Nature* 365, pp. 387–388. DOI: 10.1038/365387a0 (cit. on p. 46).

Atkins, P. and J. de Paula (2010). *Physical Chemistry*. 9th ed. W. H. Freeman (cit. on p. 23).

Bailey, N. P., U. R. Pedersen, N. Gnan, T. B. Schrøder, and J. C. Dyre (2008a). "Pressure-energy correlations in liquids. I. Results from computer simulations". In: *J. Chem. Phys.* 129, p. 184507. DOI: 10.1063/1.2982247 (cit. on pp. i, ii, 11, 12, 38–40, 43, 58, 62).

Bailey, N. P., U. R. Pedersen, N. Gnan, T. B. Schrøder, and J. C. Dyre (2008b). "Pressure-energy correlations in liquids. II. Analysis and consequences". In: *J. Chem. Phys.* 129, p. 184508. DOI: 10.1063/1.2982249 (cit. on pp. i, ii, 11–13, 18, 19, 27, 28, 58).

Bailey, N. P., L. Bøhling, A. A. Veldhorst, T. B. Schrøder, and J. C. Dyre (Nov. 2013). "Statistical mechanics of Roskilde liquids: Configurational adiabats, specific heat contours, and density dependence of the scaling exponent". In: *J. Chem. Phys.* 139.18, 184506, p. 184506. DOI: 10.1063/1.4827090 (cit. on pp. 21, 28, 36, 62).

Barkema, G. T., D. Panja, and J. M. J. van Leeuwen (2011). "Structural modes of a polymer in the repton model". In: *J. Chem. Phys.* 134.15, p. 154901. DOI: 10.1063/1.3580287 (cit. on p. 53).

Barrat, J.-L., J. Baschnagel, and A. Lyulin (2010). "Molecular dynamics simulations of glassy polymers". In: *Soft Matter* 6, pp. 3430–3446. DOI: 10.1039/b927044b (cit. on p. 50).

Bennemann, C., W. Paul, K. Binder, and B. Dünweg (1998). "Molecular-dynamics simulations of the thermal glass transition in polymer melts: α-relaxation behavior". In: *Phys. Rev. E* 57.1, pp. 843–851. DOI: 10.1103/PhysRevE.57.843 (cit. on p. 49).

Bennemann, C., C. Donati, J. Baschnagel, and S. C. Glotzer (1999a). "Growing range of correlated motion in a polymer melt on cooling towards the glass transition". In: *Nature* 399, pp. 246–249 (cit. on p. 49).

Bennemann, C., W. Paul, J. Baschnagel, and K. Binder (1999b). "Investigating the influence of different thermodynamic paths on the structural relaxation in a glass-forming polymer melt". In: *J. Phys.: Condens. Matter* 11, pp. 2179–2192 (cit. on p. 49).

Bennemann, C., J. Baschnagel, and W. Paul (1999c). "Molecular-dynamics simulation of a glassy polymer melt: Incoherent scattering function". In: *Eur. Phys. J. B* 19, pp. 323–334 (cit. on pp. 49, 67).

Bennemann, C., J. Baschnagel, W. Paul, and K. Binder (1999d). "Molecular-dynamics simulations of a glassy polymer melt: Rouse model and cage effect". In: *Computational and theorectical Polymer Science* 9, pp. 217–226 (cit. on pp. 49, 53, 66).

Berg, J. I. and R. Simha (1976). "Pressure-volume-temperature relations in liquids and glassy selenium". In: *J. Non-Cryst. Solids* 22, pp. 1–22. DOI: 10.1016/0022-3093(76)90002-8 (cit. on p. 85).

Binder, K., J. Baschnagel, C. Bennemann, and W. Paul (1999). "Monte Carlo and molecular dynamics simulation of the glass thransition in polymers". In: *J. Phys.: Condens. Matter* 11, A47–A55 (cit. on p. 49).

Binder, K., J. Baschnagel, and W. Paul (2003). "Glass transition of polymer melts: test of theoretical concepts by computer simulation". In: *Prog. Polym. Sci.* 28, pp. 115–172 (cit. on p. 50).

Bird, R. B., C. F. Curtiss, R. C. Armstrong, and O. Hassager (1987). *Dynamics of polymeric liquids*. 2nd. Vol. 2. Wiley Interscience (cit. on p. 74).

Biroli, G. and J. P. Garrahan (Mar. 2013). "Perspective: The glass transition". In: *J. Chem. Phys.* 138, 12A301. DOI: 10.1063/1.4795539 (cit. on p. 1).

Bøhling, L., T. S. Ingebrigtsen, A. Grzybowski, M. Paluch, J. C. Dyre, and T. B. Schrøder (2012). "Scaling of viscous dynamics in simple liquids: theory, simulation and experiment". In: *New J. Phys.* 14, p. 113035. DOI: 10.1088/1367-2630/14/11/113035 (cit. on pp. i, ii, 21, 39, 48, 70).

Bøhling, L., A. A Veldhorst, T. S. Ingebrigtsen, N. P. Bailey, J. S. Hansen, S. Toxvaerd, T. B. Schrøder, and J. C. Dyre (2013). "Do the repulsive and attractive pair forces play separate roles for the physics of liquids?" In: *J. Phys.: Condens. Matter* 25.3, p. 032101. DOI: 10.1088/0953-8984/25/3/032101 (cit. on p. 15).

Bøhling, L., N. P. Bailey, T. B. Schrøder, and J. C. Dyre (2014). "Estimating the density-scaling exponent of a monoatomic liquid from its pair potential". In: *arXiv:1401.2606* (cit. on p. 30).

Brooks, B. R. et al. (2009). "CHARMM: The biomolecular simulation program". In: *J. Comput. Chem.* 30.10, pp. 1545–1614. DOI: 10.1002/jcc.21287 (cit. on p. 73).

Buckingham, R. A. (1938). "The classical equation of state of gaseous helium, neon and argon". In: *Proc. R. Soc. London A* 168, pp. 264–283. DOI: 10.1098/rspa.1938.0173 (cit. on p. 106).

Casalini, R. and C. M. Roland (2004). "Thermodynamical scaling of the glass transition dynamics". In: *Phys. Rev. E* 69 (6), p. 062501. DOI: 10.1103/PhysRevE.69.062501 (cit. on p. 5).

Casalini, R. and C. M. Roland (2005). "Temperature and Density Effects on the Local Segmental and Global Chain Dynamics of Poly(oxybutylene)". In: *Macromolecules* 38, pp. 1779–1788. DOI: 10.1021/ma0476902 (cit. on p. 71).

Cavagna, A. (2009). "Supercooled liquids for pedestrians". In: *Phys. Rep.* 476, pp. 51–124. DOI: 10.1016/j.physrep.2009.03.003 (cit. on pp. 1, 3).

Cheng, A., M. L. Klein, and C. Caccamo (Aug. 1993). "Prediction of the phase diagram of rigid C_{60}". In: *Phys. Rev. Lett.* 71.8, pp. 1200–1203. DOI: 10.1103/PhysRevLett.71.1200 (cit. on p. 46).

Colby, R. H., L. J. Fetters, and W. W. Graessley (Sept. 1987). "The melt viscosity-molecular weight relationship for linear polymers". In: *Macromolecules* 20.9, pp. 2226–2237. DOI: 10.1021/ma00175a030 (cit. on p. 55).

Cornell, W. D., P. Cieplak, C. I. Bayly, I. R. Gould, K. M. Merz, D. M. Ferguson, D. C. Spellmeyer, T. Fox, J. W. Caldwell, and P. A. Kollman (1995). "A Second Generation Force Field for the Simulation of Proteins, Nucleic Acids, and Organic Molecules". In: *J. Am. Chem. Soc.* 117.19, pp. 5179–5197. DOI: 10.1021/ja00124a002 (cit. on p. 73).

Davies, R.O. and G.O. Jones (1953a). "The irreversible approach to equilibrium in glasses". In: *Proc. R. Soc. London A* 217, pp. 26–42. DOI: 10.1098/rspa.1953.0044 (cit. on p. 85).

Davies, R.O. and G.O. Jones (1953b). "Thermodynamic and kinetic properties of glasses". In: *Adv. Phys.* 2, pp. 370–410. DOI: 10.1080/00018735300101252 (cit. on p. 85).

De Gennes, P. G. (July 1971). "Reptation of a Polymer Chain in the Presence of Fixed Obstacles". In: *J. Chem. Phys.* 55.2, pp. 572–579. DOI: 10.1063/1.1675789 (cit. on p. 56).

Debenedetti, P. G. and F. H. Stillinger (Mar. 2001). "Supercooled liquids and the glass transition". In: *Nature* 410, pp. 259–267. DOI: 10.1038/35065704 (cit. on pp. 1, 2).

Debye, P. and E. Hükel (1923). "The theory of electrolytes. I. Lowering of freezing point and related phenomena". In: *Physikalische Zeitschrift* 24, pp. 185–206 (cit. on p. 23).

Derjaguin, B. and L. Landau (1941). "Theory of the stability of strongly charged lyophobic sols and of the adhesion of strongly charged particles in solutions of electrolytes". In: *Acta Physicochim. URSS* 14, pp. 633–662 (cit. on p. 23).

Dingwell, D. B., R. Knoche, and S. L. Webb (1993). "A volume temperature relationship for liquid GeO2 and some geophysically relevant derived parameters for network liquids". In: *Phys. Chem. Miner.* 19.7, pp. 445–453. DOI: 10.1007/BF00203184 (cit. on p. 90).

Doi, M. and S. F. Edwards (1986). *The theory of polymer dynamics*. Oxford Science Publications (cit. on pp. 51, 56, 65).

Donth, E. (2001). *The glass transition: Relaxation dynamics in liquids and disordered materials*. Ed. by R. Hull, R. M. Osgood, H. Sasaki, and A. Zunger. Springer (cit. on p. 1).

Dreyfus, C., A. Aouadi, J. Gapinski, M. Matos-Lopes, W. Steffen, A. Patkowski, and R. M. Pick (2003). "Temperature and pressure study of Brillouin transverse modes in the organic glass-forming liquid orthoterphenyl". In: *Phys. Rev. E* 68 (1), p. 011204. DOI: 10.1103/PhysRevE.68.011204 (cit. on p. 4).

Dyre, J. C. (2006). "Colloquium: The glass transition and elastic models of glass-forming liquids". In: *Rev. Mod. Phys.* 78, pp. 953–972. DOI: 10.1103/RevModPhys.78.953 (cit. on p. 1).

Dyre, Jeppe C. (Feb. 2013). "*NVU* perspective on simple liquids' quasiuniversality". In: *Phys. Rev. E* 87 (2), p. 022106. DOI: 10.1103/PhysRevE.87.022106 (cit. on p. 31).

Dzugutov, M. (1996). "A universal scaling law for atomic diffusion in condensed matter". In: *Nature* 381, pp. 137–139 (cit. on pp. 16, 22).

Edberg, R., D. J. Evans, and G. P. Morriss (1986). "Constrained molecular dynamics: Simulations of liquid alkanes with a new algorithm". In: *J. Chem. Phys.* 84.12, pp. 6933–6939. DOI: 10.1063/1.450613 (cit. on p. 50).

Ediger, M. D. and P. Harrowell (2012). "Perspective: Supercooled liquids and glasses". In: *J. Chem. Phys.* 137.8, p. 080901. DOI: 10.1063/1.4747326 (cit. on p. 1).

Ellegaard, N. L., T. Christensen, P. Voetmann Christiansen, N. Boye Olsen, U. R. Pedersen, T. B. Schrøder, and J. C. Dyre (2007). "Single-order-parameter description of glass-forming liquids: A one-frequency test". In: *J. Chem. Phys.* 126, p. 074502. DOI: 10.1063/1.2434963 (cit. on p. 86).

Everaers, R. (July 1999). "Entanglement effects in defect-free model polymer networks". In: *New Journal of Physics* 1.1, p. 12. DOI: 10.1088/1367-2630/1/1/312 (cit. on p. 56).

Farouki, R. T. and S. Hamaguchi (1994). "Thermodynamics of strongly?coupled Yukawa systems near the one?component?plasma limit. II. Molecular dynamics simulations". In: *The Journal of Chemical Physics* 101.11, pp. 9885–9893. DOI: 10.1063/1.467955 (cit. on p. 24).

Ferry, J. D. (1980). *Viscoelastic properties of polymers*. 3rd ed. John Wiley & Sons (cit. on p. 51).

Flory, P. J. (1949). "The Configuration of Real Polymer Chains". In: *J. Chem. Phys.* 17.3, pp. 303–310. DOI: 10.1063/1.1747243 (cit. on p. 52).

Fortov, V. E., A. V. Ivlev, S. A. Khrapak, A. G. Khrapak, and G.E. Morfill (Oct. 2005). "Complex (dusty) plasmas: Current status, open issues, perspectives". In: *Phys. Rep.* 421, pp. 1–103. DOI: 10.1016/j.physrep.2005.08.007 (cit. on p. 24).

Frenkel, D. and B. Smit (2002). *Understanding Molecular Simulation*. 2nd ed. Academic Press (cit. on pp. 6, 7, 25).

Galliero, G. and C. Boned (2009). "Thermal conductivity of the Lennard-Jones chain fluid model". In: *Phys. Rev. E* 80.6, p. 061202. DOI: 10.1103/PhysRevE.80.061202 (cit. on p. 50).

Galliero, G., C. Boned, and J. Fernández (2011). "Scaling of the viscosity of the Lennard-Jones chain fluid model, argon and some normal alkanes". In: *J. Chem. Phys.* 134.6, p. 064505. DOI: 10.1063/1.3553262 (cit. on pp. 50, 59).

Gee, G. (1947). "Some thermodynamic properties of high polymers and their molecular interpretation". In: *Q. Rev. Chem. Soc.* 1 (3), pp. 265–298. DOI: 10.1039/QR9470100265 (cit. on p. 85).

Gilvarry, J. J. (Apr. 1956). "The Lindemann and Grüneisen Laws". In: *Phys. Rev.* 102.2, pp. 308–316. DOI: 10.1103/PhysRev.102.308 (cit. on p. 28).

Girifalco, L. A. (1992). "Molecular properties of C_{60} in the gas and solid phases". In: *J. Phys. Chem.* 96, pp. 858–861 (cit. on pp. 45, 46).

Glotzer, S. C. and W. Paul (2002). "Molecular and mesoscale simulation methods for polymer materials". In: *Annu. Rev. Mater. Res.* 32, pp. 401–36. DOI: 10.1146/annurev.matsci.32.010802.112213 (cit. on p. 50).

Gnan, N., T. B. Schrøder, U. R. Pedersen, N. P. Bailey, and J. C. Dyre (2009). "Pressure-energy correlations in liquids. IV. "Isomorphs" in liquid phase diagrams". In: *J. Chem. Phys.* 131.23, p. 234504. DOI: 10.1063/1.3265957 (cit. on pp. i, ii, 11, 14, 15, 17, 21, 25, 28, 30, 43, 61, 62, 69).

Gnan, N., C. Maggi, T. B. Schrøder, and J. C. Dyre (2010). "Predicting the effective temperature of a glass". In: *Phys. Rev. Lett.* 104.23, p. 125902. DOI: 10.1103/PhysRevLett.104.125902 (cit. on p. 70).

Goel, T., C. Nath Patra, T. Mukherjee, and C. Chakravarty (2008). "Excess entropy scaling of transport properties of Lennard-Jones chains". In: *J. Chem. Phys.* 129.16, p. 164904. DOI: 10.1063/1.2995990 (cit. on p. 50).

González-Melchor, M., C. Tapia-Medina, L. Mier-y-Terán, and J. Alejandre (2004). "Surface tension at the liquid-vapor interface of screened ionic mixtures". In: *Condens. Matter Phys.* 7.4, pp. 767–778 (cit. on p. 24).

González-Melchor, M., G. Hernández-Cocoletzi, J. López-Lemus, A. Ortega-Rodríguez, and P. Orea (2012). "Interfacial and coexistence properties of soft spheres with a short-range attractive Yukawa fluid: Molecular dynamics simulations". In: *J. Chem. Phys.* 136, p. 154702. DOI: 10.1063/1.3703507 (cit. on p. 24).

Grest, G. S. and K. Kremer (1986). "Molecular dynamics simulation for polymers in presence of a heath bath". In: *Phys. Rev. A* 33, pp. 3628–3630. DOI: 10.1103/PhysRevA.33.3628 (cit. on pp. 49, 50, 73).

Gundermann, D. et al. (2011). "Predicting the density-scaling exponent of a glass-forming liquid from Prigogine?Defay ratio measurements". In: *Nat. Phys.* 7, pp. 816–821. DOI: 10.1038/nphys2031 (cit. on pp. 13, 85, 90).

Gupta, P. K. and C. T. Moynihan (1976). "Prigogine?Defay ratio for systems with more than one order parameter". In: *J. Chem. Phys.* 65, p. 4136. DOI: 10.1063/1.432870 (cit. on pp. 85, 90).

Gurnett, D. A. and A. Bhattacharjee (2005). *Introduction to plasma physics*. Cambridge University Press (cit. on p. 24).

Habasaki, J., R. Casalini, and K. L. Ngai (2010). "Molecular Dynamics Study of Thermodynamic Scaling of the Glass-Transition Dynamics in Ionic Liquids over Wide Temperature and Pressure Ranges". In: *J. Phys. Chem. B* 114, pp. 3902–3911. DOI: 10.1021/jp911157k (cit. on p. 5).

Hagen, M. H. J., E. J. Meijer, G. C. A. M. Mooij, D. Frenkel, and H. N. W. Lekkerkerker (Sept. 1993). "Does C_{60} have a liquid phase?" In: *Nature* 365, pp. 425–426. DOI: 10.1038/365425a0 (cit. on p. 46).

Hamaguchi, S., R. T. Farouki, and D. H. E. Dubin (1997). "Triple point of Yukawa systems". In: *Phys. Rev. E* 56.4, pp. 4671–4682. DOI: 10.1103/PhysRevE.56.4671 (cit. on pp. 25, 28, 33).

Hansen, J.-P. and I. R. McDonald (1986). *Theory of simple liquids*. Academic Press (cit. on p. 15).

Hasegawa, M. and K. Ohno (1999). "Monte Carlo simulation study of the high-temperature phase diagram of model C_{60} molecules". In: *J. Chem. Phys.* 111.13, pp. 5955–5963. DOI: 10.1063/1.479891 (cit. on p. 46).

Hynninen, A.-P. and M. Dijkstra (2003). "Phase diagram of hard-core repulsive Yukawa particles". In: *Phys. Rev. E* 68, p. 021407. DOI: 10.1103/PhysRevE.68.021407 (cit. on p. 24).

Ingebrigsten, T. S., T. B. Schrøder, and J. C. Dyre (2012a). "Isomorphs in model molecular liquids". In: *J. Phys. Chem. B* 116, pp. 1018–1034. DOI: 10.1021/jp2077402 (cit. on pp. i, ii, 39, 48, 58–60, 62, 69).

Ingebrigsten, T. S., T. B. Schrøder, and J. C. Dyre (2012b). "What is a simple Liquid?" In: *Phys. Rev. X* 2, p. 011011. DOI: 10.1103/PhysRevX.2.011011 (cit. on p. 28).

Ingebrigtsen, T. S., L. Bøhling, T. B. Schrøder, and J. C. Dyre (2012). "Communication: Thermodynamics of condensed matter with strong pressure-energy correlations". In: *J. Chem. Phys.* 136.6, p. 061102. DOI: 10.1063/1.3685804 (cit. on pp. i, ii, 11, 20, 21, 25, 36, 70).

Ingebrigtsen, T. S., A. A. Veldhorst, T. B. Schrøder, and J. C. Dyre (2013). "Communication: The Rosenfeld-Tarazona expression for liquids' specific heat: A numerical investigation of eighteen systems". In: *J. Chem. Phys.* 139.17, p. 171101. DOI: http://dx.doi.org/10.1063/1.4827865 (cit. on p. 22).

Jones, J. E. (Oct. 1924). "On the determination of molecular fields. II. From the equation of state of a gas". In: *Proc. R. Soc. London A* 106, pp. 463–477. DOI: 10.1098/rspa.1924.0082 (cit. on pp. 6, 106).

Jover, J., A. J. Haslam, A. Galindo, G. Jackson, and E. A. Müller (2012). "Pseudo hard-sphere potential for use in continuous molecular-dynamics simulation of spherical and chain molecules". In: *J. Chem. Phys.* 137.14, p. 144505. DOI: 10.1063/1.4754275 (cit. on p. 38).

Khrapak, S. A., O. S. Vaulina, and G. E. Morfill (2012). "Self-diffusion in strongly coupled Yukawa systems (complex plasmas)". In: *Phys. Plasmas* 19, p. 034503. DOI: 10.1063/1.3691960 (cit. on p. 25).

Kilpatrick, J. E., W. E. Keller, and E. F. Hammel (1955). "Second Virial Coefficients of Helium from the Exp-Six Potential". In: *Phys. Rev.* 97.1, p. 9. DOI: 10.1103/PhysRev.97.9 (cit. on p. 106).

Kirk, D. B. and W.-M. W. Hwu (2010). *Programming massively parallel processors*. Morgan Kaufmann (cit. on p. 8).

Kivelson, S. A. and G. Tarjus (2008). "In search of a theory of supercooled liquids". In: *Nature Mater.* 7, pp. 831–833. DOI: 10.1038/nmat2304 (cit. on p. 1).

Kniaź, K., J. E. Fischer, L. A. Girifalco, A. R. McGhie, R. M. Strongin, and A. B. Smith III (1995). "Fullerene Alloys". In: *Solid State Commun.* 96.10, pp. 739–743. DOI: 10.1016/0038-1098(95)00541-2 (cit. on p. 46).

Kob, W. and H. C. Andersen (1994). "Scaling behavior in the β-relaxation regime of a supercooled Lennard-Jones mixture". In: *Phys. Rev. Lett.* 73.10, p. 1376. DOI: 10.1103/PhysRevLett.73.1376 (cit. on pp. 40, 106).

Koči, L., R. Ahuja, A.B. Belonoshko, and B. Johansson (2007). "Study of the high-pressure helium phase diagram using molecular dynamics". In: *J. Phys.: Condens. Matter* 19, p. 016206. DOI: 10.1088/0953-8984/19/1/016206 (cit. on p. 106).

Kopf, A., B. Dünweg, and W. Paul (1997). "Dynamics of polymer ?isotope? mixtures: Molecular dynamics simulation and Rouse model analysis". In: *J. Chem. Phys.* 107.17, pp. 6945–6955. DOI: 10.1063/1.474934 (cit. on p. 50).

Kremer, K. and G. S. Grest (1990). "Dynamics of entangled linear polymer melts: a molecular-dynamics simulation". In: *J. Chem. Phys.* 92.8, pp. 5057–5086 (cit. on pp. 49, 57).

Kremer, K., G. S. Grest, and I. Carmesin (1988). "Crossover from Rouse to reptation dynamics: A molecular-dynamics simulation". In: *Phys. Rev. Lett.* 61.5, pp. 566–569 (cit. on p. 49).

Kroto, H. W., J. R. Heath, S. C. O'Brian, R. F. Curl, and R. E. Smalley (Nov. 1985). "C_{60}: Buckminsterfullerene". In: *Nature* 318, pp. 162–163. DOI: 10.1038/318162a0 (cit. on p. 45).

L.Bøhling (Feb. 2013). "Computer simulations of viscous liquids and aspherical particles". PhD thesis. Roskilde University. URL: http://glass.ruc.dk/pdf/phd_afhandlinger/LasseB_thesis.pdf (cit. on p. 36).

Leach, A. R. (2001). *Molecular modelling: principles and applications*. 2nd ed. Pearson Education (cit. on p. 73).

Lewis, L. J. and G. Wahnström (May 1993). "Relaxation of a molecular glass at intermediate times". In: *Solid State Communications* 86.5, pp. 295–299. DOI: 10.1016/0038-1098(93)90376-X (cit. on p. 58).

Lewis, L. J. and G. Wahnström (Nov. 1994). "Molecular-dynamics study of supercooled *ortho*-terphenyl". In: *Phys. Rev. E* 50 (5), pp. 3865–3877. DOI: 10.1103/PhysRevE.50.3865 (cit. on p. 58).

Lodge, T. P. (Oct. 1999). "Reconciliation of the Molecular Weight Dependence of Diffusion and Viscosity in Entangled Polymers". In: *Phys. Rev. Lett.* 83 (16), pp. 3218–3221. DOI: 10.1103/PhysRevLett.83.3218 (cit. on p. 57).

López, E. R., A. S. Pensado, M. J. P. Comuñas, A. A. H. Pádua, J. Fernández, and K. R. Harris (2011). "Density scaling of the transport properties of molecular and ionic liquids". In: *J. Chem. Phys.* 134, p. 144507. DOI: 10.1063/1.3575184 (cit. on p. 5).

Marrink, S. J., H. J. Risselada, S. Yefimov, D. P. Tieleman, and A. H. de Vries (2007). "The MARTINI Force Field:? Coarse Grained Model for Biomolecular Simulations". In: *J. Phys. Chem. B* 111.27. PMID: 17569554, pp. 7812–7824. DOI: 10.1021/jp071097f (cit. on p. 73).

Mason, E. A. and W. E. Rice (1954). "The intermolecular potentials for some simple nonpolar molecules". In: *J. Chem. Phys.* 22.5, pp. 843–851. DOI: 10.1063/1.1740200 (cit. on pp. 13, 106).

Meijer, E. J. and D. Frenkel (1991). "Melting line of Yukawa stystems by computer simulation". In: *J. Chem. Phys.* 94.3, pp. 2269–2271. DOI: 10.1063/1.459898 (cit. on p. 25).

Meyer, H., J. P. Wittmer, T Kreer, P. Beckrich, A. Johner, J. Farago, and J. Baschnagel (2008). "Static Rouse modes and related quantities: corrections to chain ideality in polymer melts". In: *Eur. Phys. J. E* 26, pp. 25–33. DOI: 10.1140/epje/i2007-10250-0 (cit. on p. 53).

Moynihan, C. T. and P. K. Gupta (1978). "The order parameter model for structural relaxation in glass". In: *J. Non-Cryst. Solids* 29, pp. 143–158. DOI: 10.1016/0022-3093(78)90110-2 (cit. on p. 85).

Nielsen, J. K. (1999). "Linear response theory for thermodynamic properties". In: *Phys. Rev. E* 60, pp. 471–481. DOI: 10.1103/PhysRevE.60.471 (cit. on p. 86).

Nielsen, J. K. and J. C. Dyre (1996). "Fluctuation-dissipation theorem for frequency-dependent specific heat". In: *Phys. Rev. B* 54, p. 15754. DOI: 10.1103/PhysRevB.54.15754 (cit. on p. 86).

Oels, H.-J. and G. Rehage (1977). "Pressure-Volume-Temperature Measurements on Atactic Polystyrene. A Thermodynamic View". In: *Macromolecules* 10.5, pp. 1036–1043. DOI: 10.1021/ma60059a030 (cit. on p. 85).

Ohta, H. and S. Hamaguchi (Nov. 2000). "Molecular dynamics evaluation of self-diffusion in Yukawa systems". In: *Phys. Plasmas* 7.11, pp. 4506–4514. DOI: 10.1063/1.1316084 (cit. on p. 24).

Paluch, M., C. M. Roland, S. Pawlus, J. Zioło, and K. L. Ngai (Sept. 2003a). "Does the Arrhenius Temperature Dependence of the Johari-Goldstein Relaxation Persist above $T - g$?" In: *Phys. Rev. Lett.* 91.11, p. 115701. DOI: 10.1103/PhysRevLett.91.115701 (cit. on p. 39).

Paluch, M., R. Casalini, A. Patkowski, T. Pakula, and C. M. Roland (2003b). "Effect of volume changes on segmental relaxation in siloxane polymers". In: *Phys. Rev. E* 68, p. 031802. DOI: 10.1103/PhysRevE.68.031802 (cit. on p. 4).

Paluch, M., S. Haracz, A. Grzybowski, M. Mierzwa, J. Pionteck, A. Rivera-Calzada, and C. Leon (2010). "A Relationship between Intermolecular Potential, Thermodynamics, and Dynamic Scaling for a Supercooled Ionic Liquid". In: *J. Phys. Chem. Lett.* 1, pp. 987–992. DOI: 10.1021/jz9004653 (cit. on p. 5).

Pedersen, U. R. (Jan. 2009). "Long-time simulations of vicous liquids". PhD thesis. Roskilde University. URL: http://glass.ruc.dk/pdf/phd_afhandlinger/Ulf-afhandling.pdf (cit. on pp. 86, 90).

Pedersen, U. R. (Sept. 2013). "Direct calculation of the solid-liquid Gibbs free energy difference in a single equilibrium simulation". In: *J. Chem. Phys.* 139.10, 104102, p. 104102. DOI: 10.1063/1.4818747 (cit. on p. 62).

Pedersen, U. R., T. Christensen, T. B. Schrøder, and J. C. Dyre (2008a). "Feasibility of a single-parameter description of equilibrium viscous liquid dynamics". In: *Phys. Rev. E* 77, p. 011201. DOI: 10.1103/PhysRevE.77.011201 (cit. on p. 90).

Pedersen, U. R., N. P. Bailey, T. B. Schrøder, and J. C. Dyre (2008b). "Strong pressure-energy correlations in van der Waals liquids". In: *Phys. Rev. Lett.* 100, p. 015701. DOI: 10.1103/PhysRevLett.100.015701 (cit. on pp. i, ii, 11–13).

Pedersen, U. R., T. B. Schrøder, and J. C. Dyre (2010). "A repulsive reference potential reproducing the dynamics of a liquid with attractions". In: *Phys. Rev. Lett.* 105.15, p. 157801. DOI: 10.1103/PhysRevLett.105.157801 (cit. on p. 19).

Pensado, A. S., A. A. H. Pádua, M. J. P. Comuñas, and J. Fernández (2008). "Relationship between Viscosity Coefficients and Volumetric Properties Using a Scaling Concept for Molecular and Ionic Liquids". In: *J. Phys. Chem. B* 112, pp. 5563–5574. DOI: 10.1021/jp711752b (cit. on p. 59).

Press, W. H., S. A. Teukolsky, W. T. Vetterling, and B. P. Flannery (2007). *Numerical Recipes*. 3rd ed. Cambridge University Press (cit. on pp. 86–88, 90).

Prigogine, I. and R. Defay (1954). *Chemical Thermodynamics*. Longman, London (cit. on p. 85).

Puosi, F. and D. Leporini (2011). "Scaling between Relaxation, Transport, and Caged Dynamics in Polymers: From Cage Restructuring to Diffusion". In: *J. Phys. Chem. B* 115, pp. 14046–14051. DOI: 10.1021/jp203659r (cit. on p. 50).

Puosi, F. and D. Leporini (2012). "Communication: Fast and local predictors of the violation of the Stokes-Einstein law in polymers and supercooled liquids". In: *J. Chem. Phys.* 136, p. 211101. DOI: 10.1063/1.4725522 (cit. on p. 50).

Rapaport, D. C. (2004). *The art of Molecular Dynamics simulation*. 2nd ed. Cambridge University Press (cit. on p. 6).

Riggleman, R. A., G. N. Toepperwein, G. J. Papakonstantopoulos, and J. J. de Pablo (2009). "Dynamics of a Glassy Polymer Nanocomposite during Active Deformation". In: *Macromolecules* 42, pp. 3632–3640. DOI: 10.1021/ma802865n (cit. on pp. 50, 74).

Riggleman, R. A., J. F. Douglas, and J. J. de Pablo (2010). "Antiplasticization and the elastic properties of glass-forming polymer liquids". In: *Soft Matter* 6, pp. 292–304. DOI: 10.1039/b915592a (cit. on p. 74).

Robbins, M. O., K. Kremer, and G. S. Grest (1988). "Phase diagram and dynamics of Yukawa systems". In: *J. Chem. Phys.* 88.5, pp. 3286–3312. DOI: 10.1063/1.453924 (cit. on p. 25).

Roe, R.-J. (1977). "Thermodynamics of the glassy state with multiple order parameters". In: *J. Appl. Phys.* 48, pp. 4085–4091. DOI: 10.1063/1.323434 (cit. on p. 85).

Roed, L. A., D. Gundermann, J. C. Dyre, and K. Niss (2013). "Communication: Two measures of isochronal superposition". In: *J. Chem. Phys.* 139, p. 101101. DOI: 10.1063/1.4821163 (cit. on p. 81).

Roland, C. M. (2007). "The effect of thermodynamic variables on polymer chain dynamics". In: *Curr. Opin. Solid State Mater. Sci.* 11, pp. 41–46. DOI: 10.1016/j.cossms.2008.04.002 (cit. on p. 72).

Roland, C. M. (2010). "Relaxation phenomena in vitrifying polymers and molecular liquids". In: *Macromolecules* 43.19, pp. 7875–7890. DOI: 10.1021/ma101649u (cit. on pp. 5, 39, 59).

Roland, C. M. and R. Casalini (2004). "Comment on: "Disentangling density and temperature effects in the viscous slowing down of glass forming liquids" [J. Chem. Phys. **120**, 6135 (2004)]". In: *J. Chem. Phys.* 121.22, pp. 11503–11504. DOI: 10.1063/1.1814974 (cit. on p. 5).

Roland, C. M., M. Paluch, and R. Casalini (2004). "Effects of the volume and temperature on the global and segmental dynamics in poly(propylene glycol) and 1,4-polyisoprene". In: *J. Polym. Sci., Part B: Polym. Phys.* 42, pp. 4313–4319 (cit. on p. 72).

Roland, C. M., S. Hensel-Bielowka, M. Paluch, and R. Casalini (2005). "Supercooled dynamics of glass-forming liquids and polymers under hydrostatic pressure". In: *Rep. Prog. Phys.* 68.6, pp. 1405–1478. DOI: 10.1088/0034-4885/68/6/R03 (cit. on pp. i, ii, 5, 39).

Roland, C. M., R. B. Bogoslovov, R. Casalini, A. R. Ellis, S. Bair, S. J. Rzoska, K. Czuprynski, and S. Urban (2008). "Thermodynamic scaling and the characteristic relaxation time at the phase transition of liquid crystals". In: *J. Chem. Phys.* 128, p. 224506 (cit. on p. 5).

Rosenfeld, Y. (1999). "A quasi-universal scaling law for atomic transport in simple fluids". In: *J. Phys.: Condens. Matter* 11, pp. 5415–5427 (cit. on pp. 16, 22).

Rosenfeld, Y. (Nov. 2000). "Excess-entropy and freezing-temperature scalings for transport coefficients: Self-diffusion in Yukawa systems". In: *Phys. Rev. E* 62.5, pp. 7524–7527. DOI: 10.1103/PhysRevE.62.7524 (cit. on p. 25).

Rosenfeld, Y. (2001). "Quasi-universal melting-temperature scaling of transport coefficients in Yukawa systems". In: *J. Phys.: Condens. Matter* 13, pp. L39–L43. DOI: 10.1088/0953-8984/13/2/101 (cit. on p. 25).

Rosenfeld, Y. and P. Tarazona (1998). "Density functional theory and the asymptotic high density expansion of the free energy of classical solids and fluids". In: *Mol. Phys.* 95.2, pp. 141–150. DOI: 10.1080/00268979809483145 (cit. on pp. 20, 22, 25).

Rouse, P. E. (1953). "A Theory of the Linear Viscoelastic Properties of Dilute Solutions of Coiling Polymers". In: *J. Chem. Phys.* 21.7, pp. 1272–1280. DOI: 10.1063/1.1699180 (cit. on pp. 52, 55).

Rowlinson, J.S. (1989). "The Yukawa potential". In: *Physica A* 156.1, pp. 15–34. DOI: 10.1016/0378-4371(89)90108-8 (cit. on p. 24).

Rubinstein, M. and R. H. Colby (2003). *Polymer Physics*. Oxford University Pess (cit. on pp. 51, 55).

Samwer, K., R. Busch, and W. L. Johnson (Jan. 1999). "Change of Compressiblity at the Glass Transition and Prigogine-Defay Ratio in ZrTiCuNiBe Alloys". In: *Phys. Rev. Lett.* 82 (3), pp. 580–583. DOI: 10.1103/PhysRevLett.82.580 (cit. on p. 90).

Sanbonmatsu, K. Y. and M. S. Murillo (Feb. 2001). "Shear Viscosity of Strongly Coupled Yukawa Systems on Finite Length Scales". In: *Phys. Rev. Lett.* 86.7, pp. 1215–1218. DOI: 10.1103/PhysRevLett.86.1215 (cit. on p. 25).

Satoh, K. (2013). "Relationship between thermodynamic parameter and thermodynamic scaling parameter for orientational relaxation time for flip-flop motion of

nematic liquid crystals". In: *J. Chem. Phys.* 138, p. 094903. DOI: 10.1063/1.4793524 (cit. on p. 5).

Schlick, T. (Aug. 2002). *Molecular Modeling and Simulation: An Interdisciplinary Guide*. Ed. by J. E. Marsden, L. Sirovich, S. Wiggins, and S. S. Antman. Vol. 21. Interdisciplinary Applied Mathematics. Springer (cit. on p. 50).

Schrøder, T. B., N. P. Bailey, U. R. Pedersen, N. Gnan, and J. C. Dyre (2009). "Pressure-energy correlations in liquids. III. Statistical mechanics and thermodynamics with hidden scale invariance". In: *J. Chem. Phys.* 131.23, p. 234504. DOI: 10.1063/1.3265955 (cit. on pp. i, ii, 11).

Schrøder, T. B., N. Gnan, U. R. Pedersen, N. P. Bailey, and J. C. Dyre (2011). "Pressure-energy correlations in liquids. V. Isomorphs in generalized Lennard-Jones systems". In: *J. Chem. Phys.* 134.16, p. 164505. DOI: 10.1063/1.3582900 (cit. on pp. 11, 62).

Sen, S., S. K. Kumar, and P. Keblinski (2005). "Viscoelastic Properties of Polymer Melts from Equilibrium Molecular Dynamics Simulations". In: *Macromolecules* 38.3, pp. 650–653. DOI: 10.1021/ma0354871 (cit. on p. 57).

Shavit, A., J. F. Douglas, and R. A. Riggleman (2013). "Evolution of collective motion in a model glass-forming liquid during physical aging". In: *J. Chem. Phys.* 138, 12A528. DOI: 10.1063/1.4775781 (cit. on pp. 50, 74).

Slater, J. C. (1928). "The normal state of Helium". In: *Phys. Rev.* 32, pp. 349–360. DOI: 10.1103/PhysRev.32.349 (cit. on p. 106).

Swiety-Pospiech, A., Z. Wojnarowska, J. Pionteck, S. Pawlus, A. Grzybowski, S. Hensel-Bielowka, K. Grzybowska, A. Szulc, and M. Paluch (2012). "High pressure study of molecular dynamics of protic ionic liquid lidocaine hydrochloride". In: *J. Chem. Phys.* 136, p. 224501. DOI: 10.1063/1.4727885 (cit. on p. 5).

Swiety-Pospiech, A., Z. Wojnarowska, S. Hensel-Bielowka, J. Pionteck, and M. Paluch (2013). "Effect of pressure on decoupling of ionic conductivity from structural relaxation in hydrated protic ionic liquid, lidocaine HCl". In: *J. Chem. Phys.* 138, p. 204502. DOI: 10.1063/1.4807487 (cit. on p. 5).

Takahara, S., M. Ishikawa, O. Yamamuro, and T. Matsuo (1999). "Structural Relaxations of Glassy Polystyrene and o-Terphenyl Studied by Simultaneous Measurement of Enthalpy and Volume under High Pressure". In: *J Phys. Chem. B* 103.5, pp. 792–796. DOI: 10.1021/jp983801l (cit. on p. 90).

Tarjus, G., D. Kivelson, S. Mossa, and C. Alba-Simionesco (2004a). "Disentangling density and temperature effects in the viscous slowing down of glassforming liquids". In: *J. Chem. Phys.* 120.13, pp. 6135–6141. DOI: 10.1063/1.1649732 (cit. on pp. 5, 20, 39).

Tarjus, G., S. Mossa, and C. Alba-Simionesco (2004b). "Response to: "Comment on 'Disentangling density and temperature effects in the viscous slowing down of glassforming liquids' " [J. Chem. Phys. **121**, 11503 (2004)]". In: *J. Chem. Phys.* 121.22, p. 11505. DOI: 10.1063/1.1814975 (cit. on pp. 5, 39).

Tölle, A. (2001). "Neutron scattering studies of the model glass former ortho - terphenyl". In: *Rep. Prog. Phys.* 64.11, p. 1473 (cit. on pp. 4, 81).

Tölle, A., H. Schober, J. Wuttke, O. G. Randl, and F. Fujara (1998). "Fast relaxation in a fragile liquid under pressure". In: *Phys. Rev. Lett.* 80 (11), pp. 2374–2377. DOI: 10.1103/PhysRevLett.80.2374 (cit. on p. 4).

Toxvaerd, S., O. J. Heilmann, T. Ingebrigtsen, T. B. Schrøder, and J. C. Dyre (2009). "Time-reversible molecular dynamics algorithms with bond constraints". In: *J. Chem. Phys.* 131.6, p. 064102. DOI: 10.1063/1.3194785 (cit. on p. 50).

Tsolou, G., V. A. Harmandaris, and V. G. Mavrantzas (2006). "Atomistic molecular dynamics simulation of the temperature and pressure dependences of local and terminal relaxations in *c*is-1,4-polybutadiene". In: *J. Chem. Phys.* 124.8, p. 084906. DOI: 10.1063/1.2174003 (cit. on p. 59).

Tycko, R., R. C. Haddon, G. Dabbagh, S. H. Glarum, D. C. Douglass, and A. M. Mujsce (1991). "Solid-state magnetic resonance spectroscopy of fullerenes". In: *J. Phys. Chem.* 95.2, pp. 518–520. DOI: 10.1021/j100155a006 (cit. on p. 45).

Urban, S. (2011). "Thermodynamic scaling of the viscosity and the longitudinal relaxation time for three nematic n-alkyl-cyclohexyl-cyanophenyls". In: *Liq. Cryst.* 38, pp. 1147–1152. DOI: 10.1080/02678292.2011.598955 (cit. on p. 5).

Urban, S. and C. M. Roland (2011). "Low frequency relaxation in liquid crystals in relation to structural relaxation in glass-formers". In: *J. Non-Cryst. Solids* 357, pp. 740–745. DOI: 10.1016/j.jnoncrysol.2010.05.093 (cit. on p. 5).

Urban, S. and A. Würflinger (2005). "Thermodynamical scaling of the low frequency relaxation time in liquid crystalline phases". In: *Phys. Rev. E* 72, p. 021707. DOI: 10.1103/PhysRevE.72.021707 (cit. on p. 5).

Urban, S., C. M. Roland, J. Czub, and K. Skrzypek (2007). "Thermodynamic analysis of the low frequency relaxation time in the smectic A and C phases of a liquid crystal". In: *J. Chem. Phys.* 127, p. 094901. DOI: 10.1063/1.2759488 (cit. on p. 5).

Vaulina, O. S. and S. A. Khrapak (2000). "Scaling law for the fluid-solid phase transition in Yukawa systems (dusty plasmas)". In: *J. Exp. Theor. Phys.* 90.2, pp. 287–289. DOI: 10.1134/1.559102 (cit. on pp. 24, 28, 33).

Veldhorst, A. A., L. Bøhling, J. C. Dyre, and T. B. Schrøder (2012). "Isomorphs in the phase diagram of a model liquid without inverse power law repulsion". In: *Eur. Phys. J. B* 85.1, p. 21. DOI: 10.1140/epjb/e2011-20506-2 (cit. on pp. 11, 13, 18–20, 43).

Veldhorst, A. A., J. C. Dyre, and T. B. Schröder (2013). "Isomorphs in flexible Lennard-Jones chains". In: *arXiv:1307.5237* (cit. on pp. 62–64, 66–71).

Verdier, P. H. (1966). "Monte Carlo studies of lattice-model polymer chains. I. correlation functions in the statistical-bead model". In: *J. Chem. Phys.* 45.6, p. 2118. DOI: 10.1063/1.1727896 (cit. on p. 53).

Verlet, L. (1967). "Computer experiment on classical fluids. I. Thermodynamical properties of Lennard-Jones molecules". In: *Phys. Rev.* 159, p. 98 (cit. on p. 6).

Verwey, E. J. W. and J. Th. G. Overbeek (1948). *Theory of the stability of lyophobic colloids*. Elsevier (cit. on p. 23).

Voyiatzis, E., F. Müller-Plathe, and M. C. Böhm (2013). "Do transport properties of entangled linear polymers scale with excess entropy?" In: *Macromolecules* 46, pp. 8710–8723. DOI: 10.1021/ma401617z (cit. on p. 50).

Warner, H. R. (1972). "Kinetic Theory and Rheology of Dilute Suspensions of Finitely Extendible Dumbbells". In: *Ind. Eng. Chem. Fundamentals* 11, pp. 379–387. DOI: 10.1021/i160043a017 (cit. on p. 74).

Whipple, E. C., T. G. Northrop, and D. A. Mendis (Aug. 1985). "The electrostatics of a dusty plasma". In: *J. Geophys. Res.* 90.A8, pp. 7405–7413. DOI: 10.1029/JA090iA08p07405 (cit. on p. 24).

Wondraczek, L. and H. Behrens (2007). "Molar volume, excess enthalpy, and Prigogine-Defay ratio of some silicate glasses with different (P,T) histories". In: *J. Chem. Phys.* 127.15, 154503, p. 154503. DOI: 10.1063/1.2794745 (cit. on p. 90).

Xu, W.-S. and K. F. Freed (2013). "Thermodynamic scaling of dynamics in polymer melts: Predictions from the generalized entropy theory". In: *J. Chem. Phys.* 138, p. 234501. DOI: 10.1063/1.4809991 (cit. on p. 59).

Yannoni, C. S., R. D. Johnson, G. Meijer, D. S. Bethune, and J. R. Salem (1991). "Carbon-13 NMR study of the C_{60} cluster in the solid state: molecular motion and carbon chemical shift anisotropy". In: *J. Phys. Chem.* 95.1, pp. 9–10. DOI: 10.1021/j100154a005 (cit. on p. 45).

Young, D. A., A. K. McMahan, and M. Ross (1981). "Equation of state and melting curve of helium to very high pressure". In: *Phys. Rev. B* 24.9, pp. 5119–5127. DOI: 10.1103/PhysRevB.24.5119 (cit. on p. 106).

Yukawa, H. (1935). "On the interaction of elementary particles. I." In: *Proc. Phys.-Math. Soc. Japan* 17, pp. 48–57 (cit. on p. 23).

Zimm, B. H. (Feb. 1956). "Dynamics of Polymer Molecules in Dilute Solution: Viscoelasticity, Flow Birefringence, and Dielectric Loss". In: *J. Chem. Phys.* 24.2, pp. 269–278. DOI: 10.1063/1.1742462 (cit. on p. 55).

Zoller, P. (1982). "A study of the pressure-volume-temperature relationships of four related amorphous polymers: Polycarbonate, polyarylate, phenoxy, and polysulfone". In: *J. Polym. Sci. Part B: Polym. Phys.* 20.8, pp. 1453–1464. DOI: 10.1002/pol.1982.180200811 (cit. on p. 90).

Appendix A

The Buckingham potential

In the Lennard-Jones potential, the repulsion between two atoms due to the Pauli exclusion principle is given by an inverse power law (IPL). This has been found to be a relatively good model for the interatomic repulsion (Jones, 1924). Slightly after this, due to the advent of quantum physics, it was possible to calculate the functional form of the short range repulsion between two atoms. The was done by Slater (1928), who found that the repulsion was better described by an exponential. Buckingham (1938) used a potential like the Lennard-Jones potential but with an repulsive exponential to calculate the equation of state of several noble gasses.

In this thesis, we have used the following form of the Buckingham potential (Koči et al., 2007; Young et al., 1981):

$$v(r) = \varepsilon \left(\frac{6}{\alpha - 6} \exp\left[\alpha \left(1 - \frac{r}{r_m} \right) \right] - \frac{\alpha}{\alpha - 6} \left(\frac{r_m}{r} \right)^6 \right). \tag{A.1}$$

This to make it easily comparable with the Lennard-Jones potential. The distance r_m is the minimum of the potential, ε the depth of the potential well, and the parameter α is related to the width of the potential well and therefore the steepness of the repulsion.

The Buckingham potential has been shown to be indeed better than the Lennard-Jones potential in the reproduction of experimental data of inert gasses (Abrahamson, 1963; Kilpatrick et al., 1955; Mason and Rice, 1954). Note also that in figure 2.2 in chapter 2 the Buckingham potential is better able to reproduce the behavior and magnitude of γ.

Despite the correctness of the Buckingham potential, it has never been able to reach the popularity of the Lennard-Jones potential in the field of computer simulations. The main reason for this is simply the extra computational time it takes to calculate an exponential.

Except figure 2.2, all simulation data of the Buckingham potential are from a Kob-Andersen binary glass-forming mixture (Kob and Andersen, 1994). The potential parameters $\varepsilon = 1$ and $r_m = 2^{1/6}$ were the same as for the Lennard-Jones potential, and $\alpha = 14.5$ is a common value for the Buckingham potential.

Appendix B

Additions to RUMD

The simulations done for this thesis were performed using the Roskilde University Molecular Dynamics (RUMD) code, which is developed by the Glass and Time group. This means I implemented several functionalities in the code because I needed them for research. Therefore here a small list of things I have implemented in the code.

- **Pair potentials:** Several of the pair potentials used in this thesis were not implemented yet, including the Yukawa, Girifalco, and the two new potentials S6 and S12-6. Luckily, RUMD has been designed to make this a relatively easy task.

- **Linear solver on the GPU:** For the simulation of rigid bonds, a set of linear equations has to be solved for each molecule to keep the bond lengths fixed. This is done fastest on the GPU, where it can be done using multiple cores per molecule and without sending data back and forth to the CPU. For the linear molecules simulated in this thesis, an optimized solver was also implemented that makes use of the fact that for these molecules, the matrix to be solved can be written in tridiagonal form.

- **Box scaling for molecules:** For the so called isomorphic "jumps" in the phase diagram that were performed in chapter 5, it was necessary to implement a function to scale the box with the centers of mass of the molecules, while keeping intramolecular distances and orientations fixed and handling the periodic boundary conditions correctly.

- **Analysis tools for molecules:** Some quantities specific for molecules and/or linear molecules have been included in the RUMD distribution, such as calculation of Rouse modes, the end-to-end vector, and their autocorrelation functions.

- **Python output manager:** An output manager has been implemented in the python interface, making it possible to define a data analysis function in the python script that is called during the simulation. This provides a means to analyze any data that are present in the program during the simulation on the fly in the simulation script.

- **Sorting for molecules:** In order to optimize the code for bigger systems, the particles were sorted in such a way that particles that are close to each other in the simulation are also close in memory. I implemented functions in the classes that handle data on molecules to keep track of the changing memory locations of these particle during the simulation.

Appendix C

Reprints of articles

Eur. Phys. J. B (2012) 85: 21
DOI: 10.1140/epjb/e2011-20506-2

THE EUROPEAN PHYSICAL JOURNAL B

Regular Article

Isomorphs in the phase diagram of a model liquid without inverse power law repulsion

A.A. Veldhorst, L. Bøhling, J.C. Dyre, and T.B. Schrøder[a]

DNRF Center "Glass and Time", IMFUFA, Dept. of Sciences, Roskilde University, P.O. Box 260, DK-4000 Roskilde, Denmark

Received 23 June 2011 / Received in final form 23 November 2011
Published online 18 January 2012
© The Author(s) 2012. This article is published with open access at Springerlink.com

Abstract. It is demonstrated by molecular dynamics simulations that liquids interacting via the Buckingham potential are strongly correlating, i.e., have regions of their phase diagram where constant-volume equilibrium fluctuations in the virial and potential energy are strongly correlated. A binary Buckingham liquid is cooled to a viscous phase and shown to have isomorphs, which are curves in the phase diagram along which structure and dynamics in appropriate units are invariant to a good approximation. To test this, the radial distribution function, and both the incoherent and coherent intermediate scattering function are calculated. The results are shown to reflect a hidden scale invariance; despite its exponential repulsion the Buckingham potential is well approximated by an inverse power-law plus a linear term in the region of the first peak of the radial distribution function. As a consequence the dynamics of the viscous Buckingham liquid is mimicked by a corresponding model with purely repulsive inverse-power-law interactions. The results presented here closely resemble earlier results for Lennard-Jones type liquids, demonstrating that the existence of strong correlations and isomorphs does *not* depend critically on the mathematical form of the repulsion being an inverse power law.

1 Introduction

Recently a series of papers has been published concerning so-called strongly correlating liquids and their physical properties [1–6]. Liquids that exhibit these strong correlations have simpler thermodynamic, structural, and dynamical properties than liquids in general. A strongly correlating liquid is identified by looking at the correlation coefficient of the equilibrium fluctuations of the potential energy $U(\mathbf{r}_1,\ldots,\mathbf{r}_N)$ and virial $W(\mathbf{r}_1,\ldots,\mathbf{r}_N) \equiv -1/3\sum_i \mathbf{r}_i\cdot\nabla_{\mathbf{r}_i}U(\mathbf{r}_1,\ldots,\mathbf{r}_N)$ [7] at constant volume:

$$R = \frac{\langle \Delta W \Delta U\rangle}{\sqrt{\langle(\Delta W)^2\rangle\langle(\Delta U)^2\rangle}}. \quad (1)$$

Here brackets denote averages in the NVT ensemble (fixed particle number, volume, and temperature), Δ denotes the difference from the average. The virial W gives the configurational part of the pressure [7],

$$pV = Nk_BT(\mathbf{p}_1,\ldots,\mathbf{p}_N) + W(\mathbf{r}_1,\ldots,\mathbf{r}_N). \quad (2)$$

Strongly correlating liquids are defined [1] as liquids that have $R \geq 0.9$.

The origin of strong WU correlations was investigated in detail in references [3,4] for systems interacting via the Lennard-Jones (LJ) potential:

$$v(r) = 4\epsilon\left[\left(\frac{\sigma}{r}\right)^{12} - \left(\frac{\sigma}{r}\right)^{6}\right]. \quad (3)$$

The fluctuations of W and U are dominated by fluctuations of pair distances within the first neighbor shell, where the LJ potential is well approximated by an extended inverse power law (eIPL), defined as an inverse power law (IPL) plus a linear term [3]:

$$v_{eIPL}(r) = Ar^{-n} + B + Cr. \quad (4)$$

The IPL term gives perfect UW correlations, whereas the linear term contributes little to the fluctuations at constant volume: when one pair distance increases, others decrease, keeping the contributions from the linear term almost constant (this cancellation is exact in one dimension). The consequence is that LJ systems inherit some of the scaling properties of the IPL potential – they have a "hidden scale invariance" [4,8]. Prominent among the properties of strongly correlating liquids is that they have "isomorphs", i.e., curves in the phase diagram along which structure, dynamics, and some thermodynamical properties are invariant in appropriate units [5,6]. The physics of strongly correlating liquids was briefly reviewed recently in reference [9].

Since the LJ system consists of two IPL terms, it is perhaps tempting to assume that a repulsive (inverse)

[a] e-mail: tbs@ruc.dk

power law is necessary for the hidden scale invariance described above. In the present paper we use the modified Buckingham (exp-six) pair potential to show that this is *not* the case. The Buckingham potential was first derived by Slater from first-principle calculations of the force between helium atoms [10]. Buckingham later used this form of the potential to calculate the equation of state for different noble gases [11]. The Buckingham potential has an exponential repulsive term, while the attractive part is given by a power law [12,13]:

$$v(r) = \epsilon \left(\frac{6}{\alpha - 6} \exp\left[\alpha\left(1 - \frac{r}{r_m}\right)\right] - \frac{\alpha}{\alpha - 6}\left(\frac{r_m}{r}\right)^6 \right). \quad (5)$$

Here ϵ is the depth of the potential well and r_m specifies the position of the potential minimum. The parameter α determines the shape of the potential well. The Buckingham potential is better able to reproduce experimental data of inert gasses than the LJ potential [14–16], but is also computationally more expensive (unless look-up tables are utilized [7]).

All simulation data in this paper were obtained from molecular dynamics in the NVT ensemble. The samples contained 1000 particles. The simulations were set up by instant cooling from a high temperature state point followed by an equilibration period, to ensure the simulations were independent from each other. The simulations were performed with the RUMD molecular dynamics package [17], which is optimized for doing computations on state-of-the-art GPU hardware.

2 Correlations in single-component Buckingham liquids

To compare the simulations with experiments [18], argon parameters from reference [14] were used; $\alpha = 14.0$, $r_m = 0.3866$ nm, $\epsilon/k_B = 123.2$ K. As can be seen in Figure 1a, the single-component Buckingham (SCB) liquid is strongly correlating ($R \geq 0.9$) in parts of the phase diagram, particularly at high densities and/or temperatures. The correlation coefficients (Eq. (1)) of the Buckingham systems are very similar to those of argon and the LJ system (dotted line in Fig. 1). This is a first indication that the actual functional form of the repulsive part of the potential does not have to be an inverse power law in order for a system to exhibit strong WU correlations.

Another interesting property of the fluctuations is the quantity γ defined [4,5] as

$$\gamma = \frac{\langle \Delta W \Delta U \rangle}{\langle (\Delta U)^2 \rangle}. \quad (6)$$

When a system is strongly correlating (R is close to one), $\Delta W \approx \gamma \Delta U$. For IPL potentials γ is constant and equal to $n/3$ and $R = 1$. For non-IPL potentials, however, $R < 1$ and γ may change with temperature and density as seen in Figure 1b [1,19]. Especially for $R < 0.9$, we find γ changing rapidly. The curves are similar for the 20.0 mol/L SCB and SCLJ systems, except for a vertical offset.

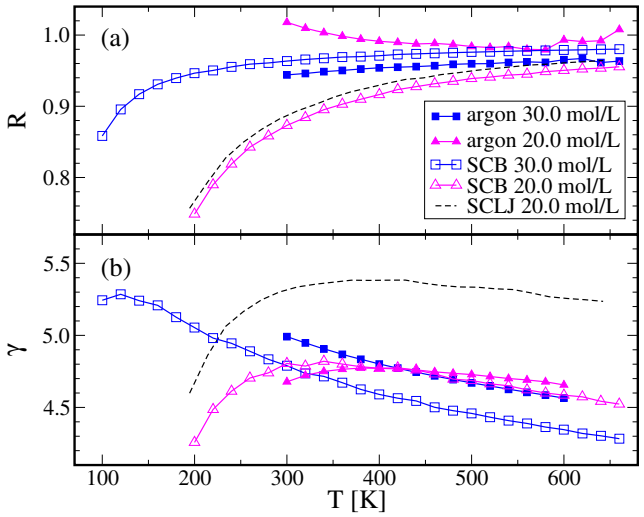

Fig. 1. (Color online) (a) The correlation coefficient, R, as a function of temperature on isochores for single-component Buckingham (SCB), single-component Lennard-Jones (SCLJ), and argon. For SCB and SCLJ argon values were used for all potential parameters [14], and R was calculated directly from equation (1). For argon R was calculated from experimental data [18] as described in references [1,3]. The correlations are strongest for state points with both high density and high temperature, and the difference between the Buckingham and the LJ potential is small. The correlation coefficient $R > 1$ for low-temperature 20.0 mol/L argon is of course unphysical and either caused by an uncertainty in the experimental data or the approximations applied in the calculation of R (see Refs. [3,20] for details). (b) The value of γ (Eq. (6)) plotted versus temperature for the same systems as in (a). For argon γ was calculated from experimental data [18] using equation (7). γ decreases slowly for increasing temperatures, except when the correlation coefficient is low ($R \lesssim 0.9$).

Fluctuations in U and W are of course only directly accessible in simulations. For experimental systems one must revert to the use of thermodynamic quantities that reflect the fluctuations in U and W. For instance, the configurational part of the pressure coefficient $\beta_V^{ex} = (\partial(W/V)/\partial T)_V$ and the configurational part of the isochoric specific heat per unit volume $c_V^{ex} = (\partial(U/V)/\partial T)_V$ can be used to to calculate γ for argon as follows [1,3,5]:

$$\gamma = \frac{\beta_V^{ex}}{c_V^{ex}}. \quad (7)$$

The values of γ for argon obtained in this way are plotted in Figure 1b, and the agreement with the Buckingham systems is good. This confirms that the Buckingham potential produces more accurate predictions of experimental argon data than the LJ potential.

Interestingly, low density argon has a higher correlation coefficient than high density argon. This is the opposite of what is found for the Buckingham and the LJ potentials. Furthermore, the buckingham data are in better agreement with the argon data at low density than at high density. At the present we do not have any explanation for these observations.

3 Isomorphs in binary Buckingham mixtures

Strongly correlating liquids are predicted to have isomorphs, which are curves in the phase diagram along which structure, dynamics, and some thermodynamical properties are invariant in appropriate reduced units [5,6]. Introducing reduced coordinates as $\tilde{\mathbf{r}}_i = \rho^{1/3}\mathbf{r}_i$, two state points (1) and (2) are defined to be isomorphic if pairs of microscopic configurations with same reduced coordinates ($\tilde{\mathbf{r}}_i^{(1)} = \tilde{\mathbf{r}}_i^{(2)}$) have proportional configurational Boltzmann weights:

$$e^{-U\left(\mathbf{r}_1^{(1)},\ldots,\mathbf{r}_N^{(1)}\right)/k_BT_1} = C_{12}e^{-U\left(\mathbf{r}_1^{(2)},\ldots,\mathbf{r}_N^{(2)}\right)/k_BT_2}. \quad (8)$$

Here the constant C_{12} depends only on the two state points and equation (8) is required to hold to a good approximation for all physically relevant configurations [6]. An isomorph is a curve in the phase diagram for which all points are isomorphic (an isomorph is a mathematical equivalence class of isomorphic state points). The isomorphic invariance of structure, dynamics, and some thermodynamical properties – all in reduced units – can be derived directly from equation (8) [5]. Only IPL liquids have exact isomorphs, but it has been shown that all strongly correlating liquids have isomorphs to a good approximation (Appendix A of Ref. [5]).

Among the thermodynamical properties that are isomorphic invariant is the excess entropy, $S_{ex} \equiv S - S_{ideal}$, where S_{ideal} is the entropy of an ideal gas at the same temperature and density. In the following, isomorphic state points were generated by utilizing that the quantity γ in equation (6) can be used to change density and temperature while keeping the excess entropy constant [5,6]:

$$\gamma = \left(\frac{\partial \ln T}{\partial \ln \rho}\right)_{S_{ex}}. \quad (9)$$

By choosing the density of a new isomorphic state point close to the density of the previous isomorphic state point, the temperature of the new state point can be calculated from the fluctuations by combining equations (6) and (9) [5]. In this way a set of isomorphic points can be obtained from one initial state point.

The predicted isomorphic invariance of the dynamics is most striking in viscous liquids, where the dynamics in general depend strongly on temperature and density. To demonstrate that systems interacting via the Buckingham potential have isomorphs, we study what we term a Kob-Andersen binary Buckingham (KABB) mixture with potential parameters being the same as for the original Kob-Andersen binary LJ (KABLJ) mixture [21]: $\epsilon_{AA} = 1.0$, $r_{m,AA} = \sqrt[6]{2}$, $\epsilon_{AB} = 1.5$, $r_{m,AB} = 0.8\sqrt[6]{2}$, $\epsilon_{BB} = 0.5$, $r_{m,BB} = 0.88\sqrt[6]{2}$. A 4:1 mixture (A:B) was used with $\alpha = 14.5$. The potentials were truncated and shifted at $r_{ij}^{cut} = 2.5r_{m,ij}/\sqrt[6]{2}$.

One of the predicted invariants on an isomorph is the structure of the system. To test this prediction, the radial distribution function in reduced coordinates $g(\tilde{r}) = g(\rho^{1/3}r)$ was plotted for isomorphic state points (Fig. 2a).

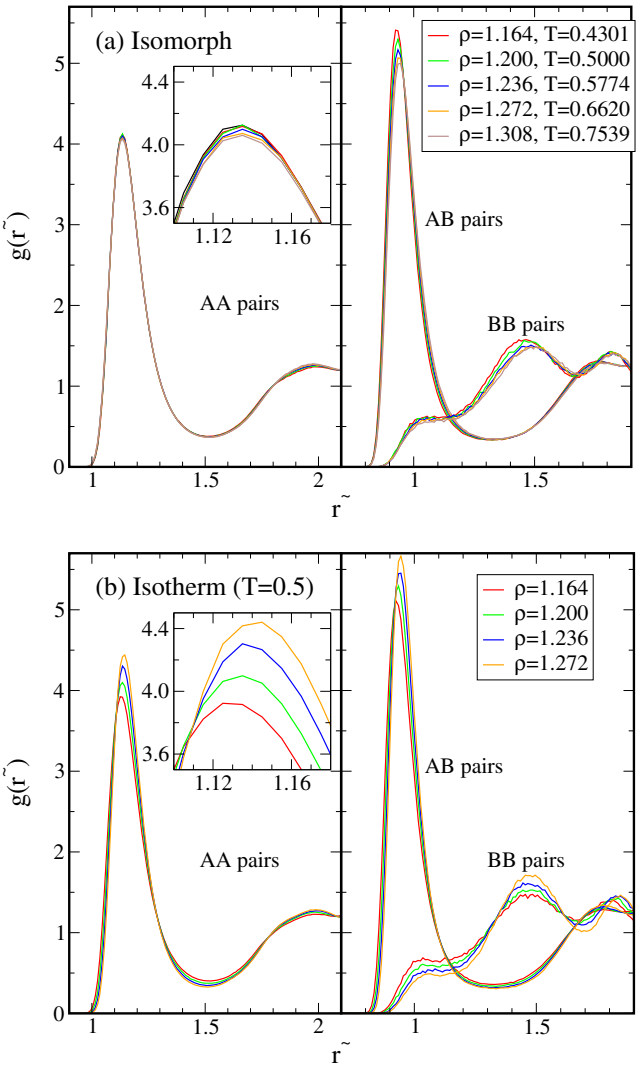

Fig. 2. (Color online) The radial distribution functions $g(\tilde{r})$ for simulations of the KABB mixture. Both graphs are in reduced units where $\tilde{r} = \rho^{1/3}r$. (a) $g(\tilde{r})$ for isomorphic state points and the three different particle combinations. The structure is invariant on the isomorph for the AA particle pairs, but for the AB and BB pairs the structure is less invariant. (b) $g(\tilde{r})$ for isothermal state points of smaller density variation. The structure is not invariant on the isotherm for any of the particle pairs.

The structure is invariant for the large (A) particle pair correlation function to a very good approximation. For the AB and BB pairs the structure is less invariant. However, when a comparison is made with Figure 2b, it is clear that $g(\tilde{r})$ for the AB and BB pairs is still more invariant on an isomorph than on an isotherm (note that the density variation on the isomorph is larger than on the isotherm). This situation is similar to what is found for the KABLJ system [5].

To investigate the dynamics of the systems, the incoherent intermediate scattering function $F_s(q,t)$ is plotted in reduced units in Figures 3a and 3b. The presence of a plateau in F_s shows that the system is in a viscous state,

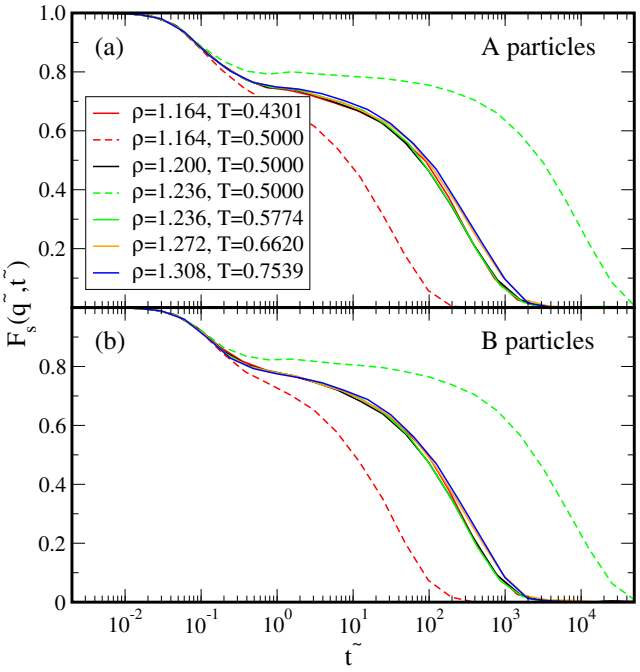

Fig. 3. (Color online) Incoherent intermediate scattering function for the A (a) and B (b) particles of the KABB system. The time is given in reduced units ($\tilde{t} = \rho^{1/3}T^{1/2}t$) and the q-vector is kept constant in reduced units: $q_A = 7.25(\rho/1.2)^{1/3}$ and $q_B = 5.5(\rho/1.2)^{1/3}$. The solid lines represent isomorphic state points, while dashed lines show isothermal density changes for comparison. The dynamics are to a good approximation invariant on an isomorph when expressed in reduced units, especially when compared to the isotherm. In contrast to $g(\tilde{r})$, this holds for both the A and the B particles.

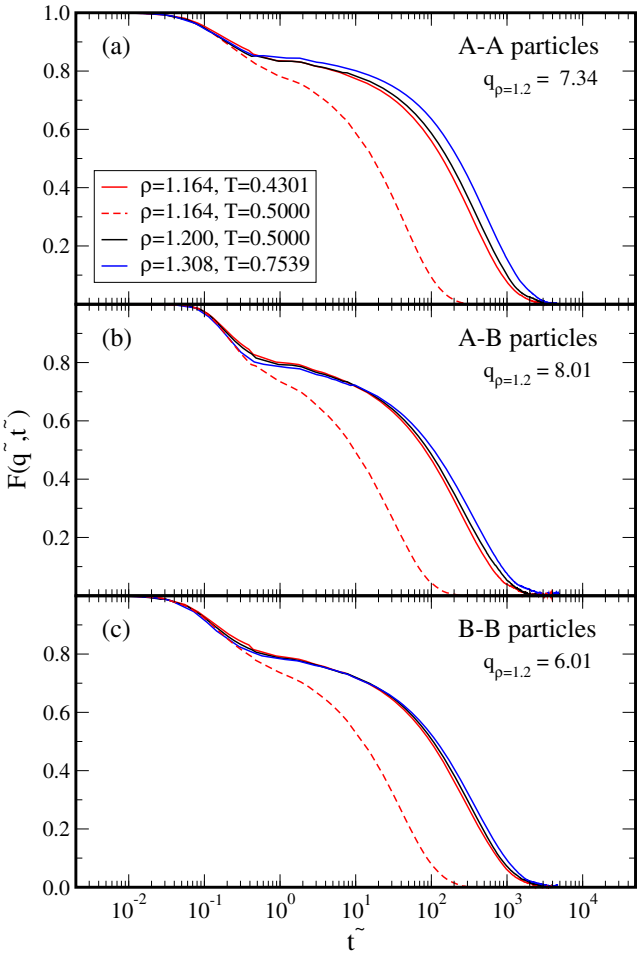

Fig. 4. (Color online) Coherent intermediate scattering function for different particle pairs on an isomorph in reduced units ($\tilde{t} = \rho^{1/3}T^{1/2}t$). The solid lines represent isomorphic state points, while dotted lines show isothermal density changes for comparison. Again, the q-vector is kept constant in reduced units: $q_{AA} = 7.34(\rho/1.2)^{1/3}$, $q_{AB} = 8.01(\rho/1.2)^{1/3}$ and $q_{BB} = 6.01(\rho/1.2)^{1/3}$. Also $F(\tilde{q},\tilde{t})$ is invariant on the isomorph. Contrary to what is seen for $g(\tilde{r})$, the invariance holds better for the AB and BB parts.

where the dynamics are highly state point dependent. The large difference in F_s for the two isothermal state points confirms this (dashed lines). For the isomorph all F_s data collapse more or less onto the same curve, showing that the dynamics are indeed invariant to a good approximation on an isomorph. In contrast to the radial distribution functions, the invariance holds well for both types of particles.

To investigate the invariance in dynamics further, the coherent intermediate scattering function was calculated (Fig. 4). The coherent intermediate scattering function was calculated from the spatial transform of the number density $\rho(q)$ [7]. In order to obtain good results, it is necessary to average over time scales that are 10–15 times longer than what is usual for the intermediate scattering function. This is the reason that there are less state points shown for the coherent-, than for the incoherent intermediate scattering function. The data confirm that the dynamics are invariant on the isomorph, especially when compared to the isothermal density change (dashed lines). However, the invariance seems to hold slightly better for the AB and BB parts, which is the opposite of what is seen for the structural invariance.

For systems described by a generalized LJ potential consisting of two IPL terms, the invariance of the structure leads to a prediction for the shape of an isomorph when plotted in the U-W plane [6] (generalized LJ potentials are a sum of inverse power laws). Since the repulsive term in the Buckingham potential is described by an exponential function, it is not possible to derive an exact equation that describes the isomorph in terms of U and W. Figure 5a shows that isomorphs for the KABB system agree well with the prediction for the 12–6 LJ system if $\alpha = 14.5$ (this value of α was chosen to demonstrate this feature). For $\alpha = 13.0$, there is a significant difference with the predicted shape at higher density and temperature. Figure 5b shows the isomorphs for both values of α after scaling U and W by the same isomorph-dependent factor, demonstrating the existence of a master isomorph [6]. This shows that master isomorphs exist not only in generalized LJ systems where they can be justified from analytical arguments [6].

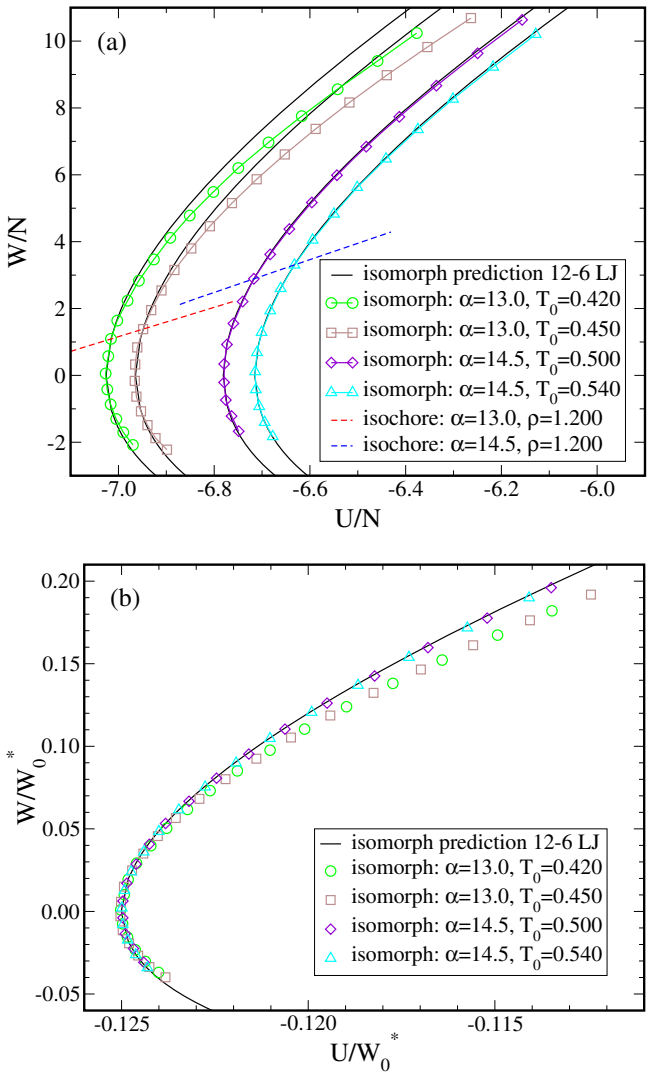

Fig. 5. (Color online) (a) Plot of the potential energy per particle versus virial per particle for the KABB system. The solid lines are the predictions of the isomorph shape for the 12–6 LJ potential [6]. For these predictions the initial state points with $\rho = 1.2$ were used as reference point. Since a new value of γ was calculated for every state point, γ is not constant on the isomorphs, but changes approximately 10% along the isomorphs. The shape of the KABB isomorph agrees very well with the predicted shape for the 12–6 LJ potential for $\alpha = 14.5$. For $\alpha = 13.0$, the shape is different. (b) The same data now scaled with W_0^* defined as the virial at $U = 0$ [6]. The isomorphs scale onto each other, forming a so called master isomorph for each value of α.

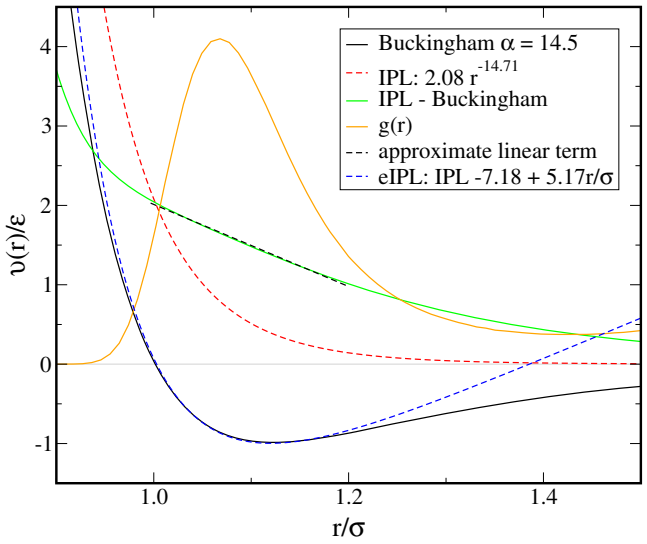

Fig. 6. (Color online) The figure shows how the Buckingham potential ($\alpha = 14.5$) can be approximated by an extended IPL potential (eIPL). The red dotted line is the IPL approximation obtained using the parameters obtained below in Figure 7. The difference of the IPL approximation and the Buckingham potential (dashed green line) is more or less linear in the first peak of $g(r)$. By subtracting this linear term from the IPL term the eIPL approximation is found (dashed blue line).

4 The inverse-power-law (IPL) approximation

As mentioned in the introduction, a generic explanation [3–5] for the existence of strong correlations and isomorphs in non-IPL systems, is the fact that some pair potentials can be well approximated by an eIPL (Eq. (4)) as shown in Figure 6. Putting this explanation to the test, it was recently demonstrated that structure and dynamics of the KABLJ system can be reproduced by a purely repulsive IPL system even in the viscous phase [22]. In the following we demonstrate that this procedure works also for the KABB system, despite its non-IPL repulsion.

Following Pedersen et al. [22], we assume that the Kob-Andersen IPL (KABIPL) system used to approximate the KABB system has the form

$$v^{IPL}(r) = A\epsilon_{ij}\left(\frac{\sigma_{ij}}{r_{ij}}\right)^n \tag{10}$$

where the parameters ϵ_{ij} and σ_{ij} are the Kob-Andersen parameters for the different types of particles and the constants A and n are independent of particle type.

For IPL liquids it is known that $W = (n/3)U$, so in principle the value of n could be calculated from γ determined from the WU fluctuations (Eq. (9)). For non-IPL liquids however, there is a slight state point dependence of γ, so instead the slope of an isochore was used to determine n (Fig. 7a) making use of the identity [5]

$$\gamma = \left(\frac{\partial W}{\partial U}\right)_V. \tag{11}$$

For the Buckingham potential with $\alpha = 14.5$ we obtained $\gamma = 4.904$ and $n = 14.71$. This is lower than the $\gamma = 5.16$ which was found for the 12–6 LJ potential [22]. This is also consistent with the data in Figure 1b where the SCB system has a lower value of gamma than the SCLJ system.

From equation (10) it follows that the total internal energy of the IPL system can be written as

$$U^{IPL} = A\sum_{i>j}\epsilon_{ij}\left(\frac{\sigma_{ij}}{r_{ij}}\right)^n. \tag{12}$$

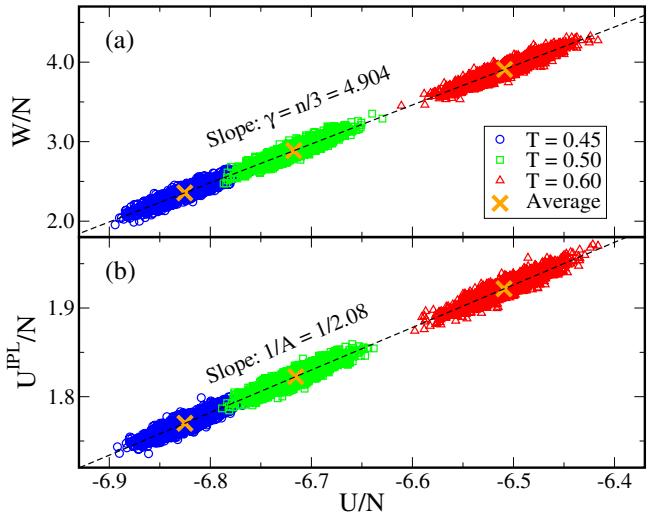

Fig. 7. (Color online) Three isochoric state points were used to obtain the parameters for the IPL potential. (a) The value of n was determined by linear regression to the mean values of the virial and the potential energy (marked by yellow crosses. (b) The method used to find the value of A of equation (12). $U^{IPL} = \sum_{i>j} \epsilon_{ij}(\sigma_{ij}/r_{ij})^n$ was calculated from configurations drawn from the KABB simulations and plotted against the energy obtained during the simulations; the value of A was then obtained from the slope of the mean energies (again marked by yellow crosses).

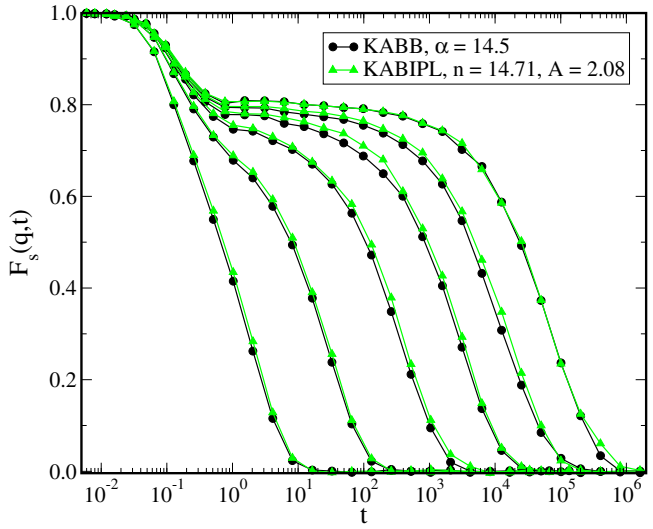

Fig. 8. (Color online) The incoherent intermediate scattering function $F_s(q,t)$, ($q = 7.25$) of the KABB and KABIPL simulations for isochoric state points with $\rho = 1.2$, $T = 0.42$, 0.44, 0.46, 0.50, 0.6, 1.0. The IPL potentials reproduce the dynamics of the Buckingham potential over a significant temperature range.

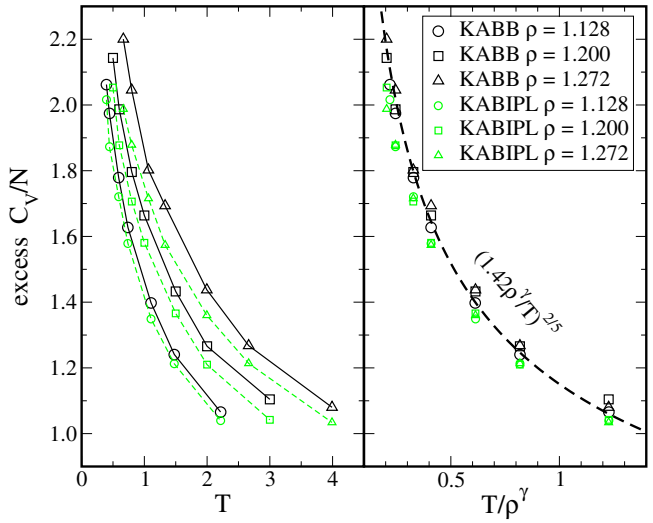

Fig. 9. (Color online) (a) The configurational part of the intensive isochoric specific heat C_V^{ex}/N as a function of temperature. Three isochores were simulated of the KABB and the KABIPL systems. At low density the agreement between the two systems is fairly good, but for higher densities the differences become larger. (b) The same data plotted versus T/ρ^γ where $\gamma = 4.904$. The data collapse on a single curve, which shows that density scaling works. The function $(1.42\rho^\gamma/T)^{2/5}$ was fitted to the data (dashed line), showing that Rosenfeld-Tarazona scaling is also obeyed.

The scaling factor A was determined from the slope of the mean values of the energies in a U, U^{IPL} plot (Fig. 7b), where U^{IPL} is given by equation (12) evaluated on configurations from simulations of the KABB mixture [22]. Using these parameters, simulations of the KABIPL systems were performed and the results were compared with the results of the KABB system. In Figure 8 the incoherent intermediate scattering function of the two systems is plotted for comparison. The KABIPL reproduces the dynamics of the KABB system very well. It should however be noted that in spite of the good reproduction of the dynamics, the KABIPL had a stronger tendency to crystallize than the KABB system at the two lowest temperatures due to the absence of attractive forces. The good agreement shown in Figure 8 only holds if both systems are in the same (supercooled) state.

From the fluctuations in the potential energy one can calculate the excess isochoric specific heat using [7]:

$$C_V^{ex} = C_V - \frac{3}{2}Nk_B = \frac{\langle(\Delta U)^2\rangle}{k_B T^2}. \qquad (13)$$

In Figure 9a C_V^{ex} is plotted for different isochores calculated from KABB and KABIPL simulations. The heat capacities for the two systems follow each other closely, although there is a small and systematic difference increasing with density. This is similar to what was found for the KABLJ system [22], but the deviations are slightly larger for the KABB mixture. Figure 9b shows that the excess heat capacity to a good approximation obeys density scaling, $C_V^{ex}/N = f(\rho^\gamma/T)$, and Rosenfeld-Tarazona scaling, $C_V^{ex}/N = g(\rho)T^{-2/5}$ [23] – again in good agreement with results for the KABLJ system [22].

5 Conclusion

The Buckingham potential has been shown to be strongly correlating like the Lennard-Jones potential. In spite of

its exponential repulsion, the Buckingham potential's dynamics and heat capacity can be closely approximated by a purely repulsive IPL system. In particular the system has good isomorphs in the phase diagram. These findings are very similar to those found for Lennard-Jones systems. We conclude that the existence of strong correlations and isomorphs is *not* dependent on the repulsion being an inverse power-law.

The centre for viscous liquid dynamics "Glass and Time" is sponsored by the Danish National Research Foundation (DNRF).

References

1. U.R. Pedersen, N.P. Bailey, T.B. Schrøder, J.C. Dyre, Phys. Rev. Lett. **100**, 015701 (2008)
2. N.P. Bailey, U.R. Pedersen, N. Gnan, T.B. Schrøder, J.C. Dyre, J. Chem. Phys. **129**, 184507 (2008)
3. N.P. Bailey, U.R. Pedersen, N. Gnan, T.B. Schrøder, J.C. Dyre, J. Chem. Phys. **129**, 184508 (2008)
4. T.B. Schrøder, N.P. Bailey, U.R. Pedersen, N. Gnan, J.C. Dyre, J. Chem. Phys. **131**, 234504 (2009)
5. N. Gnan, T.B. Schrøder, U.R. Pedersen, N.P. Bailey, J.C. Dyre, J. Chem. Phys. **131**, 234504 (2009)
6. T.B. Schrøder, N. Gnan, U.R. Pedersen, N.P. Bailey, J.C. Dyre, J. Chem. Phys. **134**, 164505 (2011)
7. M.P. Allen, D.J. Tildesley, *Computer simulations of liquids* (Oxford University Press, Oxford, 1987)
8. T.B. Schrøder, U.R. Pedersen, N.P. Bailey, S. Toxvaerd, J.C. Dyre, Phys. Rev. E **80**, 041502 (2009)
9. U.R. Pedersen, N. Gnan, N.P. Bailey, T.B. Schrøder, J.C. Dyre, J. Non-Cryst. Solids **357**, 320 (2011)
10. J.C. Slater, Phys. Rev. **32**, 349 (1928)
11. R.A. Buckingham, Proc. R. Soc. London A **168**, 264 (1938)
12. D.A. Young, A.K. McMahan, M. Ross, Phys. Rev. B **24**, 5119 (1981)
13. L. Koči, R. Ahuja, A. Belonoshko, B. Johansson, J. Phys.: Condens. Matter **19**, 016206 (2007)
14. E.A. Mason, W.E. Rice, J. Chem. Phys. **22**, 843 (1954)
15. J.E. Kilpatrick, W.E. Keller, E.F. Hammel, Phys. Rev. **97**, 9 (1955)
16. A.A. Abrahamson, Phys. Rev. **130**, 693 (1963)
17. *Roskilde University Molecular Dynamics package*, http://rumd.org
18. E.W. Lemmon, M.O. McLinden, D.G. Friend, *Thermophysical properties of fluid systems*, NIST Chemistry WebBook, NIST Standard Reference Database Number 69, http://webbook.nist.gov
19. D. Coslovich, C.M. Roland, J. Chem. Phys. **130**, 014508 (2009)
20. EPAPS document E-PRLTAO-100-033802 contains detailed information on the analysis of experimental argon data., http://www.aip.org/pubservs/epaps.html
21. W. Kob, H.C. Andersen, Phys. Rev. Lett. **73**, 1376 (1994)
22. U.R. Pedersen, T.B. Schrøder, J.C. Dyre, Phys. Rev. Lett. **105**, 157801 (2010)
23. Y. Rosenfeld, P. Tarazona, Mol. Phys. **95**, 141 (1998)

Open Access This article is distributed under the terms of the Creative Commons Attribution Noncommercial License which permits any noncommercial use, distribution, and reproduction in any medium, provided the original author(s) and source are credited.

IOP FTC

IOP PUBLISHING JOURNAL OF PHYSICS: CONDENSED MATTER

J. Phys.: Condens. Matter **25** (2013) 032101 (5pp) doi:10.1088/0953-8984/25/3/032101

FAST TRACK COMMUNICATION

Do the repulsive and attractive pair forces play separate roles for the physics of liquids?

Lasse Bøhling, Arno A Veldhorst, Trond S Ingebrigtsen, Nicholas P Bailey, Jesper S Hansen, Søren Toxvaerd, Thomas B Schrøder and Jeppe C Dyre

DNRF Centre 'Glass and Time', IMFUFA, Department of Sciences, Roskilde University, Postbox 260, DK-4000 Roskilde, Denmark

E-mail: dyre@ruc.dk

Received 2 November 2012, in final form 29 November 2012
Published 18 December 2012
Online at stacks.iop.org/JPhysCM/25/032101

Abstract
According to standard liquid-state theory repulsive and attractive pair forces play distinct roles for the physics of liquids. This paradigm is put into perspective here by demonstrating a continuous series of pair potentials that have virtually the same structure and dynamics, although only some of them have attractive forces of significance. Our findings reflect the fact that the motion of a given particle is determined by the total force on it, whereas the quantity usually discussed in liquid-state theory is the individual pair force.

(Some figures may appear in colour only in the online journal)

A liquid is held together by attractions between its molecules. At the same time, it is very difficult to compress a liquid because the molecules strongly resist closely approaching each other. These facts have been known for a long time, and today it is conventional wisdom that the repulsive and the attractive forces play distinct roles for the physics of liquids. The repulsive forces, which ultimately derive from the Fermi statistics of electrons, are harsh and short ranged. According to standard theory these forces are responsible for the structure and, in particular, for reducing considerably the liquid's entropy compared to that of an ideal gas at the same density and temperature. The attractive forces, on the other hand, are long ranged and weaker. These forces, which derive from induced dipolar interactions, reduce the pressure and energy compared to that of an ideal gas at the same density and temperature. We argue below that this physical picture, though quite appealing, overemphasizes the individual pair forces and does not provide a full understanding because it does not relate directly to the total force on a given particle.

The traditional understanding of the liquid state is based on pioneering works by Frenkel, Longuet-Higgins and Widom, Barker and Henderson, and Weeks, Chandler, and Andersen (WCA), and many others [1, 2]. The basic idea is that the attractions may be regarded as a perturbation of a Hamiltonian based on the repulsive forces, the physics of which is usually well represented by a hard-sphere reference system [3]. Perturbation theories based on this picture [1–4] are standard for calculating simple liquids' thermodynamics and structure as quantified, e.g., by the radial distribution function. We do not question the usefulness of perturbation theories, but will argue from theory and simulations that the repulsive and the attractive pair forces do not always play clearly distinguishable roles for the structure and dynamics of simple liquids.

This point is illustrated in the simplest possible way by studying systems of Lennard-Jones (LJ) particles. The LJ pair potential is given by $v_{\rm LJ}(r) = 4\varepsilon[(r/\sigma)^{-12} - (r/\sigma)^{-6}]$. This function is plotted in figure 1 for a number of different choices of the parameters ϵ and σ. In the following we adopt the unit system in which $\epsilon_0 = \sigma_0 = 1$ and $k_{\rm B} = 1$. We use the same unit system for all the potentials. Consider a simulation of the potential with $(\epsilon, \sigma) = (1.25, 0.947)$ at the state point

 © 2013 IOP Publishing Ltd Printed in the UK & the USA

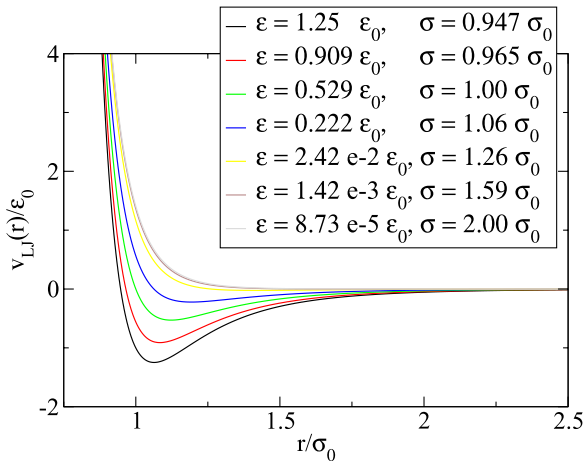

Figure 1. Lennard-Jones pair potentials $v_{\rm LJ}(r) = 4\varepsilon\,[(r/\sigma)^{-12} - (r/\sigma)^{-6}]$ predicted to give virtually the same physics at the state point $(\rho, T) = (1, 1)$ using the unit system defined by $\epsilon_0 = \sigma_0 = 1$ and $k_{\rm B} = 1$. Visually, these potentials have little in common; in particular, they have very different contributions from attractive forces. These pair potentials were constructed analytically using the isomorph theory, as detailed in the text after figure 2.

$(\rho \equiv N/V, T) = (1, 1)$. Clearly, it would lead to exactly the same structure and dynamics (after appropriate rescaling) doing a simulation of the potential with $(\epsilon, \sigma) = (8.73 \times 10^{-5}, 2.0)$ at the temperature $T = 8.73 \times 10^{-5}/1.25$ and the density $\rho = (0.947/2.00)^3$—this simply reflects the fact that the physics is determined by the two dimensionless parameters T/ϵ and $\sigma^3\rho$. We show below however that, in addition to this trivial fact, the two potentials also give (to a good approximation) the same structure and dynamics when *both* potentials are investigated at the state point $(\rho, T) = (1, 1)$. In fact, all the potentials in figure 1 were chosen to give virtually the same structure and dynamics at the state point $(\rho, T) = (1, 1)$. The paper mainly focuses on this state point, but results for a few other state points are also given, confirming the findings at $(\rho, T) = (1, 1)$.

The potentials of figure 1 all have attractive forces, but for some of the potentials the attractive forces are entirely insignificant. To show that these potentials nevertheless have virtually the same structure and dynamics, *NVT* computer simulations of systems of 1000 particles were performed using the RUMD software that runs on graphics processing units [5].

Figure 2(a) shows the radial distribution function $g(r)$ for the seven LJ pair potentials of figure 1 at the state point $(\rho, T) = (1, 1)$. For comparison, simulations at the same state point are shown in figure 2(b) for seven potentials with the same ε variation, but fixed $\sigma = 0.947$. Figure 2(c) shows the radial distribution functions at the state point (1, 1) for the pair potentials of figure 1 cut off according to the Weeks–Chandler–Andersen (WCA) recipe, i.e., by cutting the potentials at their minima and shifting them to zero there.

Figure 3 shows results for the dynamics, with (a) giving the mean-square displacement for the seven potentials of figure 1. Figure 3(b) compares the results for the diffusion constants with those of WCA simulations.

By the Henderson uniqueness theorem [6] the pair potentials of figure 1 cannot have exactly the same pair

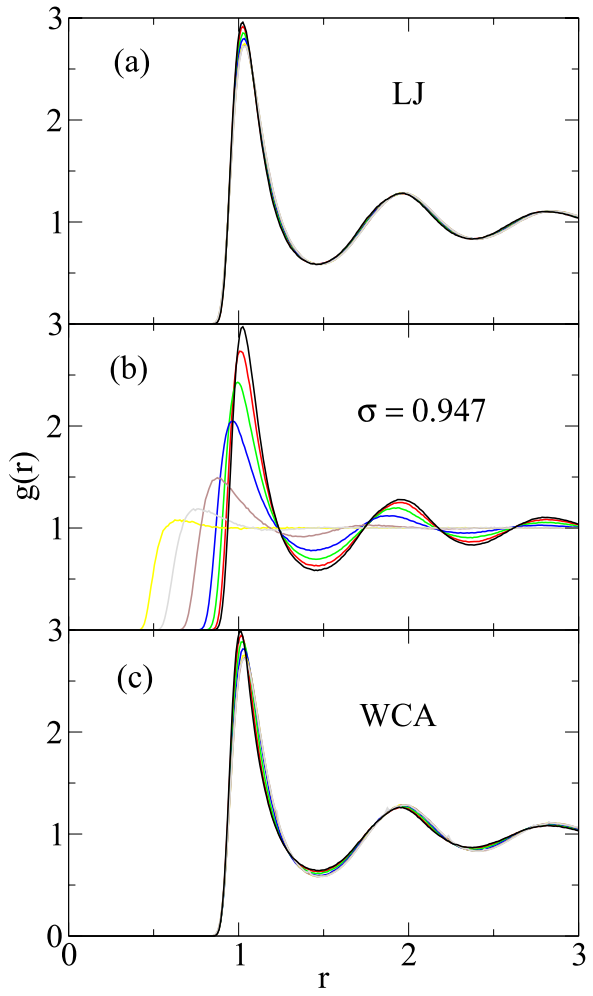

Figure 2. Radial distribution functions at the state point $(\rho, T) = (1, 1)$ for different sets of potentials: (a) the LJ pair potentials of figure 1; (b) a series of LJ pair potentials with fixed σ parameter and the ϵ-values listed in figure 1; (c) results for the series of Weeks–Chandler–Andersen (WCA) potentials corresponding to the LJ potentials of figure 1.

distribution functions. Based on figures 2 and 3 we see that, nevertheless, the potentials lead to very similar structure and very similar dynamics. In fact, both structure and dynamics among the potentials of figure 1 are closer to each other than to the WCA versions of the same potentials.

How were the pair potentials of figure 1 determined and why do they have almost the same structure and dynamics? The starting point is the existence of isomorphs in the phase diagram of liquids with strong correlations between *NVT* virial and potential-energy equilibrium fluctuations [7, 8] (which we recently argued provides a useful definition of a simple liquid [9]). Two state points with density and temperature (ρ_1, T_1) and (ρ_2, T_2) are termed isomorphic [7] if all pairs of physically relevant microconfigurations of the two state points, which trivially scale into one another, i.e., $\rho_1^{1/3}\mathbf{r}_i^{(1)} = \rho_2^{1/3}\mathbf{r}_i^{(2)}$ for all particles i, have proportional configurational Boltzmann factors: $\exp[-U(\mathbf{r}_1^{(1)}, \ldots, \mathbf{r}_N^{(1)})/k_{\rm B}T_1] = C_{12}\exp[-U(\mathbf{r}_1^{(2)}, \ldots, \mathbf{r}_N^{(2)})/k_{\rm B}T_2]$ in which the constant of proportionality is independent of the microconfiguration.

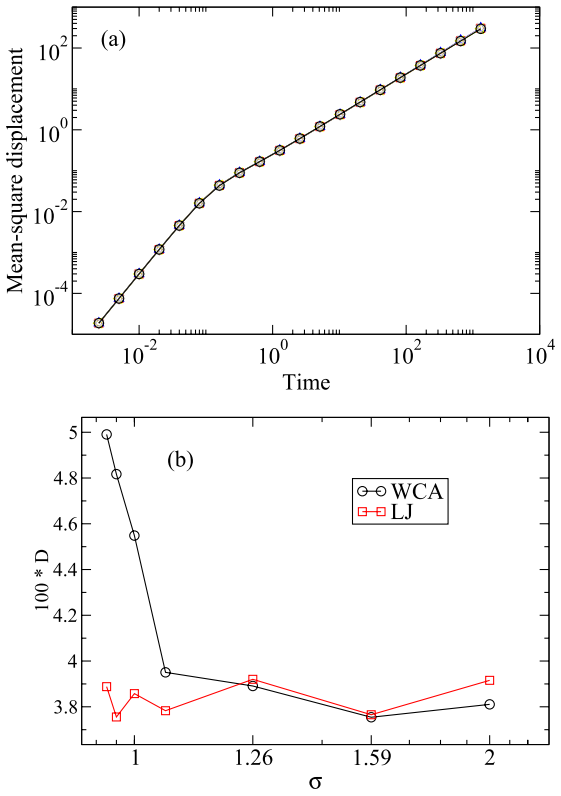

Figure 3. (a) The mean-square displacement for the LJ pair potentials of figure 1 at the state point $(\rho, T) = (1, 1)$. (b) Diffusion constants as functions of σ for the full potentials of figure 1 (red) and for the WCA versions of the potentials (black). At high σ the WCA results are accurate because these potentials are almost purely repulsive.

LJ systems are strongly correlating and thus have isomorphs to a good approximation [8]. The invariance of the canonical probabilities of scaled configurations along an isomorph has several implications [7]. Excess entropy and isochoric specific heat are both isomorph invariant, the dynamics in reduced units are invariant for both Newtonian and Brownian equations of motion, reduced-unit static density correlation functions are invariant, a jump between two isomorphic state points takes the system instantaneously to equilibrium, etc. For Newtonian dynamics, using reduced units corresponds to measuring length in units of $\rho^{-1/3}$, time in units of $\rho^{-1/3}\sqrt{m/k_BT}$ where m is the particle mass, and energy in units of k_BT. Thus the reduced particle coordinates are defined by $\tilde{\mathbf{r}}_i = \rho^{1/3}\mathbf{r}_i$.

An isomorph was generated using the recently derived result [10] that liquids with good isomorphs have simple thermodynamics in the sense that the temperature is a product of a function of excess entropy per particle s and a function of density,

$$T = f(s)h(\rho). \tag{1}$$

The function $h(\rho)$ inherits the analytical structure of the pair potential in the sense that, if the latter is given by the expression $v(r) = \sum_n v_n r^{-n}$, then $h(\rho) = \sum_n C_n \rho^{n/3}$, in which each term corresponds to a term in the pair potential [10]. Since $h(\rho)$ is only defined within an overall

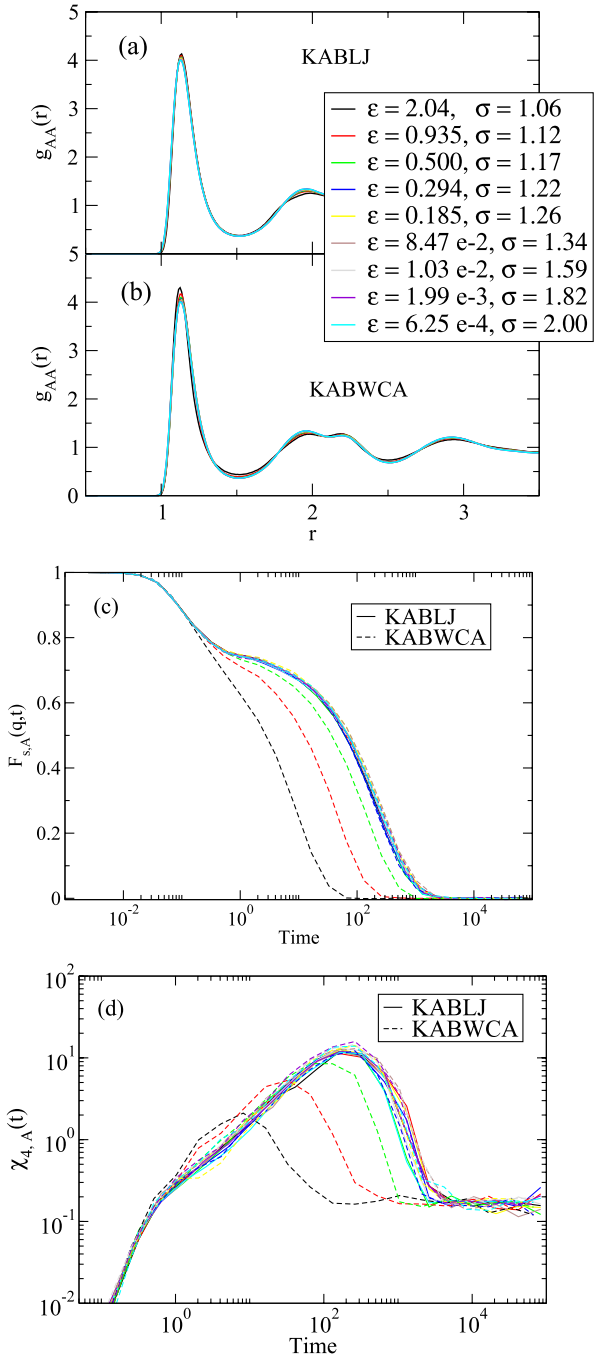

Figure 4. (a) The AA particle radial distribution function of the Kob–Andersen binary Lennard-Jones (KABLJ) mixture for a family of isomorphic pair potentials similar to those of figure 1. (b) The AA particle radial distribution function of the KABLJ mixture with the corresponding WCA potentials. (c) The A particle incoherent intermediate scattering function for the same family of potentials as a function of time at the wavevector defined from the maximum of $g(r)$ (full curves). The full dotted curves show the WCA predictions [12]. (d) The function $\chi_4(t)$ for the A particles for the same pair potentials (full curves) and the WCA predictions (dashed curves).

multiplicative constant, one can write for the LJ pair potential

$$h(\rho) = \alpha\rho^4 + (1-\alpha)\rho^2. \tag{2}$$

The constant α was determined from simulations at the state point $(\rho, T) = (1, 1)$ for $\varepsilon = 1.25$ and $\sigma = 0.947$, which is

a typical liquid state point of the LJ system. This was done by proceeding as follows [11]. We have previously [7, 10] derived the identities

$$\gamma \equiv \left(\frac{\partial \ln T}{\partial \ln \rho}\right)_{S_{\rm ex}} = \frac{\mathrm{d}\ln h}{\mathrm{d}\ln \rho} = \frac{\langle \Delta W \Delta U\rangle}{\langle (\Delta U)^2\rangle}, \qquad (3)$$

in which W is the virial, U the potential energy, and the angular brackets denote NVT equilibrium ensemble averages. Combining equations (2) and (3) with the simulation results for the fluctuations of W and U leads to $\alpha = \gamma/2 - 1 = 1.85$.

An isomorph is a set of state points with almost the same structure and dynamics in reduced units [7]. Via appropriate rescaling, however, an isomorph can be interpreted differently: as defining a set of *different* LJ pair potentials that give invariant properties at the *same state point*. These are simply two different ways of looking at an invariant Boltzmann factor: equation (1) implies that $\exp\left(-U(\rho^{-1/3}\tilde{\mathbf{r}}_1, \ldots, \rho^{-1/3}\tilde{\mathbf{r}}_N)/[f(s)h(\rho)]\right) = \exp(-[1/f(s)]\sum_{i<j} v_{\rm LJ}(\rho^{-1/3}\tilde{r}_{ij})/h(\rho))$, where r_{ij} is the distance between particles i and j. Along an isomorph $f(s)$ is a constant; if we consider the isomorph which includes the state point $\rho = T = 1$, then given the normalization of equation (2) we have $f(s) = 1$. The shift in interpretation now comes by noticing that the same Boltzmann factor is obtained by considering a configuration at unit density and unit temperature and a family of *isomorphic pair potentials* $v_{\rm LJ}^d(r) \equiv v_{\rm LJ}\left(d^{-1/3}r\right)/h(d)$, where we have dropped the tilde from positions and replaced ρ with d to emphasize the shift in perspective. These pair potentials are still LJ potentials, but with different energy and length parameters; the potentials plotted in figure 1 were arrived at in this way.

The single-component LJ system does not have a broad dynamic range because it cannot be deeply supercooled. To test the robustness of the predicted invariance of the physics for families of 'isomorphic' pair potentials, we simulated also the Kob–Andersen binary LJ (KABLJ) mixture [13], which is easily supercooled into a highly viscous state. For this system the constant $\alpha = 1.29$ was identified from simulations of 1000 particles at the state point $(\rho, T) = (1.60, 2.00)$, using again equation (3). From the function $h(\rho)$ a family of isomorphic equivalent pair potentials was generated that looks much like those of figure 1; in particular, some of them have a vanishingly small attraction.

Figure 4(a) shows the AA particle radial distribution functions for these different pair potentials and figure 4(b) shows the same quantity for the WCA version of the potentials. Figure 4(c) shows the A particle incoherent intermediate scattering function and, with dashed lines, simulations of the corresponding WCA systems. Even though the WCA approximation has the correct repulsive forces, its physics differs considerably from the isomorphic pair potentials, as noted already by Berthier and Tarjus [12]. We also calculated $\chi_4(t)$, a measure of dynamic heterogeneities. The results shown in figure 4(d) are more noisy, but confirm the predicted invariance of the dynamics for the different pair potentials. The corresponding WCA results are shown with dashed lines.

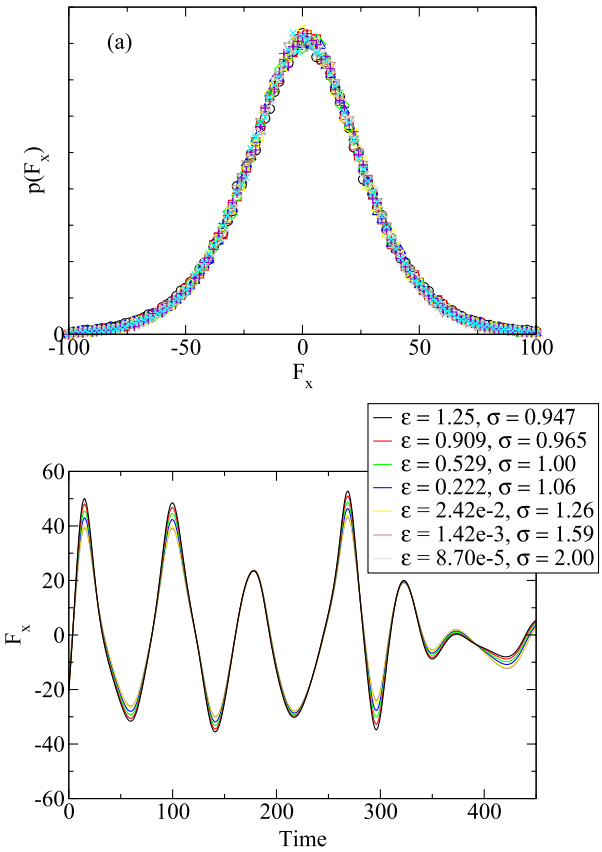

Figure 5. (a) Probability distribution of x-components of the total forces on individual particles, $p(F_x)$, for the different single-component LJ potentials of figure 1 at the state point $(\rho, T) = (1, 1)$. (b) Snapshot of the x-component of the force F_x on one particle as a function of time. The system simulated is defined by $\varepsilon = 1.25$ and $\sigma = 0.947$, and F_x was subsequently evaluated for the same series of configurations for the six other potentials. These figures show that, even though the pair potentials are quite different, the forces are virtually identical except at the extrema.

It would require extraordinary abilities to know from inspection of figure 1 that these pair potentials have virtually the same structure and dynamics. The potentials have neither the repulsive nor the attractive terms in common, so why is it that they have such similar behavior? The answer is that they result in virtually the same forces (figure 5). The force on a given particle is the *sum* of contributions from (primarily) its nearest neighbors, and plotting merely the pair potential can be misleading. We conclude that, by reference to the pair potential alone, one cannot identify separate roles for the repulsive and the attractive forces in a many-particle system. There simply are no 'repulsive' and 'attractive' forces as such.

The above reported simulations focused for each system on one particular state point. If the potentials in figure 1 are to be regarded as equivalent with respect to structure and dynamics, however, one should also test other state points. We have done this briefly, and the results are shown in figure 6. Clearly, the degree of similarity observed at the state point $(\rho, T) = (1, 1)$ is also maintained for the other state points (for comparison, figure 6(c) reproduces the $(\rho, T) = (1, 1)$ results from figure 2(a)).

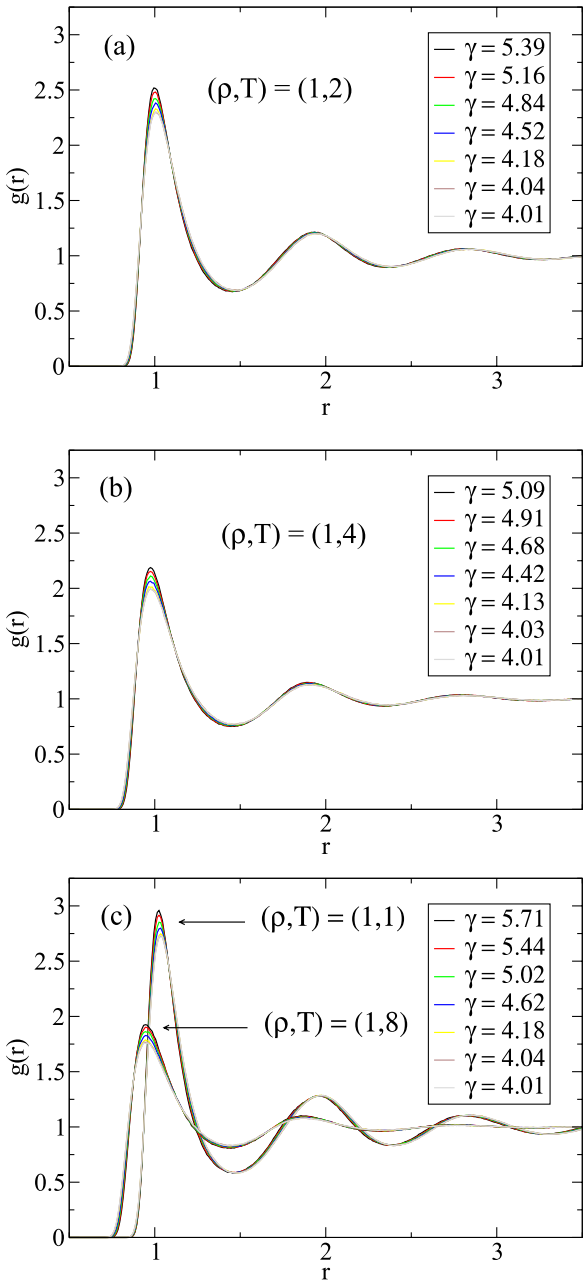

Figure 6. Radial distribution functions for the potentials of figure 1 at other state points than the state point $(\rho, T) = (1, 1)$ studied above. For reference we give in each subfigure the value of γ defined in equation (3). (a) $(\rho, T) = (1, 2)$; (b) $(\rho, T) = (1, 4)$; (c) $(\rho, T) = (1, 8)$—the γ-values reported in this subfigure are those of the state point $(\rho, T) = (1, 1)$.

What are the implications of the above results? For liquid-state perturbation theory the WCA theory is rightfully renowned for its ability to make semi-analytic predictions for thermodynamic properties of simple liquids. The focus of liquid-state theory has moved on, however, in part because modern computers make it straightforward to simulate the kinds of liquid for which WCA theory can make accurate predictions. We do not claim to have a better way to do perturbation theory in the sense of WCA. While WCA theory is based upon an *assumed* equivalence between two potentials differing by the removal of attractions, the present work describes a *predicted and observed* equivalence between apparently quite different potentials. This observation will not facilitate perturbation theory, but it could potentially be useful as a check on perturbation theories and other theories of the liquid state, for example density functional theory; such theories should be consistent with the observed invariance as the parameters of the potential are changed.

The center for viscous liquid dynamics 'Glass and Time' is sponsored by the Danish National Research Foundation (DNRF).

References

[1] Frenkel J 1955 *Kinetic Theory of Liquids* (New York: Dover)
Fisher I Z 1964 *Statistical Theory of Liquids* (Chicago, IL: University of Chicago)
Rice S A and Gray P 1965 *The Statistical Mechanics of Simple Liquids* (New York: Interscience)
Temperley H N V, Rowlinson J S and Rushbrooke G S 1968 *Physics of Simple Liquids* (New York: Wiley)
Hansen J P and McDonald J R 2005 *Theory of Simple Liquids* (New York: Academic)
[2] Longuet-Higgins H C and Widom B 1964 *Mol. Phys.* **8** 549
Barker J A and Henderson D 1967 *J. Chem. Phys.* **47** 4714
Widom B 1967 *Science* **157** 375
Neece G A and Widom B 1969 *Annu. Rev. Phys. Chem.* **20** 167
Weeks D, Chandler D and Andersen H C 1971 *J. Chem. Phys.* **54** 5237
Barker J A and Henderson D 1976 *Rev. Mod. Phys.* **48** 587
Chandler D, Weeks J D and Andersen H C 1983 *Science* **220** 787
[3] Zwanzig R W 1954 *J. Chem. Phys.* **22** 1420
[4] Sarkisov G N 1999 *Phys.—Usp.* **42** 545
Zhou S and Solana J R 2009 *Chem. Rev.* **109** 2829
[5] http://rumd.org
[6] Henderson R L 1974 *Phys. Lett.* A **49** 197
[7] Gnan N *et al* 2009 *J. Chem. Phys.* **131** 234504
[8] Pedersen U R *et al* 2008 *Phys. Rev. Lett.* **100** 015701
Bailey N P *et al* 2008 *J. Chem. Phys.* **129** 184508
Gnan N *et al* 2010 *Phys. Rev. Lett.* **104** 125902
Pedersen U R *et al* 2010 *Phys. Rev. Lett.* **105** 157801
[9] Ingebrigtsen T S, Schrøder T B and Dyre J C 2012 *Phys. Rev.* X **2** 011011
[10] Ingebrigtsen T S, Bøhling L, Schrøder T B and Dyre J C 2012 *J. Chem. Phys.* **136** 061102
[11] Bøhling L, Ingebrigtsen T S, Grzybowski A, Paluch M, Dyre J C and Schrøder T B 2012 *New J. Phys.* **14** 113035
[12] Berthier L and Tarjus G 2009 *Phys. Rev. Lett.* **103** 170601
Berthier L and Tarjus G 2011 *J. Chem. Phys.* **134** 214503
[13] Kob W and Andersen H C 1994 *Phys. Rev. Lett.* **73** 1376

THE JOURNAL OF CHEMICAL PHYSICS **139**, 171101 (2013)

Communication: The Rosenfeld-Tarazona expression for liquids' specific heat: A numerical investigation of eighteen systems

Trond S. Ingebrigtsen,[a] Arno A. Veldhorst, Thomas B. Schrøder, and Jeppe C. Dyre
DNRF Centre "Glass and Time," IMFUFA, Department of Sciences, Roskilde University, Postbox 260, DK-4000 Roskilde, Denmark

(Received 11 September 2013; accepted 17 October 2013; published online 1 November 2013)

We investigate the accuracy of the expression of Rosenfeld and Tarazona (RT) for the excess isochoric heat capacity, $C_V^{\text{ex}} \propto T^{-2/5}$, for 18 model liquids. Previous investigations have reported no unifying features of breakdown for the RT expression. Here, liquids with different stoichiometric composition, molecular topology, chemical interactions, degree of undercooling, and environment are investigated. The RT expression is a better approximation for liquids with strong correlations between equilibrium fluctuations of virial and potential energy, i.e., "Roskilde-simple" liquids [T. S. Ingebrigtsen, T. B. Schrøder, and J. C. Dyre, Phys. Rev. X **2**, 011011 (2012)]. This observation holds even for molecular liquids under severe nanoscale confinement which does not follow from the original RT bulk hard-sphere fluid perturbation theory arguments. The density dependence of the specific heat is predicted from the isomorph theory for Roskilde-simple liquids, which in combination with the RT expression provides a complete description of the specific heat's density and temperature dependence. © *2013 Author(s). All article content, except where otherwise noted, is licensed under a Creative Commons Attribution 3.0 Unported License.* [http://dx.doi.org/10.1063/1.4827865]

Fundamental theories for the temperature and pressure (or density) dependence of thermodynamic quantities have gained renewed attention in the last decade. These theories can serve as a valuable input to equations of state,[1,2] but also as input to scaling strategies which relate key dimensionless transport coefficients to thermodynamic quantities, such as the excess (or "residual") entropy[3] (with respect to an ideal gas) or the excess isochoric heat capacity.[4] Predicting dynamical quantities from first principles is a challenging task. One such theory is mode-coupling theory[5] which relates the dynamic density correlations of a fluid to its static structure. Alternative theories which relate dynamics to thermodynamics such as that of Adam and Gibbs[6] and Rosenfeld's excess entropy scaling,[3] consider the dynamics also in the highly supercooled liquid regime.[7,8] Excess entropy scaling strategies, as proposed by Rosenfeld, have proven successful in predicting the dynamics of not only single-component atomic fluids,[3] but also binary mixtures,[7,8] ionic substances,[9,10] small molecules,[11,12] and polymers.[13] In fact, excess entropy scaling strategies have been used as reliable predictors even for the perplexing dynamics of nanoconfined liquids[4,14] which exhibit stratification and position-dependent relaxation processes.

To fully harness the power of predicting dynamics from thermodynamics, however, it is imperative to develop reliable theories for the temperature and pressure (or density) dependence of thermodynamic quantities. Rosenfeld and Tarazona[15] (RT) argued for a mathematically simple expression for the temperature and density dependence of the potential energy U for fluids. Their arguments are based on thermodynamic perturbation theory, using a functional for hard-spheres in combination with an expansion of the free energy around the $\eta = 1$ packing fraction. The arguments are not easy to follow, but their expressions have found widespread application.[1,2,11,15–24]

From the potential energy one gains access to thermodynamic quantities such as the excess isochoric heat capacity $C_V^{\text{ex}} = (\partial U/\partial T)_V$ and the excess entropy S_{ex} via $C_V^{\text{ex}} = T(\partial S_{\text{ex}}/\partial T)_V$. Both of these quantities enter the aforementioned strategies. For a long time only few studies focused on the heat capacity.[25] Recently, however, the heat capacity of liquids has begun to receive more attention.[26] The RT expressions for the potential energy and excess isochoric heat capacity read

$$U(\rho, T) = \alpha(\rho)T^{3/5} + \beta(\rho), \tag{1}$$

$$C_V^{\text{ex}}(\rho, T) = 3/5\alpha(\rho)T^{-2/5}, \tag{2}$$

where $\alpha(\rho)$ and $\beta(\rho)$ are extensive functions of density ρ that relate to the specific system.[15]

Several numerical investigations have tested the applicability of the RT expressions for various model liquids. These liquids span from simple atomic model fluids to liquids showing a wide range of structural, dynamical, and thermodynamical anomalies in their phase diagram. More specifically, the RT expressions have been investigated for single-component atomic fluids,[15–17] binary mixtures,[2,18,19] ionic substances,[1,20] hydrogen-bonding liquids,[11,21,22] small molecules,[23] and sheared liquids.[24] These investigations showed that the RT expressions give a good approximation for a range of systems, but are less accurate when applied to systems known not to have strong virial/potential energy correlations,[27] such as the Dzugutov liquid and Gaussian core model, as well as for SiO_2 and BeF_2 in their anomalous

[a]Electronic mail: trond@ruc.dk

 © Author(s) 2013

regions. For SPC/E water different results for the applicability of RT have been reported.[11,21,22]

The purpose of this paper is to investigate the conditions under which RT applies by simulating 18 different model systems possessing different stoichiometric composition, molecular topology, chemical interactions, degree of undercooling, and environment. We use GPU-optimized *NVT* molecular dynamics computer simulations (http://rumd.org; in total over 40 000 GPU hours) to calculate the potential energy and excess isochoric heat capacity along a single isochore for each of these 18 model systems (for the single-component Lennard-Jones (SCLJ) liquid we also vary the density). Here and henceforth quantities are reported in dimensionless units, e.g., by setting $\sigma = 1$, $\epsilon = 1$, etc. The heat capacity is calculated via Einstein's fluctuation formula $C_V^{\text{ex}} = \langle(\Delta U)^2\rangle/k_B T^2$. Table I presents the 18 investigated model systems, which range from simple atomic fluids to molecules under severe nanoscale confinement. The densities represent typical liquid-state densities.

Figure 1 shows the excess isochoric heat capacity at constant density as a function of temperature for selected systems of Table I. The inset shows NIST equation of state data for supercritical argon at $\rho = 20$, 25, 32.6, 35 mol/L and 200 K $\leq$ T $\leq$ 700 K. The orange lines represent linear regression fits of the individual isochores, testing the correct RT power-law exponent dependence. In all cases, the excess isochoric heat capacity decreases with increasing temperature.

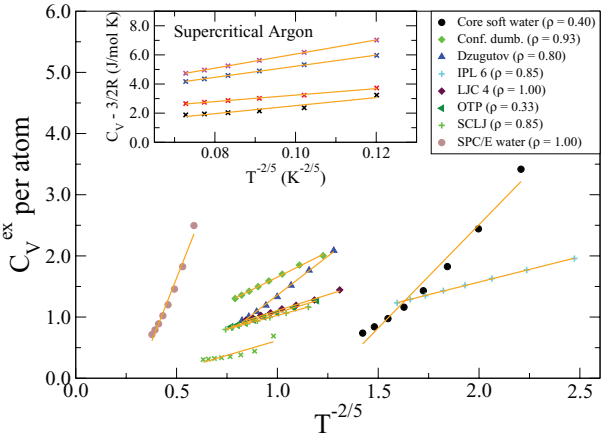

FIG. 1. Isochores studied for selected model systems of Table I. The inset shows NIST equation of state data for supercritical argon at $\rho = 20$, 25, 32.6, 35 mol/L and 200 K $\leq$ T $\leq$ 700 K. The orange lines represent linear regression fits of the individual isochores, testing the correct RT power-law exponent dependence. The excess isochoric heat capacity $C_V^{\text{ex}} = \langle(\Delta U)^2\rangle/k_B T^2$ per atom is shown as a function of $T^{-2/5}$. For all liquids C_V^{ex} decreases with increasing temperature.

TABLE I. The 18 model systems investigated. D_U and $D_{C_V^{\text{ex}}}$ are the coefficient of determination (Eq. (3)) for the potential energy and excess isochoric heat capacity, respectively, for the isochore of density ρ. The virial/potential energy correlation coefficient R is given for the lowest temperature state point T_{min}. The abbreviations used are: Kob-Andersen binary Lennard-Jones mixture (KABLJ); inverse power-law fluid with exponent n (IPL n); LJ polymer chain of length n (LJC n); Lewis-Wahnström o-terphenyl (OTP); single-component Buckingham liquid (SCB); single-component LJ liquid (SCLJ); Wahnström binary LJ mixture (WABLJ). The "Nanoconfined dumbbell" is confined to a (smooth) slit-pore of width $H = 8.13$, corresponding to roughly 16 molecular lengths.

System	ρ	T_{min}	D_U	$D_{C_V^{\text{ex}}}$	R
Core-soft water[28]	0.40	0.138	0.974	0.473	0.10
Dumbbell[29]	0.93	0.380	>0.999	0.999	0.96
Nanoconfined dumbbell[4]	0.93	0.600	>0.999	0.998	0.91
Dzugutov[30]	0.80	0.540	0.997	0.786	0.71
Girifalco[31]	0.40	0.840	0.999	−0.664	0.91
KABLJ[32]	1.20	0.420	>0.999	0.984	0.93
IPL 6	0.85	0.104	>0.999	0.997	1.00
IPL 12	0.85	0.195	>0.999	>0.999	1.00
IPL 18	0.85	0.271	>0.999	0.988	1.00
LJC 10[33]	1.00	0.450	>0.999	0.998	0.86
LJC 4	1.00	0.510	>0.999	0.991	0.90
Molten salt[34]	0.37	0.018	>0.999	0.952	0.15
OTP[35]	0.33	0.640	>0.999	0.995	0.91
Repulsive LJ[36]	1.00	0.360	>0.999	0.995	1.00
SCB[37]	1.00	0.960	>0.999	0.991	0.99
SCLJ	0.85	0.700	>0.999	0.974	0.96
SCLJ	0.82	0.660	>0.999	0.962	0.94
SCLJ	0.77	0.740	>0.999	0.940	0.90
SCLJ	0.70	0.860	>0.999	0.954	0.82
SCLJ	0.66	0.910	>0.999	0.959	0.75
SCLJ	0.61	0.980	>0.999	0.859	0.64
SCLJ	0.59	0.990	>0.999	0.729	0.56
SCLJ	0.55	1.050	>0.999	0.644	0.51
SPC/E water[38]	1.00	3.800	0.987	0.558	0.07
WABLJ[39]	1.30	0.670	>0.999	0.911	0.98

The data points of the main plot of Fig. 1 (and Table I) were generated by the following procedure.

1. First the system is cooled at constant density until one of the following happens: The system crystallizes or the pressure becomes negative or the relaxation time is of the order 10^5 time units. This happens at the temperature T_{min}. The system is then equilibrated at $T = T_{min}$; in the case of crystallization or negative pressure, the temperature is increased slightly (and this new temperature defines T_{min}).
2. Next, the temperature is increased from T_{min} up to $T_{max} = 3T_{min}$, probing state points along the isochore with a spacing of $\Delta T = 2/7\, T_{min}$. A total of eight equilibrium state points are hereby generated for each isochore.

Turning now to the RT expressions, we show in Figs. 2(a) and 2(b) the coefficient of determination[40] D for the potential energy and excess isochoric heat capacity as a function of $1 - R$ (see below) for all model systems. For a generic quantity X, the coefficient of determination D_X is defined by

$$D_X = 1 - \frac{\sum_{i=1}^{N}(X_i - f(X_i))^2}{\sum_{i=1}^{N}(X_i - \langle X\rangle)^2}, \tag{3}$$

where $f(X_i)$ is a function that provides the model values, and the average $\langle X\rangle$ is taken over a set of data points $\mathbf{X} = \{X_1, \ldots, X_N\}$. In our case $f(X_i)$ is given by best fits to the data points in $\mathbf{X}$ using, respectively, $U = A_0\, T^{3/5} + A_1$, and $C_V^{\text{ex}} = 3/5 A_2\, T^{-2/5}$, where A_0, A_1, and A_2 are constants. D_X measures the proportion of variability in a data set that is accounted for by the statistical model;[40] $D_X = 1$ implies perfect account of the variability.

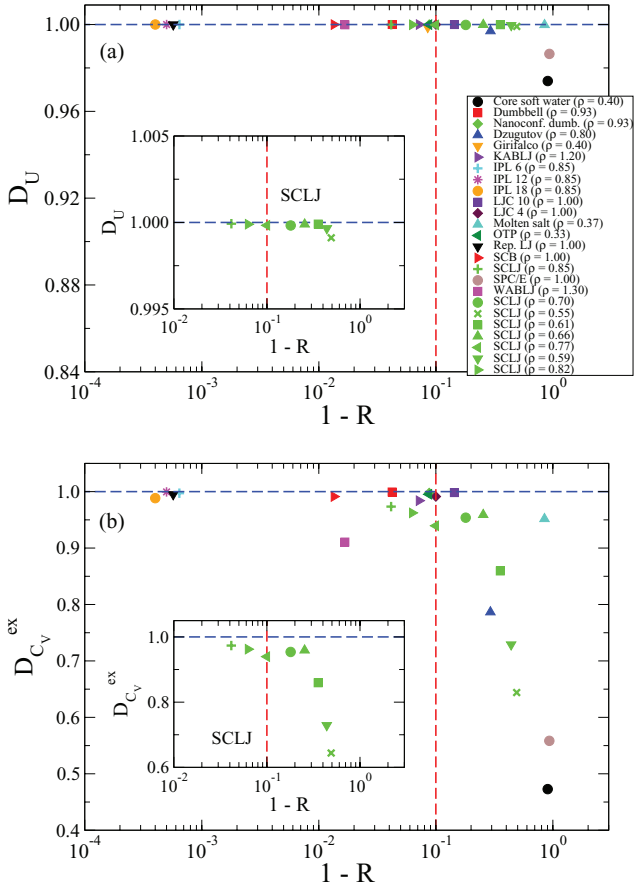

FIG. 2. The coefficient of determination D (Eq. (3)) for U and C_V^{ex} as a function of $1 - R$ for the 18 different model systems. The insets show D for the SCLJ liquid (see Table I). (a) D_U and (b) $D_{C_V^{ex}}$. The Girifalco system gives a negative value for $D_{C_V^{ex}}$ and has for clarity of presentation been left out (see Table I). For both the potential energy and the excess isochoric heat capacity, RT is seen to deteriorate as R decreases below 0.90 (to the right of the red line); in particular, see insets for the SCLJ liquid.

The virial/potential energy correlation coefficient R is defined[27] via

$$R = \frac{\langle \Delta W \Delta U \rangle}{\sqrt{\langle (\Delta W)^2 \rangle}\sqrt{\langle (\Delta U)^2 \rangle}}, \tag{4}$$

and calculated from the canonical ensemble equilibrium fluctuations at T_{min}. The "Roskilde-simple" liquids[41] are defined by $R \geq 0.90$. Only inverse power-law fluids are perfectly correlating ($R = 1$), but many models[27] as well as some experimental liquids[42] have been shown to belong to the class of Roskilde-simple liquids. We believe this class includes most or all van der Waals and metallic liquids, whereas covalently, hydrogen-bonding or strongly ionic or dipolar liquids are generally not Roskilde simple.[27]

We observe from Fig. 2(a) that for all liquids D_U gives a value close to 1, but RT provides a better approximation for liquids with R larger than 0.90 (to the left of the red line). A similar behavior is observed for $D_{C_V^{ex}}$ in Fig. 2(b) (note the change of scale). The insets of both figures show for the SCLJ liquid how RT deteriorates as R decreases below 0.90. We conclude that the RT expressions work better for systems that are Roskilde simple at the state points in question. We observe, however, also from Fig. 1 that for supercritical argon the excess isochoric heat capacity does not seem to go zero at very high temperatures which is in contrast to all simulated Roskilde liquids.

Originally,[15] RT was argued from thermodynamic perturbation theory using a bulk hard-sphere reference system and via simulation shown to describe inverse power-law systems to a high degree of accuracy. Later investigations showed that RT is a good approximation also for LJ liquids. These systems are all Roskilde simple, and a recently argued quasi-universality[43] for Roskilde simple single-component atomic systems implies this behavior. We have shown that the key determining factor for RT is not whether systems are atomic or molecular (see the results for the dumbbell model, OTP, and LJC in Fig. 2), but rather the degree of strong correlation between virial and potential energy. This was shown to be the case even for severely nanoconfined molecular systems which exhibit a completely different physics from bulk hard-sphere fluids[4] and are thus *not* expected to satisfy the original RT arguments. The latter is, in particular, true also for the elongated non-spherical molecules studied here. The observed correlation between RT and Roskilde-simple liquids is thus not trivial.

As a further validation of the above viewpoint, we relate the function $\alpha(\rho)$ in the RT expression to $h(\rho)$ for Roskilde liquids. For such liquids, temperature separates[36] into a product of a function of excess entropy per particle and a function of density via $T = f(s_{ex})h(\rho)$. Roskilde liquids are characterized by having isomorphs to a good approximation.[44] Isomorphs are curves in the thermodynamic phase diagram along which structure and dynamics in reduced units, as well as some thermodynamic quantities are invariant. Along an isomorph both C_V^{ex} and $h(\rho)/T$ are invariant, and consequently one may write

$$C_V^{ex} = F\left(\frac{h(\rho)}{T}\right). \tag{5}$$

Since by the RT expression; $C_V^{ex} = 3/5\alpha(\rho)T^{-2/5} = 3/5(\alpha(\rho)^{5/2}/T)^{2/5}$, it follows that $h(\rho) = \alpha(\rho)^{5/2}$ or, equivalently,

$$\alpha(\rho) = h(\rho)^{2/5}. \tag{6}$$

For a LJ system, it was shown in Refs. 36 and 45 that $h(\rho)$ is given by

$$h(\rho) = (\gamma_0/2 - 1)\rho^4 + (2 - \gamma_0/2)\rho^2, \tag{7}$$

in which γ_0 is calculated from the virial/potential energy fluctuations at the state point $\rho = 1$ and $T = 1$ via $\gamma_0 = \langle \Delta W \Delta U \rangle / \langle (\Delta U)^2 \rangle$.

Equation (6) is tested in Fig. 3 for the KABLJ and the repulsive LJ system (for which, respectively, $\gamma_0 = 5.35$ and $\gamma_0 = 3.56$). The latter system is defined from $v(r) = (r^{-12} + r^{-6})/2$ and has R above 99.9% in its entire phase diagram; γ varies from 2 at low density to 4 at high density. We determine $\alpha(\rho)$ for different densities by fitting Eq. (1) as a function of temperature for each isochore and system. $h(\rho)$ is calculated analytically from Eq. (7). Figure 3 shows that $\alpha(\rho)$ as predicted by the isomorph theory to a very good approximation is given by $h(\rho)^{2/5}$. Equations (2) and (7) thus provide a

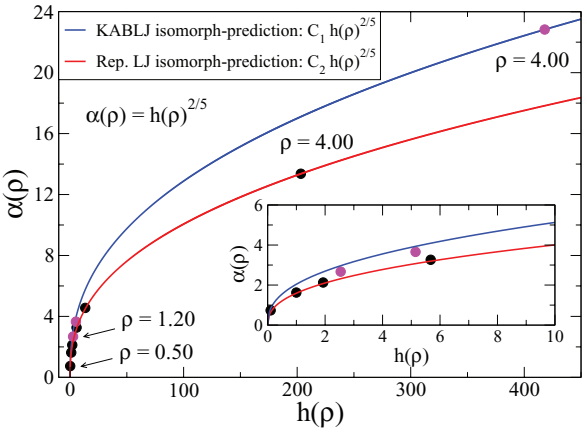

FIG. 3. $\alpha(\rho)$ in the RT expression plotted as a function of $h(\rho)$ of the isomorph theory (Eq. (7)) for the KABLJ and repulsive LJ system (see text). The red and blue curves are proportional to $h(\rho)^{2/5}$ with the proportionality constant determined from the highest density state point ($\rho = 4.00$) for each system.

complete description for the temperature and density dependence of the specific heat, i.e., $C_V^{\text{ex}} = (h(\rho)/T)^{2/5}$.

Scaling strategies which relate dynamics to thermodynamics have in the past proven useful to predict perplexing dynamical phenomena. We identified here the range of applicability for RT as the class of Roskilde liquids. By combining the RT expressions with the isomorph theory, we were able to provide also the full temperature and density dependence of the specific heat. Roskilde liquids include most or all van der Waals and metallic liquids. In contrast, water is a prime example of a non-Roskilde liquid with R close to zero near its density maximum. Water is thus not a good candidate for satisfying RT in large parts of its phase diagram as the simulation results presented here also show.

Beyond RT, Roskilde liquids also exhibit other types of simple behavior, for instance, they obey density scaling[42,46] and isochronal superposition.[47] Taking density scaling as an example, this property has been studied for a wide range of experimental liquids. A potential estimate of whether an experimental liquid obeys RT is thus to use whether this liquid obeys also density scaling.

The center for viscous liquid dynamics "Glass and Time" is sponsored by the Danish National Research Foundation via Grant No. DNRF61. We thank Lasse Bøhling for providing some of the data that establish the background for Fig. 3. Useful discussions with Truls Ingebrigtsen and Jacob Marott are gratefully acknowledged.

[1]F. J. Spera, D. Nevins, M. Ghiorso, and I. Cutler, Geochim. Cosmochim. Acta **73**, 6918 (2009).
[2]T. B. Schrøder, N. Gnan, U. R. Pedersen, N. P. Bailey, and J. C. Dyre, J. Chem. Phys. **134**, 164505 (2011).
[3]Y. Rosenfeld, Phys. Rev. A **15**, 2545 (1977).
[4]T. S. Ingebrigtsen, J. R. Errington, T. M. Truskett, and J. C. Dyre, "Predicting how nanoconfinement changes the relaxation time of a supercooled liquid," Phys. Rev. Lett. (unpublished).
[5]W. Götze, *Complex Dynamics of Glass-Forming Liquids: A Mode-Coupling Theory*, 1st ed. (Oxford University Press, New York, 2009).
[6]G. Adam and J. H. Gibbs, J. Chem. Phys. **43**, 139 (1965).
[7]J. Mittal, J. R. Errington, and T. M. Truskett, J. Chem. Phys. **125**, 076102 (2006).
[8]S. Sengupta, S. Karmakar, C. Dasgupta, and S. Sastry, Phys. Rev. Lett. **109**, 095705 (2012).
[9]M. Agarwal, M. Singh, B. S. Jabes, and C. Chakravarty, J. Chem. Phys. **134**, 014502 (2011).
[10]B. S. Jabes and C. Chakravarty, J. Chem. Phys. **136**, 144507 (2012).
[11]R. Chopra, T. M. Truskett, and J. R. Errington, J. Phys. Chem. B **114**, 10558 (2010).
[12]E. H. Abramson and H. West-Foyle, Phys. Rev. E **77**, 041202 (2008).
[13]G. Galliero, C. Boned, and J. Fernández, J. Chem. Phys. **134**, 064505 (2011).
[14]J. Mittal, J. R. Errington, and T. M. Truskett, Phys. Rev. Lett. **96**, 177804 (2006).
[15]Y. Rosenfeld and P. Tarazona, Mol. Phys. **95**, 141 (1998).
[16]R. D. Leonardo, L. Angelani, G. Parisi, and G. Ruocco, Phys. Rev. Lett. **84**, 6054 (2000).
[17]H.-O. May and P. Mausbach, Fluid Phase Equilib. **313**, 156 (2012).
[18]B. Coluzzi, M. Mézard, G. Parisi, and P. Verrocchio, J. Chem. Phys. **111**, 9039 (1999).
[19]N. Allsopp, G. Ruocco, and A. Fratalocchi, J. Comput. Phys. **231**, 3432 (2012).
[20]I. Saika-Voivod, F. Sciortino, and P. H. Poole, Phys. Rev. E **63**, 011202 (2000).
[21]A. Scala, F. W. Starr, E. L. Nave, F. Sciortino, and H. E. Stanley, Nature (London) **406**, 166 (2000).
[22]M. Agarwal, M. Singh, R. Sharma, M. P. Alam, and C. Chakravarty, J. Phys. Chem. B **114**, 6995 (2010).
[23]S. Mossa, E. L. Nave, H. E. Stanley, C. Donati, F. Sciortino, and P. Tartaglia, Phys. Rev. E **65**, 041205 (2002).
[24]L. Angelani, G. Ruocco, F. Sciortino, P. Tartaglia, and F. Zamponi, Phys. Rev. E **66**, 061505 (2002).
[25]D. C. Wallace, P. H. Sidles, and G. C. Danielson, J. Appl. Phys. **31**, 168 (1960).
[26]D. Bolmatov, V. V. Brazhkin, and K. Trachenko, Sci. Rep. **2**, 421 (2012).
[27]N. P. Bailey, U. R. Pedersen, N. Gnan, T. B. Schrøder, and J. C. Dyre, J. Chem. Phys. **129**, 184507 (2008).
[28]A. B. de Oliveira, P. A. Netz, T. Colla, and M. C. Barbosa, J. Chem. Phys. **124**, 084505 (2006).
[29]T. B. Schrøder, U. R. Pedersen, N. P. Bailey, S. Toxvaerd, and J. C. Dyre, Phys. Rev. E **80**, 041502 (2009).
[30]M. Dzugutov, Phys. Rev. A **46**, R2984 (1992).
[31]L. A. Girifalco, J. Phys. Chem. **96**, 858 (1992).
[32]W. Kob and H. C. Andersen, Phys. Rev. E **51**, 4626 (1995).
[33]K. Kremer and G. S. Grest, J. Chem. Phys. **92**, 5057 (1990).
[34]J. P. Hansen and I. R. McDonald, Phys. Rev. A **11**, 2111 (1975).
[35]L. J. Lewis and G. Wahnström, J. Non-Cryst. Solids **172–174**, 69 (1994).
[36]T. S. Ingebrigtsen, L. Bøhling, T. B. Schrøder, and J. C. Dyre, J. Chem. Phys. **136**, 061102 (2012).
[37]R. A. Buckingham, Proc. R. Soc. London, Ser. A **168**, 264 (1938).
[38]H. J. C. Berendsen, J. R. Grigera, and T. P. Straatsma, J. Phys. Chem. **91**, 6269 (1987).
[39]G. Wahnström, Phys. Rev. A **44**, 3752 (1991).
[40]R. G. D. Steel and J. H. Torrie, *Principles and Procedures of Statistics* (McGraw-Hill, New York, 1960).
[41]T. S. Ingebrigtsen, T. B. Schrøder, and J. C. Dyre, Phys. Rev. X **2**, 011011 (2012).
[42]D. Gundermann, U. R. Pedersen, T. Hecksher, N. P. Bailey, B. Jakobsen, T. Christensen, N. B. Olsen, T. B. Schrøder, D. Fragiadakis, R. Casalini, C. M. Roland, J. C. Dyre, and K. Niss, Nat. Phys. **7**, 816 (2011).
[43]J. C. Dyre, Phys. Rev. E **87**, 022106 (2013).
[44]N. Gnan, T. B. Schrøder, U. R. Pedersen, N. P. Bailey, and J. C. Dyre, J. Chem. Phys. **131**, 234504 (2009).
[45]L. Bøhling, T. S. Ingebrigtsen, A. Grzybowski, M. Paluch, J. C. Dyre, and T. B. Schrøder, New J. Phys. **14**, 113035 (2012).
[46]D. Coslovich and C. M. Roland, J. Phys. Chem. B **112**, 1329 (2008).
[47]C. M. Roland, R. Casalini, and M. Paluch, Chem. Phys. Lett. **367**, 259 (2003).

THE JOURNAL OF CHEMICAL PHYSICS **139**, 184506 (2013)

Statistical mechanics of Roskilde liquids: Configurational adiabats, specific heat contours, and density dependence of the scaling exponent

Nicholas P. Bailey, Lasse Bøhling, Arno A. Veldhorst, Thomas B. Schrøder, and Jeppe C. Dyre
DNRF Center "Glass and Time," IMFUFA, Dept. of Sciences, Roskilde University, P. O. Box 260, DK-4000 Roskilde, Denmark

(Received 26 August 2013; accepted 11 October 2013; published online 14 November 2013)

We derive exact results for the rate of change of thermodynamic quantities, in particular, the configurational specific heat at constant volume, C_V, along configurational adiabats (curves of constant excess entropy S_{ex}). Such curves are designated isomorphs for so-called Roskilde liquids, in view of the invariance of various structural and dynamical quantities along them. The slope of the isomorphs in a double logarithmic representation of the density-temperature phase diagram, γ, can be interpreted as one third of an effective inverse power-law potential exponent. We show that in liquids where γ increases (decreases) with density, the contours of C_V have smaller (larger) slope than configurational adiabats. We clarify also the connection between γ and the pair potential. A fluctuation formula for the slope of the C_V-contours is derived. The theoretical results are supported with data from computer simulations of two systems, the Lennard-Jones fluid, and the Girifalco fluid. The sign of $d\gamma/d\rho$ is thus a third key parameter in characterizing Roskilde liquids, after γ and the virial-potential energy correlation coefficient R. To go beyond isomorph theory we compare invariance of a dynamical quantity, the self-diffusion coefficient, along adiabats and C_V-contours, finding it more invariant along adiabats. © *2013 AIP Publishing LLC*. [http://dx.doi.org/10.1063/1.4827090]

I. INTRODUCTION

The traditional notion of a simple liquid-involving point-like particles interacting via radially symmetric pair potentials[1–13] (for example, the Lennard-Jones (LJ) system) is challenged by the existence of examples such as the Gaussian core model[14] and the Lennard-Jones Gaussian model[15,16] which exhibit complex behavior. Moreover, many molecular models have simple behavior in computer simulations, and experiments on van der Waals liquids show that these are generally regular with no anomalous behavior. We have recently suggested redefining a simple liquid—termed now a Roskilde-simple liquid, or just a Roskilde liquid—as one with strong correlations between the equilibrium virial (W) and potential-energy (U) fluctuations in the canonical fixed-volume (NVT) ensemble.[17] The basic phenomenology and theoretical understanding of Roskilde liquids were presented in a series of five papers published in the Journal of Chemical Physics.[18–22] In particular, Appendix A of Ref. 21 established an essential theorem of Roskilde liquids: A system has strong U, W correlations if and only if it has good isomorphs (curves in the thermodynamic phase diagram along which a number of properties are invariant in reduced units[21]). The degree of simplicity depends on the thermodynamic state point—all realistic systems lose simplicity when approaching the critical point and gas states. To illustrate this, Figure 1 shows the Lennard-Jones diagram including contours of the correlation coefficient R between U and W. We choose an (arbitrary) cut-off $R > 0.9$ as the boundary of simple-liquid behavior. It is clear from the figure that the correlation coefficient decreases rapidly as the liquid-gas spinodal is approached.

The theory of isomorphs starts with their definition and derives consequences from this which can be tested in simulations. For a system with N particles, two density-temperature state points (ρ_1, T_1) and (ρ_2, T_2) are isomorphic to each other if the Boltzmann factors for corresponding configurational microstates are proportional:

$$\exp\left(-\frac{U(\mathbf{r_1}^{(1)},\ldots,\mathbf{r_N}^{(1)})}{k_B T_1}\right) = C_{12}\exp\left(-\frac{U(\mathbf{r_1}^{(2)},\ldots,\mathbf{r_N}^{(2)})}{k_B T_2}\right). \quad (1)$$

Here U is the potential energy function and C_{12} depends on the two state points, but not on which microstates are considered. Corresponding microstates means $\rho_1^{1/3}\mathbf{r_i}^{(1)} = \rho_2^{1/3}\mathbf{r_i}^{(2)}$, or $\tilde{\mathbf{r}}_\mathbf{i}^{(1)} = \tilde{\mathbf{r}}_\mathbf{i}^{(2)}$, where a tilde denotes so-called reduced units. Reduced units for lengths means multiplying by $\rho^{1/3}$, for energies dividing by k_BT, and for times dividing by $(m/k_BT)^{1/2}\rho^{-1/3}$ (for Newtonian dynamics). An isomorph is a curve in the phase diagram consisting of points which are isomorphic to each other. From the definition it follows that all structural and dynamical correlation functions are isomorph invariant when expressed in reduced units. Thermodynamic quantities which do not involve volume derivatives, such as the excess entropy S_{ex} and excess specific heat at constant volume C_V^{ex}, are also isomorph invariant. Another consequence of the isomorph definition is that phase boundaries lying within the simple region of the phase diagram are isomorphs—note that the isomorph shown in Fig. 1 is nearly parallel to the liquid-solid coexistence lines. Reference 28

 © 2013 AIP Publishing LLC

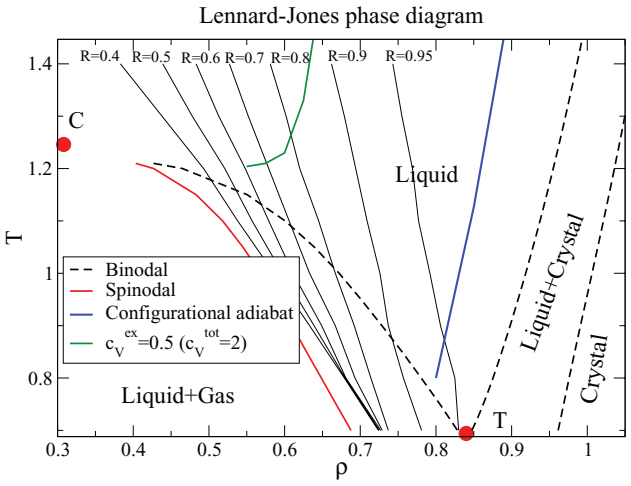

FIG. 1. Contour plot of R in (ρ, T) phase diagram for the single-component Lennard-Jones system using a shifted-potential cutoff of 4σ and system size $N = 1000$. Contour values are indicated at the top. Also indicated are binodal and spinodal obtained from the Johnson equation of state with the cutoff taken into account in a mean-field manner,[23] and the corresponding curves for solid-liquid coexistence as parameterized by Mastny and de Pablo (though for the larger cutoff 6σ).[24] T and C indicate the triple[24] and critical[23] points. The blue curve is a configurational adiabat, while the green line is the configurational isochoric specific heat contour $C_V = Nk_B/2$ (total specific heat $2Nk_B$); this is one of the criteria for the dynamic crossover separating liquid and gas regions in the phase diagram proposed by Brazhkin *et al.*[25–27] According to the theory of isomorphs both configurational adiabats and C_V-contours are isomorphs for sufficiently large R (Eq. (2)).

gives a brief review of the theory and its experimentally relevant consequences.

Only inverse power-law (IPL) systems, i.e., systems for which the potential energy is an Euler homogeneous function, have 100% virial potential-energy correlation and perfect isomorphs. Thus for realistic Roskilde liquids the isomorph concept is only approximate. Extensive computer simulations have shown, however, that the predicted isomorph invariants apply to a good approximation for several systems.[17,21,22,29–33] A few predictions have also been confirmed experimentally.[33,34]

Despite the success of the isomorph concept, it remains a "zero-order" theory, analogous to the ideal gas. In particular, there is no systematic theory for describing realistic systems in terms of perturbations about the ideal case. The purpose of this work is to examine deviations from perfect isomorph behavior in Roskilde liquids. One motivation is to understand what kind of deviations from IPL behavior (for example, constancy of the scaling exponent) are allowed while remaining in the "simple part" of the phase diagram. A second motivation is the hope of using Roskilde liquids to identify a general theory of liquids. For example, the existence of good isomorphs explains many observed connections between dynamics, structure, and thermodynamics, but also means that cause-and-effect interpretations of such connections ("the dynamics is *controlled* by . . .") must be reexamined. Given perfect isomorphs, any isomorph-invariant quantity can be said to control all the others. This puts a constraint on general theories, referred to as the "isomorph filter,"[21] but prevents one from sorting among theories that pass the filter. Examining carefully whether dynamical properties are more invariant when holding one isomorph-invariant quantity fixed versus holding another fixed could provide a means to select theories. The above applies equally well to theories of supercooled liquids and the glass transition; for example, in a theory featuring a characteristic activation energy or a characteristic temperature such as the Kauzmann temperature, then requiring the theory to pass the isomorph filter means that the characteristic energy/temperature depends on density in a specific manner.

Strong U, W correlation in the equilibrium NVT ensemble is a hallmark, and the first identified feature,[35] of Roskilde liquids. It is characterized at the level of second moments by the correlation coefficient

$$R(\rho, T) = \frac{\langle \Delta U \Delta W \rangle}{\sqrt{\langle (\Delta U)^2 \rangle \langle (\Delta U)^2 \rangle}} \tag{2}$$

and the slope

$$\gamma(\rho, T) = \frac{\langle \Delta U \Delta W \rangle}{\langle (\Delta U)^2 \rangle}. \tag{3}$$

Here Δ represents the deviation of a quantity from its NVT ensemble average. It has been shown that γ may be thought of in terms of an effective IPL potential with exponent 3γ (which in general depends on state point).[18,19] It has also a thermodynamic interpretation, namely, it is the ratio of the excess pressure coefficient $\beta_V^{\text{ex}} \equiv (1/V)(\partial W/\partial T)_V$ and excess specific heat per unit volume,

$$\gamma = \frac{\beta_V^{\text{ex}}}{c_V^{\text{ex}}}. \tag{4}$$

As mentioned, in IPL systems the correlation is indeed perfect, but non-IPL systems exist which yet have strong U, W-correlations, in particular the usual LJ fluid. While in any system the fluctuation formula for γ can be used to generate curves of constant (excess) entropy S_{ex} (configurational adiabats) via[21]

$$\left(\frac{\partial \ln T}{\partial \ln \rho}\right)_{S_{\text{ex}}} = \gamma(\rho, T), \tag{5}$$

in Roskilde-simple liquids several properties related to structure, thermodynamics, and dynamics are invariant along these curves. This leads to their designation as "isomorphs"; note that quantities must be expressed in thermodynamically reduced units to exhibit the invariance.[21] As an example of a structural quantity, the radial distribution function $g(r)$ is typically found to collapse well when plotted in reduced units along an isomorph; it could be that higher order measures of structure are less invariant, though.[36] One of the most basic isomorph-invariant quantities is the specific heat at constant volume: perfect isomorphs are also C_V-contours, while in imperfectly correlating systems the C_V contours and configurational adiabats may differ.

One might expect that the closer R is to unity, the better approximated the system would be by a single IPL potential. So it is perhaps surprising that we have recently identified systems where γ changes much more than in the LJ case, over a range in which strong U, W-correlation ($R > 0.9$) is maintained. One such system is the "repulsive Lennard-Jones" potential, in which the sign of the $1/r^6$ term is made positive.[32] It

seems that the property of strong U, W correlation and the existence of isomorphs are somehow more robust than the constancy of γ. It can be surprising how well isomorphs "work" for non-IPL systems. This robustness allows for a richer variety of behavior, since the shapes of isomorphs are no longer necessarily straight lines in a ($\ln\rho$, $\ln T$)-plot. The theory of the thermodynamics of Roskilde-simple liquids[32] implies that γ may be considered a function of ρ only. This immediately gives us a new quantity (in addition to R and γ) to characterize Roskilde liquids: $d\gamma/d\rho$, or more simply, its sign. This result depends on the assumption that configurational adiabats and C_V-contours exactly coincide. It is not clear what to expect when this does not hold exactly; this paper is an attempt to address the topic of imperfect correlation from statistical mechanical considerations. Because C_V is also a fundamental thermodynamic quantity, the difference between adiabats and C_V-contours should be a useful probe of the breakdown of perfect isomorphs as U, W-correlation becomes less than perfect, and will be the focus of this paper.

While, as mentioned above, the arguments of Ref. 32 (which assume perfect isomorphs) show that $\gamma = \gamma(\rho)$, in practice γ does depend on T but the dependence is much smaller than that on ρ, and we can ignore it most of the time. This is apparent for the single-component LJ system in Fig. 5 of Ref. 18. A more explicit quantitative comparison, of the logarithmic derivatives of γ with respect to ρ and T, was made in Ref. 33 for two molecular systems. We present further data on this below. Fluids with LJ and similar potentials (for example, generalized-LJ potentials with different exponents) tend to have $d\gamma/d\rho < 0$: It is clear that γ must converge to one third of the repulsive exponent at very high densities and temperatures while typical values are larger.[19] On the other hand, potentials may be constructed which have $d\gamma/d\rho > 0$, simply by shifting the potential radially outwards so that the repulsive divergence occurs at a finite value of pair separation. Such potentials naturally involve a hard core of absolutely excluded volume. They are relevant to experiments,[33] because tests of the isomorph theory[34] typically involve molecules rather than single atoms, with the interaction range being relatively short compared to the particle size (colloids are an even more extreme example of this, of course). The Dzugutov system,[37] although only Roskilde-simple at high densities and temperatures, is another example with $d\gamma/d\rho > 0$, but where there is no hard core. Another such system is the above-mentioned repulsive Lennard-Jones potential; in this case the effective exponent increases monotonically, interpolating between the low density limit 6 ($\gamma = 2$) and the high density limit 12 ($\gamma = 4$).

For brevity we term curves of constant $S_{\rm ex}$ *adiabats* (the qualifier "configurational" is to be understood); in this paper, unlike all our other works on isomorphs, we deliberately avoid calling them isomorphs, since the point of this work is to examine deviations from perfect isomorph behavior. We also drop the subscript ex for notational simplicity, and similarly use C_V to mean the configurational part of specific heat (the kinetic part is also isomorph invariant, though, being 3/2 for a classical monatomic system). Below we derive some exact results concerning the relation between adiabats and C_V-contours, and argue how this connects to whether γ is an increasing or decreasing function of ρ (more specifically the sign of $(\partial\gamma/\partial\rho)_S$). The argument involves relating γ to an exponent determined by derivatives of the pair potential, introduced in Ref. 19. The claim is supported by simulations of two Roskilde liquids: the LJ fluid (with $d\gamma/d\rho < 0$) and the Girifalco fluid (with $d\gamma/d\rho > 0$ at least for high densities). The Girifalco potential was constructed to model the effective interaction between C_{60} molecules, modeling the carbon atoms as Lennard-Jones particles and applying rotational averaging:[38]

$$v(r) = -\alpha\left(\frac{1}{s(s-1)^3} + \frac{1}{s(s+1)^3} - \frac{2}{s^4}\right) + \beta\left(\frac{1}{s(s-1)^9} + \frac{1}{s(s+1)^9} - \frac{2}{s^{10}}\right). \quad (6)$$

where s is the distance two molecules' centers, scaled by the diameter. We have chosen the parameters α and β such that the potential well has a depth of approximately 1 and the potential diverges at unit distance, $\beta = 0.0018141\alpha$ with $\alpha = 0.17$.

For simulations we use systems of 1000 particles simulated at constant volume and temperature (NVT) using the RUMD code[39] for simulating on NVIDIA graphical processing units (GPUs). Although the state points considered do not involve long relaxation times, the speed provided by GPUs is desirable because reasonably accurate determination of third moments requires of order 1×10^6 independent samples; we typically run 50×10^6 steps and sample every 50 steps (the time step sizes were 0.0025–0.004 for LJ and 0.0004 for Girifalco). The temperature was controlled using a Nosé-Hoover thermostat. Part (d) in Fig. 3 shows the correlation coefficient R along an adiabat for each system. Both systems are Roskilde-simple (have $R > 0.9$) in the simulated part of the phase diagram.

In Sec. II, a general fluctuation formula for derivatives of thermodynamic quantities along adiabats is derived, and applied to the case of C_V. In Sec. III we show the connection between the derivative of C_V and derivatives of γ. The results are illustrated with data from simulations. In Sec. IV a fluctuation formula for the slope of contours of C_V is derived, and illustrated with simulation data. Finally, Secs. V and VI are the discussion and a brief conclusion, respectively.

II. THERMODYNAMIC DERIVATIVES AT CONSTANT ENTROPY

A. γ as linear-regression slope

Before proceeding to thermodynamic derivatives we recall the connection between the above definition of γ and linear regression. Following Appendix C of Ref. 21 we characterize the deviation from perfect correlation via the fluctuating variable

$$\epsilon \equiv \Delta W - \gamma\Delta U, \quad (7)$$

which vanishes for perfect correlation. The linear regression slope is defined by minimizing $\langle\epsilon^2\rangle$ with respect to γ, leading to Eq. (3).[40] A consequence of this definition of γ is seen by

writing

$$\Delta W = \gamma \Delta U + \epsilon, \tag{8}$$

and correlating[41] this with ΔU:

$$\langle \Delta W \Delta U \rangle = \gamma \langle (\Delta U)^2 \rangle + \langle \Delta U \epsilon \rangle \tag{9}$$

From this and the definition of γ it follows that

$$\langle \Delta U \epsilon \rangle = 0, \tag{10}$$

that is, U and ϵ are (linearly) uncorrelated, independent of whether perfect correlation holds between U and W.

B. Density-derivatives of averages on adiabats

We are interested in the derivatives of thermodynamic quantities along certain curves in the phase diagram, in particular those of constant S, so we start by presenting general formulas for the derivatives with respect to $\ln \rho$ and $\ln T$ (holding the other constant). From standard statistical mechanics (see, for example, Appendix B of Ref. 18) we have (with $\beta = 1/(k_B T)$; in the following we set $k_B = 1$)

$$\left(\frac{\partial \langle A \rangle}{\partial \beta} \right)_\rho = - \langle \Delta U \Delta A \rangle \tag{11}$$

which implies

$$\left(\frac{\partial \langle A \rangle}{\partial \ln T} \right)_\rho = \beta \langle \Delta U \Delta A \rangle . \tag{12}$$

Likewise (see Appendix A),

$$\left(\frac{\partial \langle A \rangle}{\partial \ln \rho} \right)_T = \left\langle \frac{\partial A}{\partial \ln \rho} \right\rangle - \beta \langle \Delta W \Delta A \rangle , \tag{13}$$

where differentiation with respect to $\ln \rho$ inside an expectation value—that is, for an arbitrary configuration rather than an ensemble average—is understood to imply that the reduced coordinates of the configuration, $\tilde{\mathbf{r}}_i \equiv \rho^{1/3} \mathbf{r}_i$, are held fixed. Equations (12) and (13) can be used to construct the derivative with respect to $\ln \rho$ along an arbitrary direction; that is instead of keeping T constant (a line of zero slope) we take a direction with slope g (in $\ln \rho$, $\ln T$ space):

$$\left(\frac{\partial \langle A \rangle}{\partial \ln \rho} \right)_{[g]} = \left(\frac{\partial \langle A \rangle}{\partial \ln \rho} \right)_T + g \left(\frac{\partial \langle A \rangle}{\partial \ln T} \right)_\rho \tag{14}$$

$$= \left\langle \frac{\partial A}{\partial \ln \rho} \right\rangle - \beta \langle \Delta W \Delta A \rangle + g\beta \langle \Delta U \Delta A \rangle \tag{15}$$

$$= \left\langle \frac{\partial A}{\partial \ln \rho} \right\rangle - \beta \langle \Delta A (\Delta W - g \Delta U) \rangle . \tag{16}$$

Note that we use subscript $[g]$ to indicate that g is the slope in the $\ln \rho$, $\ln T$ plane, rather than the quantity held constant, in the derivative. This expression can be used to find formulas for the direction in which a given thermodynamic variable is constant, as we do below. For now we choose $g = \gamma$, to obtain a formula for derivatives along adiabats (Eq. (5)):

$$\left(\frac{\partial \langle A \rangle}{\partial \ln \rho} \right)_S = \left\langle \frac{\partial A}{\partial \ln \rho} \right\rangle - \beta \langle \Delta A \Delta (W - \gamma U) \rangle$$
$$= \left\langle \frac{\partial A}{\partial \ln \rho} \right\rangle - \beta \langle \Delta A \, \epsilon \rangle . \tag{17}$$

As an example, we take $A = U$. Noting that $W \equiv \partial U / \partial \ln \rho$ and Eq. (10), we get

$$\left(\frac{\partial \langle U \rangle}{\partial \ln \rho} \right)_S = \left\langle \frac{\partial U}{\partial \ln \rho} \right\rangle = \langle W \rangle , \tag{18}$$

which is a general result that can also be derived thermodynamically starting with the fundamental thermodynamic identity $TdS = dU + pdV = dU + Wd \ln(V) = dU - Wd \ln \rho$ (here the variables U, W refer to macroscopic, or thermally averaged quantities, the omission of angle-brackets notwithstanding). As a second application of Eq. (17), consider a system with perfect correlation. Then $\epsilon \equiv 0$, and we get

$$\left(\frac{\partial \langle A \rangle}{\partial \ln \rho} \right)_S = \left\langle \frac{\partial A}{\partial \ln \rho} \right\rangle , \tag{19}$$

which means that in such systems the derivative along an adiabat is given entirely by the "intrinsic" density dependence for individual configurations; fluctuations do not contribute. This is of course the case of perfect isomorphs, where the probabilities of scaled configurations are identical along an isomorph.

C. Variation of C_V on adiabats

We consider the derivative of C_V with respect to $\ln \rho$ on an adiabat. From $C_V = \langle (\Delta U)^2 \rangle / T^2$, we have

$$\left(\frac{\partial C_V}{\partial \ln \rho} \right)_S = \frac{1}{T^2} \left(\frac{\partial \langle (\Delta U)^2 \rangle}{\partial \ln \rho} \right)_S - \frac{2}{T^3} \langle (\Delta U)^2 \rangle \left(\frac{\partial T}{\partial \ln \rho} \right)_S \tag{20}$$

$$= \frac{1}{T^2} \left(\frac{\partial \langle (\Delta U)^2 \rangle}{\partial \ln \rho} \right)_S - \frac{2\gamma}{T^2} \langle (\Delta U)^2 \rangle . \tag{21}$$

Writing $\langle (\Delta U)^2 \rangle = \langle U^2 \rangle - \langle U \rangle^2$ and making use of the general result of Eq. (17), after some algebra (see Appendix B) we obtain the simple result

$$\left(\frac{\partial C_V}{\partial \ln \rho} \right)_S = -\beta^3 \langle (\Delta U)^2 \Delta (W - \gamma U) \rangle = -\beta^3 \langle (\Delta U)^2 \epsilon \rangle . \tag{22}$$

This is a major result of this paper. Note that the right side vanishes for perfect correlation ($\epsilon = 0$)—in which case C_V is constant on the same curves that S is; in other words, C_V is a function of entropy only. For less than perfect correlation, the most interesting feature is the sign, which we argue in Sec. III, is the opposite of that of $d\gamma/d\rho$.

III. CONNECTION BETWEEN $(\partial C_V/\partial\rho)_S$ AND DERIVATIVES OF γ

A. Relation to temperature-dependence of γ

We wish to understand the sign of $\langle(\Delta U)^2\epsilon\rangle$. We know from Eq. (10) that U and ϵ are linearly uncorrelated; we must now consider higher order correlations. Recall that γ may also be interpreted[18] as the slope of isochores in the W, U phase diagram—the linear regression of the scatter-plot of instantaneous W, U values at one state point gives the slope of $\langle W\rangle$ versus $\langle U\rangle$ at fixed density. The triple correlation is related to the curvature of the isochore, and thus to $(\partial\gamma/\partial T)_\rho$. We obtain the exact relation by differentiating γ with respect to β:

$$\left(\frac{\partial\gamma}{\partial\beta}\right)_\rho = \frac{1}{\langle(\Delta U)^2\rangle}\left(\frac{\partial\langle\Delta U\Delta W\rangle}{\partial\beta}\right)_\rho - \frac{\langle\Delta U\Delta W\rangle}{\langle(\Delta U)^2\rangle^2}\left(\frac{\partial\langle(\Delta U)^2\rangle}{\partial\beta}\right)_\rho \tag{23}$$

$$= -\frac{\langle(\Delta U)^2\Delta W\rangle}{\langle(\Delta U)^2\rangle} - \frac{\gamma}{\langle(\Delta U)^2\rangle}\left(-\langle(\Delta U)^3\rangle\right) \tag{24}$$

$$= -\frac{\langle(\Delta U)^2(\Delta W-\gamma\Delta U)\rangle}{\langle(\Delta U)^2\rangle} \tag{25}$$

$$= -\frac{\left\langle(\Delta U)^2\epsilon\right\rangle}{\left\langle(\Delta U)^2\right\rangle}, \tag{26}$$

where we have used Eq. (11) and some algebraic manipulation as in Appendix B. Combining this result with Eq. (22) gives

$$\left(\frac{\partial C_V}{\partial\ln\rho}\right)_S = \beta^2\langle(\Delta U)^2\rangle\beta\left(\frac{\partial\gamma}{\partial\beta}\right)_\rho = -C_V\left(\frac{\partial\gamma}{\partial\ln T}\right)_\rho, \tag{27}$$

or more concisely

$$\left(\frac{\partial\ln C_V}{\partial\ln\rho}\right)_S = -\left(\frac{\partial\gamma}{\partial\ln T}\right)_\rho. \tag{28}$$

B. Relation to density-dependence of γ via the effective IPL exponent $n^{(2)}(r)$

The last result implies, in particular, that the sign of the density-derivative of C_V along an isomorph is opposite to that of $(\partial\gamma/\partial T)_\rho$. Since the latter derivative is neglected in the theory of isomorphs, it is useful to find a connection with a density derivative of γ. The relevant derivative turns out not to be $(\partial\gamma/\partial\rho)_T$ but $(\partial\gamma/\partial\rho)_S$, i.e., the derivative of γ along the adiabat. For many systems of interest this derivative has the same sign as $(\partial\gamma/\partial T)_\rho$, while those signs can be positive or negative depending on the system (or even for a given system). We shall now argue that this sign-equivalence is to be expected by considering how γ is related to the pair potential $v(r)$. This is an interesting question in its own right, and was explored in Ref. 19. For potentials with strong repulsion at short distances, we can indeed relate γ directly, albeit approximately, to $v(r)$, or more precisely, to its derivatives. As discussed in Ref. 19 the idea is to match an IPL to the actual potential; γ is then one third of the "effective IPL exponent." There are many ways to define such an exponent, but a key insight is that it should involve neither the potential itself (because shifting the zero of potential has no consequences), nor its first derivative (because the contributions to the forces from a linear term tend to cancel out in dense systems at fixed volume).[19] The simplest possibility within these constraints involves the ratio of the second and third derivatives. For an IPL, $v(r)\propto 1/r^n$, and indicating derivatives with primes, we have $v'''(r)/v''(r) = -(n+2)/r$, so n can be extracted as $-rv'''(r)/v''(r) - 2$. For a general pair potential this quantity will be a function of r, and thus we define the r-dependent second-order effective IPL exponent $n^{(2)}(r)$ as[19]

$$n^{(2)}(r) \equiv -\frac{rv'''(r)}{v''(r)} - 2. \tag{29}$$

The superscript "(2)" indicates which derivative appears in the denominator; one can similarly[19] define $n^{(p)}(r)$ for $p = 0, 1, \ldots$; $p = 2$ is the first not involving v or v'. Interestingly, the IPL is not the only solution to $n^{(2)}(r) = n$ with constant n; so is the so-called extended IPL

$$v_{\mathrm{eIPL}}(r) = A/r^n + Br + C, \tag{30}$$

introduced in Ref. 19. The resemblance of the Lennard-Jones potential to such a form can be considered an explanation of why it inherits many of the properties of the IPL potential. For a general potential, the question that now arises is at which r one should evaluate $n^{(2)}$. It was argued in Ref. 19 that $n^{(2)}/3$ evaluated at a point near the maximum of $g(r)$—let us call it r_γ—should correspond to γ. One expects that, like the peak in $g(r)$, $r_\gamma = \Lambda\rho^{-1/3}$, where Λ is of order unity and depends weakly on temperature, but we do not know it precisely *a priori*. There are two crucial things we can say, however: First, we can certainly identify r_γ *a posteriori* by inspection for a given state point: That is, having simulated a reference state point $(\rho_{\mathrm{ref}}, T_{\mathrm{ref}})$ and determined γ_{ref} there, it is straightforward to (typically numerically) solve the equation $n^{(2)}(r_\gamma)/3 = \gamma_{\mathrm{ref}}$ for r_γ. The second crucial point is that whatever details of the liquid's statistical mechanics determine r_γ (for instance, a kind of $g(r)$-weighted average), *these details do not vary along an isomorph* (this argument assumes good isomorphs, so that the statement can be applied to adiabats). Therefore, r_γ is an isomorph invariant—more precisely its reduced-unit form $\rho^{1/3}r_\gamma = \Lambda$ is constant along an adiabat, which implies $\Lambda = \Lambda(S)$. So γ is given by

$$\gamma(\rho, S) = \frac{1}{3}n^{(2)}(\Lambda(S)\rho^{-1/3}), \tag{31}$$

or

$$\gamma(\rho, S) = \frac{1}{3}n^{(2)}\left(r_{\gamma,\mathrm{ref}}(S)\frac{\rho^{-1/3}}{\rho_{\mathrm{ref}}^{-1/3}}\right). \tag{32}$$

In the form with Λ we explicitly recognize that Λ is constant on an isomorph, or equivalently, that it depends on S; the second form shows how Λ can be determined using a simulation at one density to identify r_γ there.

For the Lennard-Jones potential $n^{(2)}(r)$ decreases as r decreases (corresponding to as ρ increases), while for potentials such as the Girifalco potential with a divergence at finite r (see Fig. 3), it increases as r decreases (ρ increases), although at low densities the opposite behavior is seen. The validity of Eq. (31) has been investigated by Bøhling *et al.*[42] Under which circumstances does Eq. (31) give a good estimate of the density dependence of γ? The system must have sufficiently strong W, U correlations, since as $R \to 0$, γ must also vanish irrespective of $n^{(2)}$'s behavior. (For example, in a Lennard-Jones-like liquid, as r increases, the curvature of the pair potential becomes negative at some r, at which point $n^{(2)}$ diverges. At or below the corresponding density, and not too high temperature, a single phase is likely to have a negative pressure and be mechanically unstable, giving way to liquid-gas coexistence. In this regime W, U correlations tend to break down completely and γ goes to zero; see Figs. 3(c) and 3(d), in particular the Girifalco data.)

Equation (31) shows how γ depends on ρ, but we need to consider temperature dependence in order to connect with the result for C_V along an adiabat. This comes in through $\Lambda(S)$. We cannot right away determine how Λ depends on S but we know it is a weak dependence, since r_γ is expected to remain close to the peak in $g(r)$.[42] For liquids with a repulsive core this peak moves slowly to shorter distances as temperature, and hence entropy, increase at fixed ρ. We expect the same to be true for Λ, since in the high-temperature limit potential energy and virial fluctuations, and thus γ, are dominated by ever smaller pair separations. Thus we expect that

$$\frac{d\Lambda(S)}{dS} < 0, \tag{33}$$

while the weak dependence on entropy/temperature at fixed density can be expressed as

$$C_V \frac{d\ln\Lambda(S)}{dS} \ll 1, \tag{34}$$

(the use of C_V to make the left side dimensionless, instead of, for example, differentiating with respect to $\ln S$, is done for convenience below; note that C_V varies slowly and has a similar order of magnitude to the entropy differences between isomorphs in the liquid region of the phase diagram). From Eq. (33) it follows that both increasing ρ at fixed S, and increasing T at fixed ρ, decrease the argument of $n^{(2)}$. (Recall that in the earliest work on Roskilde liquids it was noted that the slope of the W, U correlation converges down towards $12/3 = 4$ for the LJ case both in the high temperature and the high density limits.[35]) Taking the appropriate derivatives of Eq. (31) yields

$$\left(\frac{\partial\gamma}{\partial\ln\rho}\right)_S = -\frac{\Lambda(S)\rho^{-1/3}}{9}\left.\frac{dn^{(2)}(r)}{dr}\right|_{r=\Lambda(S)\rho^{-1/3}}, \tag{35}$$

$$\left(\frac{\partial\gamma}{\partial\ln T}\right)_\rho = \frac{\Lambda(S)\rho^{-1/3}}{3}\left.\frac{dn^{(2)}(r)}{dr}\right|_{r=\Lambda(S)\rho^{-1/3}}\frac{d\ln(\Lambda(S))}{dS}C_V. \tag{36}$$

TABLE I. Validity of Eq. (38) for several potentials. For each system the signs of $(\partial\gamma/\partial T)_\rho$ and $(\partial\gamma/\partial\rho)_S$ have been checked for a set of adiabats. For the Lennard-Jones, Buckingham and Dzugutov system the density range gives the lowest densities of the simulated adiabats while the temperature range gives the range of temperatures simulated for each adiabat. For the Girifalco and repulsive Lennard-Jones the density range indicates the range of densities simulated for each adiabat, while the temperature range indicates the lowest temperatures. Data near extrema of γ have not been included.

Potential	ρ-range	T-range	$(\partial\gamma/\partial T)_\rho$	$(\partial\gamma/\partial\rho)_S$
Lennard-Jones	0.6–1.2	0.8–5.0	−	−
Buckingham	0.7–1.2	2–6	−	−
Dzugutov	0.55–0.8	0.75–1.2	+	+
Girifalco	0.45–0.5	6–54	+	+
Repulsive Lennard-Jones	0.1–10	0.4–2.0	+	+

Combining these gives

$$\left(\frac{\partial\gamma}{\partial\ln T}\right)_\rho = \left(\frac{\partial\gamma}{\partial\ln\rho}\right)_S\left(-3\frac{d\ln(\Lambda(S))}{dS}C_V\right). \tag{37}$$

From Eqs. (33) and (34) the quantity in brackets on the right side is positive but much smaller than unity. We therefore have

$$\begin{aligned}&\mathrm{sgn}\left(\left(\frac{\partial\gamma}{\partial T}\right)_\rho\right) = \mathrm{sgn}\left(\left(\frac{\partial\gamma}{\partial\rho}\right)_S\right),\\ &\left|\left(\frac{\partial\gamma}{\partial\ln T}\right)_\rho\right| \ll \left|\left(\frac{\partial\gamma}{\partial\ln\rho}\right)_S\right|,\end{aligned} \tag{38}$$

which is expected to hold for liquids with repulsive cores, with sufficiently strong W, U-correlations. It remains to be investigated thoroughly to what extent Eq. (38) holds, both regarding in how large a region of the phase diagram it holds for a given liquid, and for which liquids it holds in a reasonably large region. Its validity depends both on that of Eq. (31) and the conjecture that Λ decreases, slowly, as entropy increases. Some data are shown in Table I which compares the signs of the two derivatives for different systems and Fig. 2 which compares the two derivatives at state points along an adiabat for the LJ system. For comparison the density derivative at fixed temperature is also shown, obtained via chain-rule combination of the other two derivatives. This involves a minus sign and therefore the two terms (which have the same sign) tend to cancel.

In the limit of perfect W, U correlation we know $(\partial\gamma/\partial T)_\rho$ vanishes. There is no reason to expect Λ to become constant in this limit,[43] therefore $(\partial\gamma/\partial\rho)_S$ must also vanish in the limit. This corresponds to $n^{(2)}(r)$ becoming constant: IPL or extended IPL systems (Eq. (30)). But because the dependence of Λ on S is in general weak, there is a regime—that of general Roskilde liquids—where we can neglect it, but where $n^{(2)}$ cannot be considered constant. In this approximation, then, we can write the density derivative as an ordinary derivative. Combining this with Eq. (28) we have the following result for the sign of the C_V:

$$\mathrm{sgn}\left(\left(\frac{\partial C_V}{\partial\ln\rho}\right)_S\right) = -\,\mathrm{sgn}\,(d\gamma/d\rho)\,. \tag{39}$$

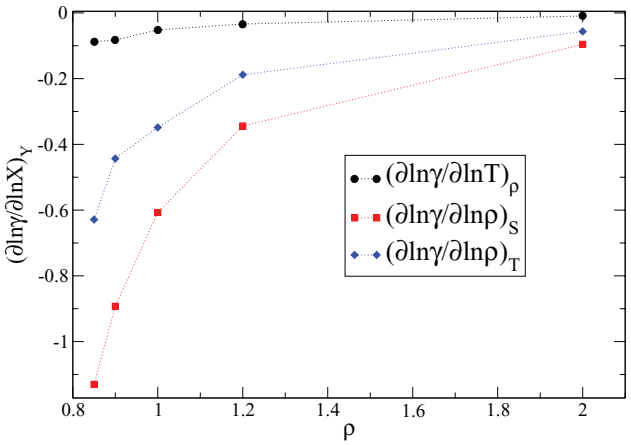

FIG. 2. Logarithmic derivatives of γ: (1) with respect to T at constant ρ, (2) respect to ρ at constant S and (3) respect to ρ at constant T, for the LJ system at points along the adiabat including $\rho = 0.85$, $T = 0.80$. The first derivative was determined via fitting $\ln(\gamma)$ versus $\ln T$ data (obtained also for neighboring adiabats) at each ρ to a quadratic function; the second analytically after making a (one-parameter) fit to the logarithmic derivative of Eq. (C5), and the third via the chain rule as a linear combination of the other two, $(\partial \ln(\gamma)/\partial \ln \rho)_T = (\partial \ln(\gamma)/\partial \ln \rho)_S - \gamma(\partial \ln(\gamma)/\partial \ln T)_\rho$. While all decrease to zero at high densities (consistent with γ converging to a constant 4 = 12/3) the temperature derivative is consistently a factor of ten smaller than the density derivative at constant S.

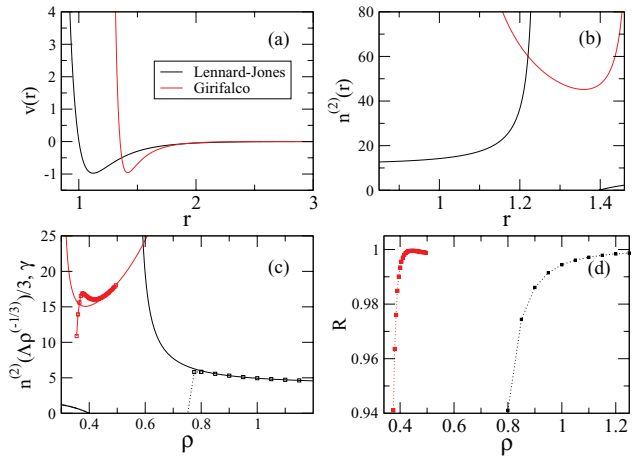

FIG. 3. (a) The pair potentials used in this work. The Girifalco potential diverges at $r = 1$. (b) $n^{(2)}(r)$ for the two potentials. (c) $n^{(2)}(\Lambda\rho^{-1/3})$ (full lines) and γ on sample adiabats for both models (symbols). The entropy was not calculated, but adiabats are uniquely specified by giving one state point, for example, $\rho = 0.80$, $T = 0.80$ for the LJ case and $\rho = 0.4$, $T = 4.0$ for the GF case. The value of Λ was fixed by requiring agreement with γ at the highest simulated density for each isomorph. (d) Correlation coefficient R from simulations, along the same adiabats as in (c).

Thus, we can predict—based on the $n^{(2)}$ estimate of γ—that the rate of change of C_V along an adiabat has the opposite sign as the density dependence of γ (along the adiabat if we need to be specific). Thus from knowing only the pair potential one can say something reasonably accurate about both the adiabats and the C_V-contours.

C. Simulation results for variation of C_V along adiabats

To confirm the relation between the sign of $d\gamma/d\rho$ and that of $(\partial C_V/\partial\rho)_S$ and exhibit the relation between adiabats and C_V contours we carried out simulations on two model systems. Figure 3(a) shows the pair potentials. Note that the Girifalco potential diverges at $r = 1$; this hard core restricts the density to be somewhat smaller than for the LJ case. Part (b) of Fig. 3 shows the effective exponent $n^{(2)}(r)$. There is a singularity where the second derivative vanishes (the transition from concave up to concave down), which can be seen in the figure at $r \simeq 1.224$ for LJ and $r \simeq 1.48$ for Girifalco; as r decreases from the singularity $n^{(2)}$ decreases monotonically in the LJ case, while in the Girifalco case it first decreases and then has a minimum before increasing and in fact diverging as $r = 1$ is approached. Part (c) of Fig. 3 shows the estimate of $\gamma(\rho)$ from Eq. (31) along with $\gamma(\rho)$ calculated in simulations along an adiabat for each system. Here Λ was determined by matching $n^{(2)}/3$ with γ at the highest density. The agreement is good for not too low densities—as mentioned above when $n^{(2)}(r)$ diverges due to the curvature of the potential vanishing, then both R and γ will rapidly approach zero, which is what we can see happening for the Girifalco system in parts (c) and (d) and low density. Note that the adiabat for the Girifalco system rapidly reaches rather high temperatures, since the exponent is always greater than 15, or roughly three times that of the LJ system. More interestingly, for the Girifalco system $d\gamma/d\rho$ changes sign at a density around 0.4, so we can expect the dependence of C_V along an adiabat to reflect this. The location and value of the minimum in γ do not match those for $n^{(2)}$, however—perhaps the vanishing of the curvature is already having an effect.

The procedure for determining adiabats is described in Appendix C. Figures 4 and 5 show $c_V = C_V/N$ along adiabats for the LJ and Girifalco systems, respectively. For the LJ case the slope is positive, which is consistent with $d\gamma/d\rho$ being negative as discussed in Sec. III. It is worth noting that the overall variation of C_V is quite small, of order 0.1 per particle for the density range shown, but it is not negligible,

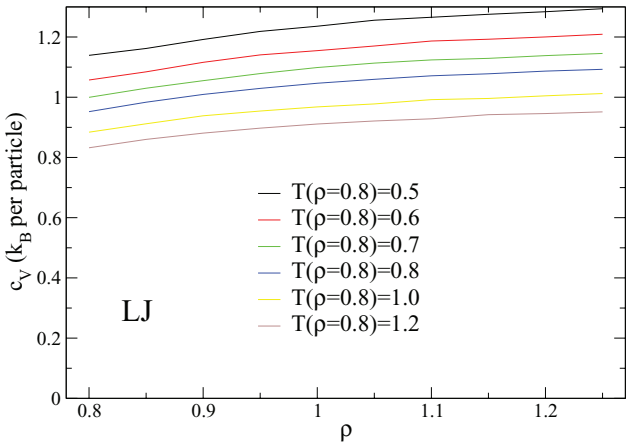

FIG. 4. Dependence of $c_V = C_V/N$ on density along six different adiabats for the LJ fluid. We label the curves by their temperature at a fixed density, here the starting density $\rho = 0.8$. The change in c_V is of order 0.1–0.15 for the ∼50% change in density shown here, small but not negligible. The slopes are positive, consistent with the negative sign of $d\gamma/d\rho$ and arguments of Sec. III.

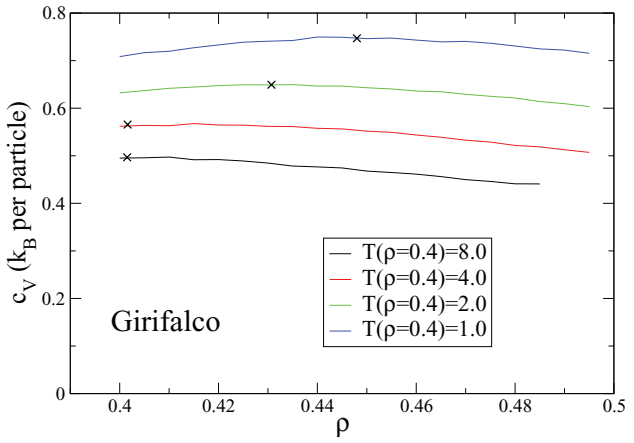

FIG. 5. Dependence of $c_V = C_V/N$ on density along four different adiabats for the Girifalco fluid. The curves are labelled by their temperature at $\rho = 0.4$. For the ∼20% changes in density shown here, c_V changes by about 0.05. It is generally decreasing in the range shown but increases at low densities and temperatures; the maxima (determined by fitting a cubic polynomial) are shown as crosses, and appear at different densities for different adiabats.

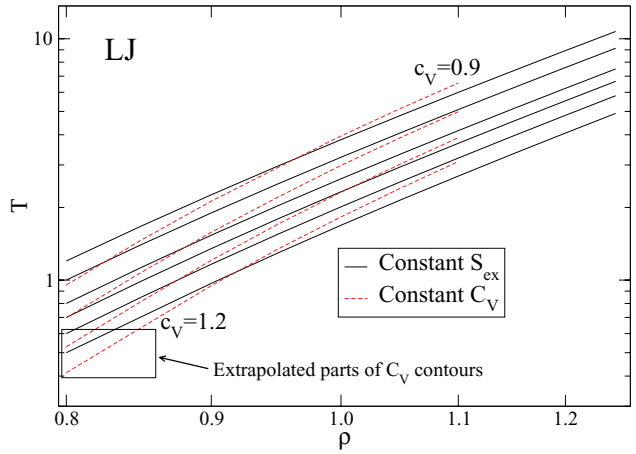

FIG. 6. Comparison of adiabats and C_V-contours for the LJ system. The adiabats are the same as those shown in Fig. 4, and were calculated using Eq. (C3), while C_V-contours (values 0.9, 1.0, 1.1, and 1.2 in units of k_B) were determined from a series of simulations on different isochores and interpolating the C_V data as a function of T (some extrapolated points, indicated, were also included).

even though the system has strong U, W correlations and the structure and dynamics have been shown to be quite invariant along the adiabats. For the Girifalco system the slope is positive at low density until a maximum is reached, with a negative slope at higher densities. This is also broadly consistent with the expectations from Fig. 3 (the locations of the maxima are not expected to be accurately given by Eq. (31)).

D. Contours of C_V and S directly compared

As an alternative to considering how C_V varies along an adiabat, we can find the contours of C_V separately. First we simulated several isochores, then the data were interpolated to allow constant-C_V curves to be constructed. Specifically, we find that the dependence of C_V on temperature along an isochore can be accurately fitted by the expression

$$C_V(T) = \frac{A(\rho)}{T^{B(\rho)}} + C(\rho), \tag{40}$$

where A, B, and C are functions of ρ. This expression was inspired by the Rosenfeld-Tarazona expression $C_V \sim T^{-2/5}$ for the specific heat;[44] we do not constrain the exponent B to be 2/5, however. The expression can easily be inverted to yield the temperature $T_{C_V}(\rho)$ corresponding to a given value of C_V, as a function of density

$$T_{C_V}(\rho) = \left(\frac{A(\rho)}{C_V - C(\rho)}\right)^{1/B(\rho)}. \tag{41}$$

The C_V contours are shown along with the adiabats in Figs. 6 and 7. Recall that in typical liquids we expect C_V to increase as T decreases or ρ increases. For the LJ case the C_V contours have a higher slope than the adiabats, therefore as ρ increases along an adiabat we cross contours corresponding to higher values of C_V. For the Girifalco system the C_V contours have initially (at low density) higher slopes than the adiabats but then bend over and have lower slopes. Thus the picture is consistent with the data for C_V along adiabats shown in Figs. 4 and 5. It cannot be otherwise, but there is more information here compared to those figures. For example, the adiabats are closer to the straight lines (in the double-log representation) expected for IPL systems, while the C_V-contours have more non-trivial shapes. Furthermore a small variation of C_V along an adiabat could hide a relatively large difference in slope between C_V-contours and adiabats (since C_V is typically a relatively slowly varying function).

IV. FLUCTUATION FORMULA FOR GENERATING CONTOURS OF C_V

Apart from investigating the variation of C_V along an adiabat, it is of interest to identify the contours of C_V; the non-constancy of C_V along an adiabat is equivalent to the statement that the C_V contours do not coincide with the adiabats, although we can expect them to be close for Roskilde liquids.

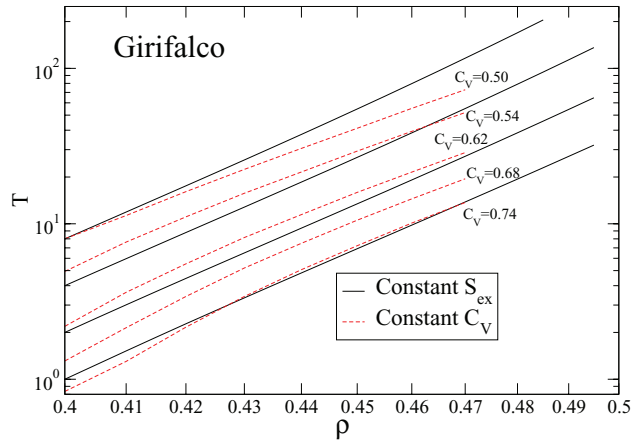

FIG. 7. Comparison of adiabats with C_V-contours for the Girifalco system. The adiabats were calculated using the definition of γ and small changes in ρ, while C_V-contours were determined from a series of simulations on different isochores and interpolating the C_V data as a function of T.

In practice, we identify C_V contours using the interpolation procedure described above, but it is potentially useful from a theoretical point of view to have a fluctuation formula for the slope of these curves. This we derive in this section.

Since the variation of C_V along an adiabat (Eq. (22)) involves the difference between two triple correlations $\langle(\Delta U)^2\Delta(W-\gamma U)\rangle$ (which vanishes for perfect correlation); it is tempting to speculate that the ratio

$$\frac{\langle(\Delta U)^2\Delta W\rangle}{\langle(\Delta U)^3\rangle}, \tag{42}$$

which equals γ for perfect correlation, gives the slope of curves of constant C_V. But it is not so simple. The total derivative of C_V with respect to $\ln\rho$ along an arbitrary slope g in the $(\ln\rho, \ln T)$ plane is

$$\left(\frac{\partial C_V}{\partial \ln\rho}\right)_{[g]} = \left(\frac{\partial C_V}{\partial \ln\rho}\right)_T + g\left(\frac{\partial C_V}{\partial \ln T}\right)_\rho. \tag{43}$$

We need to calculate the partial derivatives with respect to T and ρ. From Appendix D:

$$\left(\frac{\partial C_V}{\partial \ln T}\right)_\rho = -2\beta^2\langle(\Delta U)^2\rangle - \beta^3\frac{\partial\langle U^2\rangle}{\partial\beta} - 2\beta^3\langle U\rangle\langle(\Delta U)^2\rangle. \tag{44}$$

From Eqs. (11) and (B8) we have

$$\frac{\partial\langle U^2\rangle}{\partial\beta} = -\langle\Delta U\,\Delta(U^2)\rangle \tag{45}$$

$$= -\langle\Delta U(2\langle U\rangle\Delta U + (\Delta U)^2 - \langle(\Delta U)^2\rangle)\rangle \tag{46}$$

$$= -2\langle U\rangle\langle(\Delta U)^2\rangle - \langle(\Delta U)^3\rangle. \tag{47}$$

Inserting this into Eq. (44) gives

$$\left(\frac{\partial C_V}{\partial \ln T}\right)_\rho = -2\beta^2\langle(\Delta U)^2\rangle + \beta^3\langle(\Delta U)^3\rangle. \tag{48}$$

It might seem surprising that the third moment appears, since one expects the limit of large N that the distribution converges to a Gaussian, in accordance with the central limit theorem. A closer look at the proof of that theorem shows that when considering the summed variable (here the total potential energy), all the so-called cumulants are proportional to N, and both the second and third moments are equal to the corresponding cumulants, and therefore proportional to N. It is when one considers the average instead of the sum (potential energy per particle instead of total potential energy) that one finds the third moment and cumulant vanishing faster than the second ($1/N^2$ as opposed to $1/N$) in the limit of large N.

The density derivative of C_V,

$$\left(\frac{\partial C_V}{\partial \ln\rho}\right)_T = \beta^2\left(\frac{\partial\langle U^2\rangle}{\partial\ln\rho}\right)_T - \beta^2 2\langle U\rangle\left(\frac{\partial\langle U\rangle}{\partial\ln\rho}\right)_T, \tag{49}$$

is evaluated in Appendix D with the result

$$\left(\frac{\partial C_V}{\partial \ln\rho}\right)_T = -\beta^3\langle\Delta W(\Delta U)^2\rangle + 2\beta^2\langle\Delta U\,\Delta W\rangle. \tag{50}$$

The derivative of C_V along an arbitrary slope g is then

$$\left(\frac{dC_V}{d\ln\rho}\right)_{[g]} = C_V\left(\frac{\beta\langle(\Delta U)^3\rangle g - \beta\langle(\Delta U)^2\Delta W\rangle}{\langle(\Delta U)^2\rangle} + 2(\gamma - g)\right). \tag{51}$$

Note that with $g=\gamma$ we recover Eq. (22). When the correlation is not perfect we can set this expression to zero and solve for the slope g which gives curves of constant C_V, now calling it $\gamma_{C_V} \equiv (\partial\ln T/\partial\ln\rho)_{C_V}$:

$$\gamma_{C_V}\left(\frac{\beta\langle(\Delta U)^3\rangle}{\langle(\Delta U)^2\rangle} - 2\right) = \frac{\beta\langle(\Delta U)^2\Delta W\rangle}{\langle(\Delta U)^2\rangle} - 2\gamma \tag{52}$$

or

$$\gamma_{C_V} = \frac{\langle(\Delta U)^2\Delta W\rangle - 2T\gamma\langle(\Delta U)^2\rangle}{\langle(\Delta U)^3\rangle - 2T\langle(\Delta U)^2\rangle}. \tag{53}$$

Again we check the case of perfect correlation where we can replace ΔW by $\gamma\Delta U$ and see that we get γ as we should. We can also write this as γ plus a correction term:

$$\gamma_{C_V} = \gamma + \frac{\langle(\Delta U)^2\epsilon\rangle}{\langle(\Delta U)^3\rangle - 2T\langle(\Delta U)^2\rangle}. \tag{54}$$

Figure 8 shows the fluctuation-determined slope γ_{C_V} of a C_V contour in the $(\ln\rho, \ln T)$-plane along the $C_V = 1.0$ contour of the LJ system. We present the C_V-contour here to be able to check the validity of the exponent: The (fixed) exponent determined by a fit of the contour to a power law is also indicated for comparison. A clear trend is observed with γ_{C_V} higher than γ, and like the latter decreasing towards 4 as the density increases. There is some scatter due to the difficulty in determining third moments (compare the data for γ which are based on second moments), so this would not be a practical method for determining the contours. On the other hand, if we are interested in knowing roughly how big the difference in slope between an adiabat and a C_V-contour is, we do not need to simulate a C_V-contour–we can simu-

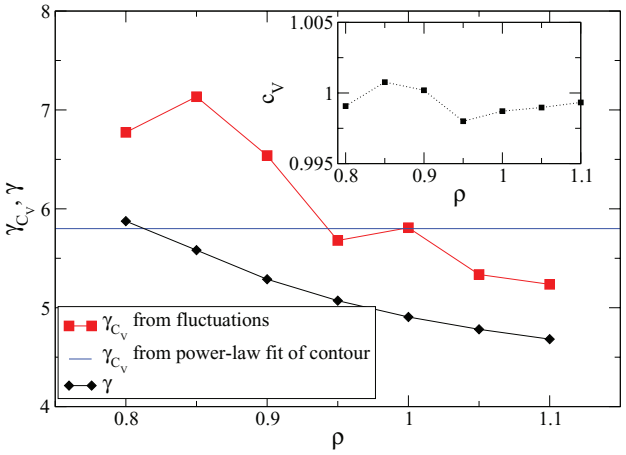

FIG. 8. Plot of $\gamma_{C_V} = (\partial\ln T/\partial\ln\rho)_{C_V}$ estimated from fluctuations, along the $C_V = 1.0$ contour for the LJ system. The contour was determined by interpolation. The horizontal line indicates the slope found by fitting the contour to a power-law form for comparison. The decrease of γ_{C_V} towards large densities is expected, just as with γ (also shown) since at high densities we expect both to converge to one third of the repulsive exponent, i.e., 4. The inset shows C_V versus ρ along the contour as a check that the contour was correctly determined.

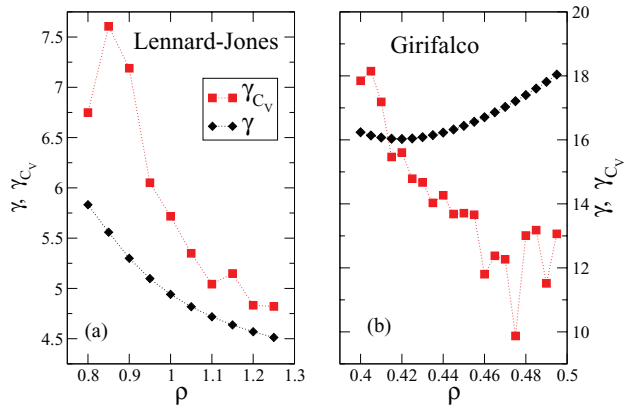

FIG. 9. Plot of $\gamma_{C_V} = (\partial \ln T/\partial \ln \rho)_{C_V}$ estimated from fluctuations, along (a) the adiabat including $\rho = 0.8$, $T = 0.8$ for the LJ system and (b) the adiabat including $\rho = 0.4$, $T = 4.0$ for the Girifalco system, as functions of ρ, compared to γ.

late a few state points, perhaps on an isochore, and estimate the γ_{C_V} from fluctuations. The scatter is not a big problem if we are not using γ_{C_V} to determine where to simulate next. Figure 9 compares γ_{C_V} with γ for both LJ and Girifalco system along an adiabat, and the trends are very clear: the C_V-contours have definitely larger slope for the LJ system, closer to 6 than 5 (they must converge to 4 at high density). For the Girifalco system the differences are quite dramatic, more so than the direct comparison of the contours in Fig. 7 (where a logarithmic temperature scale was used). It is worth noting that all the data here correspond to state points with $R > 0.985$, i.e., very strong U, W correlation, and that nothing special happens when the exponents are equal (e.g., $\rho \sim 0.42$ in Fig. 9(b)) (in any system one can define phase-space curves along which $\gamma - \gamma_{C_V} = 0$; it would be significant only if a two-dimensional region of equality existed).

V. DISCUSSION

A. Roskilde liquids are more than, and more interesting than, IPL liquids

IPL liquids are perfectly correlating and have perfect isomorphs—straight lines in the $(\ln \rho - \ln T)$ plane with slope given by one third of the IPL exponent. In this case the phase diagram is completely degenerate—the isomorphs are contours of excess entropy, C_V and all structural and dynamical properties (when expressed in reduced units). Liquids which have strong, but not perfect U, W correlation are much more interesting: we can still identify excellent isomorphs via Eq. (5), as adiabats, but these are no longer constrained to be power laws; the effective exponent can vary along an isomorph/adiabat and can exhibit non-trivial density dependence.[42] Moreover, C_V contours deviate now from the isomorphs/adiabats in a manner connected to the density dependence of γ.

It is interesting to compare the insight obtained from statistical mechanical versus thermodynamic considerations. Using statistical mechanics—the arguments leading to Eq. (38)—we have shown that $(\partial\gamma/\partial T)_\rho$ vanishes when correlation is perfect, and this occurs only for (extended) IPL systems (see Eq. (30)). We have also argued that in liquids with strong but not perfect U, W correlations the temperature derivative is relatively small, therefore as a first approximation it can be ignored, leaving the density dependence of γ as a new characteristic for a Roskilde liquid. On the other hand the purely thermodynamic arguments presented in Ref. 32 constrain only $(\partial\gamma/\partial T)_\rho$ to be zero, leaving γ free to depend on density, which allows for the richer set of behaviors just mentioned. The thermodynamic argument leads more directly (and elegantly) to the empirical truth—that in practice γ's temperature dependence is small compared to its density dependence—while the statistical mechanical arguments fill in the details of why this is the case.

B. Is isomorph theory the zeroth term in a systematic expansion?

The isomorph theory was characterized in the introduction as a "zero-order" theory, analogous to the ideal gas. For the latter there exists a systematic expansion (the virial series, with the small parameter being density times molecular volume) for obtaining the equation of state for interacting systems, or for obtaining transport properties (kinetic theory).[45,46] It is an open question whether a similar expansion exists where perfect isomorphs correspond to the zeroth term. If so, one could quantify the errors made in using the isomorph theory. A natural starting point might be thermodynamic perturbation theory using an IPL reference system, but here caution should be advised, because this would ignore that fact γ varies along an isomorph and in any case we do not have exact or near exact analytical solution for the thermodynamics and structure of the IPL system. Furthermore, traditional thermodynamic perturbation theory is primarily concerned with thermodynamics (equation of state), less so with structure, and not much at all with dynamics; isomorph theory makes predictions primarily for structure, dynamics, and some thermodynamic quantities but in general not the equation of state as such (though see Refs. 22 and 47). In particular, the use of variational perturbation theory to estimate the IPL exponent at a given state point through an optimal perturbation estimate of the free energy typically finds an exponent larger than γ.[48]

C. Status of $n^{(2)}$ and relation between different γ derivatives

The claim (38) needs to be thoroughly investigated by simulation for a wider range of systems as does the validity of Eq. (31) as an estimate of γ. While we have argued these for high temperatures and densities, their validity could turn out to depend on how strong U, W-correlation a liquid has, though it seems that $R > 0.9$ is not necessarily required, that is, they apply more generally than strong U, W correlation. One could imagine that it would be useful to derive a fluctuation formula for $(\partial\gamma/\partial\rho)_S$. We have indeed derived such a formula, see Appendix E, but it is not particularly simple, and we have not been able to use it to make a more rigorous theoretical connection with $(\partial\gamma/\partial T)_\rho$—even the sign

is far from obvious due to near cancellation of the various terms. Its usefulness in simulations is also expected to be limited since it involves fluctuations of the so-called hypervirial (the quantity used to determine the bulk modulus from fluctuations[49]) which is not typically available in a MD simulation. On the other hand, from the other results presented here, one can use the quantity $\langle(\Delta U)^2\epsilon\rangle$ or the formula for γ_{C_V} to determine the sign of $(\partial\gamma/\partial\rho)_S$ from a simulation of a single state point.

D. Adiabats versus C_V contours in non-Roskilde-simple liquids

It is interesting to consider a non-simple liquid, where there is no reason to expect that C_V-contours at all coincide with adiabats (i.e., there are not good isomorphs). We have done so for two liquids without actually determining the C_V-contours; instead we just calculated the exponent γ_{C_V} from the fluctuations. As mentioned above this is accurate enough to give an idea of the trends, in particular which way the C_V-contours are oriented with respect to the adiabats. The first example is the Dzugutov fluid.[37] Figure 10 shows γ_{C_V} and γ for this system along an adiabat. In the range shown R takes values from ~0.56 to ~0.84. As the figure shows γ_{C_V} is substantially smaller than γ. We can note also that this is consistent with the positive slope $d\gamma/d\rho$, and suggests the arguments leading to Eq. (38) do not necessarily require strong W, U correlation. The Lennard-Jones-Gaussian system[15] behaves similarly (data not shown). A very different example is the Gaussian core potential,[14] which lacks a hard core (thus particles can overlap/penetrate each other) for which data is also shown in Fig. 10. In this case there is almost no W, U correlation; $0.16 > R > 0.06$, and in fact γ_{C_V} and γ even have opposite sign (although both are close to zero). Moreover, this system clearly violates Eq. (38), since γ decreases with density on the adiabat shown, which should correspond to the case $\gamma_{C_V} > \gamma$ (as in the LJ case); this is not surprising since it does not have a hard core.

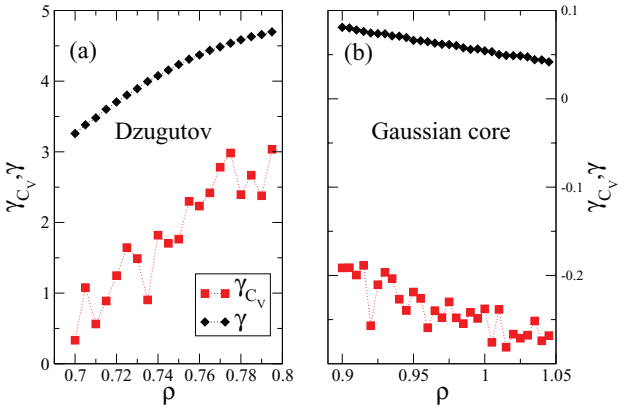

FIG. 10. Plot of $\gamma_{C_V} = (\partial \ln T/\partial \ln \rho)_{C_V}$ estimated from fluctuations, for (a) the Dzugutov system along the adiabat including $\rho = 0.70$, $T = 0.70$ and (b) the Gaussian core system along the adiabat including at $\rho = 0.90$, $T = 0.75$, as functions of ρ, compared to γ.

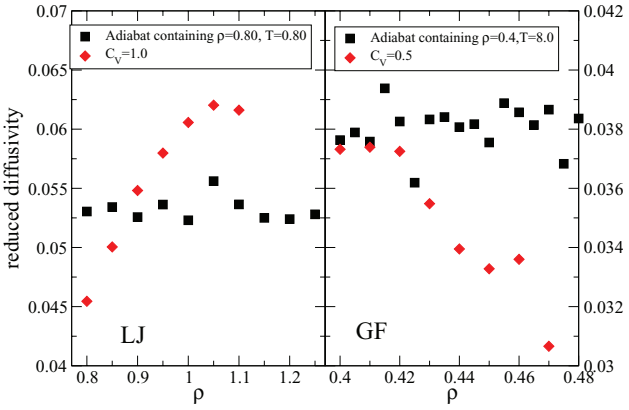

FIG. 11. Diffusivity in reduced units versus density along an adiabat and along a C_V-contour for the LJ and GF systems. It is more or less invariant on the adiabats but not on the C_V-contours.

E. Relevance of adiabats versus C_V contours

In our simulation studies of isomorphs, the procedure has always been to use Eq. (5) to generate adiabats (straightforward, since an accurate estimate of γ is readily computed from the W, U fluctuations) and then examine to what extent the other isomorph-invariant quantities are actually invariant along these curves. One could also generate C_V contours and check for invariance along them. While it is not obvious that adiabats are more fundamental, Rosenfeld proposed that transport properties are in fact governed by the excess entropy.[50] Given the not insignificant difference between adiabats and C_V-contours it is worth checking explicitly whether measures of dynamics are more invariant along one versus the other. This is done in Fig. 11 for the reduced diffusivity $\tilde{D} \equiv \left(\rho^{1/3}\sqrt{m/T}\right) D$. It is clear that by the this measure, the dynamics are more invariant along adiabats than along C_V-contours, consistent with Rosenfeld's theory. We note also that the adiabats seem to be simpler than the C_V-contours in that the exponent γ varies less than the exponent γ_{C_V}. This is true for the all the systems presented here including simple and non-simple ones. This implies γ is more practical as a liquid characteristic than γ_{C_V} and suggests that adiabats provide a more useful, and fundamental basis for describing the phase diagram than C_V-contours. In fact a (ρ, S) phase diagram would be consistent with the traditional starting point of statistical mechanics—a function $U(S, V)$ expressing the dependence of internal energy on entropy and volume (though typically the total entropy, not S, is considered).

VI. CONCLUSION

We have derived several exact results relating to Roskilde-simple liquids (previously termed strongly correlating liquids) in the form of fluctuation formulas for various thermodynamic derivatives. These include the derivative (with respect to $\ln \rho$) of an arbitrary NVT averaged dynamical variable along a configurational adiabat, Eq. (17), the derivative of C_V along an adiabat, Eq. (22), the temperature derivative of γ itself on an isochore, Eq. (27), and the slope of contours of C_V in the $(\ln \rho, \ln T)$ plane, Eq. (53). In addition to

the exact formulas we have argued that when $d\gamma/d\rho$ is negative (positive) one expects that $(\partial C_V/\partial\rho)_S$ is positive (negative) and that the slopes of C_V-contours are greater (less) than those of adiabats. This we have tested with two model Roskilde-simple liquids, the Lennard-Jones fluid with $d\gamma/d\rho < 0$ and the Girifalco potential which has $d\gamma/d\rho < 0$ at low density but switches to $d\gamma/d\rho > 0$ at high density. From this argument emerged a claim, Eq. (38) equating the sign of the temperature derivative of γ to the density derivative along an adiabat for a wide class of liquids (wider than Roskilde-simple liquids). Finally, we note that the data presented here provide support for the use of the $n^{(2)}$ exponent, determined purely by the pair potential, as a quick and convenient way to estimate γ and its density dependence.

ACKNOWLEDGMENTS

The centre for viscous liquid dynamics "Glass and Time" is sponsored by the Danish National Research Foundation's Grant No. DNRF61.

APPENDIX A: DERIVATION OF EQ. (13)

As in Appendix A of Ref. 18, we use a discrete-state notation for convenience, such that A_i is the value of observable A in microstate i and the (configurational) partition function is $Z = \sum_i \exp(-\beta U_i)$. We have

$$\left(\frac{\partial\langle A\rangle}{\partial\ln\rho}\right)_T = \frac{1}{Z}\frac{\partial\sum_i A_i\exp(-\beta U_i)}{\partial\ln\rho} - \frac{1}{Z^2}\sum_i A_i\exp(-\beta U_i)\frac{\partial\sum_j\exp(-\beta U_j)}{\partial\ln\rho} \tag{A1}$$

$$= \frac{1}{Z}\sum_i\left(\frac{\partial A_i}{\partial\ln\rho}\exp(-\beta U_i) + A_i\exp(-\beta U_i)(-\beta)\frac{\partial U_i}{\partial\ln\rho}\right) - \frac{\sum_i A_i\exp(-\beta U_i)}{Z^2}\sum_j\exp(-\beta U_j)(-\beta)\frac{\partial U_i}{\partial\ln\rho} \tag{A2}$$

$$= \left\langle\frac{\partial A}{\partial\ln\rho}\right\rangle - \beta\left(\langle AW\rangle - \langle A\rangle\langle W\rangle\right) \tag{A3}$$

$$= \left\langle\frac{\partial A}{\partial\ln\rho}\right\rangle - \beta\langle\Delta A\Delta W\rangle\,. \tag{A4}$$

In the second last step the definition of the virial for a micro-configuration, $W_i \equiv (\partial U_i/\partial\ln\rho)$ was used; the density derivative is understood to mean that the reduced coordinates are held fixed while the volume is changed.

APPENDIX B: DERIVATION OF EQ. (22)

Here we give the details of the derivation of the expression for the derivative of C_V at constant S. Writing the variance of U as $\langle(\Delta U)^2\rangle = \langle U^2\rangle - \langle U\rangle^2$ allows us to use Eq. (17) to take the derivative of $\langle U^2\rangle$ and Eq. (18) to differentiate $\langle U\rangle$:

$$\left(\frac{\partial\left\langle(\Delta U)^2\right\rangle}{\partial\ln\rho}\right)_S = \left\langle\frac{\partial U^2}{\partial\ln\rho}\right\rangle - \beta\langle\Delta(U^2)\Delta(W-\gamma U)\rangle - 2\langle U\rangle\langle W\rangle \tag{B1}$$

$$= \langle 2UW\rangle - \beta\left\langle\Delta(U^2)\Delta(W-\gamma U)\right\rangle - 2\langle U\rangle\langle W\rangle \tag{B2}$$

$$= 2\langle\Delta U\Delta W\rangle - \beta\langle\Delta(U^2)\Delta(W-\gamma U)\rangle \tag{B3}$$

$$= 2\gamma\langle(\Delta U)^2\rangle - \beta\langle\Delta(U^2)\Delta(W-\gamma U)\rangle, \tag{B4}$$

where we have used Eq. (3) to write the covariance $\langle\Delta U\Delta W\rangle$ in terms of the variance of U. Inserting this result into Eq. (21) gives the relatively simple formula

$$\left(\frac{\partial C_V}{\partial\ln\rho}\right)_S = -\beta^3\langle\Delta(U^2)\Delta(W-\gamma U)\rangle = -\beta^3\langle\Delta(U^2)\epsilon\rangle. \tag{B5}$$

We make one more change by writing $U = \langle U\rangle + \Delta U$, so that

$$\Delta(U^2) = U^2 - \langle U^2\rangle \tag{B6}$$

$$= \langle U\rangle^2 + 2\langle U\rangle\Delta U + (\Delta U)^2 - (\langle U\rangle^2 + \langle(\Delta U)^2\rangle) \tag{B7}$$

$$= 2\langle U\rangle\Delta U + (\Delta U)^2 - \langle(\Delta U)^2\rangle. \tag{B8}$$

When this is correlated with $\epsilon = \Delta W - \gamma\Delta U$, the first term vanishes because of Eq. (10) and the last term vanishes because $\langle\epsilon\rangle = 0$. Thus $\langle\Delta(U^2)\epsilon\rangle = \langle(\Delta U)^2\epsilon\rangle$ and we arrive at Eq. (22).

APPENDIX C: GENERATING CONFIGURATIONAL ADIABATS

Equation (5) indicates a general procedure for generating adiabats: (1) evaluate γ from the fluctuations at the current state point; (2) choose a small change in density, say of order 1% or less; (3) use Eq. (5) to determine the corresponding change in temperature:

$$\rho_{n+1} = \rho_n + \delta\rho, \tag{C1}$$

$$T_{n+1} = T_n\,(\rho_{n+1}/\rho_n)^{\gamma_n}\,. \tag{C2}$$

We have used this method for the Girifalco system with $\delta\rho = 0.005$ for values of ρ between 0.4 and 0.5. For generalized Lennard-Jones systems there is now an analytic expression for the ρ-dependence of γ which allows large changes in ρ, the so-called "long jump method":[32,33]

$$\rho_{n+1} = \rho_n + \delta\rho, \tag{C3}$$

$$T_{n+1} = T_n h(\alpha_n, \rho_{n+1})/h(\alpha_n, \rho_n), \tag{C4}$$

where the energy/temperature scaling function $h(\alpha, \rho)$ is defined by (see Refs. 32 and 33; the normalization is such that $h(\alpha, 1) = 1$).

$$h(\alpha, \rho) = \alpha\rho^4 + (1-\alpha)\rho^2. \tag{C5}$$

Here α is a parameter which according to the theory of isomorphs—i.e., assuming perfect isomorphs for LJ systems—is a constant. More generally one may expect that it is fixed for a given isomorph, but can vary weakly among isomorphs, analogous to $\Lambda(S)$ in Eq. (31). In fact, since $\gamma = d\ln(h)/d\ln(\rho)$,[32] there is a close connection between $h(\rho)$ and $n^{(2)}$; by identifying Eq. (31) with the logarithmic derivative of $h(\rho)$ we find that the latter can be expressed generally in terms of the curvature of the pair potential:

$$h(\rho) = \rho^{-2/3} v''(\Lambda(S)\rho^{-1/3}), \tag{C6}$$

making it clear how to include dependence on S in $h(\rho)$. This connection will be discussed in more detail elsewhere.[42] At a given density α can be evaluated via

$$\alpha = (\gamma - 2)/(4\rho^2 - 2 - \gamma\rho^2 + \gamma) \tag{C7}$$

(at $\rho = 1$ this becomes simply $\gamma/2 - 1$).

Since the theory is not exact, and α determined this way will also vary weakly along the isomorph, in order to get the best determination of the adiabats we re-evaluate α at each state point. It therefore also has an index n. We observe a systematic variation in α of at most 0.5% for a given adiabat, and a few percent variation between adiabats. We have used the long-jump formula for the LJ system with $\delta\rho = 0.05$ for values of ρ between 0.8 and 1.4. We noticed more noise in the data for the Girifalco system, but have not checked whether this is due to not having a long-jump formula or to differences in effective sampling rate (because of different relaxation times) giving different statistical errors.

APPENDIX D: DERIVATION OF C_V EXPONENT

The temperature derivative of C_V, Eq. (44), is obtained as follows:

$$\left(\frac{\partial C_V}{\partial \ln T}\right)_\rho = -\frac{\partial}{\partial \ln \beta}(\beta^2\langle(\Delta U)^2\rangle) = -\beta\frac{\partial}{\partial\beta}(\beta^2\langle(\Delta U)^2\rangle) \tag{D1}$$

$$= -2\beta^2\langle(\Delta U)^2\rangle - \beta^3\frac{\partial}{\partial\beta}(\langle U^2\rangle - \langle U\rangle^2) \tag{D2}$$

$$= -2\beta^2\langle(\Delta U)^2\rangle - \beta^3\frac{\partial\langle U^2\rangle}{\partial\beta} + 2\beta^2\langle U\rangle\beta\frac{\partial\langle U\rangle}{\partial\beta} \tag{D3}$$

$$= -2\beta^2\langle(\Delta U)^2\rangle - \beta^3\frac{\partial\langle U^2\rangle}{\partial\beta} - 2\beta^2\langle U\rangle T C_V \tag{D4}$$

$$= -2\beta^2\langle(\Delta U)^2\rangle + \beta^3\langle(\Delta(U^2)\Delta U\rangle - 2\beta^3\langle U\rangle\langle(\Delta U)^2\rangle. \tag{D5}$$

In the last line Eq. (11) was used. We can simplify by using Eq. (B8):

$$\left(\frac{\partial C_V}{\partial \ln T}\right)_\rho = -2\beta^2\langle(\Delta U)^2\rangle + \beta^3(2\langle U\rangle\langle(\Delta U)^2\rangle + \langle(\Delta U)^3\rangle) - 2\beta^3\langle U\rangle\langle(\Delta U)^2\rangle \tag{D6}$$

$$= -2\beta^2\langle(\Delta U)^2\rangle + \beta^3\langle(\Delta U)^3\rangle. \tag{D7}$$

For the density derivative of C_V, we have likewise,

$$\left(\frac{\partial C_V}{\partial \ln \rho}\right)_T = \beta^2\left(\frac{\partial\langle U^2\rangle}{\partial \ln \rho}\right)_T - \beta^2 2\langle U\rangle\left(\frac{\partial\langle U\rangle}{\partial \ln \rho}\right)_T. \tag{D8}$$

Starting with the second term, using Eq. (13),

$$\left(\frac{\partial\langle U\rangle}{\partial \ln \rho}\right)_T = -\beta\langle\Delta W\Delta U\rangle + \langle W\rangle \tag{D9}$$

while the first gives, also using Eqs. (13) and (B8),

$$\left(\frac{\partial\langle U^2\rangle}{\partial \ln \rho}\right)_T = -\beta\langle\Delta W\Delta(U^2)\rangle + \langle 2UW\rangle \tag{D10}$$

$$= -2\beta\langle U\rangle\langle\Delta W\Delta U\rangle - \beta\langle\Delta W(\Delta U)^2\rangle + 2\langle UW\rangle. \tag{D11}$$

Combining the two terms then gives

$$\left(\frac{\partial C_V}{\partial \ln \rho}\right)_T = -\beta^3 2\langle U\rangle\langle\Delta U\Delta W\rangle - \beta^3\langle\Delta W(\Delta U)^2\rangle + 2\beta^2\langle UW\rangle + 2\langle U\rangle\beta^3\langle\Delta W\Delta U\rangle - 2\langle U\rangle\beta^2\langle W\rangle \tag{D12}$$

$$= -\beta^3\langle\Delta W(\Delta U)^2\rangle + 2\beta^2\langle\Delta U\Delta W\rangle \tag{D13}$$

which is Eq. (50). Now we can assemble the derivative of C_V along an arbitrary slope g (Eq. (43)),

$$\left(\frac{dC_V}{d\ln\rho}\right)_{[g]} = -\beta^3\langle\Delta W(\Delta U)^2\rangle + 2\beta^2\langle\Delta U\Delta W\rangle + g(-2\beta^2\langle(\Delta U)^2\rangle + \beta^3\langle(\Delta U)^3\rangle) \tag{D14}$$

$$= \beta^2\langle(\Delta U)^2\rangle(-\beta\langle\Delta W(\Delta U)^2\rangle/\langle(\Delta U)^2\rangle + 2\gamma + g(-2 + \beta\langle(\Delta U)^3\rangle/\langle(\Delta U)^2\rangle)) \tag{D15}$$

which can be rewritten as Eq. (51).

APPENDIX E: FLUCTUATION FORMULA FOR THE DERIVATIVE OF γ

We include here, omitting the derivation, the fluctuation formula for the derivative of γ with respect to $\ln\rho$ at constant

S. The quantity $X \equiv dW/d\ln\rho$ is the hypervirial, which appears in fluctuation expressions for the bulk modulus.[49]

$$\left(\frac{\partial\gamma}{\partial\ln\rho}\right)_S = \frac{1}{\langle(\Delta U)^2\rangle}(\langle(\Delta W)^2\rangle + \langle\Delta U\Delta X\rangle - 2\gamma^2\langle(\Delta U)^2\rangle - \beta\langle\Delta U\epsilon^2\rangle). \quad \text{(E1)}$$

For IPL systems (and perfect correlating systems in general) we have $\Delta X = \gamma\Delta W = \gamma^2\Delta U$ and $\epsilon \equiv 0$, so that the derivative is zero.

[1] I. Z. Fisher, *Statistical Theory of Liquids* (University of Chicago, Chicago, 1964).
[2] S. A. Rice and P. Gray, *The Statistical Mechanics of Simple Liquids* (Interscience, New York, 1965).
[3] H. N. V. Temperley, J. S. Rowlinson, and G. S. Rushbrooke, *Physics of Simple Liquids* (Wiley, 1968).
[4] N. K. Ailawadi, Phys. Rep. **57**, 241 (1980).
[5] J. S. Rowlinson and B. Widom, *Molecular Theory of Capillarity* (Clarendon, Oxford, 1982).
[6] C. G. Gray and K. E. Gubbins, *Theory of Molecular Fluids* (Oxford University Press, 1984).
[7] D. Chandler, *Introduction to Modern Statistical Mechanics* (Oxford University Press, 1987).
[8] J. L. Barrat and J. P. Hansen, *Basic Concepts for Simple and Complex Liquids* (Cambridge University Press, 2003).
[9] P. G. Debenedetti, AIChE J. **51**, 2391 (2005).
[10] J. P. Hansen and I. R. McDonald, *Theory of Simple Liquids*, 3rd ed. (Academic Press, New York, 1986).
[11] J. F. Douglas, J. Dudowicz, and K. F. Freed, J. Chem. Phys. **127**, 224901 (2007).
[12] B. Kirchner, Phys. Rep. **440**, 1 (2007).
[13] B. Bagchi and C. Chakravarty, J. Chem. Sci. **122**, 459 (2010).
[14] F. H. Stillinger, J. Chem. Phys. **65**, 3968 (1976).
[15] M. Engel and H.-R. Trebin, Phys. Rev. Lett. **98**, 225505 (2007).
[16] V. Van Hoang and T. Odagaki, Physica B **403**, 3910 (2008).
[17] T. S. Ingebrigtsen, T. B. Schrøder, and J. C. Dyre, Phys. Rev. X **2**, 011011 (2012).
[18] N. P. Bailey, U. R. Pedersen, N. Gnan, T. B. Schrøder, and J. C. Dyre, J. Chem. Phys. **129**, 184507 (2008).
[19] N. P. Bailey, U. R. Pedersen, N. Gnan, T. B. Schrøder, and J. C. Dyre, J. Chem. Phys. **129**, 184508 (2008).
[20] T. B. Schrøder, N. P. Bailey, U. R. Pedersen, N. Gnan, and J. C. Dyre, J. Chem. Phys. **131**, 234503 (2009).
[21] N. Gnan, T. B. Schrøder, U. R. Pedersen, N. P. Bailey, and J. C. Dyre, J. Chem. Phys. **131**, 234504 (2009).
[22] T. B. Schrøder, N. Gnan, U. R. Pedersen, N. P. Bailey, and J. C. Dyre, J. Chem. Phys. **134**, 164505 (2011).
[23] J. K. Johnson, J. A. Zollweg, and K. E. Gubbins, Mol. Phys. **78**, 591 (1993).
[24] E. A. Mastny and J. J. de Pablo, J. Chem. Phys. **127**, 104504 (2007).
[25] V. V. Brazhkin, Y. D. Fomin, A. G. Lyapin, V. N. Ryzhov, and K. Trachenko, JETP Lett. **95**, 164 (2012).
[26] V. V. Brazhkin, Y. D. Fomin, A. G. Lyapin, V. N. Ryzhov, and K. Trachenko, Phys. Rev. E **85**, 031203 (2012).
[27] V. V. Brazhkin, Y. D. Fomin, A. G. Lyapin, V. N. Ryzhov, E. N. Tsiok, and K. Trachenko, Phys. Rev. Lett. **111**, 145901 (2013).
[28] U. R. Pedersen, N. Gnan, N. P. Bailey, T. B. Schrøder, and J. C. Dyre, J. Non-Cryst. Solids **357**, 320 (2011).
[29] A. A. Veldhorst, L. Bøhling, J. C. Dyre, and T. B. Schrøder, Eur. Phys. J. B **85**, 21 (2012).
[30] T. S. Ingebrigtsen, T. B. Schrøder, and J. C. Dyre, J. Phys. Chem. B **116**, 1018 (2012).
[31] N. Gnan, C. Maggi, T. B. Schrøder, and J. C. Dyre, Phys. Rev. Lett. **104**, 125902 (2010).
[32] T. S. Ingebrigtsen, L. Bøhling, T. B. Schrøder, and J. C. Dyre, J. Chem. Phys. **136**, 061102 (2012).
[33] L. Bøhling, T. S. Ingebrigtsen, A. Grzybowski, M. Paluch, J. C. Dyre, and T. B. Schrøder, New J. Phys. **14**, 113035 (2012).
[34] D. Gundermann, U. R. Pedersen, T. Hecksher, N. P. Bailey, B. Jakobsen, T. Christensen, N. B. Olsen, T. B. Schrøder, D. Fragiadakis, R. Casalini *et al.*, Nat. Phys. **7**, 816 (2011).
[35] U. R. Pedersen, N. P. Bailey, T. B. Schrøder, and J. C. Dyre, Phys. Rev. Lett. **100**, 015701 (2008).
[36] A. Malins, J. Eggers, and C. P. Royall, "Investigating isomorphs with the topological cluster classification," preprint arXiv:1307.5516 (2013).
[37] M. Dzugutov, Phys. Rev. A **46**, R2984 (1992).
[38] L. A. Girifalco, J. Phys. Chem. **96**, 858 (1992).
[39] See http://rumd.org for the RUMD source code.
[40] H. Robbins and J. Van Ryzin, *Introduction to Statistics* (Science Research Associates, 1975).
[41] To "correlate with" means to multiply by and take an ensemble average.
[42] L. Bøhling, N. B. Bailey, T. B. Schrøder, and J. C. Dyre, "Estimating the density-scaling exponent of a liquid from its pair potential" (unpublished).
[43] Our method of determining Λ fails when $n^{(2)}$ is constant, but the value of r where one should evaluate $n^{(2)}$ is in principle well-defined.
[44] Y. Rosenfeld and P. Tarazona, Mol. Phys. **95**, 141 (1998).
[45] H. Smith and H. H. Jensen, *Transport Phenomena* (Oxford University Press, USA, 1989).
[46] S. G. Brush, *Kinetic Theory* (Pergamon Press, 1972), Vol. 3.
[47] J. C. Dyre, Phys. Rev. E **88**, 042139 (2013).
[48] N. P. Bailey, T. B. Schrøder, and J. C. Dyre, "Non-uniqueness of effective inverse power-law exponent for Lennard-Jones potential from variational perturbation theory" (unpublished).
[49] M. P. Allen and D. J. Tildesley, *Computer Simulation of Liquids* (Oxford University Press, 1987).
[50] Y. Rosenfeld, J. Phys.: Condens. Matter **11**, 5415 (1999).

arXiv:1307.5237v3 [cond-mat.soft] 28 Mar 2014

The isomorph theory explains the dynamical scaling properties of flexible Lennard-Jones chains

Arno A. Veldhorst, Jeppe C. Dyre, Thomas B. Schrøder[a]
DNRF Center "Glass and Time", IMFUFA, Dept. of Sciences, Roskilde University, P.O. Box 260, DK-4000 Roskilde, Denmark
(Dated: March 31, 2014)

The isomorph theory provides an explanation for the so-called power law density scaling which has been observed in many molecular and polymeric glass formers, both experimentally and in simulations. Power law density scaling (relaxation times and transport coefficients being functions of ρ^γ/T, where ρ is density, T is temperature, and γ is a material specific scaling exponent) is an approximation to a more general scaling predicted by the isomorph theory. Furthermore, the isomorph theory provides an explanation for Rosenfeld scaling (relaxation times and transport coefficients being functions of excess entropy) which has been observed in simulations of both molecular and polymeric systems. Doing molecular dynamics simulations of flexible Lennard-Jones chains (LJC), we provide the first detailed test of the isomorph theory applied to flexible chain molecules. We confirm the existence of "isomorphs", which are curves in the phase diagram along which the dynamics is invariant in the appropriate reduced units. This holds not only for the relaxation times but also for the full time dependence of the dynamics, including chain specific dynamics such as the end-to-end vector autocorrelation function, and the relaxation of the Rouse modes. As predicted by the isomorph theory, jumps between different state points on the same isomorph happen instantaneously without any slow relaxation. Since the LJC is a simple coarse-grained model for alkanes and polymers, our results provide a possible explanation for why power-law density scaling is observed experimentally in alkanes and many polymeric systems. The theory provides an independent method of determining the scaling exponent, which is usually treated as a empirical scaling parameter.

I. INTRODUCTION

When a liquid or polymer melt is (super)cooled towards the glass transition, its viscosity and relaxation time increase with many orders of magnitude over a relatively small temperature range. More generally, the dynamics of a viscous liquid depends on two variables, density ρ and temperature T (or pressure and temperature). Understanding what exactly controls the viscous slowing down upon cooling and/or compression remains one of the main challenges related to the glass transition[1–3].

An indication that a single, underlying quantity determines the viscous slowing down of supercooled liquids was published in 1998 by Tölle et al.[4,5]. They showed that the dynamics of *ortho*-terphenyl, measured at different densities and temperatures, collapses on a single curve when plotted against a function of density over temperature $h(\rho)/T$. More specifically, these neutron scattering data were found to collapse for $h(\rho) = \rho^4$. Later, a similar scaling was found to work for other organic glass formers, including polymers, showing that the relaxation time is a function of $h(\rho)/T$[6–8]. There was some debate over the functional form of $h(\rho)$ and whether it could be uniquely determined given the limited density changes experimentally available[9–14]. In a famous review Roland et al.[15] demonstrated that scaling with $h(\rho) = \rho^\gamma$ with a material specific scaling exponent γ works well for a large group of organic glass formers, including polymers. We refer to this scaling as power-law density scaling. To date, many more molecular liquids have been shown to obey power-law density scaling to a good approximation, including polymers, but also ionic liquids[16–20] and liquid crystals[21–26].

The recently developed isomorph theory[27] explains and generalizes power-law density scaling. The isomorph theory states that a group of simple liquids exists that have curves (isomorphs) in their phase diagrams along which structure and dynamics are invariant in the appropriate units. The isomorphs are identified by $h(\rho)/T$ being constant on an isomorph, where $h(\rho)$ is a material specific function. Consequently relaxation times and transport coefficients are predicted[28] to be functions of $h(\rho)/T$. For sufficiently small density changes $h(\rho)$ may be approximated by a power law: $h(\rho) \propto \rho^\gamma$, which is equivalent to power law density scaling. The theory provides an independent method of determining the scaling exponent, γ. Other predictions of the theory are that certain thermodynamical quantities including the excess entropy and isochoric specific heat are invariant on the isomorph. Since both excess entropy and the relaxation times are predicted to be constant on an isomorph, the isomorph theory provides an explanation for Rosenfeld's excess entropy scaling[27,29,30], according to which a liquid's relaxation times and transport coefficients are functions of excess entropy only.

The isomorph theory has so far only been tested in detail for atomic systems[27,31], and for some small rigid molecules[32]. However, many organic glass formers are large molecules or have bulky side groups, because this makes it harder for the liquid to crystallize. These larger

[a] tbs@ruc.dk

molecules, and polymers in particular, inherently have intra molecular degrees of freedom that influence the liquid structure and dynamics. Here, we aim to bridge the gap between the simple models already shown to obey they isomorph theory, and larger flexible glass formers shown experimentally to obey power law density scaling.

Since both alkanes[18,33,34] and polymers[15,35] have been shown to obey power-law density scaling, we simulated a general viscous model liquid of linear, flexible Lennard-Jones chains (LJC). The model has been used extensively for viscous polymer melts close to the glass transition[36–40]. We show that the LJC liquid has isomorphs in its phase diagram, and we study the effect of the intra molecular degrees of freedom on the applicability of the isomorph theory.

In section II we give a short overview over the relevant aspects of the isomorph theory. We explain the LJC model in section III and present the details of our simulation method. We start our discussion of the results by showing how the isomorphs were obtained for the LJC model (section IV A) . We then verify that the dynamics (section IV B) and some aspects of the structure IV C are invariant on the isomorph. As predicted by the isomorph theory, we show in section IV D that isomorph scaling can be used to collapse the dynamics along different isochores onto a single master curve.

II. ISOMORPH THEORY

The development of the isomorph theory was preceded by the discovery of a class of liquids that have strong correlations in the equilibrium fluctuations of the configurational parts of their energy and pressure. The correlations can be quantified by the standard correlation coefficient[41,42]:

$$R = \frac{\langle \Delta W \Delta U \rangle}{\sqrt{\langle (\Delta W)^2 \rangle \langle (\Delta U)^2 \rangle}}, \tag{1}$$

where U is the potential energy, W is the virial, Δ denotes deviation from thermal average, and brackets $\langle ... \rangle$ denote average in the canonical ensemble. For liquids where the pair potential is an inverse power law (IPL), $v(r) \propto r^{-n}$, the correlation is perfect ($R = 1$), but a large group of liquids have a correlation coefficient close to one, indicating strong correlation. Liquids with a correlation larger than 0.9 were referred to as "strongly correlating", but since this term was often confused with strongly correlated quantum systems, we now refer to this class of liquids as "Roskilde-simple" liquids.

The "slope" γ of the fluctuations can be defined by

$$\gamma = \frac{\langle \Delta W \Delta U \rangle}{\langle (\Delta U)^2 \rangle}. \tag{2}$$

This definition of the slope is equal to the logarithmic density derivative of the temperature on a curve of constant excess entropy $S_{ex} \equiv S - S_{ideal}$, where S_{ideal} is the entropy of an ideal gas at the same temperature and density[27]

$$\gamma = \left(\frac{\partial \ln T}{\partial \ln \rho} \right)_{S_{ex}}. \tag{3}$$

This means that one can use the "slope" γ calculated from the fluctuations to trace out a curve of constant excess entropy in the phase diagram. One can calculate γ at a certain state point (1) with temperature $T^{(1)}$ and density $\rho^{(1)}$ using Eq. (2). If one then increments density by a sufficiently small amount to density $\rho^{(2)}$, Eq. (3) gives the temperature of state point (2) that has the same excess entropy. This can be done many times in an iterative fashion to obtain a set of state points that have the same excess entropy. We use this method to trace out curves in the phase diagram with invariant excess entropy, and check if the predicted isomorphic invariance of other properties is fulfilled. It should be noted that the invariance is only predicted to hold when quantities are considered in the appropriate reduced units, e.g., using $\rho^{-1/3}$ as the unit of length, and $k_B T$ as the unit of energy[27,43].

The isomorph theory predicts "isomorph scaling", i.e., that the dynamics is a function of $h(\rho)/T$, where $h(\rho)$ depends on the system[28,44]. For atomic systems interacting via a pair potential that is the sum of IPL potentials $v(r) = \sum_n v_n r^{-n}$, $h(\rho)$ is given by $h(\rho) = \sum_n C_n \rho^{n/3}$, where the constants C_n are the fractional contributions of each term to the heat capacity[28,44]. This includes for example the celebrated Lennard-Jones potential[44,45]. For molecular liquids $h(\rho)$ is not known analytically.

III. MODEL AND SIMULATION METHOD

We performed Molecular Dynamics simulations of flexible Lennard-Jones chains (LJCs) consisting of 10 bonded segments. Segments in different molecules and non-bonded segments within a molecule interact via the standard LJ potential, cutting and shifting the potential at 2.5σ. We simulated 200 chains in a cubic bounding box with periodic boundary conditions, in the NVT ensemble using a Nosé-Hoover thermostat. For the time step we used $\Delta t = 0.0025$, and the time constant of the thermostat was 0.2. The simulation was performed with our RUMD[46] software utilizing state of the art GPU computing.

The model has been derived from a model by Kremer and Grest[47], who did not include the attractive part of the LJ potential. Later, the attractive part has usually been included. Short LJ chains of around ten segments have been used extensively to simulate glassy polymer melts[48–51], even though real polymers easily consist of thousands of monomers. The reason for this is threefold. Firstly, the LJC is a coarse-grained model, meaning that a single Lennard-Jones particle may correspond to several monomers. Secondly, increasing the chain length in general increases the total system size, which in turn

increases the simulation time. Most importantly, it is often the equilibrium (viscous) liquid that is of interest. Both increasing the chain length and approaching the glass transition increase the equilibration time, meaning that there is always a trade-off between chain length and viscosity[52,53].

Usually, the neighboring segments in the chain are bonded by a FENE potential, although harmonic springs[38–40] and rigid bonds[34,54,55] have also been used. Here, the bond length $l_b = \sigma = 1$ was kept constant using the Time Symmetrical Central Difference algorithm[56,57]. Like other constraint algorithms, these bonds contribute to the virial[58]: $W_{total} = W_{LJ} + W_{constraint}$, but not to the energy.

With our purpose in mind, the model is of special interest since it has already been shown to obey power-law density scaling, using γ as an empirical scaling parameter.[34]. Moreover, the LJC liquid has been shown to obey Rosenfeld's excess entropy scaling[34,54,55,59].

IV. RESULTS AND DISCUSSION

A. Generating isomorphs

To generate an isomorph, a NVT simulation was performed at a state point (ρ_0, T_0), and the scaling exponent γ was calculated using Eq. (2). We then change density with 0.02 and use equation Eq. (3) to find the temperature at the new state point for which the excess entropy S_{ex} is the same. Applying this procedure iteratively we obtain a curve with constant S_{ex}. If the model conforms to the isomorph theory, this curve will be an isomorph, i.e., have invariant dynamics and structure in reduced units. Five isomorphs were generated using this procedure with $\rho_0 = 1.0$ and $T_0 = \{0.5, 0.6, 0.65, 0.7, 0.8\}$.

In Fig. 1(a), the correlation coefficient R is plotted as a function of density for the five isomorphs. For the densities we have simulated, the correlation coefficient varies between 0.81 and 0.87, which is lower then the (somewhat arbitrary) 0.9 limit for simple liquids. However, we show with this paper, that the LJC model also shows clear isomorphs in its phase diagram, and that within the density range investigated, simple power-law density scaling does not suffice.

In Fig. 1(b) we plot the values of γ calculated from Eq. (2). The isomorph theory predicts γ to depend on density but not temperature[27,45]. This is seen to be fulfilled to a good approximation; γ is seen to change much more by increasing density by 25% than by increasing temperature by 60%. The density dependence of γ means that we can only use Eq. (3) for small density changes, and indicates that simple power-law density scaling is an approximation that only works for small density changes.

The γ values found for the LJC model (6.1–7.9) are higher than for a single component LJ liquid (5.3–6.7)[42]. This increase in γ is due to the fixed constraints, which can be seen as a very steep repulsion between bonded segments. On the other hand, the high γ values is in contrast to the values found from power-law density scaling,which are generally lower for polymers than for small molecular liquids[35]. Tsolou et al[61] found $\gamma = 2.8$ from power-law density scaling of simulation data of a united atom model of *cis*-1,4-polybutadiene. A possible explanation for this low value of γ has been given by Xu[62] who showed using the generalized entropy theory that polymer rigidity significantly decreases the density scaling exponent γ. Here, polymer rigidity was quantified by the bending energy of the angle between two bonds.

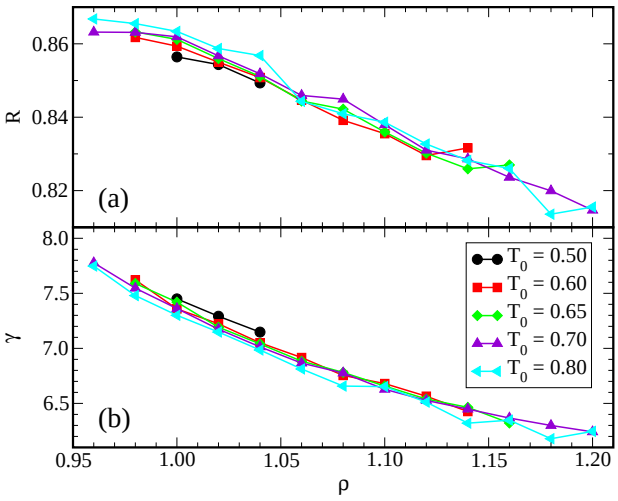

FIG. 1. (a) The correlation coefficient R, calculated from the instantaneous values of the virial W and the potential energy U using Eq. (1). Each data set corresponds to an isomorph, obtained as described in the text. The correlation coefficient is high, albeit lower than for a standard single component Lennard-Jones liquid[60]. (b) The isomorphic scaling exponent γ as defined by Eq. (2). The values found are significantly higher than for the single component Lennard-Jones liquids[60], and show a clear density dependence. The logarithmic derivatives of γ on the isochore and isotherm confirm that γ is much more dependent on the density: $(\frac{\partial \ln \gamma}{\partial \ln T})_{\rho=1} \approx 0.05$ and $(\frac{\partial \ln \gamma}{\partial \ln \rho})_{T=0.7} \approx 0.89$, as predicted by the isomorph theory.

B. Dynamics on an isomorph

In the following, we test a number of isomorph predictions focusing on the $(\rho_0, T_0) = (1.0, 0.7)$ isomorph, before returning to the question of the overall scaling properties of the model. The isomorph theory predicts dynamics and structure to be invariant on an isomorph. This invariance applies to data in reduced units, which means that distance and time are scaled using $\tilde{r} = \rho^{1/3} r$ and $\tilde{t} = \rho^{1/3}(T/m)^{1/2} t$, where m is the mass of a segment. The dynamics are of particular interest here, because the dependence on state point becomes large upon cooling and/or compression. In Fig. 2(a), different dynamical quantities are plotted. The self part of the segmental

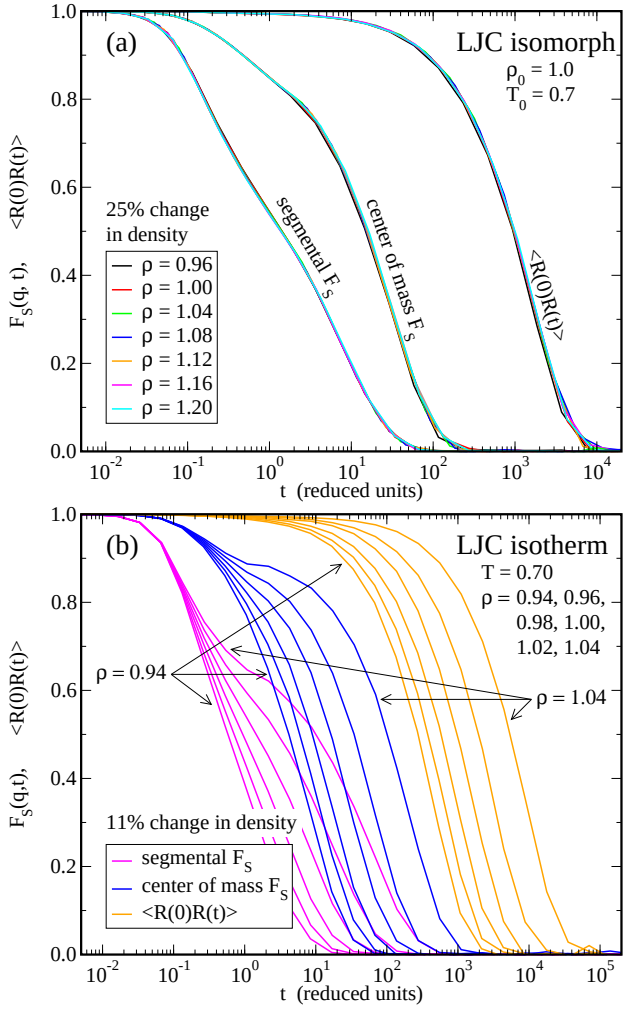

FIG. 2. The segmental and center of mass intermediate scattering function $F_S(q,\tilde{t})$, as well as the normalized orientational autocorrelation function of the end-to-end vector $\langle \mathbf{R}(t)\mathbf{R}(0)\rangle$. The position of the peak of the (segmental) static structure factor was taken as the value for q. (a) The data for 7 isomorphic state points collapse on a single master curve when plotted in reduced units, and this is the case for all three relaxation functions. (b) For isothermal state points, the curves do not collapse but are spread over a larger dynamical range.

and the center of mass intermediate scattering function $F_S(q,t)$, as well as the normalized orientational autocorrelation of the end-to-end vector $\langle \mathbf{R}(0)\mathbf{R}(t)\rangle$ are plotted as a function of reduced time. The values of q were kept constant in reduced units: $q = \tilde{q}\rho^{1/3}$. All these measures of the dynamics collapse well for the isomorphic state points compared to an isothermal density change; Increasing the density by 11% while keeping temperature constant significantly changes the dynamics, whereas increasing the density 25% while following the isomorph keeps the dynamics invariant to a really good approximation.

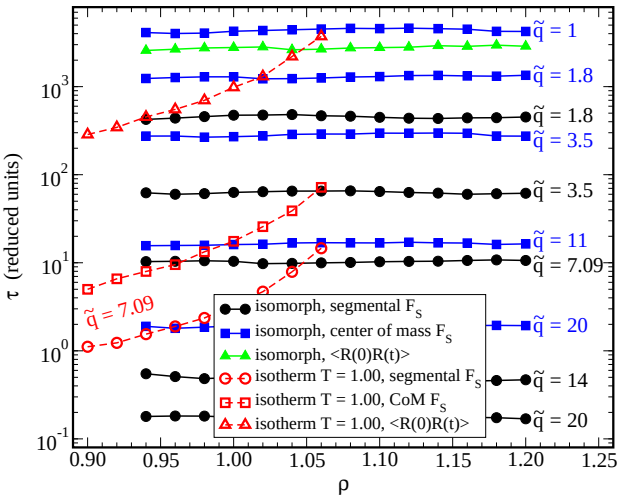

FIG. 3. Relaxation times calculated from the orientational autocorrelation of the end-to-end vector and the intermediate scattering function, as function of density. The value of the $\tilde{q}$ vector has been varied to obtain different measures of the relaxation time. Each value was kept constant in reduced units for the different densities All relaxation time measures are invariant for isomorphic state points (filled symbols). An isotherm is included for comparison (open red symbols).

We define a relaxation time for the dynamical quantities as the time where the correlation function reaches 0.2. These relaxation times are plotted in Fig. 3, this time also varying q. The different relaxation times characterizing the dynamics covers more than 4 decades in time, but each of them are to a good approximation invariant on the isomorph. In contrast, the relaxation times on the isotherm shown (open red symbols) shows a clear dependence on density.

The dynamics of flexible chains are often expressed in terms of correlation functions of Rouse modes, $\langle \mathbf{X}_p(t)\mathbf{X}_q(0)\rangle$[63,64]. The zeroth mode describes the center of mass displacement of the chain, while the other modes describe vibrations in a subchain of N/p segments. In Fig. 4 some of the Rouse mode auto correlation functions are plotted for the isomorphic state points. For the lower modes, there is an excellent collapse of the correlation functions, whereas the invariance decreases somewhat for the higher modes. It should be noted that the amplitude of the rouse modes is predicted to scale as $\langle X_p^2\rangle \propto 1/(N\sin^2(p/N))$, so the contribution of the higher modes is very small[65].

Fig. 5 shows the isomorphic invariance of the mean square displacement of both the segments and the center of mass in all regimes, including the subdiffusive regimes which is specific for polymers and other flexible molecules.

Not only equilibrium dynamics, but also out of equilibrium dynamics are predicted to be invariant on an isomorph. We test this by changing density and temperature instantaneously during a simulation. The center of

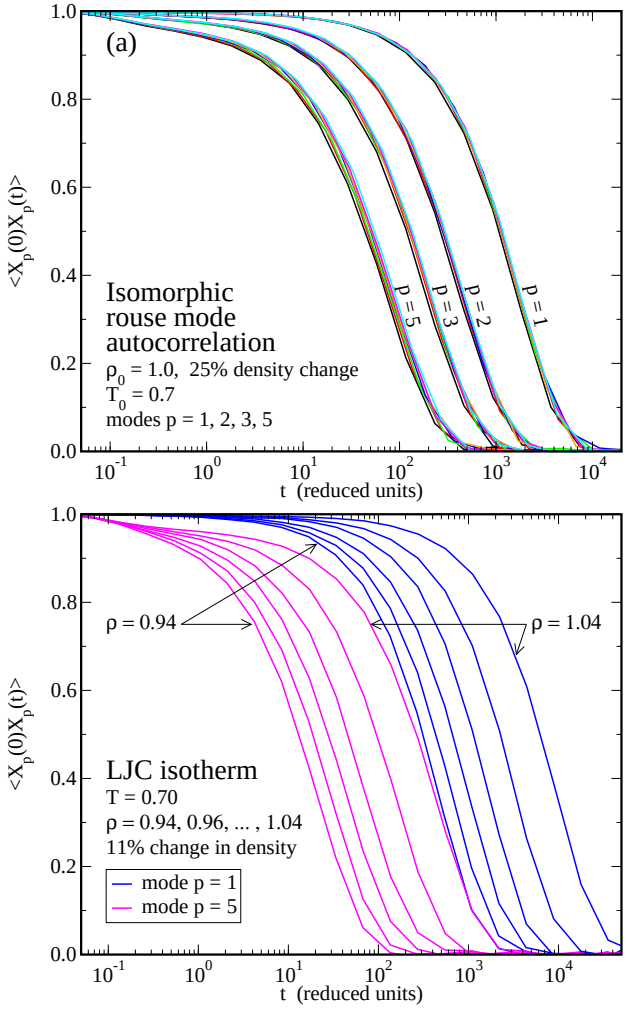

FIG. 4. Auto-correlation functions of some rouse modes. (a) For the same isomorphic state points as in Fig. 2(a). The collapse of the Rouse modes is good, especially for the lower modes. (b) Data for the same isothermal state points as in Fig. 2(b). There is no collapse of the dynamics for isothermal state points.

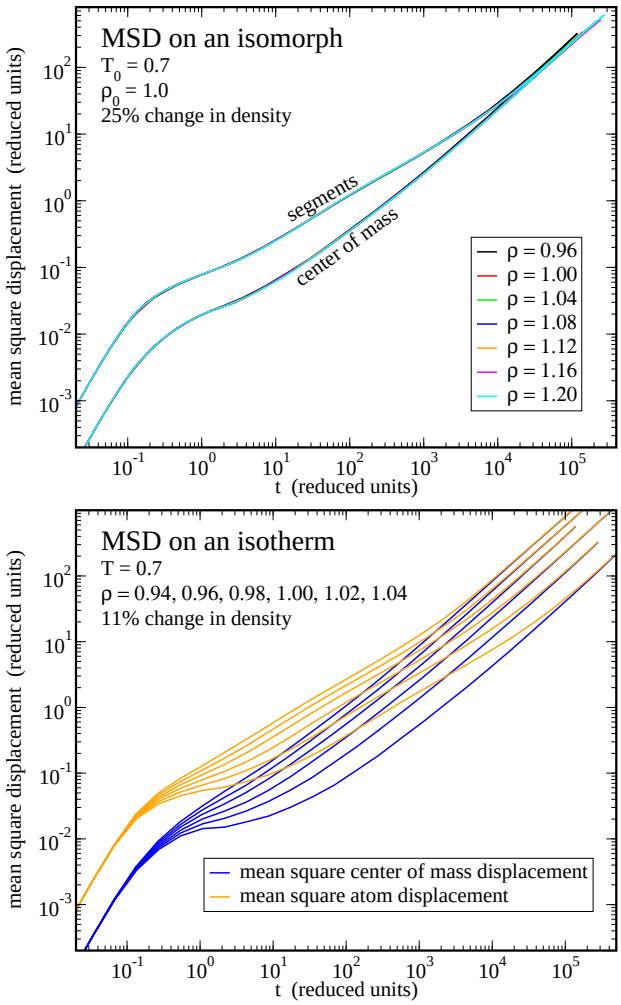

FIG. 5. The mean square displacements of the segments and the center of mass of the chains. (a) again, there is a good collapse for the mean square displacement on the isomorph, for both the segments and the center of mass. (b) This is not the case for the isotherm.

mass positions are scaled together with the box, but the intramolecular distances were kept constant. In Fig. 6 the relaxation of the potential energy is plotted after different instantaneous jumps. The figure shows that no relaxation is visible in the energy when jumping between two state points that are isomorphic to each other (black line). This is predicted by the isomorph theory: two state points on the same isomorph are equivalent with regard for aging[27]. Likewise, when jumping from two state points on the same isomorph to a third state point that is not on that isomorph, the relaxation curve is the same for the two jumps. When the density is changed, the system is immediately in equilibrium at the isomorphic state point with the new density. Any relaxation after the density jump then takes place on the isochore[66].

C. Structure on an isomorph

Also the structure is predicted to be invariant on an isomorph[27]. However, not all structural quantities are necessarily equally invariant when molecular liquids are considered. Since the length of the constrained bonds is constant in normal units and does not change with density, the bond length in reduced units will not be constant on the isomorph in reduced units. For that reason we plot the inter- and intramolecular contribution to the segmental radial distribution function $g(r)$ separately in Fig. 7. The intermolecular structure is quite constant on the isomorph, while the intramolecular structure is clearly not. The center of mass $g(\tilde{r})$ was also found to be invariant on the isomorph when plotted in reduced units (data not shown), but it is also invariant on the isochore and isotherm within the liquid (fluid) phase.

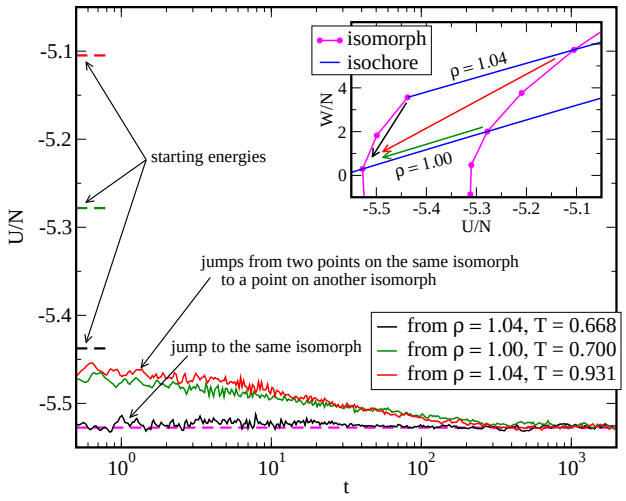

FIG. 6. Potential energy relaxation after instantaneous jumps from three different state points to $\rho = 1.00, T = 0.50$. The inset shows the direction of the jumps in the phase diagram, plotted in the U, W-plane. Black line: a jump between isomorphic state points. The energy shows no relaxation since the system is immediately in equilibrium. Red and green lines: two jumps from the same isomorph to another isomorph show the same relaxation behavior. The data of the relaxation plots are averaged of 8 independent starting configurations.

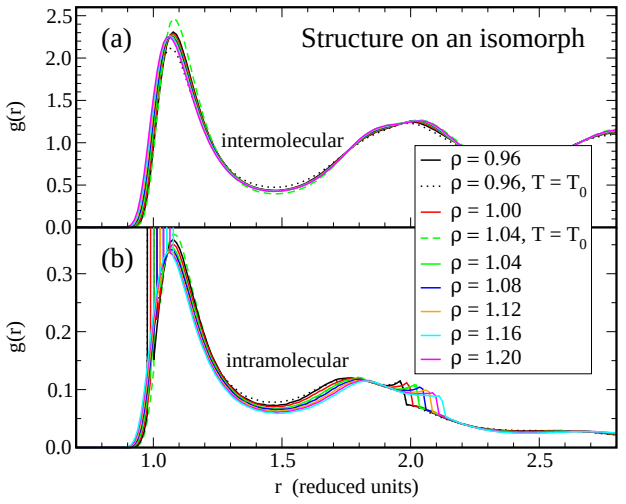

FIG. 7. Segmental and molecular structure on an isomorph for the same state points as in Fig. 2. Dashed lines correspond to isothermal density changes and are included for comparison. The data show that intermolecular structure is invariant, while intramolecular structure is not invariant on the isomorph due to the constant bond length. (a) The intermolecular (segmental) radial distribution function $g(\tilde{r})$ in reduced units on the isomorph $(\rho, T) = (1.00, 0.70)$. The intermolecular $g(r)$ is to a good degree invariant for isomorph state points, especially when compared to a (small) density change on an isotherm. (b) The intramolecular $g(r)$ is clearly not invariant on an isomorph.

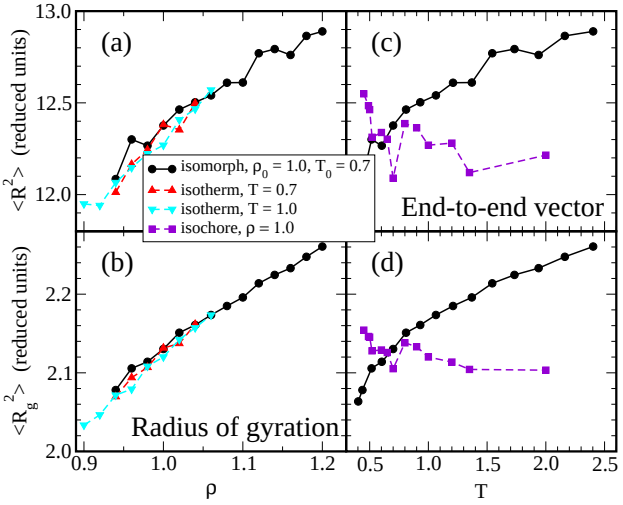

FIG. 8. Intramolecular quantities are not invariant on the isomorph (black solid lines) (a) The mean square end-to-end vector $\langle R^2 \rangle$ and the mean square radius of gyration (b) as a function of density. The temperature dependence of these quantities is similar on the isomorph and isotherms (dashed lines). It should be mentioned that when these quantities are plotted in real units, they show an (intuitive) decrease with density. (c) and (d) The same data for the isomorphic state points, now plotted as a function of temperature and compared with an isochore. These intramolecular quantities are actually more constant on the isochore, due to the fixed bond length.

To investigate the difference in inter- and intramolecular structure further, we plot the mean square radius of gyration $\langle R_g^2 \rangle$ and the mean square end-to-end vector $\langle R^2 \rangle$ in Fig. 8. These intramolecular quantities are clearly not invariant on the isomorph, changing as much with density as on the isotherm. On an isochore these quantities are even more constant than on the isomorph. The lack of temperature dependence of these quantities was already noted for a similar bead-spring model[67].

D. Scaling of the dynamics

Finally, we return to the question of the overall scaling of the dynamics of the model. As mentioned in the introduction, the isomorph theory predicts that each relaxation time characterizing the dynamics is a function of $h(\rho)/T$ where $h(\rho)$ is system dependent function. For atomic system with pair potentials being sums of power laws, we have an analytical expression for $h(\rho)$[44]. Due to the presence of the bonds, we unfortunately do *not* have an analytical expression for $h(\rho)$ in the model studied here. Fig. 9 shows the five studied isomorph in the ρ, T plane (filled symbols). The open symbols show the same data, except that the temperatures are divided by T_0 (the temperature at $\rho = 1$). The scaled data is predicted to collapse on a single curve, $h(\rho)$, which is indeed

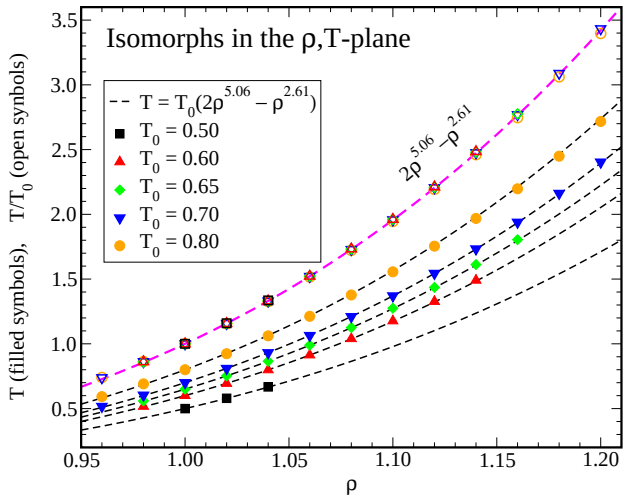

FIG. 9. Filled symbols: Shape of isomorphs in the ρ,T-plane. Open symbols: Same data with temperatures divided by T_0, showing a good collapse as predicted by the isomorph theory. Dashed lines: The function $h(\rho)$ was found by fitting to the open symbols (see text).

seen to be the case. We find $h(\rho)$ to be well approximated by $h(\rho) = 2\rho^{5.06} - \rho^{2.61}$, where the two exponents were determined by fitting.

Fig. 10 compares for three isochores the power-law density scaling and the scaling predicted by the isomorph theory. Fig. 10(a) and Fig. 10(b) show that the two smallest densities collapse using power-law density scaling with $\gamma = 7.7$, whereas the two highest densities collapse using $\gamma = 6.7$. Notice that the values of γ found by this empirical scaling is consistent with the values found from the W, U fluctuations in the respective density intervals (see Fig. 1). The power-law density scaling is thus an approximation that works for (relatively) small density changes, and the scaling exponent γ can be determined independently from the W, U-fluctuations. The more general form of scaling is the one predicted by the isomorph theory, which is tested in Fig. 10(c), using the $h(\rho)$ determined empirically in Fig. 9. The collapse is seen to be excellent. Notice that the isomorph scaling also captures the different shapes of the segmental and chain dynamics, which is also well known for power-law density scaling in a small density range[68–70].

V. CONCLUSION

To summarize, we have shown that the predictions of the isomorph theory apply to a flexible chain-like model system, despite the fact that the system is not entirely "Roskilde-simple" because the correlation coefficient of the instantaneous U, W fluctuations is less than 0.9. However, the collapse of the dynamics at different time scales is unmistakable, and works for the segmental dynamics as well as the chain dynamics. The rigid bonds

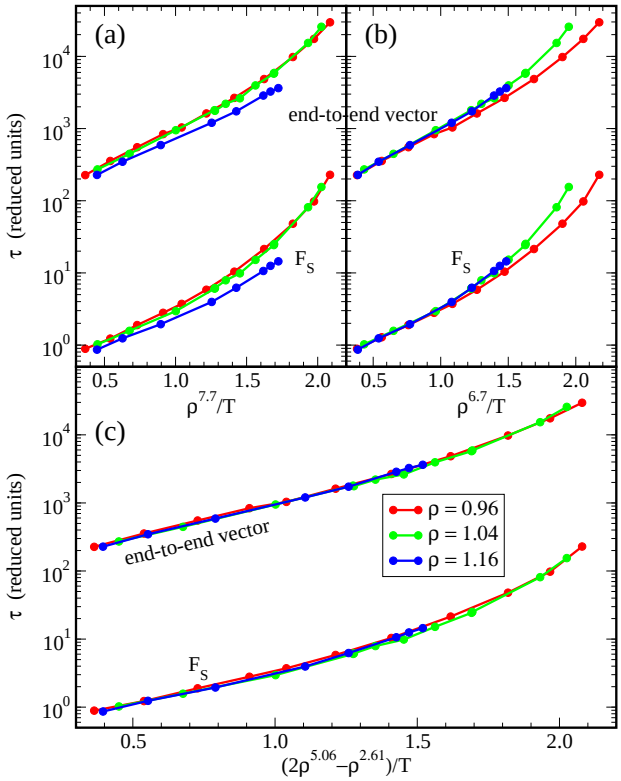

FIG. 10. Comparison between power-law density scaling and isomorph density scaling, applied to the relaxation times of the end-to-end vector and the segmental incoherent intermediate scattering function (F_S). (a) and (b) The power-law density scaling approach for two different values of γ (7.7 and 6.7), collapsing the low and high density isochores respectively. Neither value gives a good collapse of all the data. (c) Isomorph scaling approach, using the function $h(\rho) = 2\rho^{5.06} - \rho^{2.61}$ (see Fig. 9) to scale the relaxation times, giving a much better collapse.

in the model cannot scale with density and the structure can therefore not be constant on the isomorphs. We have shown that this is only the case for intramolecular structure, while the intermolecular structure stays invariant on the isomorph. This indicates that the isomorph theory may be extended to include flexible molecules. In particular this explains the experimentally observed power-law density scaling for alkanes and many polymers - and predicts that it should break down at larger density variations where isomorph scaling is needed.

ACKNOWLEDGMENTS

The authors are grateful to Søren Toxvaerd for critical reading of the manuscript. The centre for viscous liquid dynamics "Glass and Time" is sponsored by the Danish National Research Foundation via Grant No. DNRF61.

[1] P. G. Debenedetti and F. H. Stillinger, Nature **410**, 259 (2001).
[2] J. C. Dyre, Rev. Mod. Phys. **78**, 953 (2006).
[3] M. D. Ediger and P. Harrowell, J. Chem. Phys. **137**, 080901 (2012).
[4] A. Tölle, H. Schober, J. Wuttke, O. G. Randl, and F. Fujara, Phys. Rev. Lett. **80**, 2374 (1998).
[5] A. Tölle, Reports on Progress in Physics **64**, 1473 (2001).
[6] C. Alba-Simionesco, D. Kivelson, and G. Tarjus, J. Chem. Phys. **116**, 5033 (2002).
[7] C. Dreyfus, A. Aouadi, J. Gapinski, M. Matos-Lopes, W. Steffen, A. Patkowski, and R. M. Pick, Phys. Rev. E **68**, 011204 (2003).
[8] M. Paluch, R. Casalini, A. Patkowski, T. Pakula, and C. M. Roland, Phys. Rev. E **68**, 031802 (2003).
[9] G. Tarjus, D. Kivelson, S. Mossa, and C. Alba-Simionesco, J. Chem. Phys. **120**, 6135 (2004).
[10] R. Casalini and C. M. Roland, Phys. Rev. E **69**, 062501 (2004).
[11] C. M. Roland and R. Casalini, J. Chem. Phys. **121**, 11503 (2004).
[12] G. Tarjus, S. Mossa, and C. Alba-Simionesco, J. Chem. Phys. **121**, 11505 (2004).
[13] C. Alba-Simionesco, A. Cailliaux, A. Alegría, and G. Tarjus, Europhys. Lett. **68**, 58 (2004).
[14] C. Dreyfus, A. Le Grand, J. Gapinski, W. Steffen, and A. Patkowski, Eur. Phys. J. B **42**, 309 (2004).
[15] C. M. Roland, S. Hensel-Bielowka, M. Paluch, and R. Casalini, Reports on Progress in Physics **68**, 1405 (2005).
[16] M. Paluch, S. Haracz, A. Grzybowski, M. Mierzwa, J. Pionteck, A. Rivera-Calzada, and C. Leon, J. Phys. Chem. Lett. **1**, 987 (2010).
[17] J. Habasaki, R. Casalini, and K. L. Ngai, J. Phys. Chem. B **114**, 3902 (2010).
[18] E. R. López, A. S. Pensado, M. J. P. Comuñas, A. A. H. Pádua, J. Fernández, and K. R. Harris, J. Chem. Phys. **134**, 144507 (2011).
[19] A. Swiety-Pospiech, Z. Wojnarowska, J. Pionteck, S. Pawlus, A. Grzybowski, S. Hensel-Bielowka, K. Grzybowska, A. Szulc, and M. Paluch, J. Chem. Phys. **136**, 224501 (2012).
[20] A. Swiety-Pospiech, Z. Wojnarowska, S. Hensel-Bielowka, J. Pionteck, and M. Paluch, J. Chem. Phys. **138**, 204502 (2013).
[21] S. Urban and A. Würflinger, Phys. Rev. E **72**, 021707 (2005).
[22] S. Urban, C. M. Roland, J. Czub, and K. Skrzypek, J. Chem. Phys. **127**, 094901 (2007).
[23] C. M. Roland, R. B. Bogoslovov, R. Casalini, A. R. Ellis, S. Bair, S. J. Rzoska, K. Czuprynski, and S. Urban, J. Chem. Phys. **128**, 224506 (2008).
[24] S. Urban and C. M. Roland, J. Non-Cryst Solids **357**, 740 (2011).
[25] S. Urban, Liq. Cryst. **38**, 1147 (2011).
[26] K. Satoh, J. Chem. Phys. **138**, 094903 (2013).
[27] N. Gnan, T. B. Schrøder, U. R. Pedersen, N. P. Bailey, and J. C. Dyre, J. Chem. Phys. **131**, 234504 (2009).
[28] L. Bøhling, T. S. Ingebrigtsen, A. Grzybowski, M. Paluch, J. C. Dyre, and T. B. Schrøder, New Journal of Physics **14**, 113035 (2012).
[29] Y. Rosenfeld, Phys. Rev. A **15**, 2545 (1977).
[30] M. Dzugutov, Nature **381**, 137 (1996).
[31] A. A. Veldhorst, L. Bøhling, J. C. Dyre, and T. B. Schrøder, Eur. Phys. J. B **85**, 21 (2012).
[32] T. S. Ingebrigsten, T. B. Schrøder, and J. C. Dyre, J. Phys. Chem. B **116**, 1018 (2012).
[33] A. S. Pensado, A. A. H. Pádua, M. J. P. Comuñas, and J. Fernández, J. Phys. Chem. B **112**, 5563 (2008).
[34] G. Galliero, C. Boned, and J. Fernández, J. Chem. Phys. **134**, 064505 (2011).
[35] C. M. Roland, Macromolecules **43**, 7875 (2010).
[36] C. Bennemann, C. Donati, J. Baschnagel, and S. C. Glotzer, Nature **399**, 246 (1999).
[37] K. Binder, J. Baschnagel, and W. Paul, Prog. Polym. Sci. **28**, 115 (2003).
[38] R. A. Riggleman, G. N. Toepperwein, G. J. Papakonstantopoulos, and J. J. de Pablo, Macromolecules **42**, 3632 (2009).
[39] R. A. Riggleman, J. F. Douglas, and J. J. de Pablo, Soft Matter **6**, 292 (2010).
[40] A. Shavit, J. F. Douglas, and R. A. Riggleman, J. Chem. Phys. **138**, 12A528 (2013).
[41] U. R. Pedersen, N. P. Bailey, T. B. Schrøder, and J. C. Dyre, Phys. Rev. Lett. **100**, 015701 (2008).
[42] N. P. Bailey, U. R. Pedersen, N. Gnan, T. B. Schrøder, and J. C. Dyre, J. Chem. Phys. **129**, 184507 (2008).
[43] D. Fragiadakis and C. M. Roland, J. Chem. Phys. **134**, 044504 (2011).
[44] T. S. Ingebrigtsen, L. Bøhling, T. B. Schrøder, and J. C. Dyre, J. Chem. Phys. **136**, 061102 (2012).
[45] T. B. Schrøder, N. Gnan, U. R. Pedersen, N. P. Bailey, and J. C. Dyre, J. Chem. Phys. **134**, 164505 (2011).
[46] *Roskilde University Molecular Dynamics*, URL http://rumd.org.
[47] K. Kremer and G. S. Grest, J. Chem. Phys. **92**, 5057 (1990).
[48] C. Bennemann, W. Paul, K. Binder, and B. Dünweg, Phys. Rev. E **57**, 843 (1998).
[49] M. Aichele, Y. Gebremichael, F. W. Starr, J. Baschnagel, and S. C. Glotzer, J. Chem. Phys. **119**, 5290 (2003).
[50] F. Puosi and D. Leporini, J. Phys. Chem. B **115**, 14046 (2011).
[51] F. Puosi and D. Leporini, J. Chem. Phys. **136**, 211101 (2012).
[52] S. C. Glotzer and W. Paul, Annu. Rev. Mater. Res. **32**, 401 (2002).
[53] J.-L. Barrat, J. Baschnagel, and A. Lyulin, Soft Matter **6**, 3430 (2010).
[54] T. Goel, C. N. Patra, T. Mukherjee, and C. Chakravarty, J. Chem. Phys. **129**, 164904 (2008).
[55] G. Galliero and C. Boned, Phys. Rev. E **80**, 061202 (2009).
[56] S. Toxvaerd, O. J. Heilmann, T. Ingebrigtsen, T. B. Schrøder, and J. C. Dyre, J. Chem. Phys. **131**, 064102 (2009).
[57] T. Ingebrigtsen, O. J. Heilmann, S. Toxvaerd, and J. C. Dyre, J. Chem. Phys. **132**, 154106 (2010).
[58] M. P. Allen and D. J. Tildesley, *Computer simulations of liquids* (Oxford University Press, 1987).
[59] E. Voyiatzis, F. Müller-Plathe, and M. C. Böhm, Macromolecules **46**, 8710 (2013).

[60] N. P. Bailey, U. R. Pedersen, N. Gnan, T. B. Schrøder, and J. C. Dyre, J. Chem. Phys. **129**, 184508 (2008).
[61] G. Tsolou, V. A. Harmandaris, and V. G. Mavrantzas, J. Chem. Phys. **124**, 084906 (2006).
[62] W.-S. Xu and K. F. Freed, J. Chem. Phys. **138**, 234501 (2013).
[63] P. H. Verdier, J. Chem. Phys. **45**, 2118 (1966).
[64] M. Doi and S. F. Edwards, *The theory of polymer dynamics* (Oxford Science Publications, 1986).
[65] C. Bennemann, J. Baschnagel, W. Paul, and K. Binder, Computational and theorectical Polymer Science **9**, 217 (1999).
[66] N. Gnan, C. Maggi, T. B. Schrøder, and J. C. Dyre, Phys. Rev. Lett. **104**, 125902 (2010).
[67] C. Bennemann, J. Baschnagel, and W. Paul, Eur. Phys. J. B **19**, 323 (1999).
[68] C. M. Roland, M. Paluch, and R. Casalini, Journal of Polymer Science: Part B: Polymer Physics **42**, 4313 (2004).
[69] R. Casalini and C. M. Roland, Macromolecules **38**, 1779 (2005).
[70] C. M. Roland, Curr. Opin. Solid State Mater. Sci. **11**, 41 (2007).